FRP-STRENGTHENING OF WEBS OF STEEL PLATE-GIRDERS

Muhammad Aslam Bhutto

B.E. (Civil), M. Engg.

Submitted for the degree of Doctor of Philosophy

Heriot-Watt University

School of Built Environment

February 2014

ABSTRACT

Fibre-reinforced polymer, FRP, composites have been used successfully for the strengthening and repair of steel beams in order to increase the flexural strength of the beams by up to 40%. However, little attention has been given to the use of FRP composites to increase the ultimate strength of steel plate-girders where failure is initiated by shear buckling of the slender webs. This thesis presents the details and results of an experimental and numerical investigation in which the web panels of the steel plate-girders were strengthened either by bonding GFRP pultruded section stiffeners or layers of carbon or glass FRP composite fabrics. The objective of the strengthening was to obtain an increase of a minimum of 20% in the ultimate load of the steel plate-girders by increasing the out-of-plane stiffness of the web in the web panels.

The tests of one un-strengthened control specimen and seven FRP-strengthened specimens were carried out. The test results showed an increase up to 54% in the ultimate load of the FRP-strengthened specimens, compared to that of the un-strengthened control specimen. In the tests there was no breakdown of the steel-GFRP bond, at the ultimate load, in the specimens strengthened using the GFRP pultruded sections, whilst a breakdown of the steel-fabric bond occurred in the specimens strengthened using FRP fabrics. Before testing, nonlinear finite-element analyses, FEA, of the specimens were carried out using shell elements and the LUSAS FE program. Both material and geometrical nonlinearities were modelled. The test results and the FEA predictions for the un-strengthened and GFRP pultruded section strengthened specimens were in good agreement. For the FRP fabric-strengthened specimens, there was agreement between the test results and FEA predictions up to the breakdown of the steel-fabric bond.

Design procedures for FRP-strengthened plate-girders have been developed based on those in Eurocode 3. The design procedures can be used to estimate the ultimate loads of the FRP-strengthened plate-girders and to determine suitable cross-sections of GFRP pultruded sections as intermediate, load-bearing and diagonal web stiffeners. The procedures have been validated using the results of the tests and FE analyses of nine FRP-strengthened plate-girder specimens and those of the FE analyses of thirty-five models of the plate-girders. The design procedures for the FRP-strengthened plate-girders can therefore be used in practice.

DEDICATED

TO

MY PARENTS, WIFE AND CHILDREN

FOR THEIR

LOVE AND PRAYERS

ACKNOWLEDGMENTS

With the name of ALLAH the almighty, who is the most beneficent and the most merciful. He is creator, master and controller of the whole universe and can do each and every thing without help from any creation. He is the ONLY who bestowed me ability, courage and time to carry out PhD research work.

I would like to express my personal gratitude to Professor Ian M. May for his expert supervision, continued guidance, consistent motivation and valuable advices during all phases of the research work. He always gave me a patient hearing and helped me in addressing all sorts of problems during the research work.

I am extremely grateful to the Department for Transport (DfT), United Kingdom for providing financial assistance to carry out the research project. I am grateful to Mr. Brian Bell (Network Rail), Mr. Simon Frost (Walker Technical Resources) and other members of 'Project Steering Group' for their continued guidance and support throughout the project. I am also grateful to NED University of Engineering & Technology, Pakistan for granting study leave and providing the additional funding required for the research.

I would also express my gratitude to all laboratory colleagues of the School of Built Environment (SBE) particularly David Haldane, Tom Stenhouse, Steve Ritch and Graham Sorely for their assistance and understanding during the course of testing work. Thanks are also due to the SBE staff members Anne Ormston, Julie Brunton, Gillian Rae and all others for their support in the official matters.

I am greatly inedited to all my teachers at Saint Mary's High School, Sukkur; Islamia Science College, Sukkur; Quiad-e-Awam University of Engineering, Science & Technology, Nawabshah and NED University of Engineering & Technology, Karachi whose efforts enabled me to pursue PhD degree at Heriot-Watt University. I would like to express the deepest appreciations to my mentors Engr. Abul Kalam (late), Prof. S.F.A. Rafeeqi, Prof. S.H. Lodi, Prof. Asad-ur-Rahman, Prof. Noor A. Memon and Prof. A. A. Ansari for their continued support and encouragement.

Special thanks are due to my friends and colleagues Dr. Rashid A. Khan, Dr. A. J. Sangi, Dr. Atif Mustafa, Shamsoon Fareed, Qari Falaksher, Wajid A. Khan, Naseer Sattar, Ali Hasnain and many others for their help and support from time to time.

Finally, I would express my gratitude to all my family members, in particular to my father for his patience, encouragement and constant prayers and also to my brother Akram for looking after family and other matters in my absence. I would also acknowledge the contributions of great love and support from my wife and lovely kids Ali, Hussain and Sumayya without which completion of PhD would have been a dream. I always missed love and affection of my mother during entire period of the study and would take this opportunity to pray for her departed soul. Prayers are also due for my brother Zain-ul-Abideen whose departure from this world was a big and irreparable loss during the PhD work.

ACADEMIC REGISTRY
Research Thesis Submission

Name*:*	MUHAMMAD ASLAM BHUTTO		
School/PGI:	SCHOOL OF THE BUILT ENVIRONMENT		
Version: *(i.e. First, Resubmission, Final)*	FINAL	Degree Sought (Award **and** Subject area)	Ph D in Civil Engineering

Declaration

In accordance with the appropriate regulations I hereby submit my thesis and I declare that:

1) the thesis embodies the results of my own work and has been composed by myself
2) where appropriate, I have made acknowledgement of the work of others and have made reference to work carried out in collaboration with other persons
3) the thesis is the correct version of the thesis for submission and is the same version as any electronic versions submitted*.
4) my thesis for the award referred to, deposited in the Heriot-Watt University Library, should be made available for loan or photocopying and be available via the Institutional Repository, subject to such conditions as the Librarian may require
5) I understand that as a student of the University I am required to abide by the Regulations of the University and to conform to its discipline.

* *Please note that it is the responsibility of the candidate to ensure that the correct version of the thesis is submitted.*

Signature of Candidate*:*		Date:	

Submission

Submitted By *(name in capitals):*	
Signature of Individual Submitting:	
Date Submitted:	

For Completion in the Student Service Centre (SSC)

Received in the SSC by *(name in capitals):*			
1.1 Method of Submission *(Handed in to SSC; posted through internal/external mail):*			
1.2 E-thesis Submitted (mandatory for final theses)			
Signature:		Date:	

TABLE OF CONTENTS

LISTS OF TABLES

LISTS OF FIGURES

SYMBOLS AND ABBREVIATIONS

λ_w = web slenderness of shear panel

χ_w = reduction factor for the shear bucking of web depending on λ_w

A = area of cross-section

a, b = length of plate/ web in the web panel

A_f, A_w = area of cross-section of flange/ web

A_{f1}, A_{f2} = areas of cross-section of top and bottom flanges of plate-girder

AFRP = aramid fibre-reinforced polymer

b_f, b_s = width of flange/ stiffener

c = distance between plastic hinges in flanges

CFRP = carbon fibre-reinforced polymer

d_o, h_f = distance between centres of top and bottom flanges

D, d_w, h_w = depth of web/ plate

E = Young's modulus of elasticity

e = distance between end-posts or transverse stiffeners at the end supports

FE = finite element

F_e, V_{cr} = Euler/ elastic critical load

FEA = finite element analysis/ analyses

f_f = mean longitudinal stress in the flange due to bending moment

FRP = fibre-reinforced polymer

G = shear modulus

GFRP = glass fibre-reinforced polymer

GNL = geometric non-linearity

I = second moment of area

I_f = moment of inertia of flange about an axis passing through its centroid and perpendicular to the plane of web

I_{min} = minimum second moment of area

I_s = second moment of area of a transverse stiffener

K = shear buckling co-efficient

L = length/ span of steel beam/ plate-girder

M, M_{Ed} = maximum elastic bending moment of the plate-girder/ beam

$M_{f,Rd}$ = design plastic moment of resistance of flanges only = $A_f.h_f.\sigma_{yf}$

M_{pf}, M_{pw} = plastic moment capacity of flanges/ web

MGNL = material and geometric non-linearities

MNL = material non-linearity

N_{Ed} = design axial force

NL = non-linearity

N_{pl} = squash load

S_x = plastic section modulus

t, t_w = thickness of web/ plate

t_f, t_s = thickness of flange/ stiffener

$V_{b,Rd}$ = Eurocode design shear strength/ ultimate load of plate-girder

$V_{bf,Rd}$ = Eurocode design shear strength/ ultimate load contribution of flanges

$V_{bw,Rd}$ = Eurocode design shear strength/ ultimate load contribution of web

V_f = plastic shear buckling resistance of flanges

V_p, P_v = ultimate plastic load of plate/ web in shear = $\sigma_{yw}A_w/\sqrt{3}$

V_w = elastic shear buckling resistance of web panel

W = concentrically applied load

w = uniformly distributed load/length

W_c = plastic collapse load

y = distance from the neutral axis

Z_x = elastic section modulus

α = aspect ratio of the web plate/ panel = a/d_w

γ_{M0}, γ_{M1} = partial safety factors for the resistance to instability (taken as 1.0)

δ_b, δ_s = vertical displacement due to bending/ shear

δ_{max} = maximum vertical displacement

ε = $\sqrt{(235/\ \sigma_{yw}}$ in MPa)

σ_b = longitudinal stress due to elastic bending

σ_y = yield strength

σ_{yf}, σ_{ys}, σ_{yw}, $\sigma_{y\ GFRP}$ = yield strength of flange/ stiffener/ web/ GFRP

τ_{cr}, q_w = elastic shear buckling or critical shear stress

τ_y, p_v = yield stress in shear = $\sigma_y/\sqrt{3}$

τ_{yw} = yield stress of web in shear = $\sigma_{yw}/\sqrt{3}$

η = co-efficient that includes the increase of shear strength/ ultimate load at smaller web slenderness's (1.2 for S235 to S460 grades of steel)

ϑ = Poisson's ratio

DEFINITIONS

End posts or end stiffeners

Vertical stiffeners at the ends of a plate-girder

Glass fabric-strengthened plate

A steel plate (without a surrounding frame) strengthened using layers of the glass fabric sheets

Glass fabric-strengthened web panel

A steel plate surrounded by the frame of flanges and vertical stiffeners and strengthened using layers of the glass fabric sheets

Steel frame

A steel frame comprising the top and bottom flanges and vertical stiffeners

Steel frame with diagonal stiffener

A steel frame comprising the flanges and vertical stiffeners with an additional stiffener in the diagonal orientation

Steel plate

A steel plate without a surrounding frame

Steel web panel

A steel plate surrounded by the frame of flanges and vertical stiffeners

Steel web panel with stiffener(s)

A steel plate surrounded by the frame of flanges and vertical stiffeners with additional vertical or diagonal stiffener(s) either on one or both sides of the plate

Web or web plate

A steel plate in the web panel surrounded by frame

Chapter 1 Introduction

1.1 Background

Steel bridge members generally require strengthening and repair due to the increased loads, damage due to accidents and environmental conditions and initial design flaws. The conventional methods for the strengthening and repair of the steel members involve adding more steel which requires welding, large scaffoldings, heavy lifting and long disruptions. Because of these problems, new materials which can be used conveniently and efficiently in place of the steel need exploring. Fibre-reinforced polymers, FRP, composites are light-weight, have suitable strength and stiffness properties and are easy to install on site. Due to these advantages, FRP composites are considered to be the most favoured material for the strengthening and repair of structures (Cadei et al, 2004).

FRP composites are commonly formed by mixing two components, a fibrous reinforcement and a resin to form a matrix, which encapsulates the reinforcement. The fibre reinforcement generally has high strength, stiffness and strength-to-weight ratio. The matrix in comparison has lower strength and stiffness (Cadei et al, 2004). FRP composites have been used successfully in strengthening and repair of concrete beams. Carbon FRP, CFRP, is the most commonly used composite with some use of glass FRP, GFRP. Research carried out (Sundarraja & Rajamohan, 2009; Czaderski & Motavalli, 2004; Al-saidy, 2004 and Sen et al, 2001) has shown that due to FRP-strengthening, the flexural strength of concrete and steel-concrete composite beams has been increased by up to 50%. In one case, carbon composites have been proved to be a useful alternative to steel shear reinforcement in concrete beams (Czaderski, 2002).

CFRP and GFRP composites have also been used for the strengthening and repair of steel beams. The objective of such strengthening has been to increase the flexural strength of the beams, which has been obtained up to 40% compared to the un-strengthened beams (Narmashiri et al, 2010; Vatonec et al, 2002, Photiou et al, 2006 and Colombi & Poggi, 2006).

1.2 Description of problem

Steel plate-girders are a common type of thin-walled steel members often used in bridges. A plate-girder consists of a web plate, top and bottom flanges and generally a series of stiffeners. The web primarily resists the applied shear, while the flanges primarily resist the applied moment (Nilsen et al, 2012). The steel plate-girders being investigated are those which are predominantly loaded in shear. In such plate-girders, shear buckling of the thin web initiates the failure and occurs when the applied shear approaches the critical shear stress of the panel. After buckling, the additional load is carried by a tensile membrane stress field in the web and the flanges. The failure occurs when the web yields across the tensile stress field and plastic hinges develop in the top and bottom flanges (Rockey et al, 1978). Two methods can be used to increase the buckling strength of the web plate; either by increasing the web thickness to reduce its slenderness or by providing transverse steel stiffeners to reduce the aspect ratio. Therefore, one important design aspect of plate-girders is the shear buckling and failure of web elements (Alinia et al, 2009).

Shear buckling of the thin-walled members has remained a prominent cause in initiating the failure of steel bridges. Imam and Chryssanthopoulos (2010) carried out a statistical study of 164 metallic bridges to investigate the causes of failure of bridges throughout the world from the early nineteenth century up to 2010. The study comprised 87 highway and 73 railway bridges and was carried out with the help of the published literature, web and news reports. Among 164 reported cases, 87 bridges (51%) were classified as ‘collapse or major failure’ where one or more structural members had detached from the bridges. 73 bridges (47%) were classified as ‘no collapse or minor failure’ where the bridges became non-functional and were closed for repair or strengthening works. 4 bridges (3%) could not be classified and were left as ‘unknown’. Among 87 bridges in the ‘major failure’ category, the most frequently encountered modes causing the failure were scour of piers/ foundations (17%), buckling of thin-walled members (16%), fatigue (13%) and impact (13%). Of 73 bridges in ‘minor failure’ category, the dominant cause of the failure was fatigue (67%). It was also revealed that the majority of the fatigue cracking (29%) was due to the out-of-plane distortions of the members initiated by the shear buckling. Figure 1.1 shows the failure of plate-girder beams at the beam-column joint initiated by shear buckling of the webs at the Building Research Establishment's Cardington Laboratory, United Kingdom.

Figure 1.1 Failure of plate-girder beams initiated by shear buckling of the webs (Newman et al, 2001)

Due to the reasons described earlier, webs of the steel plate-girders used in the bridges may require strengthening and repair. The use of CFRP and GFRP composites for the strengthening of steel beams has generally been made to increase their flexural strengths. Little attention, however, has been given to the use of these composites to strengthen the webs of the steel plate-girders, where failure is initiated by shear buckling of the web.

Okeil et al (2009a & 2010) used GFRP pultruded sections as vertical and diagonal stiffeners to strengthen the webs of two steel plate-girders, specimens OB2 and OB3. Okeil et al named their test specimens as B1, B2 and B3. Since similar names for the specimens have been used by the author, a prefix letter 'O' is added to the names of Okeil's specimens for identification. Test results showed that the ultimate loads of GFRP-strengthened specimens OB2 and OB3 were increased by 1.40 and 1.56 times, respectively, compared to that of the un-strengthened specimen OB1. Finite element analyses, FEA, of specimens OB1 and OB2 were carried out before testing. The FEA ultimate loads of the specimens were higher, up to 3.78 times, than those in the tests. A breakdown of the steel-GFRP bond occurred in the tests of the strengthened specimens.

The preliminary work carried out by Okeil et al (2009a & 2010) for the FRP-strengthening of steel plate-girders is useful, but requires more study to determine the effectiveness of using different orientations of the GFRP stiffeners and of using different types of FRP composites for strengthening. Techniques are required to be developed to strengthen the bond between the steel and GFRP stiffeners in order to

avoid a bond breakdown. Development of the finite element models of the un-strengthened and FRP-strengthened plate-girders, which can be validated using the experimental investigations, is also required.

Guidelines for FRP-strengthening of steel structures were made available in 2004 in a report published by the Construction Industry Research and Information Association (CIRIA), United Kingdom (Cadie et al, 2004). The report focused on strengthening steel members to increase their axial and flexural strengths. No guidance was given in the report on the FRP-strengthening of thin-walled steel members. Design guidelines are therefore required to be developed for plate-girders with the webs strengthened using the FRP composites.

1.3 Research project

In order to carry out research work on the use of FRP composites for strengthening of the thin-walled steel members, a research project has been carried out at the School of Built Environment, Heriot-Watt University, Edinburgh. The project titled 'FRP-strengthening of steel bridge members' comprised the full scale tests and FE analyses of the un-strengthened and FRP-strengthened steel plate-girders. The guidelines on the use of CFRP and GFRP composites to strengthen the web of plate-girders have also been developed.

1.4 Aim and objectives of research

The aim and objectives of the research project are as follows.

1.4.1 Aim of research

The aim of present research is to investigate the use of FRP composites for strengthening of the webs of steel plate-girders and to obtain a minimum increase of 20% in the ultimate load of the plate-girders due to FRP-strengthening.

The primary fuction of a bridge is to carry traffic (live) loads in addition to its own weight (dead load). In the bridges, the ratio of live to dead loads is less than unity for long spans and more than unity for short spans, with a general approximation as unity, i.e. 1:1. The usual increase required in the live loads due to vehicular traffic is 35-40% (Sparks, 2008). The methods for strengthening and repair of the bridge members due to

addition of materails have a very small effect, less than 2%, in increasing the dead load and can be ignored. Therefore, in order to carry the 35-40% increased live loads, the increase required in the overall load capacity of the bridge member (plate-girder) would be half of that, i.e. about 20%, which has accordingly be made the aim of the reserach.

1.4.2 Objectives of research

In view of the aim of the research, the objectives are as follows.

- To investigate use of carbon and glass FRP, CFRP and GFRP, composites to strengthen webs of the steel plate-girders.

- To increase the load at which shear buckling of the web occurs by using FRP-strengthening in order to obtain a minimum increase of 20% in the ultimate load of FRP-strengthened plate-girders compared to that of the un-strengthened plate-girders.

- To carry out experimental investigations of un-strengthened and FRP-strengthened steel plate-girders.

- To carry out studies of un-strengthened and FRP-strengthened steel plate-girders using FE modelling to be validated using the experimental investigations.

- To determine the effectiveness of FRP-strengthening of the webs of steel plate-girders by using GFRP pultruded sections as intermediate, load-bearing and diagonal web stiffeners and using layers of carbon and glass fabric sheets.

- To develop procedures for the design of FRP-strengthened plate-girders.

- To use the results of the tests and FE analyses to validate the design procedures.

1.5 Content of the thesis

The thesis consists of seven chapters. Chapter 1 describes, briefly, the failure mechanism in steel plate-girders and the use of FRP composites for the strengthening of structures. It also describes the problem to be investigated and the aim and objectives of the research. Finally, it outlines the content of the thesis.

Chapter 2 commences with a description of the various theories developed to explain the failure mechanism of steel plate-girders and methods for the design of transverse web stiffeners. An introduction to FRP composites and the significance of their use in strengthening of structures is given. This is followed by a review of the literature pertaining to the use of FRP composites for strengthening and repair of the concrete and steel structures. Finally, it describes the significance of bond between the steel and FRP surfaces in the FRP-strengthened structures and the effect of various factors upon the strength of the steel-FRP bond.

Chapter 3 presents the details of an experimental investigation comprising the tests of eight specimens, one un-strengthened control specimen, B1, and the seven FRP-strengthened specimens, B2 to B8. The tests were carried out on the end web panels of steel plate-girders. The plate-girders were manufactured in two series, S1 and S2. The S1 and S2 plate-girders were similar in construction; but had different yield and ultimate tensile strengths of the steel in the web. In four of the strengthened specimens, the webs of the end panels were bonded with GFRP pultruded section stiffeners and in the remaining three specimens with layers of the carbon and glass fabrics. The testing procedure, the strengthening techniques employed and FRP composites used for the strengthening of the specimens are described. The test results for the specimens are presented, discussed and compared.

Chapter 4 describes the details of a validation study in which the FE analyses of nine models and thirty-eight test specimens were carried out using the LUSAS FE program, Version 14.3 (LUSAS, 2008). The models were a steel beam, a steel frame, steel plate and web panel, frame and web panel with diagonal stiffeners, glass fabric-strengthened plate and web panel and a steel plate-girder. The test specimens were thirty-five steel plate-girders of Rockey and Skaloud (1968 & 1972) and three plate-girders, one un-strengthened and two GFRP-strengthened, of Okeil et al (2009 & 2010). The results of the FE analyses are compared to the theoretical predictions and test results.

Chapter 5 presents the details and results of FE analyses carried out on models of the test specimens. FE models of the eight test specimens, B1 to B8, were analysed to predict the behaviour of specimens in the tests. Because of the good agreement between the test and FEA results of control specimen B1, a model of the un-strengthened

specimen B9 was analysed and used as the control for the test specimens and models using the S2 plate-girders. The details of the element, mesh size and material properties used and the loading and boundary conditions applied are described. The ultimate loads, modes of the failure, load-deflection responses and locations of the plastic hinges developed in specimens obtained from the FE analyses are compared to those in the tests.

Chapter 6 presents the design procedures which have been developed for the steel plate-girders with the webs strengthened using GFRP pultruded section stiffeners or layers of the FRP composite fabrics. The design procedures for estimation of the ultimate load of the strengthened plate-girders and for the design of suitable cross-sections of GFRP stiffeners are developed from those in Eurocode 3, EC3 (ENV 1993-1-5, 2006). The design procedures have been used to estimate the ultimate loads of test specimens B2 to B8 and to determine the cross-sections of the GFRP stiffeners required for specimens B2, B5, B6 and B8. The design procedures have also been used to estimate the ultimate loads and to determine the cross-sections of the GFRP stiffeners required for specimens OB2 and OB3 of Okeil et al (2009a, 2009b & 2010). The results of the design procedures for all specimens are compared to those in the tests and FE analyses for validation.

Chapter 7 presents the main findings of the tests and FE analyses of the specimens B1 to B9. It is followed by a comparison of the results of the specimens B1 to B9 predicted by the design procedures and those in the tests and FE analyses. It also describes the work suggested to be carried in future.

Appendices A to G give the details of calculations made for the estimation of the ultimate loads of models and test specimens, B1 to B9 and OB1 to OB3, and the determination of suitable cross-sections of the GFRP stiffeners of specimens B2, B5, B6, B8, OB2 and OB3.

Chapter 2 Review of Literature

2.1 Introduction

Thin-walled steel beams such as plate-girders are commonly used as bridge members. In plate-girders, the flanges primarily resist the applied moment, while the web primarily resists the applied shear. Due to the slenderness of the web plates, they can buckle at an early stage of loading. To avoid web buckling, transverse or longitudinal steel stiffeners are used (Nilsen et al, 2012 & Alinia et al, 2009). This Chapter commences with a description of shear buckling in thin steel plates and steel plate-girders. The various theories developed to explain the failure mechanism of steel plate-girders are then described. Methods developed to for the design of transverse stiffeners to strengthen the slender webs are also described.

A description is given of fibre-reinforced polymers, FRP, composite materials, their component parts, types and properties of FRP composites and the use of the FRPs in strengthening of structures together with a discussion of advantages and limitations of their use. Due to suitable strength and stiffness properties, FRP composites have extensively been used in strengthening and repair of concrete and steel structures (Cadei et al, 2004). The literature pertaining to the use of FRP composites for strengthening and repair of the concrete structures with particular focus on reinforced concrete beams is reviewed. It is followed by a review of the experimental, numerical and analytical research carried on the use of the FRP composites for the flexural and shear strengthening of the steel beams. Preliminary work carried on the use of the FRP composites to strengthen the webs of steel plate-girders has also been presented. Finally, the significance of the adhesively bonded joints in the FRP-strengthened structures and various factors affecting the bond strength are discussed.

2.2 Shear buckling in thin steel plates

A thin steel plate in shear is a representation of the dominant loading case of a slender web in the web panel of a steel plate-girder. In the thin plate in shear, the principal tensile and compressive in-plane stresses would develop as shown in Figure 2.1. When the principal compressive stress exceeds the elastic shear buckling stress of the plate, the plate cannot resist any additional compressive loading and buckles out-of-plane along the tensile diagonal (Da Silva et al, 1999). The elastic shear buckling stress of the

plate depends upon the slenderness and aspect ratios of the plate and the boundary conditions applied along its edges (Trahair et al, 2001).

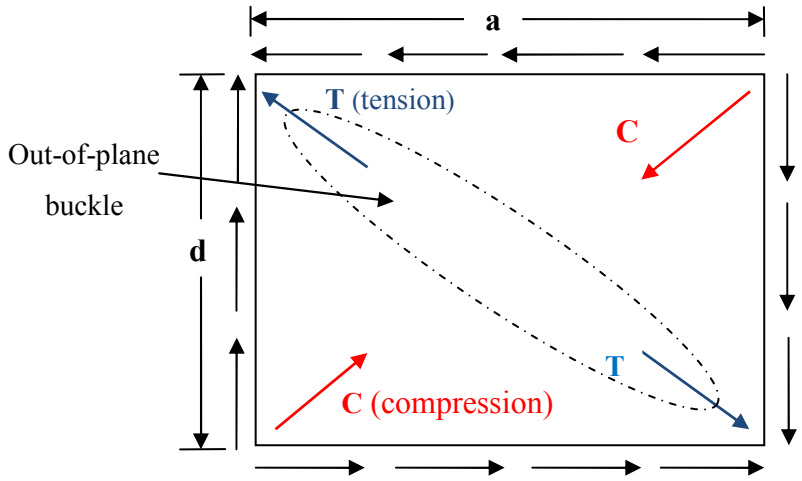

Figure 2.1 Principal tensile and compressive stresses in thin plate subjected to shear

2.3 Failure in steel plate-girders

Steel plate-girders are fabricated by welding together two flanges, a web and a series of transverse stiffeners if provided. In plate-girders, the flanges primarily resist the applied moment, while the web primarily resists the applied shear and maintains the relative distance between flanges. Generally, the ratio of depth of the web to its thickness, known as slenderness ratio, is high. Due to the high slenderness ratio of the web, shear buckling in the web occurs at an early stage of loading. The webs are therefore strengthened with transverse or longitudinal stiffeners to increase their shear buckling strength (Nilsen et al, 2012 and Alinia et al, 2009).

The failure in a steel plate-girder predominantly loaded in shear is initiated by the shear buckling of the web. After buckling of the web, the additional load is carried by a tensile membrane stress field in the web and the flanges. The failure occurs when the web yields across the tensile stress field and plastic hinges develop in the top and bottom flanges (Rockey et al, 1978). There are three basic contributions to the ultimate strength of the transversely stiffened plate-girders. These include elastic buckling and post-buckling strengths of the web and the frame action of the flanges (White & Barker, 2008). Therefore, one important design aspect of plate-girders is the shear buckling and failure of web elements. A proper web design involves finding a combination of optimum plate thickness and stiffener spacing that renders the required load capacity and economy in terms of material and fabrication cost (Alinia et al, 2009).

2.4 Design theories for steel plate-girders

Extensive research has been carried out and several theories have been developed to predict the failure behaviour of steel plate-girders loaded in shear and bending and to determine their ultimate load carrying capacity. The most important amongst them are discussed below.

2.4.1 Basler theory

Basler (1961) carried out research into the shear strength of the steel plate-girders and proposed a design theory which utilizes the post-buckling strength offered by the transverse stiffeners of plate-girders. The following assumptions were made.

1. The web in the web panel of plate-girder acts as a thin plate simply supported along all edges.

2. The thin web of the plate-girder subjected to shear would reach a stage at which the diagonal compressive stresses cease to increase as the web deflects and as the load is increased. At this stage, the diagonal tensile stresses would continue to increase and develop a uniform membrane tension stress field in the web's cross-section. The ultimate load contribution resulting from the tension field depends upon its inclination 'Φ' with the flanges and has a maximum value at '$\Phi = 45^{o}$'.

3. A flange of a conventionally built welded plate-girder cannot resist the vertical component of the tensile stresses at the web-flange juncture due to very little bending rigidity in the plane of the web. So the flanges do not serve as anchors for the tensile stress field. The situation at the boundaries of the web along the transverse stiffeners is different where the tensile strip can transmit the stresses.

In view of the above assumptions, it was concluded that in plate-girders with slender webs, neither a pure beam action nor a pure tension field action occurs alone, but rather the combination of both. Failure would occur when the shaded area of the web in Figure 2.2(c) yields. The results of this research formed the basis of the design procedures used in the United States (AISC, 1961).

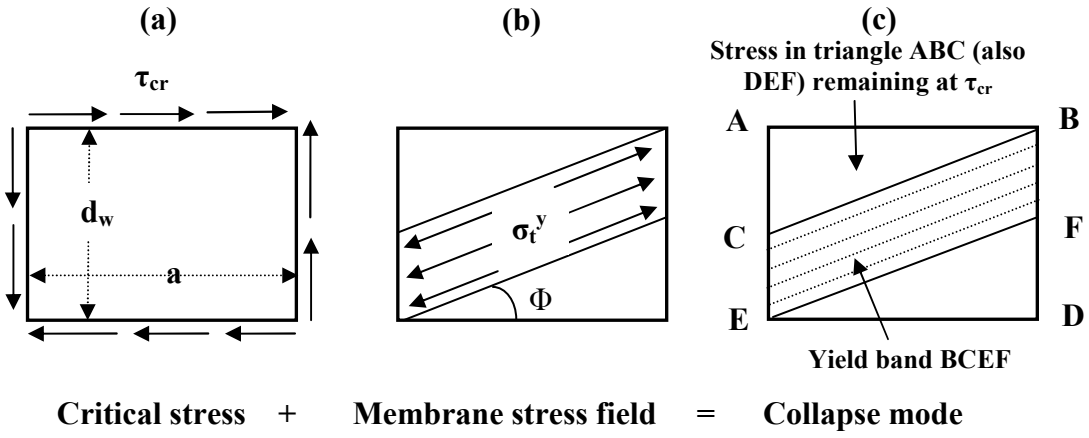

Figure 2.2 Failure behaviour of steel plate-girder (Basler, 1961)

Using this structural model, Basler developed Equation 2.1 to determine the ultimate load of a shear web panel, V_{ult}, of a plate-girder.

$$V_{ult} = d_w t_w \left[\tau_{cr} + \frac{\sqrt{3}}{2}\frac{\tau_{yw}}{\sqrt{1+\alpha^2}}\left\{1 - \frac{\tau_{cr}}{\tau_{yw}}\right\}\right] \qquad \text{Equation 2.1}$$

Where,

τ_{yw} = yield stress of the web in shear $= \sigma_{yw}/\sqrt{3}$

σ_{yw} = yield strength of the steel in web

τ_{cr} = elastic critical/ buckling shear stress of web

d_w, t_w = depth/ thickness of web plate

2.4.2 Rockey and Skaloud theory

Rockey and Skaloud (1968) carried out tests of 24 steel plate-girders and examined the effect of flexural strength of the flanges upon the ultimate load carrying capacity of the plate-girders. Later, tests of a further 21 plate-girders were carried out (Rockey & Skaloud, 1972).

The test results showed that by increasing the flexural strength of the flanges, the ultimate load capacity of the plate-girder could be increased by up to approximately 60%. A plastic method of design for steel plate-girders which allowed for the influence of the flexural strength of the flanges upon the post-buckled behaviour of webs was presented. It was considered that conventionally welded steel plate-girders have flanges of low torsional rigidity and the influence of residual stresses is present in the web and flanges. Based upon this consideration, it was assumed that the web in a shear web

panel should be treated as simply supported on all edges. A failure mechanism of the plate-girders comprising the three stages, shown in Figure 2.3 and described below, was also presented.

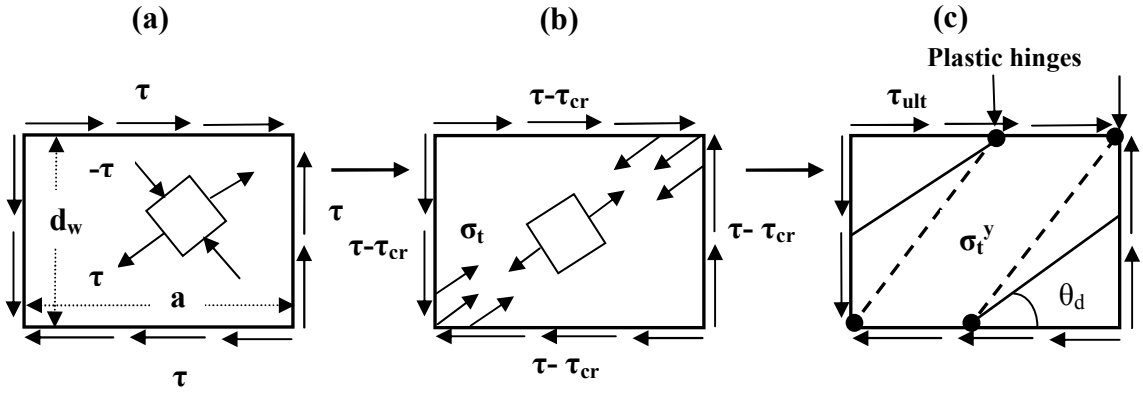

Figure 2.3 Failure behaviour of steel-plate girder (Rockey & Skaloud, 1972)

(a) ***Pure shear stage***

When the applied shear 'τ' is less than the critical shear stress 'τ_{cr}', the web remains in pure shear, Figure 2.3(a).

(b) ***Post-buckling or tension field action stage***

When the applied shear 'τ' exceeds the critical shear stress 'τ_{cr}', the web buckles and carries the additional shear 'τ-τ_{cr}' by a truss action and imposes the lateral and axial loadings on the flanges and stiffeners, Figure 2.3(b).

(c) ***Failure stage***

The web yields throughout the diagonal strip, Figure 2.3(c), together with the development of tension field action and the formation of plastic hinges in the flanges. The angle 'θ_d' of the tension field developed in the web was taken to be equal to the inclination of the geometrical diagonal of the web panel. The plastic hinges were assumed to occur in the flanges at the boundaries of the diagonal tension field. The position of the plastic hinges varied with the flexural strength of the flanges; for very thick flanges the plastic hinges occurred at mid span. If the diagonal tension was insufficient to develop plastic hinges in the flanges, then after the web has yielded any additional load is carried by the frame action acting as a Vierendeel girder.

Rockey et al (1978) suggested Equation 2.2 to determine the ultimate load, V_S, for the plate-girder predominantly loaded to shear.

$$V_s = V_{yw}\left[\frac{\tau_{cr}}{\tau_{yw}} + \sqrt{3}\mathrm{Sin}^2\theta\left(\mathrm{Cot}\theta - \frac{a}{d_w}\right)\frac{\sigma_t^y}{\sigma_{yw}} + 4\sqrt{3}\,\mathrm{Sin}\theta\left\{\sqrt{\frac{\sigma_t^y M_p^*}{\sigma_{yw}}}\right\}\right] \quad \text{Equation 2.2}$$

$$\text{Where, } \sigma_t^y = \sigma_{yw}\left[\frac{\sqrt{3}}{2}\frac{\tau_{cr}}{\tau_{yw}}\mathrm{Sin}2\theta + \sqrt{1 + \left(\frac{\tau_{cr}}{\tau_{yw}}\right)^2\left(\frac{3}{4}\mathrm{Sin}^2\theta - 1\right)}\right] \quad \text{Equation 2.3}$$

σ^y_t = tension field web membrane stress

θ = inclination of tension field to flange = $2\theta_d/3$

θ_d = inclination of web panel diagonal

a = length of web between the stiffeners

M_{pf} = plastic moment of the flange

M_p^* = $M_{pf}/d_w^2\, t_w\, \sigma_{yw}$

V_{yw} =ultimate plastic load of the web in shear = $\tau_{yw}\, d_w\, t_w$

2.4.3 Hoglund theory

Hoglund (1973) carried out a detailed study of the behaviour of steel plate-girders and developed a theory known as the 'Rotated stress field method'. The rotated stress field method was originally developed for plate-girders with web stiffeners at supports only, a structure for which the other tension field methods, for example Basler's and Rockey's, were very conservative (Hoglund, 1997). Later, the method with some modifications was found to give very good agreement with the test results of 273 steel and 93 aluminium plate-girders and was applicable to un-stiffened, transversely and longitudinally stiffened and trapezoidal corrugated webs. According to this theory, the inclination 'θ' of the principal tensile stresses decreases when the ratio of the ultimate to critical shear stress, τ_u/τ_{cr}, increases, this is why it is known as the 'rotated stress field method'.

This theory is the basis of the design rules in Eurocode 3, EC3 (ENV 1993-1-5, 2006) for the determination of the ultimate load of the plate-girders. Equation 2.4 was proposed to determine the shear strength/ ultimate load, V_{ult}, of the plate-girders (Hoglund, 1973).

$$V_{ult} = V_w + V_f \qquad \text{Equation 2.4}$$

Where 'V_w' and 'V_f' are the ultimate load contributions of the web and flanges respectively.

In determining 'V_w', the web panels were represented in the post-buckling stage with a system of perpendicular bars in compression and tension, Figure 2.4(a). When the load increases, the stress 'σ_c' in the compression bars remains constant and equal to the elastic shear buckling stress 'τ_{cr}' while the stress 'σ_t' in the tension bars increases as its inclination with the flange 'θ' decreases. This behaviour produces a net axial membrane tension in the web and a tension stress field 'EHGK' as shown in Figure 2.4(b) is developed in the web. This tension stress field differs from the tension field described by Rockey and Skaloud (1968) in which it is assumed to be developed between the flanges only. The tensile stresses in the tension stress field produce a stiffening effect on the web (this effect is favourable to the load-carrying capacity) at the same time as the bending stresses increase in the web (this effect is mostly unfavourable). In order to develop simple design rules, it is assumed that the favourable and unfavourable effects neutralize each other and the ultimate load/ shear resistance of the web 'V_w' is not changed by the tension field.

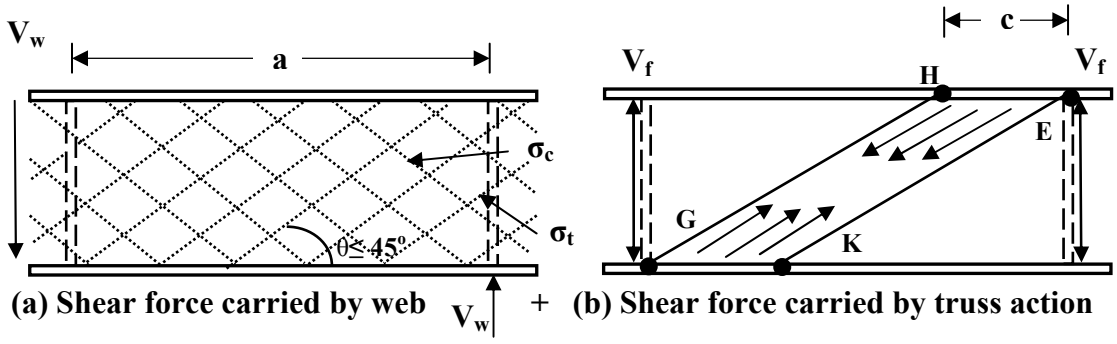

Figure 2.4 Behaviour of steel plate-girder in post-buckling range (Hoglund, 1973)

At failure, four hinges shown as E, H, G and K in Figure 2.4(b) form in the top and bottom flanges. The moment in each hinge is assumed to be equal to the plastic moment capacity '$Z_f.\sigma_{yf}$' of the flanges. For the rectangular section of the flanges, the plastic moment of resistance 'Z_f' is given by '$b_f t_f^2/4$' and 'σ_{yf}' is the lower yield strength of the flange material. The shear force in the hinges 'H' and 'K' is assumed to be zero. The

shear force 'V_f' which is transmitted by the tension stress field is obtained from the equilibrium of flange portion 'c' and is given by Equation 2.5.

$$V_f = {}^{b_f t_f^2 \sigma_{yf}}/_{c} \qquad \text{Equation 2.5}$$

If the applied moment 'M' is less than the moment capacity 'M_f' of the flanges and an axial force is present in the flanges, the ultimate contribution of the flanges 'V_f' is reduced by a factor of '$[1-(M/M_f)^2]$'.

2.4.4 Eurocode 3

The Eurocode 3, EC3, (ENV 1993-1-5, 2006) provides design guidance for stiffened and un-stiffened plates which are subject to in-plane forces. For an un-stiffened or stiffened web, the design shear resistance/ ultimate load, $V_{b,Rd}$, of the web panel of a steel plate-girder is given by Equation 2.6.

$$V_{b,Rd} = V_{bw,Rd} + V_{bf,Rd} \leq \frac{\eta d_w t_w \sigma_{yw}}{\sqrt{3}\gamma_{M1}} \qquad \text{Equation 2.6}$$

Where,

$$V_{bw,Rd} = \frac{\chi_w d_w t_w \sigma_{yw}}{\sqrt{3}\gamma_{M1}} \qquad \text{Equation 2.7}$$

$$V_{bf,Rd} = \frac{b_f t_f^2 \sigma_{yf}}{c\gamma_{M0}}\left[1 - \left\{\frac{M_{Ed}}{M_{f,Rd}}\right\}^2\right] \qquad \text{Equation 2.8}$$

$$\lambda_w = 0.76\sqrt{\frac{\sigma_{yw}}{\tau_{cr}}} \qquad \text{Equation 2.9}$$

$$\tau_{cr} = \frac{\pi^2 KE}{12(1-\vartheta^2)}\frac{t_w^2}{d_w^2} \qquad \text{Equation 2.10}$$

$$\chi_w = \frac{0.83}{\lambda_w} \text{ for non} - \text{rigid end post} \qquad \text{Equation 2.11}$$

$$c = a\left[0.25 + \frac{1.6 b_f t_f^2 \sigma_{yf}}{d_w 2 t_w \sigma_{yw}}\right] \qquad \text{Equation 2.12}$$

Also, $V_{bf,Rd}$ = Shear strength/ ultimate load contribution of flanges

$V_{bw,Rd}$ = Shear strength/ ultimate load contribution of web

η = co-efficient that includes the increase of shear resistance at smaller web slendernesses (1.2 for S235 to S460 grades of steel)

γ_{M0}, γ_{M1} = partial safety factors for the resistance to instability

χ_w = reduction factor for the ultimate load of web depending on λ_w

λ_w = web slenderness of shear panel

A_{f1}, A_{f2} = areas of cross-section of top and bottom flanges respectively

b_f, t_f = width and thickness of flange

K = shear buckling co-efficient of the web panel

The Eurocode also provides various types of transverse stiffeners which can be used at the end supports of stiffened and un-stiffened plate girders and are generally known as end posts, Figure 2.5.

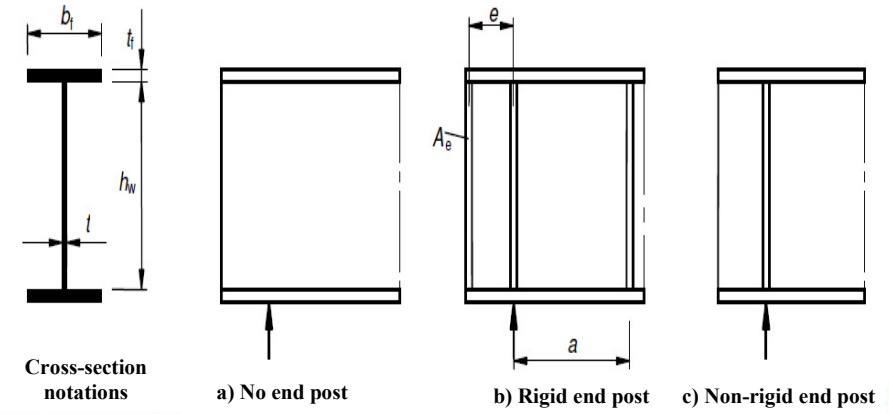

Figure 2.5 Types of end posts/ external stiffeners of plate-girders (ENV 1993-1-5, 2006)

2.4.5 Real et al thoery

Real et al (2007) studied the plastic behaviour of stainless steel plate-girders predominantly subjected to shear loading with the help of experimental, analytical and numerical investigations. The objective of the study was to understand the behaviour of the stainless steel-plate girders and to develop a design method. Nine stainless steel plate-girders with different slenderness ratios for the web and the different aspect ratios of the web panels were tested and analysed. Each plate-girder had two web panels and a central applied load and was simply supported at the ends. The FE analyses were carried out using shell elements and the ABAQUS FE program. Both geometric and material nonlinearities were modelled. The first buckling mode of the plate-girder obtained from by eigenvalue analysis was used to account for the initial imperfections in the web.

The ultimate loads of the test specimens were determined using three methods of the Eurocode and were compared with the test and FEA results. The three methods included the simple post-critical (ENV 1993-1-4, 1996), the stainless steel tension field (ENV

1993-1-1, 1993) and the stainless steel rotated stress field (ENV 1993-1-5, 2006). The post-critical method ignores the contribution of the flanges in resisting the shear, so gives conservative results for the ultimate load of a plate-girder. The tension field and rotated stress field methods are described earlier in the Sections 2.4.2 and 2.4.3. The test and FEA results for the ultimate loads of the plate-girders were in good agreement. The ultimate loads given by the tension field and rotated stress field methods were in reasonable agreement with those of the tests and the FE analyses. The post-critical method, as expected, underestimated the ultimate loads of the plate-girders.

It was concluded that the behaviour of stainless steel plate-girders was similar to the carbon steel plate-girders. In stainless steel plate-girders, a tension band is developed after reaching the shear buckling load, but their behaviour is influenced by the material nonlinearity. In the most slender plate-girders, shear buckling of the web, geometric nonlinearity, occurred before material nonlinearity, yielding, appeared. In girders of intermediate slenderness, the effect of the material nonlinearity appeared before geometric nonlinearity. In stocky girders, yielding of the web occurred before its shear buckling and were therefore subjected to a pure shear state throughout the test.

2.4.6 Lee and Yoo theory

Lee and Yoo carried out the nonlinear FE analyses (Lee & Yoo, 1998) and tests (Lee & Yoo, 1999) of ten steel plate-girders and developed a failure model. The plate-girders mainly differed in the aspect ratios of the web in web panels and the thicknesses and widths of the flanges. It was concluded that Basler and Rockey models could predict the ultimate loads of the plate-girders adequately. However, the failure mechanisms assumed by these models might not correctly represent actual behaviours of the web panels due to the following observations.

1. The boundary condition at the flange-web juncture of web in a plate-girder in practical designs is much closer to fixity. Therefore the assumption that the web is simply supported at the juncture sometimes leads to considerable underestimation of the ultimate shear strength because of the underestimation of the elastic shear buckling strength.

2. The flange rigidity affected the elastic buckling strength of the web due to the degree of restraint at the flange-web juncture provided and had a little effect on the post-buckling strength.

3. In all existing assumed failure mechanisms, the thorough-thickness bending stress effects of the web on the ultimate load are neglected. It has been found that at failure, very high bending stresses develop in the web. Tension field action neglecting the out-of-plane bending stresses effects of the web could give satisfactory results for the ultimate load of the girders with an aspect ratio of the web up to 1.50.

4. An anchoring system for the web, such as flanges, is not required for the development of the post-buckling strength of the web. A simply supported plate without any anchors like flanges can develop the same post-buckling strength as the web plate with heavy flanges.

Equation 2.13 was proposed to determine the ultimate load/ shear strength 'V_u' of the plate-girders.

$$V_u = R_d V_p (0.6C + 0.4) \qquad \text{Equation 2.13}$$

Where, V_p = ultimate plastic load = $A_w.\sigma_{yw}/\sqrt{3}$

The above equation was developed based on the results of FE analyses of plate girders by including the effects of initial lateral out-of-plane imperfections in the web (Lee & Yoo, 1998) and was later validated using the test results of the girders (Lee & Yoo, 1999). According to the Bridge Welding Code (AASHTO/AWS D1.5, 1996), allowable initial imperfections in the web vary from 'a/80' to 'a/130' depending upon the panel dimensions and stiffeners configuration. The FE analyses were however carried out using the initial lateral imperfections in the web between an upper-bound value of 'D/120' and a very small value of 'D/120,000'. The FEA results showed that due to the larger initial imperfections, the reduction in the ultimate load of the plate-girders was less than 2% for higher web slendernesses, $d_w/t_w \geq 180$, and was approximately 20% for lower web slendernesses, $d_w/t_w \leq 120$. A strength reduction factor, R_d, depending on the web slenderness was included in the equation to account for the larger initial imperfections in the web and has to be determined as follows.

$$R_d = 1.0 \quad \text{for } \frac{d_w}{t_w} > \frac{12000\sqrt{K}}{\sqrt{\sigma_{yw}}}$$

$$R_d = 0.8 + 0.2\left[\frac{\left\{\frac{d_w}{t_w}\frac{\sqrt{\sigma_{yw}}}{\sqrt{K}} - 6000\right\}}{6000}\right] \quad \text{for } \frac{6000\sqrt{K}}{\sqrt{\sigma_{yw}}} \leq \frac{d_w}{t_w} \leq \frac{12000\sqrt{K}}{\sqrt{\sigma_{yw}}}$$

$$R_d = 0.8 \quad \text{for } \frac{d_w}{t_w} < \frac{6000\sqrt{K}}{\sqrt{\sigma_{yw}}}$$

$$C = 1.0 \quad \text{for } \frac{d_w}{t_w} < \frac{6000\sqrt{K}}{\sqrt{\sigma_{yw}}}$$

$$C = \frac{6000\sqrt{K/\sigma_{yw}}}{d_w/t_w} \quad \text{for } 6000\sqrt{K/\sigma_{yw}} \leq \frac{d_w}{t_w} \leq 7500\sqrt{K/\sigma_{yw}}$$

$$C = 4.5 \times 10^7 \frac{6000\,K/\sigma_{yw}}{\left(d_w/t_w\right)^2} \quad \text{for } \frac{d_w}{t_w} > 7500\sqrt{K/\sigma_{yw}}$$

2.4.7 Alinia et al theory

Alinia and Dastfan (2006) investigated, using FE analyses, the effects of the relative stiffness of surrounding members, i.e. beams and columns, on the overall behaviour of thin steel plate shear walls. The FE analyses were carried out using shell element and the ANSYS FE program. The surrounding members were connected to each other by hinges, so no frame action was developed. The shear walls, columns and beams were similar to the webs in panels, flanges and transverse stiffeners, respectively, of plate-girders. The structural system, however, did not fully represent the behaviour of the plate-girder because the bending effect of the frame was negligible and the shear deformation was dominant. In linear elastic buckling analyses, eight shear walls with different dimensions and aspect ratios were analysed, while five shear walls were analysed in nonlinear post-buckling analyses. Each model was analysed with a variety of stiffnesses of the supporting members.

It was concluded that the thin steel plate shear walls should not be considered as simply supported along the edges. The torsional stiffness of the supporting members, i.e. the beams and columns, is highly effective in increasing the elastic critical load; it however does not affect the post-buckling strength. The flexural rigidity of the supporting members neither influences the elastic critical load nor the post-buckling strength.

Later, Alinia et al (2009) carried out nonlinear FE analyses of steel plate-girder models to study the failure mechanism and to understand the formation of plastic hinges. Eighteen models, comprising 2, 4 and 6 square web panels and subjected three-point loading, were analysed. Different thicknesses of the web, flange and stiffeners and three types of end posts shown in Figure 2.5 were used. The FE analyses were carried out using shell element and the ABAQUS FE program. For validation of the analyses, the steel plate-girder tested by Real et al (2007) were modelled, analysed and the results validated. The following conclusions were made.

1. The failure mode of a steel plate-girder is dependent of the ratio of thicknesses of the flange to web 't_f/t_w'. If $t_f/t_w \geq 3$, the failure mode is always shear. If $t_f/t_w \leq 2$, the failure mode is always flexure. In the $2 < t_f/t_w < 3$, the failure depends on the web slenderness ratio. Thicker webs, $d_w/t_w<200$, fail in flexure, while more slender webs have a shear failure mode.
2. In the shear failure mode, plastic hinges are formed in the flanges of end web panels after diagonal yielding of the web. The plastic hinges are formed due to the differential shear deformation of the end panels and not due to the stresses imposed by the inclined tension field because the shear stress distributions in the web panels of 4 and 6-panel plate-girders were almost similar. The plastic hinges did not occur in the middle panels of 4 and 6-panel plate-girders although the bending moments in the middle panels are higher than the end ones.
3. The end posts or end stiffeners provide more fixity to the flange plates and increase the ultimate load of plate-girders. The end-posts have no effect on the initial stiffness of plate-girders and only become effective after the web yields in shear.

2.4.8 Comparison of design theories

1. Basler (1961) assumed that a uniform tension stress field develops through the web and ignored the flexural strength of the flanges upon the ultimate load/ shear strength of steel plate-girders. Rockey and Skaloud (1972) showed that the stress distribution and inclination of the tension stress field in the buckled web varies significantly with the flexural strength of the flanges and by simply increasing the flexural strength of the flanges, the ultimate load of plate-girders could be increased up to approximately 60%. Basler's assumption of the uniform stress field would therefore lead to an overestimation of the ultimate contribution of the thin webs in which buckling occurs before the yielding.

2. Lee and Yoo (1999) contradicted the well-known hypothesis that a web panel must be provided with sufficient rigid anchors, such as heavy flanges, to resist diagonal tension and to develop the complete post-buckling strength. They found in FE analyses that longitudinal stresses in the flanges were much lower than the yield stresses at the ultimate strength point.

3. Alinia et al (2011) compared the results of elastic critical loads and ultimate loads of the steel plate-girders predicted by their FE analyses with those of various design theories. It has been found that all the available theories, assuming the webs to be simply supported along the edges, are conservative in predicting the elastic critical loads of the webs. However, except Eurocode 3 (ENV 1993-1-5, 2006), all the other design theories overestimate the ultimate load of the plate-girders.

All the design theories discussed above assume that the end posts or end stiffeners of plate-girders are strong enough to deform plastically at failure. The behaviour of plate-girders has to be investigated if the end stiffeners, not being strong enough, cannot resist the formation of plastic hinges.

2.5 Design of transverse stiffeners of steel plate-girders

Most of the design theories for steel plate-girders with the un-stiffened or transversely stiffened web panels and predominantly loaded in shear assume that the web remains in pure shear until elastic critical shear buckling occurs; subsequently bands of tension form to carry further increases in shear. What is not agreed upon at present is the role of intermediate transverse stiffeners when the tension field develops and in particular, what are the forces they attract (Hendy et al, 2011). A brief review of some important methods for the design of intermediate stiffeners for steel plate-girders is given below.

2.5.1 Rockey's method

Transverse stiffeners in steel plate-girders have the following three functions to fulfil (Rockey et al, 1981).

1. To increase the buckling resistance of the web plate.
2. To remain effective when the web plates buckles and develops a tension field.
3. To restrict the tendency of the flanges to approach each other.

Rockey et al (1981) presented a detailed approach to the design of intermediate transverse stiffeners for steel plate-girders with slender webs at the ultimate state based on the tests of eleven plate-girders. The plate-girders were identical except for the dimensions of the stiffeners. It was shown that intermediate stiffeners behaved as eccentrically loaded columns subjected to axial loading due to the tension field action and bending due to a disturbing action from the buckled web plate. It was concluded that the evaluation of the load carrying capacity of an intermediate stiffener was complicated. A simple approach was developed which proposed that the force, P_N, the stiffener should be designed be taken as the difference between the ultimate and elastic critical loads, V_{ult} and V_{cr}, of the web plate. To resist the disturbing action of the web, the stiffener should also have a minimum second moment of area, $I_{s\,min}$, given by.

$$I_{s\,min} = \frac{4}{\pi^2} \frac{t_w d_w^4}{a} \frac{\tau_{cr}}{E} \qquad \text{Equation 2.14}$$

2.5.2 Hoglund's method

According to Hoglund (1973), transverse stiffeners of steel plate-girders between supports should satisfy the following conditions.

1. They should have the following minimum second moment of area, $I_{s\,min}$, in order to prevent the web from deflecting along the web-stiffener juncture.

$$I_{s\,min} = \left[\frac{d_w}{50}\right]^4 \qquad \text{Equation 2.15}$$

2. They should have the following minimum area of the cross-section, $A_{s\,min}$, in order to become capable to act as compression struts when truss action has developed.

$$A_{s\,min} = \frac{b_s t_s^2}{a} \frac{\sigma_{yf}}{\sigma_{ys}} . D \qquad \text{Equation 2.16}$$

Where D = 1.0 for flat plate stiffeners on both sides of the web

D = 1.8 for L-shaped stiffener on one side of the web

D = 2.4 for flat plate stiffener on one side of the web

3. In order to avoid the stiffener buckling, the width-to-thickness ratio, b_s/t_s, of the stiffeners(s) should be less than '$0.55 \sqrt{(E/\sigma_{ys})}$'.

2.5.3 Eurocode 3 method

Eurocode 3 (ENV 1993-1-5, 2006) lists the following criteria to be satisfied for the intermediate stiffeners.

1. Intermediate transverse stiffeners should act as rigid supports to the interior panels of the web and be designed for 'strength and stiffness'.

2. The effective section of intermediate stiffeners should have a minimum second moment of area, $I_{s\,min}$, given by.

$$I_{s\,min} > \frac{1.5\, d_w^3\, t_w^3}{a^2} \quad \text{if } \frac{a}{d_w} < \sqrt{2} \qquad \text{Equation 2.17}$$

$$I_{s\,min} > 0.75 d_w t_w^3 \quad \text{if } \frac{a}{d_w} \geq \sqrt{2} \qquad \text{Equation 2.18}$$

3. When checking the buckling resistance, the effective section of stiffeners should be taken as the gross area comprising the stiffener plus a width of the web plate equal to '15εt' but not more than the actual dimension available on each side of the stiffener avoiding any overlap of contributing parts of the adjacent stiffeners, Figure 2.6, where ε = √(235/ σ_{yw} in MPa).

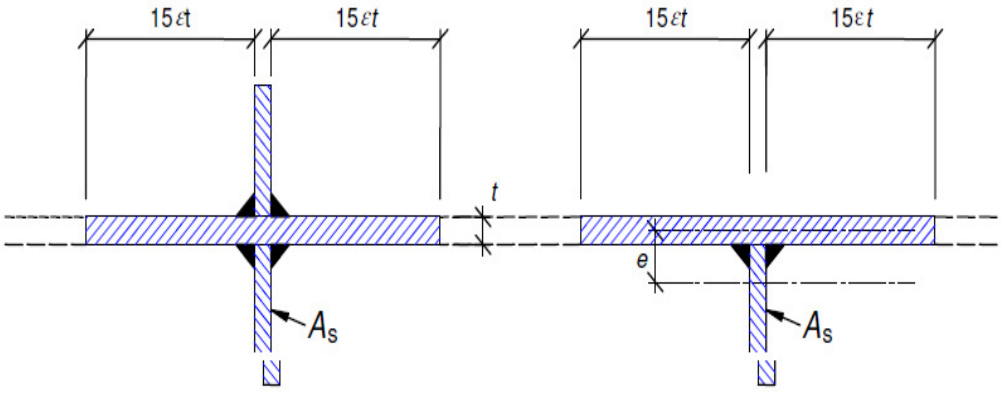

Figure 2.6 Effective cross-section of stiffener (ENV 1993-1-5, 2006)

4. Intermediate steel stiffener may be designed for an axial force, N_{Ed}, equal to $\left[V_{Ed} - \frac{1}{\lambda_w^2} \frac{\sigma_{yw} d_w t_w}{\sqrt{3}\,\gamma_{M1}}\right]$.

2.5.4 Hendy et al method

Hendy et al (2011) studied the behaviour of transversely stiffened plate-girders in bending and shear using nonlinear finite element, FE, analyses. In some of the analyses, the axial forces were applied to the intermediate stiffeners to examine their effect. It was observed that the axial forces in the stiffeners had an influence on the ultimate load of the plate-girder, but had a limited effect on the stiffener forces. It was concluded that the intermediate transverse stiffener could be designed safely on the basis of a 'stiffness only approach' as contained in Eurocode 3 (ENV 1993-1-5, 2006). However, in order to include the effect of the tensile filed passing through the intermediate stiffeners, the stiffener design force, N_{Ed}, could be taken as the difference between the ultimate loads of the web panel and the web only '$V_{Ult} - V_{bw,Rd}$'.

2.5.5 Comparison of design methods

1. The main difference between Rockey's and Hoglund's methods is the load which the stiffeners are required to carry. Rockey's method requires the stiffeners to act as compression members in the truss with the web plate acting as the tension diagonals. Hoglund's method requires the stiffeners to carry only a small part of the load due to the tension field anchored by the flanges at the collapse as no force is induced in the stiffener in mobilizing post-buckling resistance of the web.

2. Eurocode 3 was developed on the basis of Hoglund's theory which gives the 'a stiffness only approach' for the design of the intermediate transverse stiffeners. The method, however, was modified and the stiffener design based on 'a combined stiffness and strength approach' was included in the Eurocode.

3. The method of Hendy et al requires that the intermediate stiffener can be designed safely on the basis of 'a stiffness only approach' instead of 'a combined stiffness and strength approach' as required by Eurocode 3.

It has been observed by the author that all methods have discussed the design and load carried by the web stiffeners in a vertical orientation. An investigation into the design and behaviour of the stiffeners is required if the stiffeners are to be used in a diagonal orientation.

2.6 Fibre-reinforced polymers

Fibre-reinforced polymers, FRPs, are composite materials commonly formed by mixing of two major components, a fibrous reinforcement and a continuous medium (resin) to form a matrix, which encapsulates the reinforcement. The fibre reinforcement generally has high strength and stiffness at relatively low mass density. The matrix in comparison has lower strength and stiffness. Under stress, the fibres utilize the plastic flow of the matrix to transfer the load to each other; this results in a composite of suitable strength and stiffness. Depending on the type of fibre used in the manufacture, FRP composites are classified as carbon, aramid and glass FRP composites and are abbreviated as CFRP, AFRP and GFRP respectively (Cadei et al, 2004).

2.6.1 Properties of FRP composites

Table 2.1 gives the properties of carbon, aramid and glass FRP composites manufactured by the pultrusion technique using epoxy resin and long directionally aligned fibre reinforcements with a fibre-matrix ratio of 60% (Hollaway & Teng, 2008).

Table 2.1 Properties of FRP composites (Hollaway & Teng, 2008)

Property	CFRP	AFRP	GFRP
Tensile modulus (GPa)	150-350	70-110	40-55
Tensile Strength (MPa)	1400-2670	1150-1400	750-1650
Density (Kg/m^3)	1600-1800	1450	1800-1900

The properties of the FRP composites largely depend upon the following factors.

1. Fibre volume fraction and arrangement
2. Orientation of fibres and the direction of loading
3. Method of manufacture
4. Type and properties of the composite fibre used
5. Type and properties of the composite matrix used

2.6.1.1 Fibre volume fraction

The strength of the final FRP composite depends upon the volume of the fibre contained in it; the greater the volume of the fibre, the stronger will be the composite and vice versa. For the rehabilitation of structural members, composites with a fibre-volume fraction of 55 to 60% are generally used (Hollaway & Teng, 2008).

2.6.1.2 Orientation of fibres

The direction or orientation of the fibres in FRP composites also determines the strength and stiffness of the composite. In flexural plate bonding solutions, the fibres are uni-directionally aligned along the longitudinal length of the member. In order to maintain the alignment, particularly during the manufacturing procedure, it may be necessary to add a small percentage of fibres in the transverse direction.

2.6.1.3 Methods of manufacture

Methods used for manufacturing FRP composites have an influence on the mechanical properties of the final component. The main reasons for this influence on the mechanical properties are due to the temperature used for curing the matrix resin and the degree of the compaction applied.

2.6.1.4 Composite fibres

Fibres are the load-carrying components of the FRP composites and generally consist of a number of long filaments. The fibre filaments are extremely fragile, but possess higher strength and stiffness than the matrix. Three types of fibres, carbon, aramid and glass, are generally used in FRP composites (Cadei et al, 2004). Table 2.2 gives the properties of the composite fibres.

Table 2.2 Properties of composite fibres (Cadei et al, 2004)

Property	**Carbon fibre**			**Aramid fibre**	**Glass fibre**
	High-strength (HS)	High-modulus (HM)	Ultra-high-modulus (UHM)		
Tensile modulus (GPa)	230-240	295-390	440-640	125-130	70-85
Tensile strength (MPa)	4300-4900	2740-5940	2600-4020	3200-3600	2460-2580
Density (Kg/m^3)	1800	1730-1810	1910-2120	1390-1470	2600
Coefficient of thermal expansion ($10^{-6}/^oC$)	-0.38	-0.83	-1.1	2.1	4.9

Carbon fibres have both high strength and high stiffness. They are light in weight and have a low coefficient of thermal expansion, but high electrical conductivity. They are available in variety of different grades according to the manufacturing processes and can be classified as high-strength, HS, high-modulus, HM, and ultra-high-modulus,

UHM. With carbon fibres, there is a play-off between tensile strength and modulus of elasticity; the higher the strength, the lower the modulus and vice versa.

Aramid fibres have high tensile strength, moderate stiffness and low density. They are resistant to fatigue and have low compressive and shear strengths. Unlike carbon fibres, they are electrically non-conductive.

Glass fibres are the least stiff and the least strong of all the three fibres, but are considerably cheaper than either carbon or aramid fibres.

2.6.1.5 Composite matrix (Resin)

The composite matrix or polymer is an organic material composed of molecules made from many repeats of the same simpler unit called the monomer. It binds and protects the fibres, transfers force into the fibres by interfacial shear and protects the delicate fibres against aggressive environments. The durability of a composite largely depends upon the matrix material, which determines the heat, fire and chemical resistance of the composite. The commonly used types of matrices are epoxy, polyester, phenolic and polyurethane (Cadei et al, 2004). Table 2.3 gives general properties of the matrix resins.

Table 2.3 Properties of matrix resins (Cadei et al, 2004)

Property	**Epoxy**	**Polyester**	**Phenolic**	**Polyurethane**
Tensile modulus (GPa)	2.6-3.8	3.1-4.6	3.0-4.0	0.5
Tensile strength (MPa)	60-85	50-75	60-80	15-25
Density (Kg/m^3)	1110-1200	1110-1250	1000-1250	1150-1200
Coefficient of thermal expansion ($10^{-6}/^oC$)	30-70	30-70	80	40

2.6.2 Deformation in FRP composites

There are two stages, I and II, of deformation within an FRP composite (Callister, 2000) which are described below and illustrated in Figure 2.7.

1. In the first stage I, both the fibre and the matrix deform elastically.

2. In the second stage II, the matrix yields and deforms plastically whilst the fibres continue to deform elastically. In this stage, the proportion of load carried by the fibres increases with the load. Eventually fibres start to fail and the load carried out by these is initially transferred to the surrounding fibres. Further load increases lead to successive fibre failure and eventual failure of the structure.

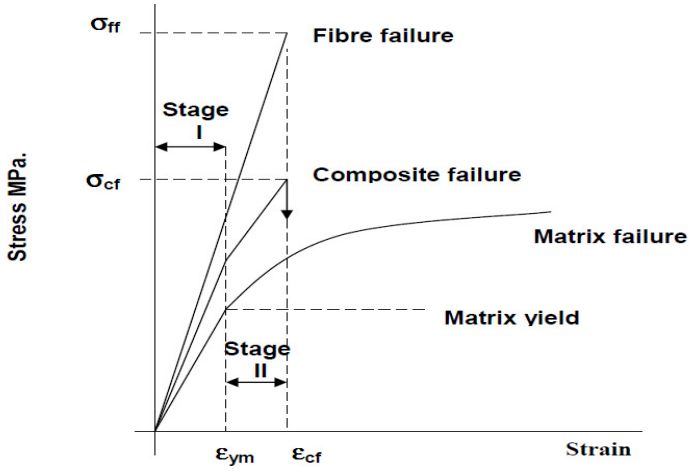

Figure 2.7 Stress-strain curve for fibre, matrix and composite (Callister, 2000)

2.7 FRP-strengthening of structures

There are several situations in which a structure could require strengthening, rehabilitation or repair. These could be due to lack of strength in flexure, shear, etc., lack of stiffness, lack of ductility or loss of durability (Cadei et al, 2004). Some of the more common situations where a structure needs strengthening during its life span are:

1. Upgraded loading requirements
2. Damage caused by accidents and environmental conditions
3. Initial design flaws
4. Change of use of the structure
5. Seismic retrofit to satisfy current code requirements

Because FRP composites are light-weight, have suitable strength and stiffness properties and are easy to install on site, they are considered to be the most favoured material in many strengthening applications. Externally-bonded FRP-strengthening is a powerful technique of extending the life of structures including those made of steel. The overall cost of the whole strengthening job using FRP materials can be as competitive as using conventional materials, in addition to being quick and easy to handle on site

with minimum interruption to the use of the facility. In some situations, FRP composites are the only plausible material that could be used for strengthening especially in the places where neither access of heavy machinery is possible nor closure of the facility is practical. The choice of strengthening material and method is dictated by the following considerations (Cadei et al, 2004).

1. Extent and type of strengthening required
2. Shape of the structural member to be strengthened
3. Regularity, in particular flatness of the substrate
4. Available surface area to which the reinforcement is required
5. Cross-sectional area of the FRP reinforcement required to be applied
6. Feasibility of the installation process and site conditions
7. Required appearance.

CFRP composites are the best suited for strengthening of the structures that are either weight sensitive or have high stiffness and strength requirements. Aramid FRPs are suitable for use in structures requiring high tensile strength and impact resistance. GFRPs are used for the structures that are not weight critical.

2.7.1 Advantages

FRP composite materials are widely used in the strengthening of structures in aerospace, automotive, marine, and construction industries. Generally, they are selected for various structural applications due to the following advantages (Hollaway, 2010).

1. They possess low density and good mechanical properties (e.g. high tensile strength, suitable stiffness, etc) giving low mass components.
2. They possess high environmental durability and are more chemically resistant than most of the metals.
3. They offer great ease in transportation, lifting and installation due to the low mass density.
4. There are several health and safety benefits with reduced lifting requirements of FRPs.
5. They can easily be jointed either to another FRP material or to any other material such as concrete, steel, etc using adhesive bonding techniques.

6. FRP-strengthening methods require either no or very little false-work and scaffoldings.
7. FRP-strengthening methods can be applied more rapidly compared to other strengthening options.

2.7.2 Limitations

The application of FRP-strengthening is still a relatively new technique, so there are practical limitations which should be taken care of before their use. Some of them are given below.

1. FRP composites are more expensive than conventional construction materials, such as steel.
2. They have less resistance to high and low temperatures and fire which can affect their strength and stiffness properties.
3. There is no accurate prediction for service life of FRPs.
4. FRP-strengthening critically relies on high quality adhesive joints, and thus requires the high quality workmanship and the correct environmental conditions during cure.

2.7.3 Early Use of FRP composites in structures

The building industry was an early user of FRP composites with its use in the construction of radomes during the Second World War (1939-1945). A radome, radar dome, is a weather-proof structural enclosure that protects a microwave or radar antenna. The material used was glass fibre-reinforced polymer, GFRP, as it minimally attenuates the radio waves passing through them. The use of FRP then spread slowly, initially with its use for marine craft, to the point where they are utilized in demanding areas such as pressure vessels, pipes and blast panels on offshore oil and gas platforms. Carbon fibre-reinforced polymers, CFRP, were developed by Royal Aircraft Establishment at the end of 1960s (Hollaway, 2010).

2.8 FRP-strengthening of concrete structures

In buildings, architectural appearance rather than structural performance and durability motivated the early applications of FRP composites. By the end of 1970s, semi-load bearing and infill GFRP panels were fabricated and used. The examples in the UK include classroom structures at Fulwood, Lancashire; the Mondial House, London; and

the Amex House, Brighton (Hollaway, 2010). During the period from 1980 to 1997, there were at least 32 documented new bridge construction projects, 20 with vehicular traffic, using concrete with FRP reinforcement. Of these, 6 were constructed in Europe, 7 in North America and 19 in Japan. In general CFRP was used for the reinforcement, although there were also GFRP and AFRP applications (Bakis et al, 2002).

In 1984, Urs Meier and his team at the Swiss Federal Laboratories for Material Testing and Research (EPMA) began research into the use of CFRP composites for the strengthening of structures (Motavalli & Czaderski, 2007). The work done at EPMA between 1984 and 1989 enabled a consequent wide spread use of CFRP external reinforcements to strengthen structures. Based upon these developments, one of the earliest applications of CFRP to strengthen a bridge took place in Lucerne, Switzerland in the early 1990s. Ibach Bridge was a multi-span continuous box bridge, which had one of its pre-stressed tendons damaged during drilling to install new traffic signals. Although the material cost of CFRP was several times more than that of steel plates, but the use of 6.2 Kg of CFRP composites instead of 175 Kg of steel and the completion of the entire work in two night-shifts from a mobile platform without any scaffolding was sufficient to justify the use of the CFRP over the steel plates (Meier et al, 1992).

Sometimes deficiencies in the initial design have required strengthening to be carried out during the service life of a bridge. After World War II, a number of pre-stressed concrete multi-span bridges were built in Germany. Later on, these bridges exhibited cracks at joints due to the development of excessive tensile stresses at the bottom due to the restraint of temperature movements which had not been taken into account at the initial design stage. The cracks were initially repaired by strengthening the joints with bonded steel plates. During 1986-87, ten joints of the Kattenbusch Bridge were strengthened by bonding GFRP plates to the joint using a technique developed by Professor F. S. Rostasy and his colleagues from Technische Universitat Braunschweig. With the help of loading tests, they observed a reduction of 50% in crack width and 36% decrease in the tensile stress amplitude, thus extending the fatigue life of the joint (Motavalli & Czaderski, 2007).

In the early 1990s, pre-stressed concreted beams were taken from an old deteriorated highway bridge in England for testing. CFRP plates of various lengths were bonded to

the bottom surface with Sikadur®-31 or Sikadur®-30 high strength adhesives and in some cases some pre-stressing steel wires were also removed. After load tests, it was observed that the CFRP plates provided significant improvement in crack control, increased beam stiffness in flexure and load carrying capacity without any anchorage failures. Similarly 400 mm deep reinforced concrete joists of the roof of Kings College Hospital in London were strengthened by adding pultruded CFRP strips to the bottom. The installation took place quickly and conveniently by using only 2 Kg of CFRP instead of 60 Kg of steel (Chakrabarti et al, 2011).

Czaderski and Motavalli (2004) investigated the suitability of pre-fabricated L-shaped CFRP plates for shear strengthening of the reinforced concrete T-beams, Figure 2.8(a). Test specimens comprised two control beams S1 and S2 and four CFRP-strengthened beams S3 to S6, details are given in Table 2.4. The four strengthened beams were bonded with the L-shaped CFRP plates, 1.4 mm thick and 40 mm wide, using Sikadur®-30 epoxy-adhesive. The CFRP plates in all beams were bonded to the sides of the web and passed through in holes drilled in the flange, Figure 2.8(a). All beams were tested to the failure under a four-point loading system, Figure 2.8(b). Further details of loading of the each beam are given in Table 2.4.

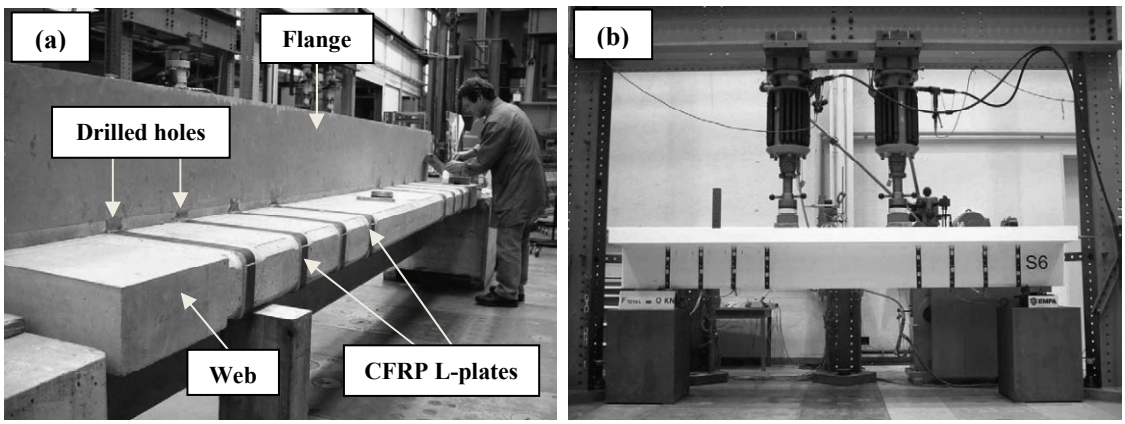

Figure 2.8 (a) Application of CFRP L-shaped plates to web of specimen beam S6 and (b) testing set-up (Czaderski & Motavalli, 2004)

The test results, Table 2.4, showed that there was a small improvement of 5% in the ultimate load of the beam S4 due to CFRP-strengthening, compared to that of the beam S1. However, the CFRP-strengthening increased the ultimate load of the beam S3 by approximately 100%, compared to that of the beam S2. The ultimate loads of the beams S4, S5 and S6 remained approximately the same. The CFRP L-shaped plates however

remained undamaged during the 5 million load cycles fatigue test showing their suitability to be used in the shear strengthening of RC T-beams for fatigue reasons (Czaderski, 2002).

Table 2.4 Details of reinforcement, loading and ultimate loads of beams S1 to S6 (Czaderski & Motavalli, 2004)

Beam No.	Reinforcement		Type of loading applied	Ultimate load (kN)	Ratio of ultimate loads
	Steel	CFRP			
S1	Provided	None	Static loading to failure	723	S1/S2= 2.22
S2	None	None	Static loading to failure	325	S2/S1= 0.45
S3	None	Provided	Static loading to failure	634	S3/S2=1.95
S4	Provided	Provided	Static loading to failure	757	S4/S1=1.05
S5	Provided	Provided	First pre-loading, then CFRP application and finally static loading to failure	761	S5/S4=1.005
S6	Provided	Provided	Fatigue test and then static loading to failure	765	S6/S4=1.01

GFRP has also been used for shear strengthening of reinforced concrete beams. Sundarrraja and Rajamohan (2009) investigated the effect of epoxy-bonded inclined GFRP fabric strips on the shear capacity of concrete beams with the help of an experimental program. A total of 13 beams were tested. Five beams, C1 to C5, were control specimens without any GFRP-strengthening. Among them, the beam C1 was fully-reinforced in shear, while the remaining four beams, C2 to C5, were made shear-deficient either by decreasing the longitudinal steel reinforcement or by increasing the spacing of the shear reinforcement. Four beams, RF2 to RF5, were strengthened with GFRP strips on both sides of the web, Figure 2.9(a), and the remaining four beams, RFU2 to RFU5, strengthened using GFRP U-wraps, Figure 2.9(b). The beams C2, RF2 and RFU2 had the same steel reinforcement which was also same in case of the beams C3 to 5, RF3 to 5 and RFU3 to 5 respectively. A four-point loading system as shown in Figure 2.10 was used. A comparison of the test ultimate loads is given in Table 2.5.

Figure 2.9 GFRP-strengthened beams using inclined (a) side strips and (b) U-strips (Sundarrraja & Rajamohan, 2009)

Figure 2.10 Testing set-up (Sundarrraja & Rajamohan, 2009)

Table 2.5 Comparison of ultimate loads of beams (Sundarrraja & Rajamohan, 2009)

Beam No.	**Ultimate load (kN)**	**Beam No.**	**Ultimate load (kN)**	**Beam No.**	**Ultimate load (kN)**	**Ratio of ultimate loads**	
						RF/C	RFU/C
C1	49	---	---	---	---		
C2	47	RF2	53	RFU2	55	1.13	1.13
C3	33	RF3	50	RFU3	52	1.56	1.62
C4	32	RF4	48	RFU4	55	1.50	1.72
C5	32	RF5	49	RFU5	50	1.53	1.56

The results showed that:

1. Due to a reduction in the steel shear reinforcement, the ultimate loads of control beams C3, C4 and C5 were 33% less that of the beam C1 and the ultimate load of beam C2 was 4% less than the beam C1.
2. The ultimate loads of the GFRP-strengthened beams, RF2 to RF5, using method 1 were increased by up to 56%, compared to those of the respective control beams, C2 to C5.

3. The ultimate loads of the GFRP-strengthened beams, RFU2 to RFU5, using method 2 were increased by up to 72%, compared to those of the respective control beams, C2 to C5.
4. In the all GFRP-strengthened beams, the ultimate load was either equal to or up to 10% more than that of the control beam C1 which had the full steel shear reinforcement.
5. Shear cracks formed in the GFRP-strengthened beams at 80% to 150% higher loads than the respective un-strengthened beams.
6. All the un-strengthened beams failed in shear, while flexural failure was more prominent in the GFRP-strengthened beams.

One of the significant causes of deterioration of steel-composite bridge structures is corrosion due to the extensive use of de-icing salts in winter. Sen et al (2001) investigated the feasibility of using CFRP strips to repair steel-concrete composite bridge members with the help of the tests and FE analyses. Six specimens were tested and have been named as S1 to S6; details are given in Table 2.6. The test specimens were obtained by cutting each of two steel-concrete composite bridge models into three parts, Figure 2.11(a). The resulting cross-section is shown in Figure 2.11(b). The normal weight concrete used had an average compressive strength of approximately 50 MPa.

Table 2.6 Details of beams with comparison of ultimate loads (Sen et al, 2001)

Beam No.	Yield strength of steel (MPa)	Thickness of CFRP plate applied (mm)	Bonding method	Ultimate load (kN)	Ult. load of strengthened to control
Control 1	310	---	---	196*	---
S1	310	5	Epoxy only	169***	0.86
S2	310	5	Epoxy & bolting	298**	1.52
S3	310	2	Epoxy & bolting	237**	1.21
Control 2	370	---	---	249*	---
S4	370	2	Epoxy only	271**	1.09
S5	370	2	Epoxy only	272**	1.09
S6	370	5	Epoxy & bolting	329**	1.32

* Values predicted by FE analyses
** Values obtained in tests
*** Maximum load in the test which was not continued after a premature bond failure

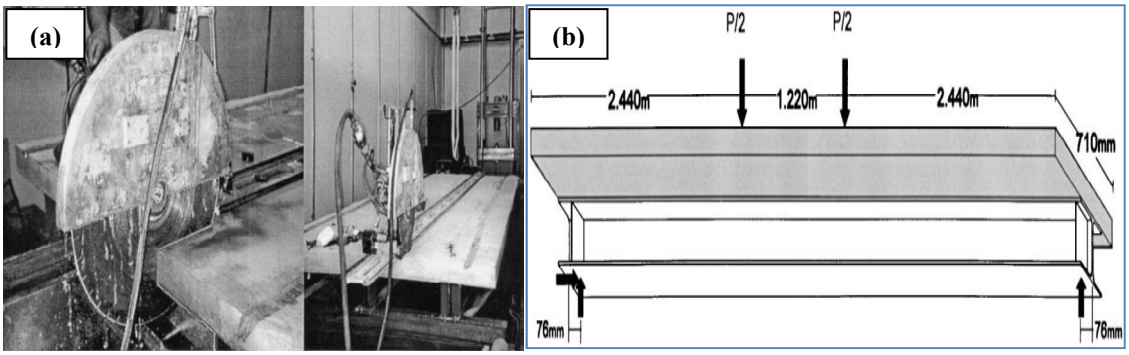

Figure 2.11 (a) Cutting of bridge into three beam sections and (b) simply supported composite bridge section (Sen et al, 2001)

In order to simulate the severe service distress, all the specimens were pre-loaded to give permanent deformations in each member before CFRP-repairing. The average loads applied for the pre-loading were 142 and 187 kN for the specimens with the steel yield strengths of 310 and 370 MPa respectively. Three specimens S1, S2 and S6 were repaired by applying 5 mm thick CFRP strips and the remaining three S3, S4 and S5 with 2 mm thick strips. The width of the CFRP strips was 165 mm, to match the flange-width of the steel beam, and the length was 3.65 m. In three of the six specimens, S2, S3 and S6, the CFRP strips were provided with steel clamps, secured with bolts, at the ends to resist the peeling stresses. No un-strengthened control beam was tested and the ultimate loads of the control beams predicted by finite element, FE, analyses were used for comparisons with CFRP-repaired beams.

The beam S1 was not tested up to it ultimate load because of a premature breakdown of the steel-CFRP bond at a load of 169 kN. Except for the beam S1, the test results indicated significant gains, 9% to 52%, in the ultimate load of the CFRP-repaired beams, compared to that of the un-repaired beams; details are given in Table 2.6. Non-linear FE analyses for the repaired beams were carried out using the PCFRAME program. The FEA results were in good agreement with the test results.

With the help of testing and analytical modelling, Al-Saidy et al (2004) studied behaviour in steel–concrete composite girder beams first by damaging, intentionally, the tension flange of the beam to simulate the field corrosion and then by repairing the beam with bonded CFRP strips applied to the tension side. The main focus of the study was to investigate the effect of the CFRP-repairing on the flexural capacity of the beams.

A total of six steel-concrete composite specimens, two undamaged control beams, one un-repaired damaged beam and three CFRP-repaired damaged beams, were tested. The control beam consisted of a concrete slab 76 mm thick by 812 mm wide attached at mid-span to a 3.4 m long W8x15 grade A572 structural steel section by stud-type shear connectors, Figure 2.12. The normal weight concrete used had an average compressive strength of approximately 33 MPa, the A572 steel had a yield strength of 364 MPa and the pultruded CFRP strips had a modulus of elasticity of 200 GPa. To simulate the field corrosion, damage to three of the four damaged beams was induced by removing 50% area of cross-section of the bottom flange and to the remaining one by removing 75% area of cross-section.

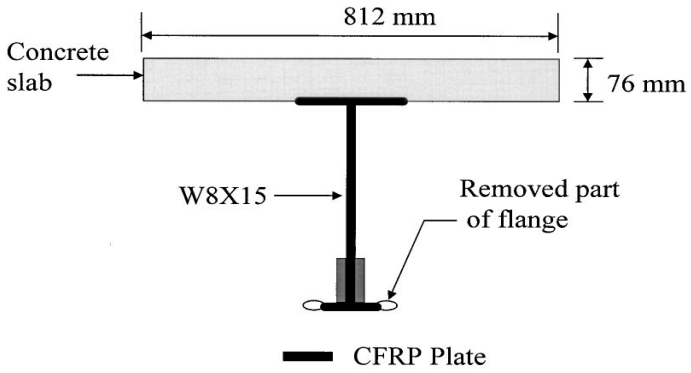

Figure 2.12 Repair scheme 1: CFRP strip bonded to tension flange (Al-Saidy et al, 2004)

The repairing of the three damaged beams was achieved by attaching 1.4 mm thick CFRP strips to the tension side of the steel sections. In two of the three repaired beams with the 50% and 75% bottom flange area removed respectively, 102 mm wide CFRP strips were applied on both sides of the web at lower ends. In the remaining repaired beam with the 50% bottom flange area removed, 51 mm wide strips were applied on both sides of the web at lower ends as well as to the bottom flange. All the six beams were tested in a four-point static loading system. The test results showed that:

1. The ultimate flexural strength of the damaged beams was reduced by approximately 20% compared to the control beams due to removing 50% of the area of cross-section of the bottom flange.
2. Following the CFRP-repair using the strips, the ultimate strength of the damaged beams was not only fully restored to that of original undamaged beams, but it was also further increased by 4 to 20%.

3. The undamaged and damaged beams failed due to yielding of the steel beam followed by crushing of the concrete slab, while the CFRP-repaired beams failed due to slip at the steel-concrete surface followed by the crushing of the concrete slab. No de-bonding of the CFRP strips was observed at failure of the repaired beams.

Before testing, the ultimate loads of the un-damaged, the damaged and the repaired beams were predicted numerically using the measured stress-strain relationships of the materials. The numerical predictions were in good agreement with the test results.

Attari et al (2012) investigated the use of CFRP, GFRP and hybrid FRP fabric sheets to strengthen simply supported concrete beams. Seven test specimens comprising an un-strengthened control beam and six FRP fabric-strengthened beams were tested in a four-point loading system. The control beam, PC, was a 1500 mm long concrete beam; 160 mm deep and 100 mm wide. The FRP fabric-strengthened beams were divided into two series 'A' and 'B'. In series 'A', two beams PA1 and PA2 were strengthened using two and three layers of unidirectional carbon and glass fabric sheets respectively. The third beam PA3 was strengthened by bonding one layer each of the unidirectional glass and carbon fabrics. In series 'B', three beams PB4, PB5 and PB6 were bonded with three, two and three layers of bidirectional carbon-glass hybrid sheets respectively. In five of the six strengthened beams, PA1 to PB5, the fabric sheets were bonded to the bottom and both sides of the beam in U-wraps and to the bottom only in the sixth beam PB6. The test results showed that:

1. Compared to the control beam, increases in the ultimate loads of the series 'A' strengthened beams, PA1, PA2 and PA3, using unidirectional carbon and glass fabrics were 114%, 118% and 138% and those of the series 'B' beams, PB4, PB5 and PB6, using bidirectional hybrid fabrics were 114%, 88% and 52%, respectively. The fabric-strengthening also improved the stiffness and reduced mid-span deflections of the beams.
2. The load-deflection responses of all strengthened beams PA1, PA2 and PA3 in series 'A' were almost similar. Likewise, the responses of two of the three beams, PB4 and PB5, in series 'B' were similar, Figure 2.13.

3. In series 'B' beams, a small difference, 14%, in the ultimate loads of beams PB4 and PB5 using two and three layers of hybrid fabric showed that there was a threshold beyond which the addition of strengthening material did not contribute much to increase the strength of the beam.
4. A comparison of the test results of beams PB4 and PB6 using the same, three, number of layers showed that due to U-anchorage clamping of the fabric sheets, not only the ultimate load of PB4 was increased by 40% compared to that of PB6; but PB4 also showed more ductility than PB6, Figure 2.13.

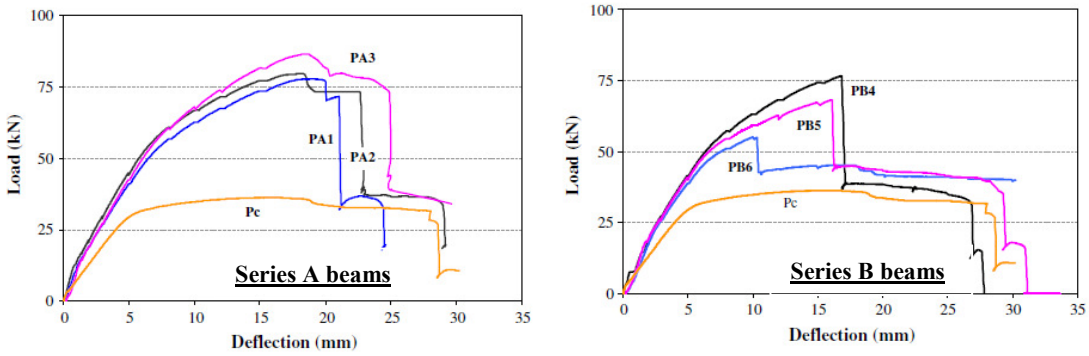

Figure 2.13 Load vs. mid-span deflections of series A and B beams (Attari et al, 2012)

Mostofinejad and Kashani (2013) carried out tests of 32 concrete beams subjected to a four-point loading system. Each beam was 560 mm long, 85 mm deep and 70 mm wide. Eight beams were un-strengthened control beams, while the remaining twenty-four beams were strengthened using 85 mm long and 40 mm wide CFRP strips. In the 6 strengthened beams, the surface of the concrete was not prepared before bonding CFRP strips, while in the other 8 strengthened beams the concrete surface was prepared with grinding followed by air pressure cleaning. In the remaining 10 strengthened beams, 10 mm deep and 5 mm wide grooves were made in the concrete beam by grinding. After grinding, all grooves were cleaned by air and filled in with epoxy Dur 31N glue. The grooves were then covered with epoxy Dur 300 and CFRP strips were attached to the concrete surface.

Test results showed that the ultimate loads of the CFRP-strengthened beams without any concrete surface preparation were increased by up to 10% compared to those of the un-strengthened beams. The increases in the ultimate loads of the CFRP-strengthened beams with the concrete surface prepared using grinding and the grinding and grooving methods were up to 13% and 23% respectively.

It has transpired that FRP externally bonded to concrete structures are susceptible to damage from collisions, high temperatures, fire and ultraviolet rays. To overcome these drawbacks, the Near Surface Mounting Reinforcement, NSMR, technique has been proposed, whereby slits with a depth smaller than the concrete cover are cut into the concrete structure and then CFRP strips or bars are bonded within these slits. Tests have shown that a higher anchoring capacity of the structure was obtained with these bonded CFRP strips. One of the first applications of this procedure, in Stuttgart, Germany, was the flexural strengthening in the negative bending moment region of a concrete bridge deck, Figure 2.14 (Motavalli & Czaderski, 2007).

Figure 2.14 Near Surface Mounting Reinforcement, NSMR, in Stuttgart, Germany (Motavalli & Czaderski, 2007)

FRP-confinement has also been applied to structural members in compression, with the aim of enhancing their load bearing capacity or in case of seismic upgrading, to increase their ductility in the potential plastic hinge region. The RC columns of Reggio Emillia football stadium in Italy were strengthened by FRP-confinement in March 2006 by applying CFRP fabrics, using the wet lay-up technique, around them. Analysis of the stadium with the new Italian Seismic Code had shown that the existing stirrups at the base of the columns were not sufficient to withstand the expected seismic loads. Another application was the seismic retrofitting of the column-beam joints, using CFRP fabrics, in the Aigaleo football stadium in Athens, Greece, Figure 2.15. The CFRP fabric was anchored to the RC deck using steel plates (Motavalli & Czaderski, 2007).

Figure 2.15 CFRP-confinement of column-beam joints at Aigaleo football stadium in Athens, Greece (Motavalli & Czaderski, 2007)

Research work has shown that pre-stressing of FRP composite strips prior to the bonding procedure is a more economical use of materials but requires special clamping devices. The roof of the sports hall at Thorl Secondary School, Styria in Austria had to be strengthened due to the large deformations under dead loads and insufficient load capacity for high snow loads. Assessment showed that the tensile resistance and flexural stiffness in the transverse beams across the sports hall were insufficient. Reduction of the deflections and increasing the load bearing capacity was achieved by applying pre-stressed CFRP strips, Figure 2.16(a). In 2003, the 585-metre long Neckar Highway Bridge in Heilbronn, Germany, built in 1964, had to be strengthened because all the coupling joints of the structure were cracked. The rehabilitation of coupling joints was achieved by applying pre-stressed CFRP strips, Figure 2.16(b), with steel plates for clamping the strip ends (Motavalli & Czaderski, 2007).

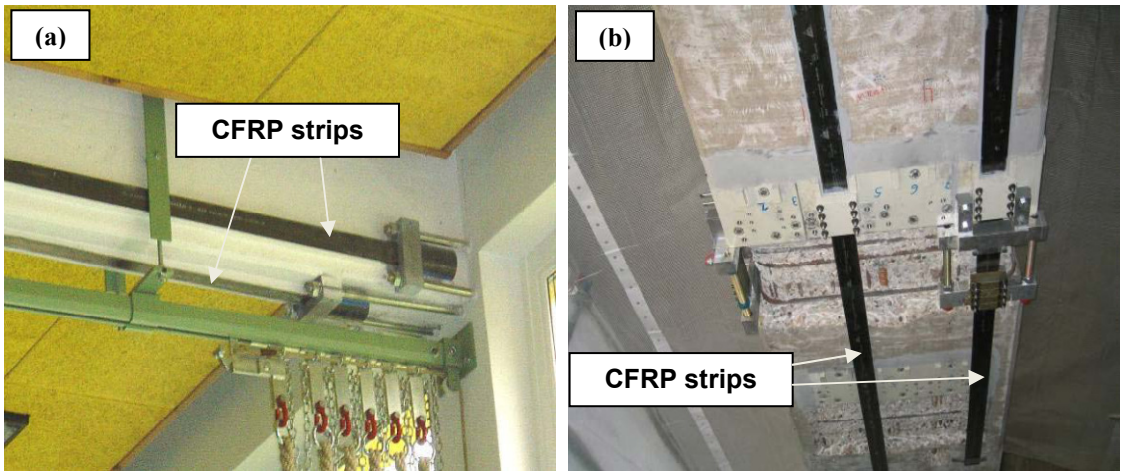

Figure 2.16 Strengthening using CFRP-pre-stressed strips at (a) Thorl Secondary School, Austria and (b) Neckar Highway Bridge, Germany (Motavalli & Czaderski, 2007)

2.9 FRP-strengthening of steel structures

It can be observed from the work described in Section 2.8 that due to FRP-strengthening, the flexural and shear strengths of concrete and steel-concrete composite beams were increased by up to 50%. The successful use of FRP composites in the concrete and steel-concrete composite beams led the researchers to use the FRP composites for the strengthening and repair of steel structures in place of conventional methods using steel sections. Besides the requirements of welding, large scaffoldings and heavy lifting, one of the major disadvantages of the conventional methods of repairing and strengthening using the steel is that they can cause considerable disruption to the users for longer periods. FRP-strengthening may offer techniques that can be applied in a shorter time and with a minimum possible disruption. Although the use of FRP composite materials for the strengthening of steel structures started in the late twentieth century, the momentum has increased since the start of twenty-first century (Okeil et al, 2009b). A review of the use of FRP composites for strengthening of steel structures is given as follows.

Vatonec et al (2002) investigated the behaviour of steel tubes strengthened with different configurations of pultruded CFRP strips. The configurations comprised of bonding the CFRP strips on the top, the bottom and both the top and bottom walls of steel tubes. Ten steel tubes, two un-strengthened and eight CFRP-strengthened were tested. All specimens were 3.35 m long, TS6x6x3/16 grade A500 steel tubes. The CFRP strips had modulus of elasticity and ultimate strength of 165 GPa and 2800 MPa respectively. In tests of the first two specimens, the local buckling of the flanges limited the full potential for the CFRP mobilization. Therefore, middle-half length of the remaining eight specimens was filled with normal-weight concrete to eliminate the flange local buckling. All the beams were tested in a four-point loading system. The testing was terminated either when the load ceased to increase or after the geometry of the test machine prevented continuation of the test due to excessive deflections. Test results showed that:

1. The increases, 6% to 26%, in the flexural strength of the concrete-filled CFRP-strengthened steel tubes, compared to un-strengthened concrete-filled tubes, were associated with the increase in the number of CFRP strips.

2. The specimen with the single top CFRP strip exhibited the minimum increase of 6% in the flexural strength, while that with the single top and double bottom strips exhibited the maximum increase of 26%, compared to that of the un-strengthened specimens.
3. The CFRP strips debonded in tests of all the strengthened tubes and the top strips debonded prior to the bottom strips in all the cases.

Harries et al (2009) carried out tests to investigate the suitability of using FRP composites to control global and local buckling in steel T sections subjected to cyclic loading. Small amounts of high strength, HS, CFRP and ultra-high modulus, UHM, GFRP composites were applied to the flanged steel sections for increasing the resistance to flange and/or web local buckling. The purpose of the FRP was to provide the cross-sectional stability to the columns, but not necessarily to increase the load carrying capacity. The test specimens, Figure 2.17(a), were T steel sections, WT 155 x 10.5, A 992 grade 50 steel, with a tensile strength of 345 MPa. A total of 20 specimens, 4 un-strengthened columns and 16 FRP-strengthened columns, were tested for elastic and inelastic buckling.

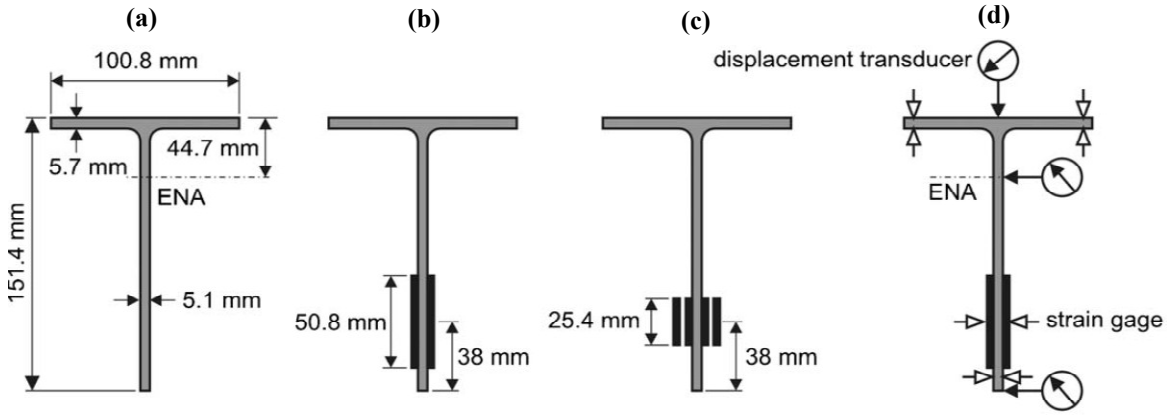

Figure 2.17 Specimen details (a) Control specimen, (b) CFRP-1 and GFRP-1, (c) CFRP-2 and GFRP-2 and (d) instrumentation (Harries et al, 2009)

FRP-strengthening was made by adhesively bonding the CFRP and the GFRP strips to both sides of the web. Two types of strengthening, Figure 2.17(b) and (c), were used, (i) single strips, 50.8 mm wide by 1.4 mm thick and (ii) double strips, each 24.5 mm wide by 1.4 mm thick, placed on top of each other. The bonded strips were centred 38 mm from tip of the column web. The tensile strength and modulus of elasticity of the CFRP strips were 2790 MPa and 155 GPa respectively, while those for the GFRP strips were

895 MPa and 41.4 GPa respectively. Concentric axial compression cyclic loading was applied by a 1300 kN capacity universal test machine.

In the first set of tests for the elastic buckling, the columns were 1664 mm long. Five steel sections, one un-strengthened and four FRP-strengthened, one of each case, were tested. The strong and weak-axis bifurcation loads were assessed as the loads at which an abrupt change in lateral displacement occurred about these axes. Results showed that the strong and weak-axis bifurcation loads of the un-strengthened specimen were increased by up to 60% and 13% respectively by the FRP-strengthening. However, a very small increase, up to 9%, in the axial capacity in FRP-strengthened sections was observed as compared to that of the un-strengthened section.

In the second set of tests for the inelastic buckling, the length of the specimen was reduced to 356 mm to avoid the flange local and torsional buckling. 15 specimen, 3 un-strengthened and 12 FRP-strengthened, 3 of each case, were tested. FRP applications led to improvements of 9 to 17% in web local buckling, WLB, bifurcation loads, compared to those of the control specimens. An increase of 4 to 14% was observed in the axial capacity due to FRP-strengthening. The specimens with two 25.4 mm wide FRP strips performed better than those with one 50.8 mm strips. Debonding of FRP strips occurred in all tests usually at about 75% of the peak loads, Figure 2.18.

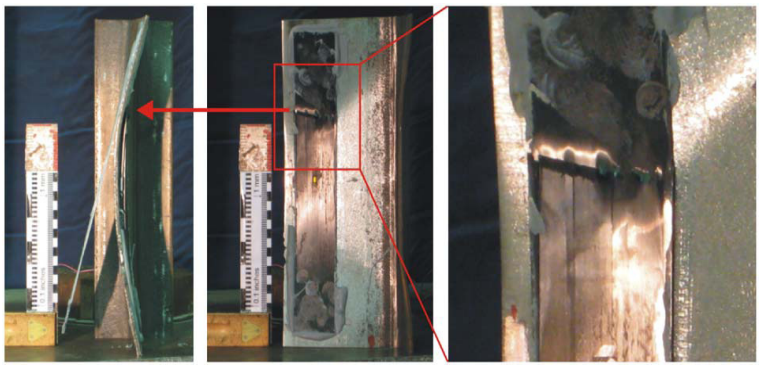

Figure 2.18 Debonding of CFRP strips in specimen CFRP-2 (Harries et al, 2009)

Colombi and Poggi (2006) presented the results of an experimental and numerical programme to characterize the static behaviour of steel I-beams strengthened by pultruded CFRP strips. Four beams, one un-strengthened and three CFRP-strengthened were tested. The control specimen, TR0, was a 2.5 m long HEA 140 steel beam. Two of the three strengthened beams, TR1 and TR2, had the bottom flange bonded with one

layer of two parallel pultruded CFRP strips, 60 mm wide and 1.4 mm thick, using the epoxies Sikadur®30 and Sikadur®330 respectively, Figure 2.19. The third strengthened beam, TR3, had the bottom flange bonded with two layers of the CFRP strips with the two parallel strips in each layer using epoxy resin Sikadur ®30, Figure 2.20. The two epoxies differed in mechanical properties. The elastic modulus and tensile strength for Sikadur®30 were 4500 and 24.8 MPa and those for Sikadur®330 were 3800 and 30 MPa respectively.

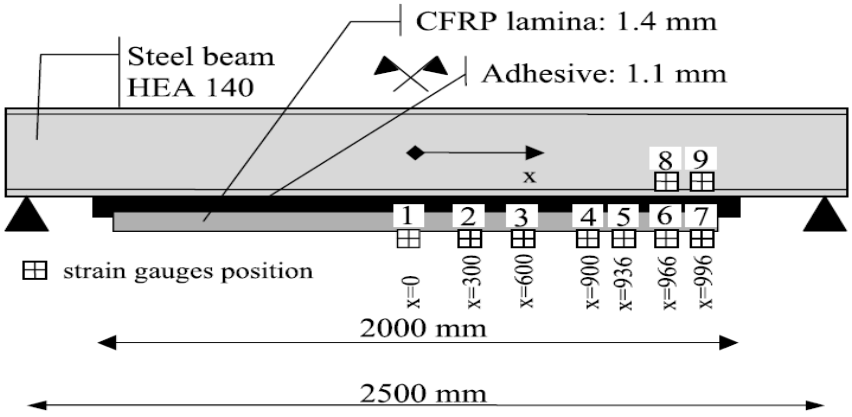

Figure 2.19 Specimen details for beams TR1 and TR2 (Colombi & Poggi, 2006)

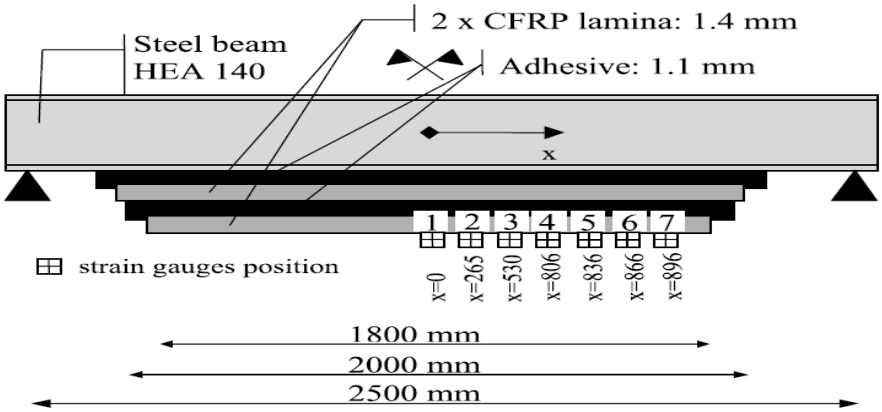

Figure 2.20 Specimen details for beam TR3 (Colombi & Poggi, 2006)

Three point bending tests were performed using the test frame shown in Figure 2.21. The specimens TR0, TR2 and TR3 were provided with lateral supports to prevent lateral torsional buckling, which occurred in the test of the specimen TR1 which had no lateral support.

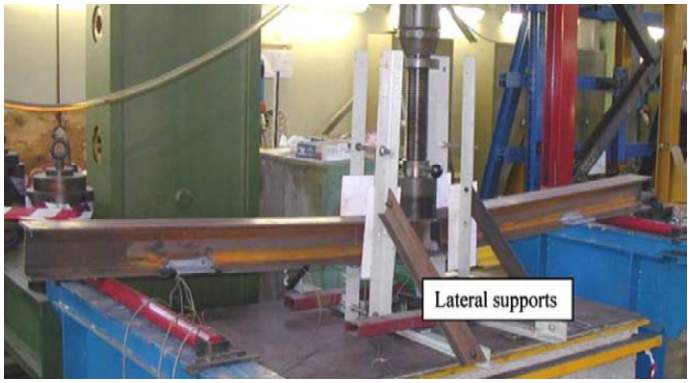

Figure 2.21 Testing set-up with lateral supports setup for specimens TR0, TR2 and TR3 (Colombi & Poggi, 2006)

The test results showed 14%, 31% and 40% increases in the ultimate loads of the CFRP-strengthened beams TR1, TR2 and TR3 respectively, compared to that of the control specimen TR0. No significant differences were observed between the responses of specimens TR1 and 2, which had the same CFRP-strengthening but had different epoxy adhesives. Finite element analyses, FEA, of the test specimens were performed using the ABAQUS FE program. The FEA results were in good agreement with the experimental results.

Photiou et al (2006a) used a combination of CFRP and GFRP pre-peg laminates in two geometric shapes to repair/strengthen the artificially degraded (damaged) rectangular hollow section, RHS, steel beams. The objective was to restore the flexural strength of the damaged beams to that of the undamaged beams and to compare the effectiveness of using two types of the CFRP composites and two geometric shapes with each other. The damage to the beams was caused by removing the half of thickness of the tension (bottom) flange. In order to obtain a flexure mode of the failure of the beams, a Class 1 compact section was used.

Four FRP-repaired beams were tested in a four-point loading system, Figure 2.22. Two damaged beams were repaired by bonding layers of the FRP pre-peg laminates in U-shaped unit to the tension flange and the other two in a flat plat unit. In each geometric shape, two layers each of an ultra-high modulus CFRP, UHM-CFRP, and a high modulus CFRP, HM-CFRP, were used respectively with a combination of the layers of a low modulus GFRP laminate as shown in Figure 2.23. The laminates were bonded using a film adhesive which was compatible with the resin system of composite pre-

pegs. No control beam was tested. The ultimate loads of the undamaged and damaged steel beams are determined using the elasto-plastic analyses of the beams.

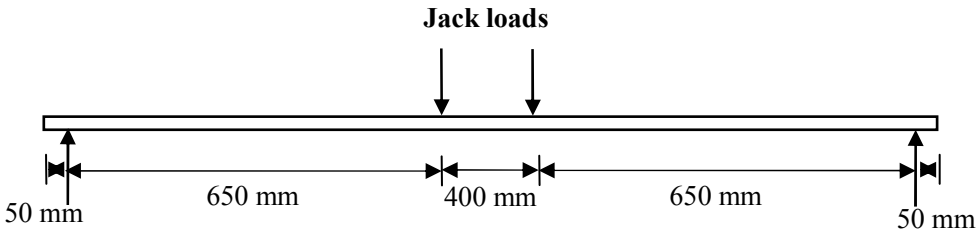

Figure 2.22 Four point loading set-up (Photiou et al, 2006a)

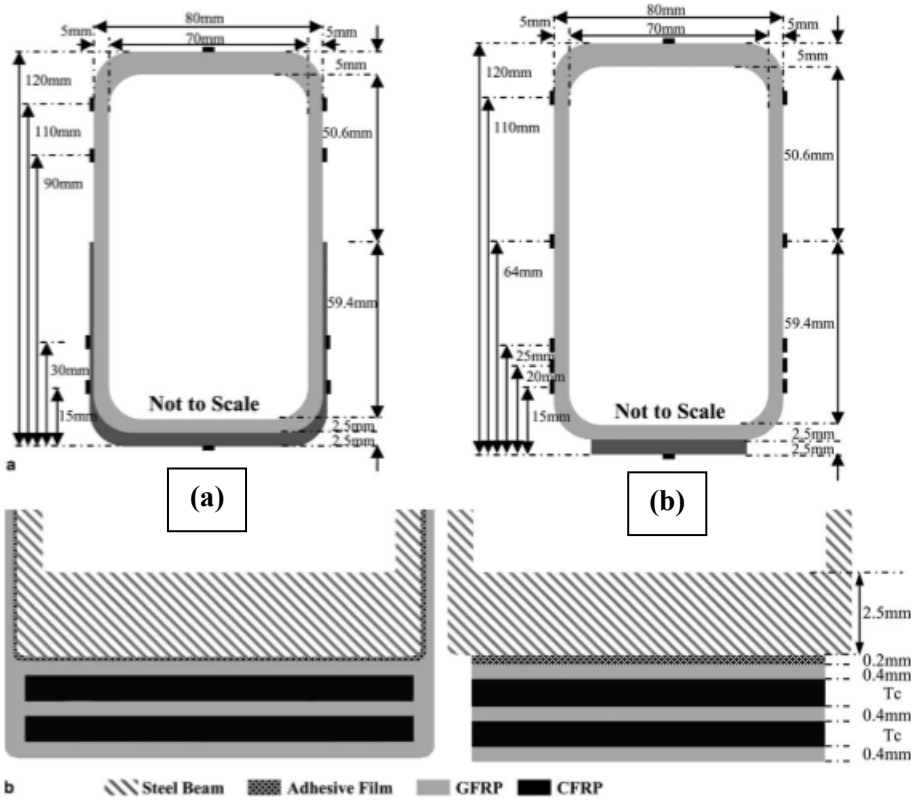

Figure 2.23 Schematic diagrams of RHS steel beams repaired using (a) U-shaped CFRP/GFRP and (b) flat plate pre-peg laminates (Photiou et al, 2006a)

The selection of using a combination of CFRP and GFRP pre-peg composites with a film adhesive was made on the basis of the tests of double-lap strap FRP-steel joints (Photiou et al, 2006b & Hollaway, 2005). The adhesives used were (i) a film adhesive compatible with the resin system used in pre-peg composites, (ii) a standard two-part epoxy adhesive Sikadur 31 used for rigid FRP plate bonding in construction industry and (iii) a two-part epoxy adhesive 3M9323 used for high-grade bonding applications in aerospace industry. The pre-peg composites used were (i) UHM-CFRP (ii) HM-CFRP

and (iii) GFRP. The test results showed that the strengths of the CFRP-steel joints using the film adhesive were approximately 16% higher than those using Sikadur 31 adhesive. The 3M9323 adhesive performed even better than the film adhesive. The advantage of using a film adhesive however was that since it was compatible with matrix of the composite pre-peg, so the curing was done in one operation. The ultimate loads of joints using the HM-CFRP laminates were approximately 20% higher than those using the UHM-CFRP. The ultimate loads of joints using the UHM-CFRP/GFRP laminates were approximately 26% higher than those using the UHM-CFRP.

Table 2.7 gives the ultimate loads and modes of the failure of the CFRP-repaired and unrepaired beams.

Table 2.7 Ultimate loads and modes of failure of un-repaired and FRP-repaired beams (Photiou et al, 2006a and Hollaway, 2005)

Beam details with FRP combination & shape of repairing system	**Ultimate load per jack (kN)**	**Ratio of ultimate loads**		**Mode of failure**
		Repaired /Beam 5	Repaired /Beam 6	
Beam 1 (UHM-CFRP/GFRP) U-shaped	45	1.18	1.43	Yielding of steel and CFRP laminate in high moment region
Beam 2 (HM-CFRP/GFRP) U-shaped	50	1.30	1.59	Yielding of steel, test stopped due to excessive deflections
Beam 3 (UHM-CFRP/GFRP) Flat plate	45	1.18	1.43	Yielding of steel and CFRP laminate, breakdown of steel-CFRP bond
Beam 4 (HM-CFRP/GFRP) Flat plate	50	1.30	1.59	Yielding of steel, test stopped due to excessive deflections
Beam 5 (Un-repaired) Undamaged	*38.2	1.0	1.21	*Yielding of steel in high moment region
Beam 6 (Un-repaired) Damaged	*31.4	0.82	1.0	*Yielding of steel in high moment region

* determined using elasto-plastic analyses

Test results show that:

1. The ultimate load of the damaged beam was reduced by approximately 18% compared to that of the undamaged beam due to removing half thickness of the bottom flange.
2. Following the CFRP-repair using either U-shaped or flat plate laminates, the ultimate load of the damaged beam was not only fully restored to that of undamaged beam, but it was also further increased by up to 30%.
3. The ultimate loads of the repaired beams using either U-shaped or flat plate laminates were identical.
4. The ultimate loads of the repaired beams using the HM-CFRP laminates were approximately 11% higher than those using the UHM-CFRP laminates because the latter had a lower ultimate strain of 0.4%.
5. Due to a higher ultimate strain, the failure of the HM-CFRP-repaired beams was ductile; while that of UHM-CFRP-repaired beams was brittle.

Okeil et al (2009a) carried out the FRP-strengthening of steel plate-girders by providing additional out-of-plane stiffness to the buckling-prone webs with the help of the tests and finite element, FE, analyses. Two specimens, one control OB1 and the other GFRP-strengthened OB2, were tested. The control specimen was an un-strengthened end web panel of a 2083 mm long steel plate-girder, 532 mm deep with a 3.2 mm thick web, and 279 mm wide and 13 mm thick flanges, Figure 2.24. The slenderness ratio of the web was 159 and it consisted of four panels divided by five vertical steel stiffeners, 9.5 mm thick and 114 mm wide, on both sides at an equal spacing of 521 mm. Because the mode of failure of the plate-girder to be the investigated was that initiated by web buckling, so all other possible modes causing failure, for example flange buckling and stiffener buckling, were designed to be avoided in the plate-girder.

The strengthened specimen OB2 was the web panel at other end of the plate-girder with the addition of two vertical GFRP pultruded T-sections as the additional stiffeners on both sides of the web. A single point load, Figure 2.24, was applied at the first internal stiffener on one end of the plate-girder causing the end web panel, test panel, to be subjected to 3 times the load acting on rest of the plate-girder.

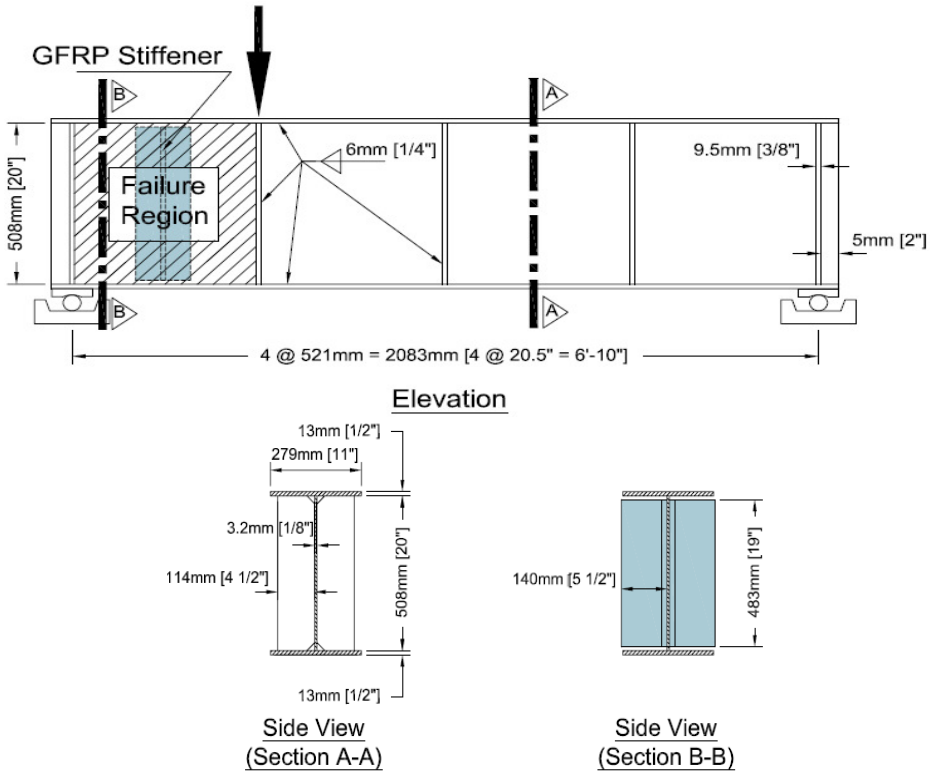

Figure 2.24 Control and GFRP-strengthened specimens, OB1 and OB2 (Okeil et al, 2009a)

Test results showed that the ultimate load, 389 kN, of the GFRP-strengthened specimen OB2 was 40% greater than that, 278 kN, of the control specimen OB1. If loads at the initiation of buckling of the web are considered, there was an improvement of 56% because the buckling initiated at 389 kN with failure in the GFRP-strengthened specimen and at 249 kN in the un-strengthened specimen. Failure in the GFRP-strengthened specimen was initiated by a breakdown of the steel-GFRP bond followed by immediate buckling of the web.

Before testing, FE analyses of specimens OB1 and OB2 were carried out using 8-node solid elements in the ANSYS 2008 program. Inconsistency between the test and FEA results was observed. The FEA ultimate load, 330 kN, of the control specimen was 19% greater than the test ultimate load of 278 kN. For the GFRP-strengthened specimen, the FEA ultimate load, 1485 kN, was about 4 times of the test ultimate load of 389 kN. The test and FEA modes of the failure of the GFRP-strengthened specimen were also different, Figure 2.25.

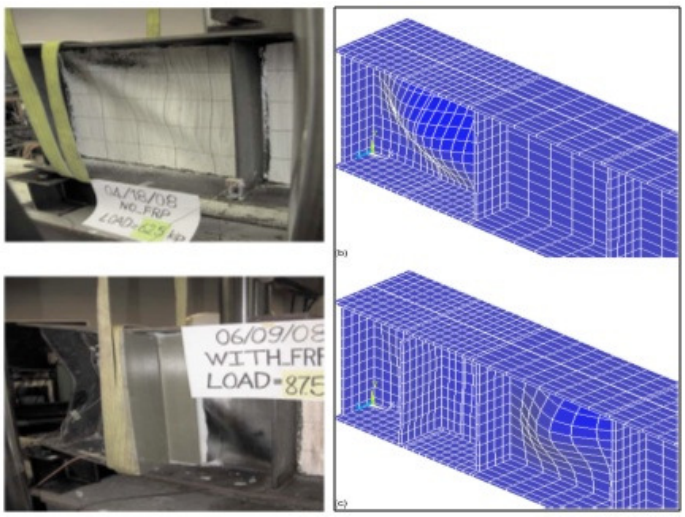

Figure 2.25 Test and FEA modes of failure of specimens, OB1 and OB2 (Okeil et al, 2009a)

It was observed that the incorrect predictions of the analyses presented in the above research were due to (i) the choice of wrong element in the FEA and (ii) the mesh, 8 x 11, for the web in panels that had been used for the model plate-girders not being fine enough. It will be demonstrated later in Chapter 4 that shell elements perform well and give better results compared to the solid elements with the same mesh. The authors did not provide load-deflection plots of the FEA or test results to demonstrate the elastic and the plastic behaviour of the two specimens. The problem of bond breakdown between the steel and GFRP, which occurred in the test of the GFRP-strengthened specimen, could affect the ultimate load capacity of the specimen by not allowing it to reach its full strength. No attempts were made to reduce the stress concentrations in the adhesive at the end of GFRP stiffeners which leads to the bond breakdown. No information on the tested values of material properties, such as tensile yield strength and modulus of elasticity, for the steel and the pultruded GFRP sections used in tests was available. The properties of the steel and GFRP should have been obtained by testing in order to get the correct results in the FE analyses.

Later the authors (Okeil et al, 2011) realised some of the shortcomings in the FE analyses and rectified them by using a finer mesh of 17x28 for the web in web panels, Figure 2.26, in the models of the control and GFRP-strengthened specimens. The same 8-node solid element in the ANSYS 2008 program was used for modelling the steel, the GFRP and the adhesive layer. GFRP and epoxy were assigned linear elastic material properties. The first buckling modes predicted by the eigenvalue analyses were used to

account for geometrical imperfections in the web. Nonlinear FE analyses of specimens were then carried out by modelling both the material and geometric nonlinearities. The results showed that the FEA and test ultimate loads of specimen OB1 were same, i.e. 278 kN, while the FEA ultimate load of specimen OB2, 403 kN, was approximately 4% greater than that, 389 kN, in the test. The FEA modes of failure of the two specimens were same as those in the tests.

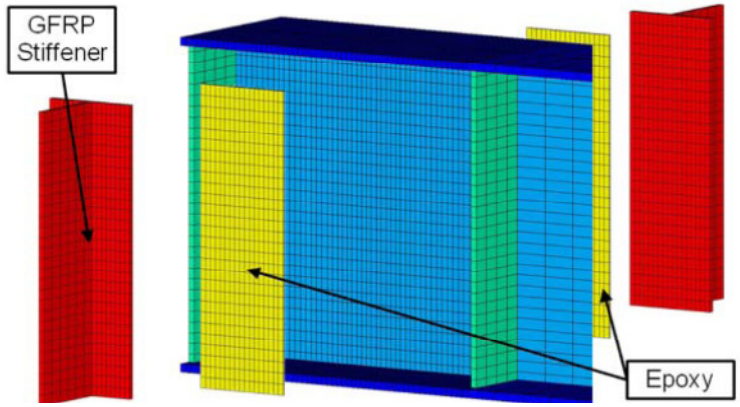

Figure 2.26 Model of GFRP-strengthened specimen OB2 (Okeil et al, 2011)

Okeil et al (2010) tested one more strengthened specimen OB3, which was bonded with one GFRP pultruded T-section as additional diagonal stiffener on one side of the web in the end web panel. The test results showed that the ultimate load, 435 kN, of the specimen OB3 was increased by 56% than that, 278 kN, of the control specimen OB1 and by 12% than that, 389 kN, of the specimen OB2 strengthened with vertical GFRP stiffeners. Further details about carrying out the FE analysis of the specimen OB3 were not provided by the authors.

Zhao and Al-Mahiadi (2009) investigated the effect of CFRP-strengthening on the web-buckling capacity of light steel beams, LSBs, having slender webs and subjected to compressive loading. 28 specimens comprising 7 control beams and 21 CFRP-strengthened beams were tested. The seven control specimens, LSB1 to LSB7, had web slenderness ratios ranging from 62.5 to 125. Three strengthening techniques were used for each type of specimen. CFRP plates with a unidirectional fibre orientation were adhesively bonded to their webs on (a) the outer sides, (b) the inner sides or (c) both sides, Figure 2.27. The direction of CFRP fibre was kept perpendicular to the longitudinal axis of the beam.

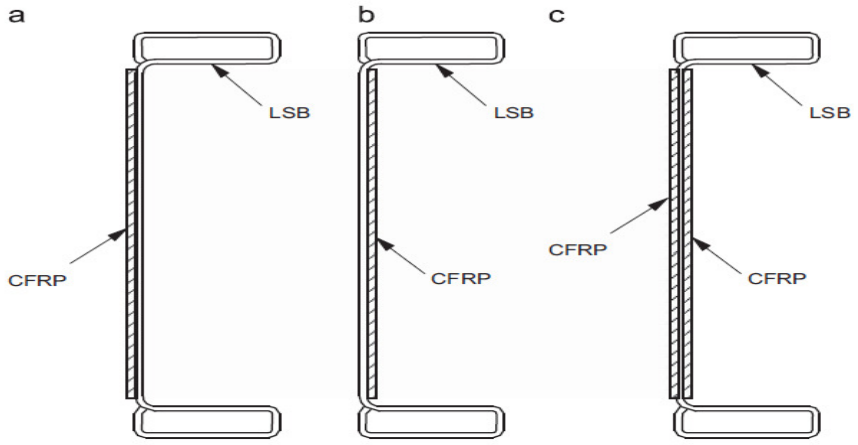

Figure 2.27 CFRP-strengthening of LSBs (a) outer side, (b) inner side and (c) both sides (Zhao & Al-Mahiadi, 2009)

The test results showed significant increases in the ultimate load of the CFRP-strengthened beams for all three types of strengthening techniques, compared to that of the respective control beams.

1. Strengthening method 1 using the CFRP strips on the outer sides of the web increased the ultimate loads of the beams by 40 to 200% compared to the respective un-strengthened beams.
2. Method 2 using the CFRP strips on the inner sides of the web increased the ultimate loads by 140 to 300%.
3. Method 3 using the CFRP strips on both sides of the web showed the highest increases of 250 to 500% in the ultimate loads of the strengthened beams.
4. Increases in the ultimate loads due to the CFRP-strengthening were proportional to the web slenderness ratios of the beams; the higher the web slenderness ratio of the control beam, the more the increase in the ultimate strength of the respective strengthened beams and vice versa.
5. Debonding of CFRP strips occurred for all the three types of strengthening, but the LSBs with CFRP on the inner web surfaces using methods 2 and 3 continued to carry the load even after partial debonding had occurred.
6. The modes of the failure of the un-strengthened and the CFRP-strengthened beams are shown in Figure 2.28.

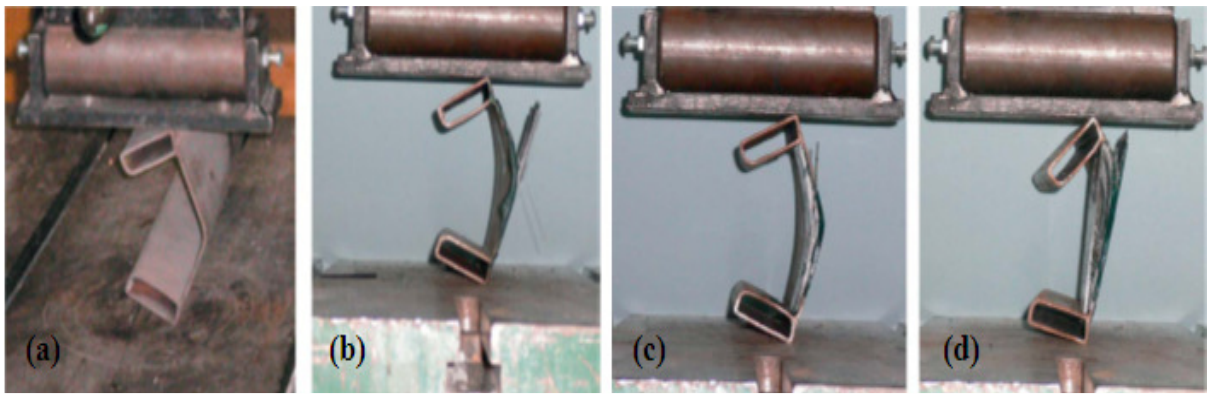

Figure 2.28 Modes of failure of LSBs (a) un-strengthened beam, (b) CFRP on outer side, (c) CFRP on inner side and (d) CFRP on both sides (Zhao & Al-Mahiadi, 2009)

Before testing, the ultimate loads, N_b, of the un-strengthened beams were predicted with the help of the Equation 2.19 used for the buckling capacity of columns in Australian standards (Standards Australia, 1998).

$$N_b = \alpha_c k_f A \sigma_y \qquad \text{Equation 2.19}$$

Where 'α_c' is member slenderness reduction factor, 'k_f' is form factor, 'A' is the cross-sectional area of the beam and 'σ_y' is the yield strength of steel. The analytically predicted ultimate loads of the un-strengthened beams, LSB1 to LSB7, agreed reasonably with the experimental results.

Narmashiri et al (2010) investigated, using FE analyses and experimental testing, the effectiveness of bonded pultruded CFRP strips for shear strengthening of steel I-beams. Five specimens, one control NB1 and four CFRP-strengthened NB2 to NB5, were tested. The un-strengthened control specimen NB1 was a 1.3 m long beam, 150 mm deep with a 6.6 mm thick web and 100 mm wide and 10 mm thick flanges as shown in Figure 2.29.

Specimen NB2 was strengthened using 3 CFRP strips applied to each shear zone at each end of the beam on both sides of the web, Figure 2.29. The shear zone was the region of web surrounded by two partial height stiffeners and two flanges near the supports and was 200 mm wide and 130 mm deep. Specimen NB3 was strengthened in a similar way to NB2 except that instead of 3, 2 CFRP strips were applied to the each shear zone. Specimen NB4 was strengthened using 3 CFRP strips applied to the one shear zone at the right end of the beam on the one side of the web and 3 strips applied to one shear

zone at left end of the beam on the other side of the web. Specimen NB5 was strengthened in a similar way to NB4 except that instead of 3, 2 CFRP strips were applied to the each shear zone. All the specimens were tested in four-point loading system, Figure 2.29.

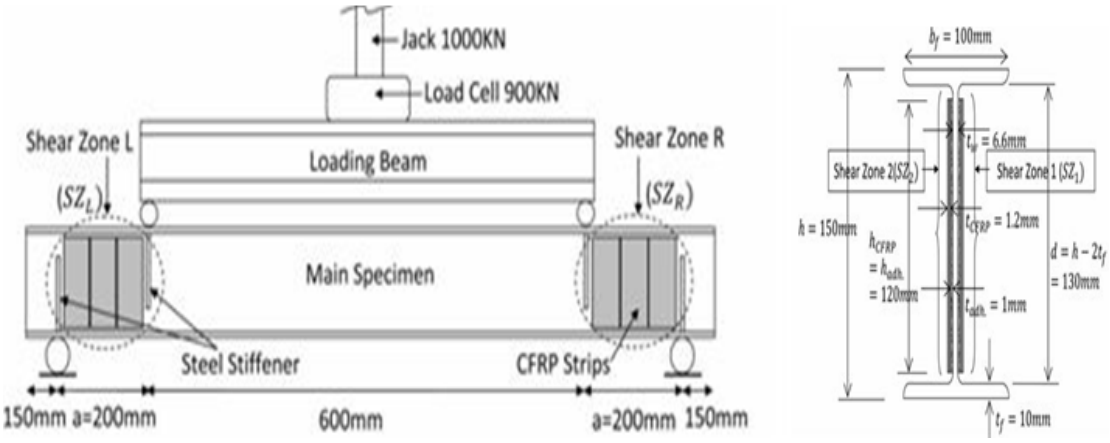

Figure 2.29 CFRP-strengthening and loading of specimen NB2 (Narmashiri et al, 2010)

The test results showed that:

1. The increase in the ultimate load of the strengthened specimens NB2 and NB3, using 3 and 2 CFRP strips on both sides of the web respectively, was the same, approximately 52%, compared to that of the control specimen NB1.
2. For the strengthened specimens NB4 and NB5, using 3 and 2 strips on one side of the web only, the increases in the ultimate loads were 43% and 35% respectively, compared to that of the control specimen NB1.
3. The control specimen failed due to the flange twisting and the web crippling.
4. Failure in the strengthened specimens was initiated either by the longitudinal delamination of CFRP strips in the area near the applied loads or debonding of the CFRP strips; firstly in compressive and then in tensile regions. The CFRP-strengthening decreased the lateral deflection and twisting of the compression flange and shear buckling of the web.

To evaluate the testing, FE analyses of the specimens were carried out using the ANSYS program. The test and FEA ultimate loads of the specimens showed good agreement. It was recommended to use two CFRP strips to each shear zone in the case of shear strengthening on the both sides of the web. However, in the case of shear strengthening on one side of the web only, which is economical as well as practicable, use of three CFRP strips to the shear zone, was proposed.

Islam and Young (2013) carried out tests to investigate the effects of using different FRP composites, adhesives and surface treatment methods on the behaviour of stainless steel tubular sections. 57 specimens, 9 un-strengthened control and 48 FRP-strengthened, were tested under end-two-flange (ETF) and interior-two-flange (ITF) loading conditions, Figure 2.30. Specimens were either rectangular hollow sections (RHS) or square hollow sections (SHS). The specimen lengths 'L' were N+1.5d and N+3d for ETF and ITF loading conditions respectively, where 'N' was bearing length 50 mm and 'd' was the overall depth of steel tubular sections.

Following methods of the surface preparation and types of the FRP composites and adhesives were used in the tests.

1. Two methods of the surface preparation of the steel using (i) electric sander and (ii) electric grinder were employed.
2. Six types of FRP composites with different tensile strengths and elastic modulus were used. They included two wrap sheets (i) Sika Wrap-300C/60 carbon fibre and (ii) Sika Wrap-430G/25 glass fibre, and four laminate plates (iii) Tyfo UC laminate, (iv) Sika Carbodur S1214, (v) Sika Carbodur M614 and (vi) Sika Carbodur H514.
3. Six types adhesive with different tensile strength, elastic modulus and elongation after failure were used. They included (i) Sika 330, (ii) Sika 30, (iii) Tyfo TC, (iv) Araldite 2011, (v) Araldite 2015 and (vi) Araldite 420.

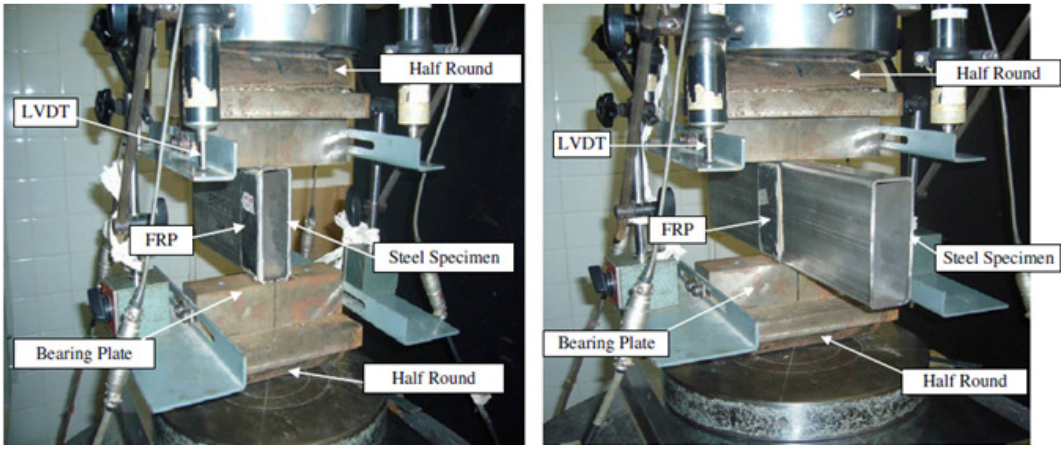

Figure 2.30 Testing set-up of ETF and ITF loading conditions (Islam & Young, 2013)

The tests results showed that:

1. The ultimate loads of the strengthened specimens using 'sander' treatment were slightly higher than those using the 'grinder'.

2. The adhesive 'Araldite 2015' showed better performance than others. The specimens strengthened using this adhesive gave higher ultimate loads.
3. Of six different FRP composites used for the strengthening of specimens, carbon laminate 'Sika Carbodur H514 carbon' provided the best performance by giving the higher ultimate loads.
4. The CFRP-strengthening was found to be the most effective when the CFRP width was the same as that of the bearing length of the stainless steel tubular section; any further increase did not provide much improvement in the web crippling capacity.
5. The web crippling capacity of the un-strengthened sections was increased by up to 51% due to the FRP-strengthening.
6. Five failure modes were observed in the FRP-strengthened specimens. They include adhesion, cohesion, combination of adhesion and cohesion, inter-laminar failure of FRP plate and delamination of FRP. Generally adhesion failure was observed for the section with stocky webs, while either inter-laminar CFRP or combination of adhesion and cohesion failures were observed for the sections with slender webs.

It has been observed that the majority of the published work has focused on the use of GFRP and CFRP composites to the tension regions of the steel beams in order to increase the flexural strength of the beams. Little attention has been given to the use of FRP composites to strengthen the thin-walled members of steel beams, for example webs of the steel plate-girders, where the failure is initiated by out-of-plane shear buckling of the thin-walled members. Although some use of the GFRP pultruded sections as intermediate and diagonal stiffeners to strengthen the webs of the steel plate-girders has been made, but their use as the load-bearing stiffeners has not been investigated. The webs of the plate-girders can also be strengthened using FRP composite fabrics or pre-pegs which also needs attention of the researchers.

2.10 Bonding of FRP composites for strengthening

FRP composites used to strengthen steel structures are generally bonded to the steel surfaces using adhesives. Adhesives join materials primarily by attaching to their surfaces within a layer of molecular dimensions, i.e. of the order of 0.1-0.5 nm. Being liquid, adhesives flow over and into the irregularities of a solid surface, coming into contact with the solid and as a result, interact with its molecular forces. The adhesive

then solidifies to form the joint. The basic requirements for good adhesive bonding are intimate contact between the adhesives and substrates and absence of weak layers or contamination at the interface. It has been observed that the best chance of success for FRP applications to steel structures can be achieved by using two part cold-curing paste epoxy adhesives that have been developed for use on site (Hollaway & Teng, 2008).

Durability and strength of the FRP-strengthened steel and other structures depend upon the durability and integrity of adhesive joints between the strengthening and the strengthened members. FRP-strengthened structures usually fail due to the failure of these joints. Failure of the adhesively bonded joints can be divided into the following six categories, which are also shown in Figure 2.31(a) to (f) (Tomblin et al, 2003).

1. Adherend failure away from the joint
2. Adherend failure at the joint
3. Cohesive failure in shear
4. Cohesive failure in peel
5. Adhesive failure in shear
6. Adhesive failure in peel

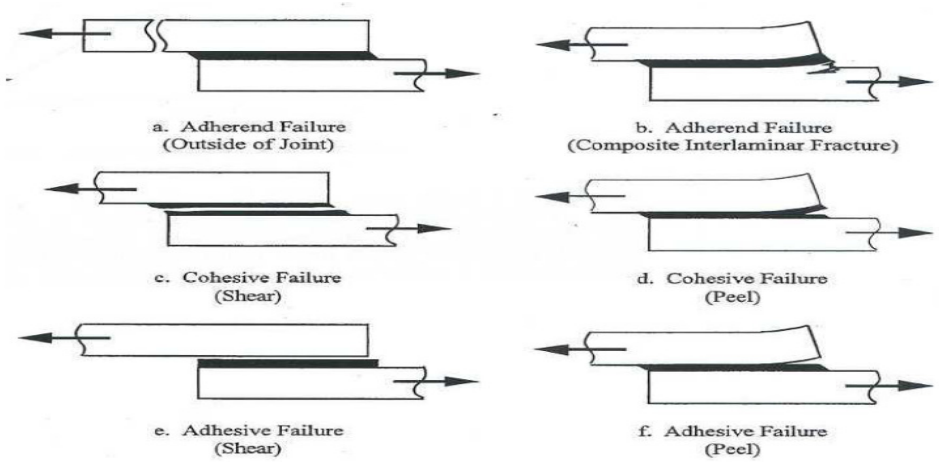

Figure 2.31 Modes of failure of the adhesively bonded joints (Tomblin et al, 2003)

2.10.1 Surface preparation

In order to avoid the failure of adhesively bonded joints and to get effective adhesive bonding of FRP composites to steel surfaces, one of the most important aspects in is the proper surface preparation of the solid surfaces of FRP and the steel to be bonded. The purpose of surface preparation is to remove contaminations and weak surface layers and to change the surface topography of the substrates. Surface preparation has a much

greater influence on long-term bond than it does on initial bond strength so that a high standard of surface preparation is essential for promoting long-term bond integrity and durability. Some of the commonly used techniques for the surface preparation of mild steel members are given below (Hollaway & Teng, 2008).

1. Removing dust or grease with a suitable solvent or alkaline cleaner, such as acetone.
2. Dry or wet grit-blasting.
3. Removing release agents and resin-rich surface layers by mechanical abrasion, such as grinding, wire-brushing, etc.

Surface preparation of a solid FRP composite is done by stripping-off a peel-ply layer which is usually 0.2 mm thick and laid-up on the outermost surfaces (Hollaway & Teng, 2008).

2.10.2 Other Factors affecting bond strength

Besides the surface preparation of the FRP composites and the steel, there are several others factors such as the thickness of the adhesive layer, length of adhesive joints, end shapes of bonded FRP composites, etc, which can affect the ultimate strength and durability of the adhesive bond joints. Lang (Lang, 2008) has reviewed the work carried out using FE analyses and the experimental investigations to determine the effects of the aforementioned factors on the bond strength. The main conclusions are as follows.

1. Adams et al (1997) and Adams (1990) carried out stress analyses of the adhesively bonded joints. They assumed that the adhesive deformed only in shear and the adherends deformed only in tension. It was found that the distribution of shear stress was not uniform along the length of the adhesive joint. The shear stresses were a maximum at the joint ends and were of the order of two to four times the average shear stress in the joint.

2. Investigations into the adhesive edge shapes at the ends of rigid adherends have shown that the position of maximum stress within the adhesive is dependent of the end shape of the adhesive. Using adhesive spew angles of 45^0 at the ends of bonded joints can reduce stress concentrations by up to 20% (Crocombe & Adams, 1981).

3. Vallee and Keller (2006) carried out tensile tests on epoxy bonded double lap joints composed of pultruded GFRP profiles to investigate the effect of adhesive layer thickness and influence chamfering (tapering) of the adherends at the ends. A two-component epoxy adhesive SikaDur 330 was used. The results showed that the maximum shear and peel stresses at the ends of the bonded joints were reduced by up to 50% for the joints with tapered adherend ends compared to those with non tapered adherend ends. The test results for joint failure loads for a range of adhesive thickness from 1 mm to 3 mm showed that the adhesive thickness had only a small influence on the joint strength.

4. In order to minimize the intensity of shear and peel stresses in adhesives at ends of the adherend, the ends of FRP pultruded sections should be tapered to the angle of 30^{o} or less (Lang, 2008).

5. Tomblin et al (2001) carried out thin-adherend lap shear tests to investigate in situ properties of the adhesive joints using the test methods given in D-1002, D-3165 and D-5656 of ASTM standards. It was found that the shear strength of an adhesive joint also depends upon the bending stiffness of the adherend irrespective of the thickness of the adhesive.

6. Joints with thin adherends had lower shear strengths due to adherend's bending and the resultant high peeling stresses. The shear strength of an adhesive joint is found to decrease when it is exposed to heat and moisture. The joint strength is also affected by the glass transition temperature, T_g, of the adhesive. The glass transition temperature is the temperature at which the matrix material transforms from a hard and brittle state to a rubbery and plastic state, thereby affecting the joint stiffness (Lang, 2008).

It has been observed that end-tapered FRP pultruded sections, which can minimize the intensity of shear and peel stresses in adhesives has not been used for the strengthening of the steel or concrete beams. In order to strengthen the bond between the FRP composites and steel or concrete surfaces, another method can also be used in which the adherends are to be held together till the curing of the adhesive.

2.11 Conclusions

Steel plate-girders are commonly used as the bridge members. This Chapter has presented a review of well-known theories developed to explain the failure mechanism and to estimate the ultimate load of the steel plate-girders. The failure of a plate-girder is initiated by shear buckling of the web and occurs when the web yields across a tensile stress field and four plastic hinges develop in the flanges (Rockey et al, 1978). All the theories assume that the vertical stiffeners at the ends of the plate-girders known as end posts, being strong and rigid enough, do not deform at failure. Eurocode 3 (ENV 1993-1-5, 2006) provides a simple procedure to estimate the ultimate load of the plate-girders. This is followed by the review of methods for the design of transverse steel stiffeners to strengthen the webs of plate-girders. The design methods mainly differ in the load carried by the stiffeners. It has however been shown that the intermediate stiffener can be designed safely by satisfying the 'stiffness requirement' only (Hendy et al, 2011). The mode of failure of the plate-girders has to be investigated if the end posts are non-rigid and deform at the failure. An investigation into the design and behaviour of the stiffeners is also required if the stiffeners are made of another material such as FRP pultruded sections and are to be used in a diagonal orientation.

The literature pertaining to the use of fibre-reinforced polymer, FRP, composites for strengthening and repair of the concrete structures has also been reviewed. Carbon FRP has been found to be the most commonly used composite with some use of glass FRP. FRP composites have successfully been used to increase the flexural strength of concrete and steel-concrete composite beams by up to 50%. In a few cases, FRP composites have also been used for the shear strengthening of the concrete beams. In one case, carbon composites have been proved to be a useful alternative to steel shear reinforcement in concrete beams (Czaderski, 2002).

CFRP and GFRP composites have been also used for the strengthening and repair of steel beams. The objective of such strengthening and repair has been to increase the flexural strength of the beams, which has been obtained up to 40% compared to the un-strengthened beams. Little attention has been given to use FRP composites to increase the ultimate strength of thin-walled steel sections, such as the webs of steel plate-girders, where failure is initiated in the web. Some work has been done by Okeil et al (2009a, 2009b & 2011), but it is at a very early stage and needs more study to determine

the effectiveness of using different orientations of the GFRP stiffeners and of using different types of FRP composites, such as fabrics and pre-pegs, for strengthening. Development of the finite element models of FRP-strengthened plate-girders and their validation using the tests are also required.

The review has also revealed that durability and strength of the FRP-strengthened steel and other structures depend upon the durability and integrity of adhesive joints between the strengthening and the strengthened members. Failure in FRP-strengthened structure is generally initiated by a breakdown of the adhesive bond. The literature further reveals that for a strong adhesive bond, one of the most important factors to be considered is the proper preparation of the surface to be strengthened and of the FRP composites in case of the use of pultruded sections as the strengthening material. The stress concentrations at the ends of the adhesive bond layers, which are one of the major reasons for the debonding, can be minimized by tapering the ends of bonded solid FRP composites to the angles less than 30^{o}. The adhesive thickness has only a small influence on the strength of the adhesive joint. In order to further strengthen the bond between the FRP composites and steel or concrete surfaces, the adherends after bonding should be held together till the curing of the adhesive is complete.

Chapter 3 Experimental Study

3.1 Introduction

This Chapter presents the details of an experimental investigation comprising the tests of eight specimens, one un-strengthened and the seven fibre-reinforced polymer, FRP, strengthened. The tests were carried out on the un-strengthened or the FRP-strengthened end web panels of steel plate-girders. The plate-girders were manufactured in two series, S1 and S2, each comprising four specimens. The S1 and S2 plate-girders were similar in construction; but the steel used in the webs had different yield and ultimate tensile strengths. The testing procedure, the strengthening methods employed and FRP composites used for the strengthening of the specimens are described.

Based upon method used for the FRP-strengthening, the test specimens were divided into three groups, G1, G2 and G3. Group G1 comprised the control specimens without any FRP-strengthening. An un-strengthened test specimen was used as control for the test specimens using the S1 plate-girders, while an FE model of the un-strengthened specimen was analysed and used as the control for the specimens using the S2 plate-girders. In G2 and G3 specimens, the end web panels were strengthened using GFRP pultruded section stiffeners and layers of carbon and glass FRP fabric sheets respectively. The test results of all the specimens have been presented, discussed and compared. The results have been used for the validation of finite element, FE, analyses of the test specimens described in Chapter 5.

3.2 Tests

3.2.1 Objectives of tests

The tests were carried with the main objective of investigating the use of carbon and glass FRP composites to increase the ultimate strength of steel plate-girders by increasing the out-of-plane stiffness of the web panels. Further objectives of the tests of the specimens were as follows.

1. To obtain an increase of a minimum of 20% in the ultimate load of the FRP-strengthened specimens compared to that of the un-strengthened control specimen.

2. To understand the behaviour of the test specimens strengthened using different types of FRP composite materials and different strengthening methods.

3. To validate by testing the results of the FE analyses performed on models of the proposed test specimens.

4. To investigate the issues of breakdown of the steel-FRP bond, the optimal orientation of GFRP stiffeners and effectiveness of using different types of FRP composites for strengthening.

5. To use the test results to validate the design procedures to be developed for the FRP-strengthened plate-girders.

3.2.2 Steel plate-girders

Four steel plate-girders with slender web panels were used in the experimental investigation. The plate-girders were manufactured using S275 grade of steel in two series, S1 and S2, each comprising two plate-girders. Each plate-girder allowed two tests to be carried out, one for each of the two end web panels. Because the mode of failure of the plate-girders to be the investigated was that initiated by out-of-plane buckling of the web, all other possible modes causing failure, for example flange buckling and stiffener buckling, were designed to be avoided in the girder. The plate-girders tested were similar to those tested by Okeil et al (2009a). Figure 3.1 shows the plate-girders and Figure 3.2 gives the dimensions of the S1 and S2 plate-girders.

The S1 and S2 plate-girders were of similar construction except a small difference in lengths of the flanges and web plate. The top and bottom flanges and web plate in the S2 plate-girders were extended by 50 mm at both ends of the plate-girders in an attempt to avoid plastic hinges formed in the end steel stiffeners during the tests of the S1 plate-girders. Besides, each of the four plate-girders was 524 mm deep with a 3 mm thick web; and 300 mm wide and 12 mm thick flanges. Each plate-girder consisted of four web panels divided by five vertical steel stiffeners, 8 mm thick and 125 mm wide, on both sides of the web at an equal spacing of 500 mm. The slenderness ratio of the web was approximately 167 and the aspect ratio of each of the four web panels was 1.0.

Figure 3.1 Views of S1 and S2 plate-girders used in tests

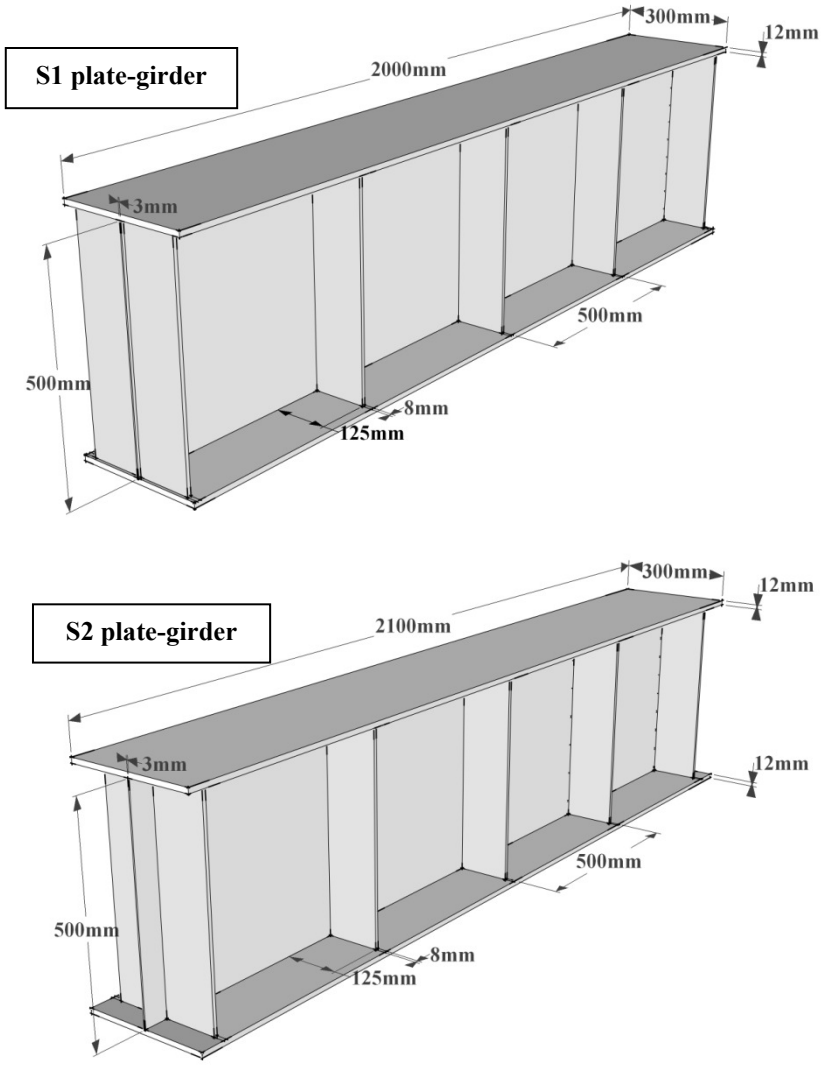

Figure 3.2 Dimensions of S1 and S2 plate-girders

3.2.3 Tensile testing of steel

To determine the yield strength and the ultimate tensile strength of grade S275 steel used in the S1 and S2 plate-girders, tensile testing of the steel was carried out in accordance with the British/ European Standards (BS EN ISO 6892-1, 2009). A total of thirteen tensile specimens, details in Table 3.1, were tested. Two specimens each were taken from the flanges, webs and stiffeners of the plate-girders. A third tensile specimen from the web of S1 plate-girder was also tested to investigate the apparent inconsistency in the results of the second test.

Table 3.1 Properties of steel obtained from tensile tests

Specimen No.	**S1 plate-girders**			**S2 plate-girders**		
	Flange	Web	Stiffener	Flange	Web	Stiffener
Yield strength (MPa)						
1	320.2	280.4	311.2	333.8	340.1	346.0
2	323.7	237.7	305.6	325.9	365.7	321.0
3	---	304.3	---	---	---	---
Mean	**322**	**274**	**308**	**330**	**353**	**334**
Ultimate tensile strength (MPa)						
1	445.4	366.6	466.8	436.8	471.8	449.9
2	447.6	356.5	458.4	442.4	474.0	449.4
3	---	403.2	---	---	---	---
Mean	**446**	**375**	**463**	**440**	**473**	**450**

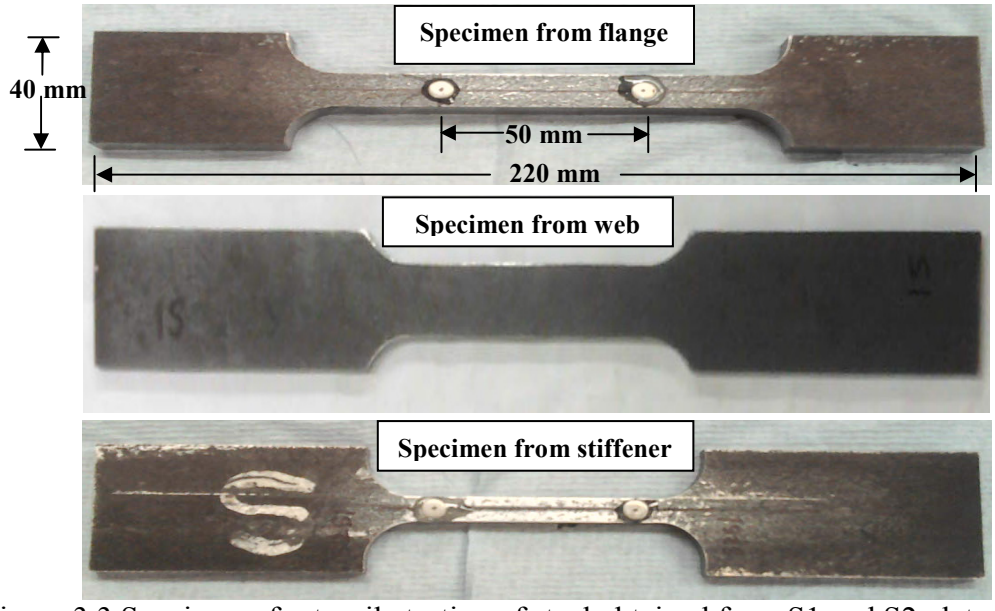

Figure 3.3 Specimens for tensile testing of steel obtained from S1 and S2 plate-girders

Each tensile specimen, Figure 3.3, was 220 mm long and had a gauge length of 50 mm. The widths of the gauge lengths of specimens were adjusted according to the code requirements for the given thicknesses and were 12, 15 and 8 mm for the specimens taken from the flanges, webs and stiffeners respectively. All the specimens were taken by saw cutting, Figure 3.4, from the second web panels of the S1 and S2 plate-girders and were cut keeping a distance of approximately 30 mm away from the welds. The Instron 8803 machine having a loading strength of 500 kN was used for the tensile testing. The properties of the steel obtained from the tensile tests are given in Table 3.1. The results of the tensile tests show that the tensile yield and ultimate strengths of the flanges and stiffeners of the S2 plate-girders were slightly higher, up to 1.08 times, than those of the S1 plate-girders. The two strengths of the webs of the S2 plate-girders were significantly higher, about 1.30 times, than those of the S1 plate-girders.

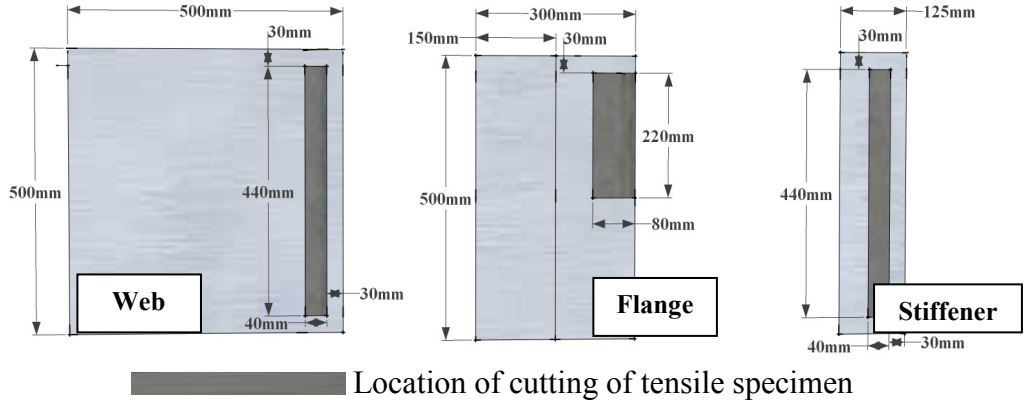

Figure 3.4 Locations of cutting for tensile specimens from S1 and S2 plate-girders

3.2.3.1 Thicknesses of girder members

Using the steel sections cut out for the tensile specimens, the thicknesses of the flange, web and stiffener of the S1 and S2 of plate-girders were measured using a digital vernier calliper and are given in the Table 3.2.

Table 3.2 Thicknesses of flange, web and stiffener of S1 and S2 plate-girders

Reading No.	S1 plate-girders			S2 plate-girders		
	Thickness (mm)			Thickness (mm)		
	Flange	**Web**	**Stiffener**	**Flange**	**Web**	**Stiffener**
1	12.08	3.16	8.28	12.21	3.05	8.06
2	12.12	3.19	8.27	12.13	3.15	8.16
3	12.14	3.18	8.29	12.10	3.14	8.27
4	12.27	3.24	8.27	12.05	3.12	8.08
5	12.14	3.04	8.26	12.08	3.18	8.12
6	12.34	3.09	8.25	11.96	3.07	8.18
Mean	**12.18**	**3.14**	**8.27**	**12.12**	**3.10**	**8.16**

3.2.3.2 Stress-strain curves of tensile tests

Figure 3.5 shows the stress-strain curves of the steel in flanges, webs and stiffeners of the S1 and S2 plate-girders obtained from the results of the tensile tests.

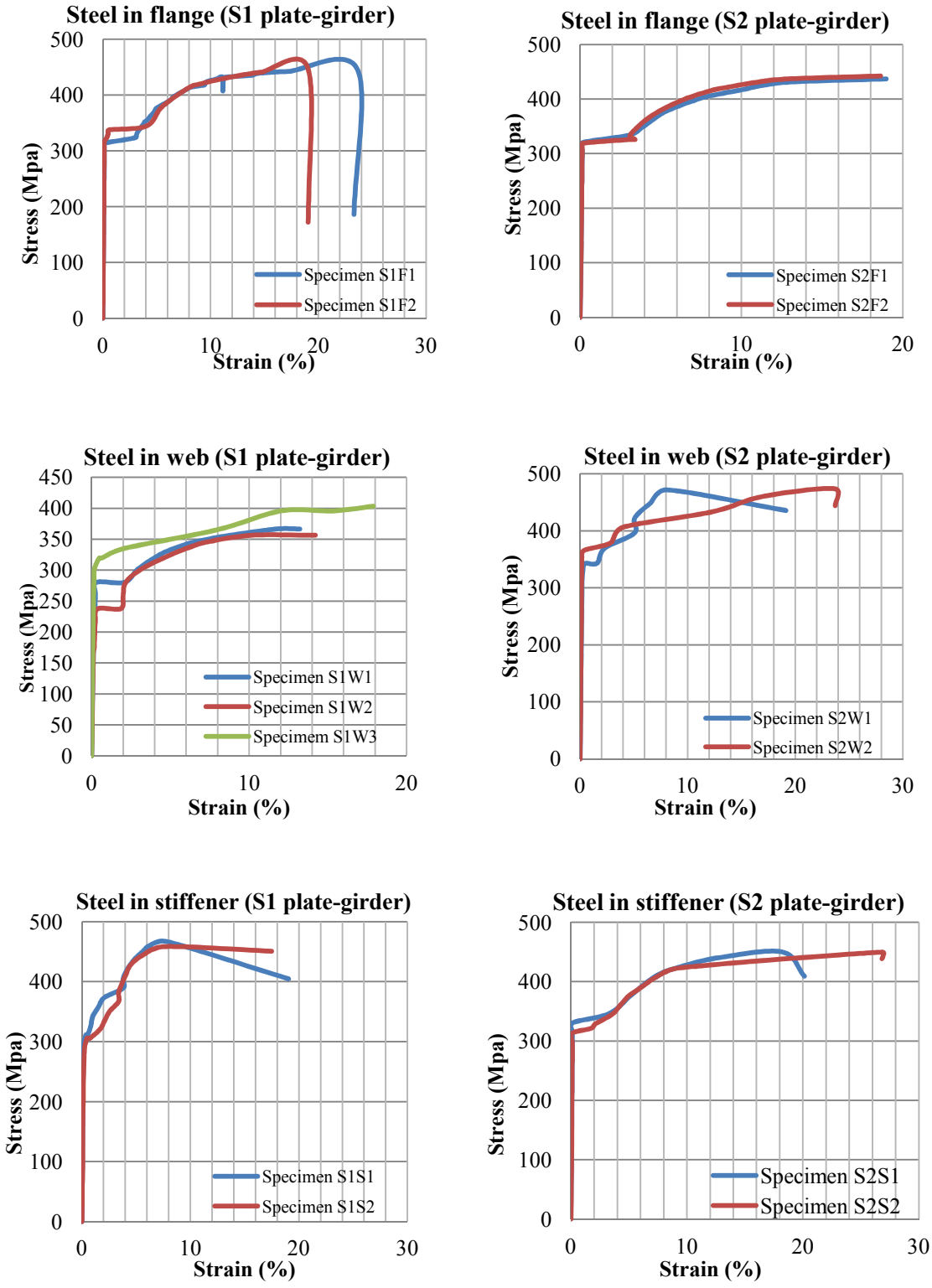

Figure 3.5 Tensile stress-strain curves of the steel in flanges, webs and stiffeners

3.3 Test specimens

As mentioned earlier, all the eight test specimens, B1 to B8, were either un-strengthened or FRP-strengthened end web panels of steel plate-girders. Because of a good agreement between the test and the FEA results of un-strengthened control specimen B1 for the series S1 plate-girders, an FE model of un-strengthened specimen B9 was used as the control for the test specimens using S2 plate-girders. Details of the FE analyses are given in Chapter 5. Brief details of the specimens and the objective of the each test are given in Table 3.3.

Table 3.3 Description and strengthening of test specimens B1 to B8 and FE model B9

Specimen No. (Series)	FRP-strengthening method used	Figure of specimen	Objective of test
B1 (S1)	None	Figure 3.6	Control specimen for S1 plate-girder tests
B2 (S1)	2 vertical GFRP pultruded section stiffeners, one on each side of the web	Figure 3.12	Effectiveness of using the additional GFRP stiffeners in the vertical direction on both sides of web
B3 (S1)	4 layers of carbon fabric on one side of the web only	Figure 3.23	Effectiveness of using carbon fabric sheets for strengthening
B4 (S1)	8 layers of glass fabric on one side of the web only	Figure 3.24	Effectiveness of using glass fabric sheets for strengthening
B5 (S2)	1 vertical GFRP stiffener on one side of the web only	Figure 3.14	Effectiveness of using the additional GFRP stiffener in the vertical direction on one side of web only
B6 (S2)	1 diagonal GFRP stiffener on one side of the web only	Figure 3.16	Effectiveness of using an additional GFRP stiffener in diagonal orientation
B7 (S2)	4 layers of glass fabric on one side of the web only	Figure 3.25	Reduced number of layers of glass fabric to avoid a breakdown of the steel-fabric bond
B8 (S2)	2 vertical GFRP stiffeners, one on each side of the web beneath the load	Figure 3.18	GFRP stiffeners used as replacement of the load-bearing steel stiffeners
B9 (S2)	None	Figure 3.7	Control FE model for S2 plate-girder tests

3.3.1 Grouping of specimens

Based upon the type of FRP strengthening provided to the end web panels, test panels, the specimens have been divided into three groups namely G1, G2 and G3. Table 3.4 shows the test specimens in each of the three groups.

Table 3.4 Grouping of test specimens B1 to B8 and FE model B9

Specimen group	Group description	Specimen No.	Girder series No.
G1	Un-strengthened control specimen/ FE model	B1	S1
		B9	S2
G2	Glass FRP pultruded section strengthened specimens	B2	S1
		B5	S2
		B6	S2
		B8	S2
G3	FRP fabric strengthened specimens	B3	S1
		B4	S1
		B7	S2

3.4 Group G1 specimens

Group G1 comprised the control specimen B1 for the S1 girder tests and the control FE model B9 for the S2 girder tests, with un-strengthened end web panels.

3.4.1 Control specimen B1

The objective of testing a control specimen was to determine its ultimate load and to identify the behaviour of an un-strengthened steel girder. The results are a benchmark for comparisons with the FRP-strengthened specimens.

The control specimen, B1, was an un-strengthened steel web panel at one end of a S1 steel plate-girder surrounded by the top and bottom flanges and two steel stiffeners, Figure 3.6.

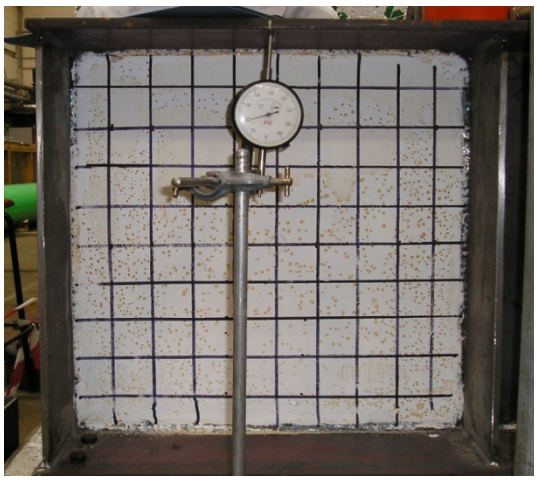

Figure 3.6 Control specimen B1 for S1 plate-girders

3.4.2 Control FE model B9

Since there was only a small increase in the length of the S2 steel plate-girders compared to the S1 plate-girders, a control specimen was not tested for the S2 girder tests. However, after the tensile tests, it was observed that there was a significant difference in the material properties, especially in the yield strength of the webs of the S1 and S2 plate-girders. Therefore, a direct comparison of S2 specimens with the S1 control specimen B1 was not possible. Hence, for comparison of the test results of the S2 specimens, a model of an un-strengthened control specimen B9, Figure 3.7, was analysed using the LUSAS FE program. Full details of the model are given in the Chapter 5 of the FE analyses.

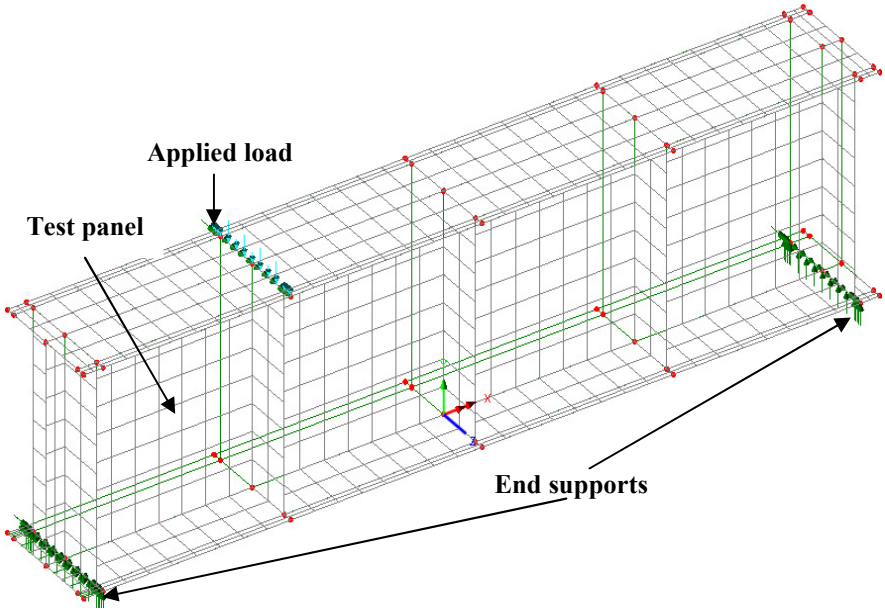

Figure 3.7 FE model of control specimen B9 for S2 plate-girders

3.5 Group G2 specimens

Group B2 comprised the four specimens B2, B5, B6 and B8 which were strengthened using GFRP pultruded T-section stiffeners either on one or both sides of the web.

3.5.1 FRP-strengthening of G2 specimens

For the FRP-strengthening of the G2 specimens, the T-section stiffeners were cut from GFRP pultruded T or I section profiles and were bonded to the end web panels of the steel plate-girders using a two-component epoxy adhesive. The advantages of this type of FRP-strengthening include the minimum amount of surface preparation due to small area of bonding, easy clamping of the GFRP stiffeners after bonding to ensure a better bond and less chances of breakdown of the bond between GFRP and the steel. The main disadvantage is putting a rigid stiffener on to an uneven surface.

3.5.1.1 GFRP pultruded T and I-section profiles

The GFRP pultruded T-section composite profiles were 41.1 mm wide by 25.3 mm deep, Figure 3.8, and were manufactured by Strongwell Corporation, Bristol, Virginia USA and supplied by Pipex Limited, Plymouth, UK. The stiffeners obtained from these sections were used in the strengthening of the specimen B2.

The GFRP pultruded I-section composite profiles were 152 mm wide by 152 mm deep, Figure 3.8, and were manufactured and supplied by DURA Composites Limited, Essex, UK. The stiffeners obtained from these sections were used in the strengthening of the specimens B5, B6 and B8.

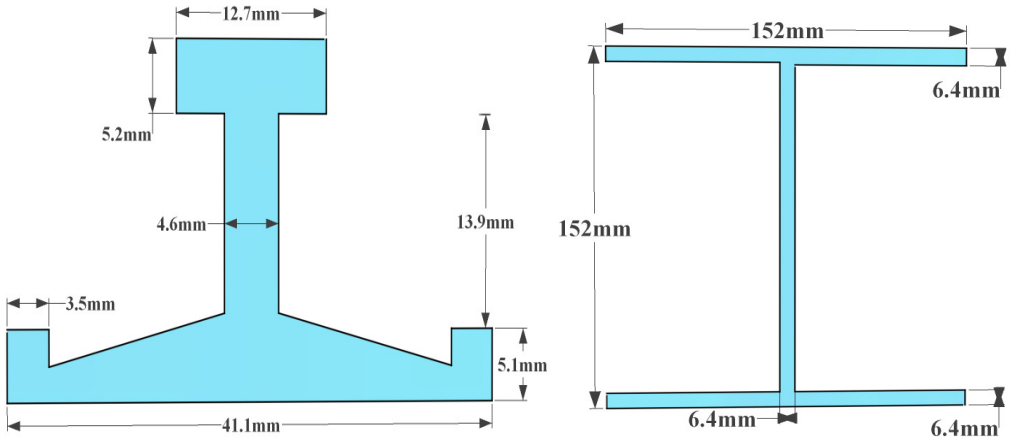

Figure 3.8 GFRP pultruded T and I-section profiles (Not to scale)

3.5.1.2 Testing of GFRP sections

To determine the ultimate strength and modulus of elasticity of GFRP sections, the specimens were taken from the webs and flanges of the GFRP sections and were cut to size, Figure 3.9(a), and tested in accordance with the ASTM standards (D3039/D 3039M-08, 2008). During the tensile testing in the Instron machine, the GFRP specimens either slipped or cracked at the grips before the failure. Of a number of specimens tested, the results of the only three specimens could be obtained, Figure 3.9(b), and were used to determine the modulus of elasticity. For determining the ultimate strength, flat plate specimens were tested. The specimens for the tensile tests were 350 mm long and 20 mm wide by 4 mm thick and those for the compression tests were 40 x 40 mm in section and 6.2 mm thick. The properties of the GFRP pultruded sections are given in Table 3.5.

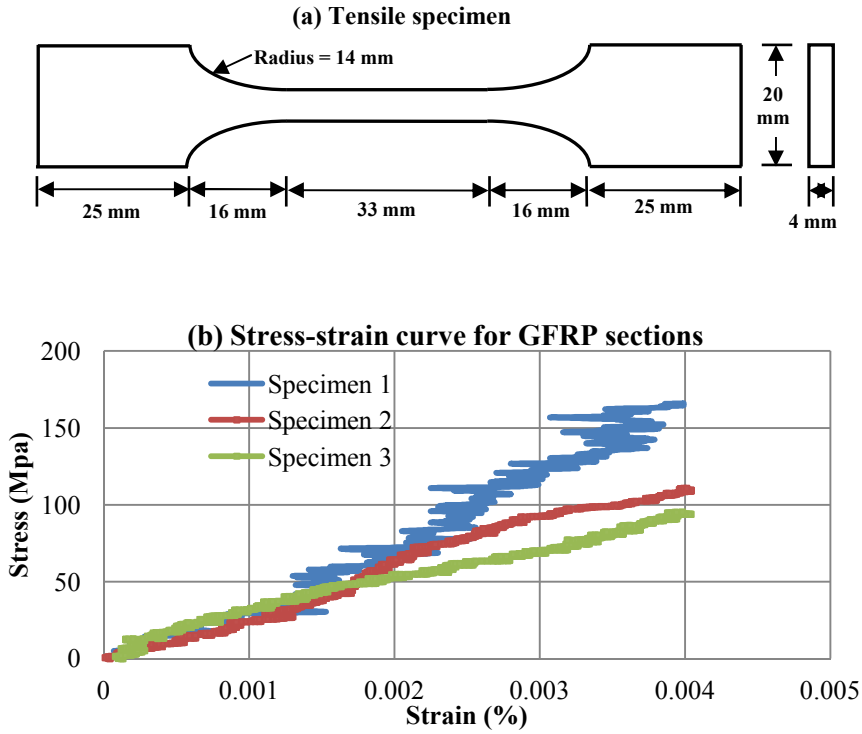

Figure 3.9 (a) Tensile specimen and (b) stress-strain curves of GFRP pultruded sections

Table 3.5 Properties of GFRP pultruded T and I-sections (DURADRID T-3500, 2010) and (DURA RAL7001, 2012)

Name of property		GFRP T-section	GFRP I-section
Ultimate strength (MPa)	Tensile	350-400**	350-400**
	Compressive	---	200-250**
Modulus of elasticity (GPa)		36**	36**
Poisson's Ratio		0.15*	0.15*
Density (Kg/m^3)		1700*	1600-2100*

* Value supplied by manufacturer ** Test values obtained by author

3.5.1.3 Plio-Grip epoxy adhesive

A two-component epoxy, Plio-Grip® 7770/220 high strength structural adhesive, comprising a resin and hardener was used to bond the GFRP pultruded section stiffeners to the webs of the steel plate-girders. The adhesive was selected because of its good resistance to the elevated temperatures, moisture, most solvents and chemicals. It has long opening and painting times and can also be applied in a thick bond line. It was manufactured by Ashland Performance Materials, Dublin, USA. The properties of the adhesive as supplied by the manufacturer are given in Table 3.6.

Table 3.6 Properties of Plio-Grip epoxy adhesive
(PLIO-GRIP 7770/220, 2011)

Tensile strength (MPa)	29
Modulus of Elasticity (GPa)	1.184
Density (Kg/m^3)	1230
Elongation at failure (%)	63
Open time (minutes)	30
Working time (minutes)	45
Colour	Green
Sanding/painting time	150 minutes

As supplied by the manufacturer

3.5.1.4 Surface Preparation

Before bonding the GFRP pultruded section stiffeners to the end web panels of the steel plate-girders, the required areas of the steel surface and the GFRP pultruded sections were prepared. The steel surface was first cleaned using coarse sand paper followed by a steel brush. It was then ground with the help of an angle grinder using a grinding disc at an angle of approximately 45^o. The steel surface was ground until its colour was apparently changed to silver, Figure 3.10. The disc is used for general purpose grinding on metals and was of grade A30RBF and 100 mm in diameter. To enhance bonding, the glazed surface of the pultruded sections was removed and irregular scratches were made using a machine belt with a surface finish of 150 grits. Grit measures the number of scratches per linear inch of abrasive pad. Both surfaces were finally cleaned with acetone to remove residual particles in order to prepare the surfaces for bonding.

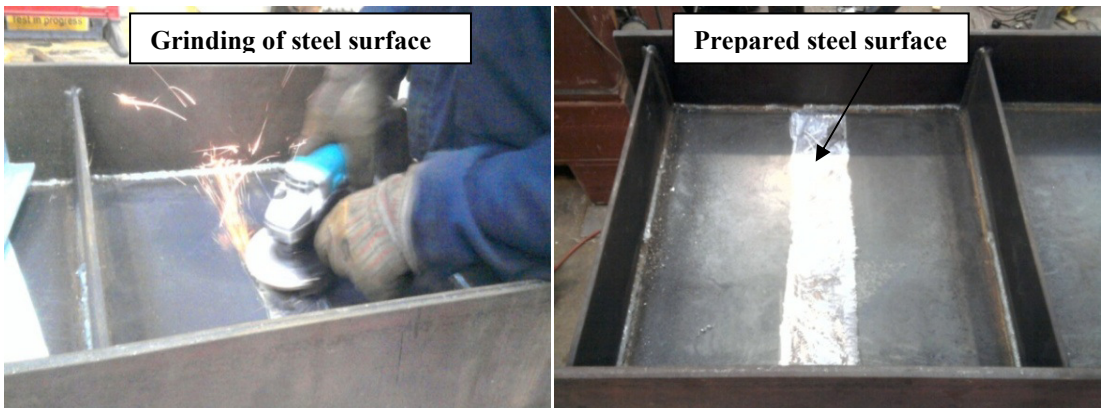

Figure 3.10 Grinding of steel surface and prepared steel surface for bonding GFRP pultruded section stiffener

3.5.1.5 Bonding

A mixture of epoxy resin and the hardener to a ratio of 1:1 was obtained using a plastic mixer. The mixer was attached to the epoxy cartridge and both were mounted in a gun. The epoxy adhesive was then applied to the cleaned steel and GFRP surfaces using the gun, Figure 3.11. Each of the GFRP stiffeners was positioned in the desired location on the prepared steel surface keeping a distance of approximately 8 mm from the flanges to allow for the 6 mm welds at the flange/web juncture, Figure 3.11. The GFRP stiffener was then clamped using a grooved wooden plank and two steel clamps. The steel clamps were hand-tightened and were removed after remaining in the tightened position for a minimum time period of 72 hours for the epoxy to cure.

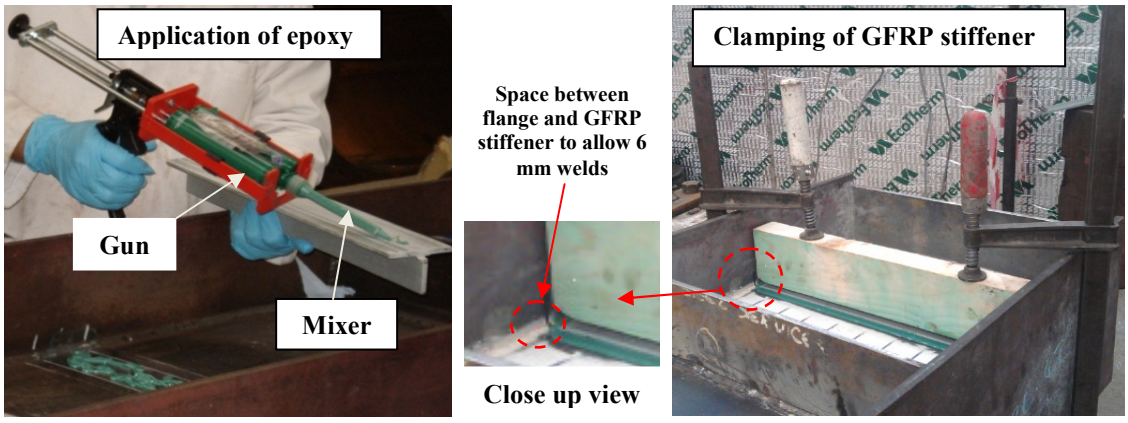

Figure 3.11 Application of epoxy adhesive and clamping of GFRP pultruded section stiffener after bonding

3.5.2 Specimen B2 (two vertical GFRP stiffeners)

Specimen B2 was the end web panel of an S1 steel plate-girder and was strengthened using two vertical GFRP pultruded T-section stiffeners, approximately 25 mm wide by 40 mm deep, one on each side of the web, Figure 3.12. The stiffeners were obtained by cutting to size a GFRP pultruded T-section composite profile, Figure 3.8.

It has been described in Chapter 1 that in order to minimize the intensity of shear and peel stresses in adhesives at ends of the adherend, the ends of FRP pultruded sections should be tapered to the angle of 30 degrees or less (Lang, 2008). Linear eigenvalue analyses of a simply supported plate with the intermediate GFRP stiffeners with the ends tapered between the angles of 20 to 30 degrees were carried out and a small difference of less than 2% in the FEA elastic critical loads of the plate was obtained. Since the intensity of shear and peel stresses in adhesives at ends of the GFRP stiffeners could be decreased by reducing the angle of the stiffeners, the ends of the GFRP stiffener were tapered to an angle of approximately 20 degrees, Figure 3.13.

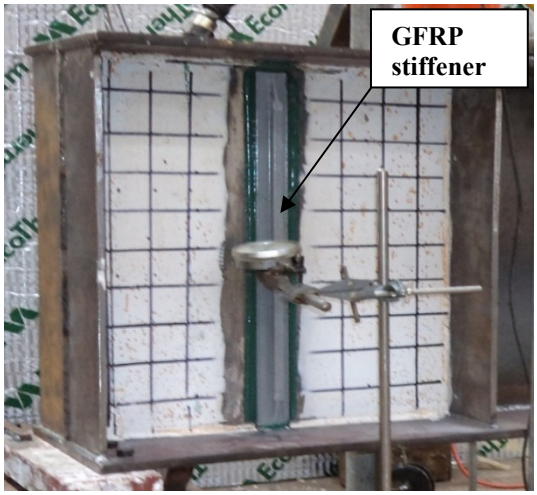

Figure 3.12 GFRP-strengthened specimen B2

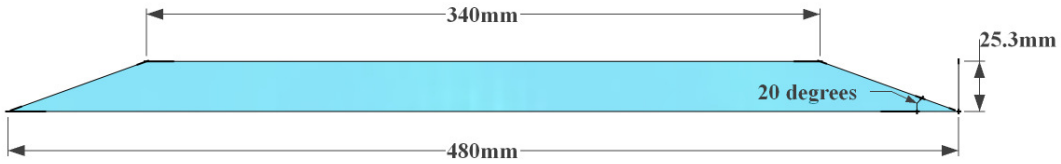

Figure 3.13 Longitudinal section of GFRP stiffener used in specimen B2

3.5.3 Specimen B5 (one vertical GFRP stiffener)

Specimen B5 was the end web panel of an S2 steel plate-girder and was strengthened using one vertical GFRP pultruded T-section stiffener, 80 mm wide by 50 mm deep, on one side of the web, Figure 3.14. The stiffener was obtained by cutting to size a GFRP pultruded I-section composite profile, Figure 3.8. To reduce the shear and peel stresses in the adhesive at ends of the GFRP stiffener, the ends were tapered to an angle of approximately 20 degrees, Figure 3.15. The stiffness, EI, of the GFRP stiffener was about 1.30 times the combined stiffness of two GFRP stiffeners used in the specimen B2, Appendix-A.

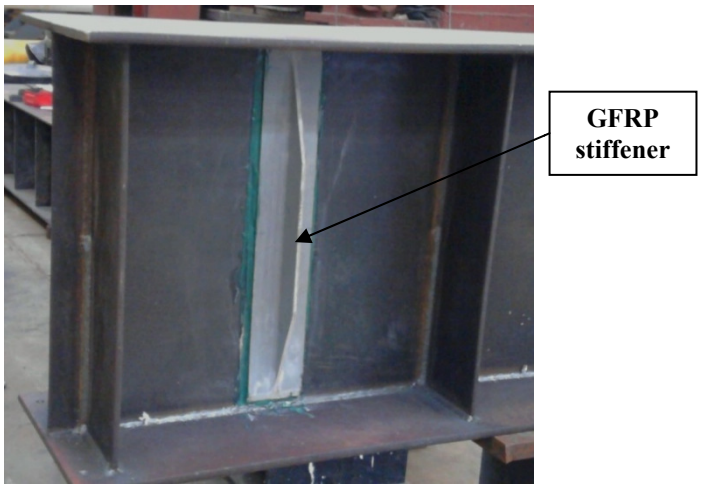

Figure 3.14 GFRP-strengthened specimen B5

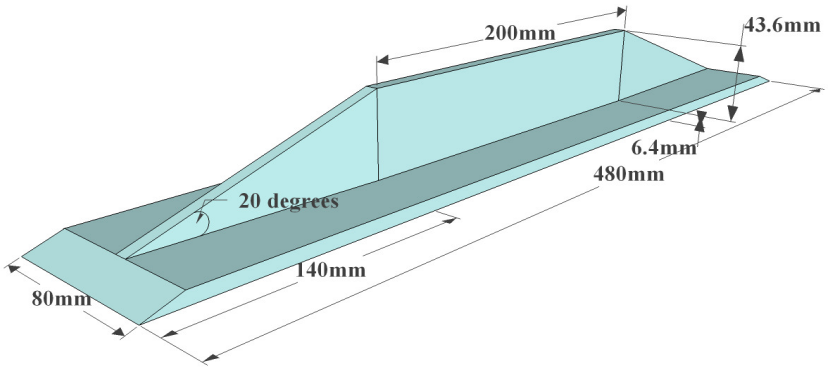

Figure 3.15 Vertical GFRP pultruded section stiffener used in specimen B5

3.5.4 Specimen B6 (one diagonal GFRP stiffener)

Specimen B6 was the end web panel of an S2 steel plate-girder with a diagonal GFRP pultruded T-section stiffener, 80 mm wide by 50 mm deep, on one side of the web, Figure 3.16. The stiffener was obtained by cutting to size a GFRP pultruded I-section composite profile, Figure 3.8. In order to fit into the steel web panel, the flange of the

stiffener was cut to an angle of approximately 45 degrees at all four ends, Figure 3.17. The flange length was also reduced by 7.5 mm at both ends, compared to the web; in order to allow for the 6 mm welds at the flange/web juncture in the plate-girder.

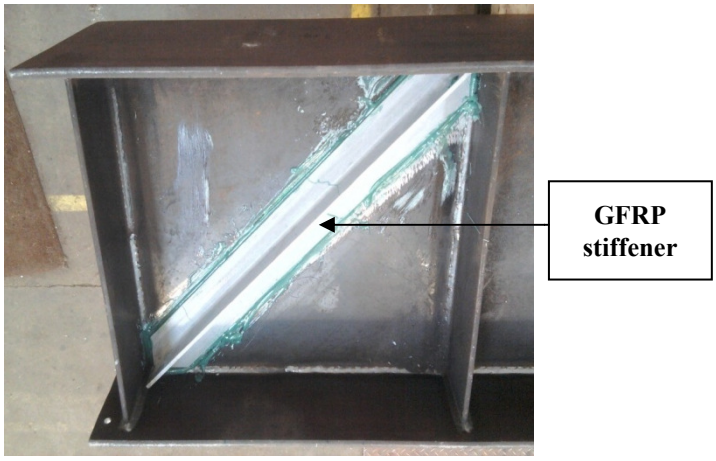

Figure 3.16 GFRP-strengthened specimen B6

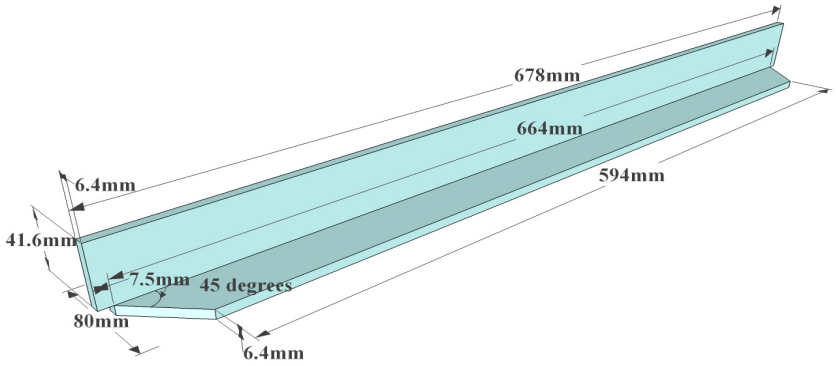

Figure 3.17 Diagonal GFRP pultruded section stiffener used in specimen B6

3.5.5 Specimen B8 (load-bearing GFRP stiffeners)

Specimen B8 was strengthened using two GFRP T-section stiffeners, 80 mm wide by 50 mm deep, on both sides of the web of an S2 plate-girder beneath the applied load, Figure 3.18, at the same place of the load-bearing steel stiffeners in the FE model B9. The ratio of stiffness, EI, of each of the two GFRP stiffeners used in B8 to that of the steel stiffener in B9 was approximately 1:43, Appendix-A. The GFRP stiffeners were obtained by cutting to size a GFRP pultruded I section composite profile, Figure 3.8. The flanges at the ends of each of the two GFRP stiffeners were reduced by 7.5 mm in order to allow for the 6 mm welds at the flange/web juncture in the plate-girder as shown in Figure 3.19.

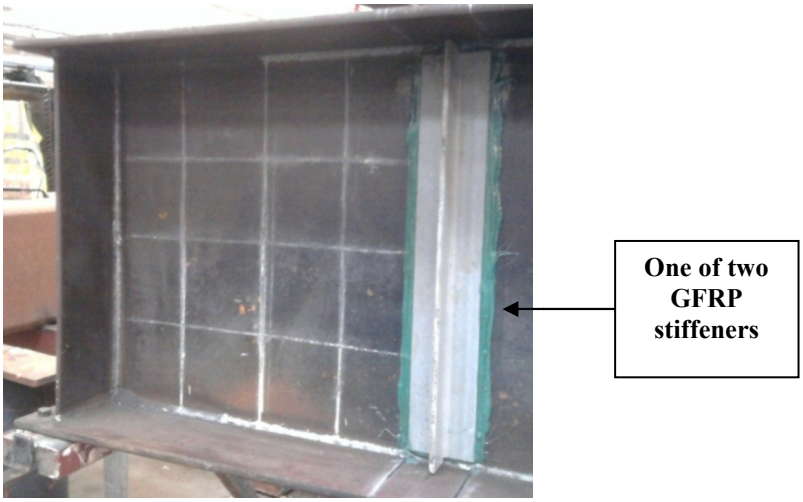

Figure 3.18 Specimen B8 with GFRP stiffeners beneath applied load

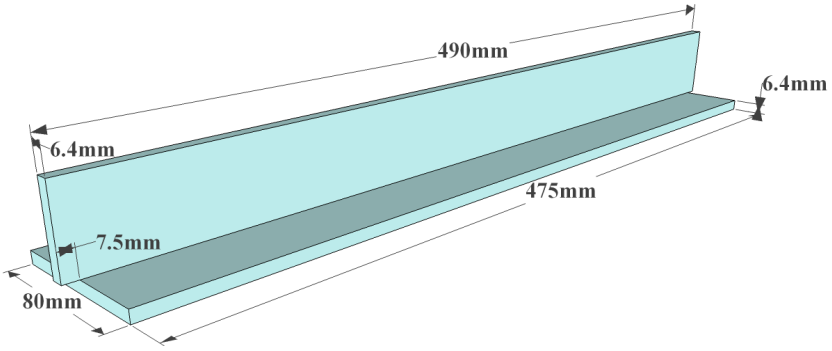

Figure 3.19 Vertical GFRP pultruded section stiffener used in specimen B8

3.6 Group G3 specimens

Group B3 comprised the three specimens B3, B4 and B7 which were strengthened using either four or eight layers of carbon or glass fabric on one side of the web in the end web panels.

3.6.1 FRP-strengthening of G3 specimens

In FRP-strengthening of the G3 specimens, the carbon or glass FRP fabric sheets were cut to a size of 480 mm x 480 mm to fit into the web panel of the steel plate-girder and were bonded to the web using two-component epoxy adhesive. The advantages of this type of the FRP-strengthening include less effort for the cutting of the FRP fabric sheets and their easy application on to the steel surface. The disadvantages include the requirement of preparation of the entire steel surface for bonding, the requirement of ensuring an effective bond by use of a roller on the FRP fabric layers after application of the adhesive and the difficulty of clamping the fabric layers after bonding. There is also a significant chance of breakdown of the bond between the FRP and the steel due to the different shear stress distributions in two materials when loaded.

3.6.1.1 Carbon and glass fabric sheets

The carbon and glass fabric composite sheets were manufactured and supplied by Walker Technical Resources Limited, Aberdeen, UK. Both fabrics had three-axial layup of woven fibres. In the three-axial layup, the main fibres are woven along the longitudinal axis of the fabric sheets and carry the axially applied load. The secondary fibres are woven in such a way to maintain distance between the main fibres and provide lateral support to them. In both the carbon and glass fabric sheets, the direction of the main fibres was parallel to the longitudinal axis of the fabric sheets. The directions of two secondary fibres were mutually perpendicular to each other and at angles of 45 and 135 degrees to the main fibres, Figure 3.20.

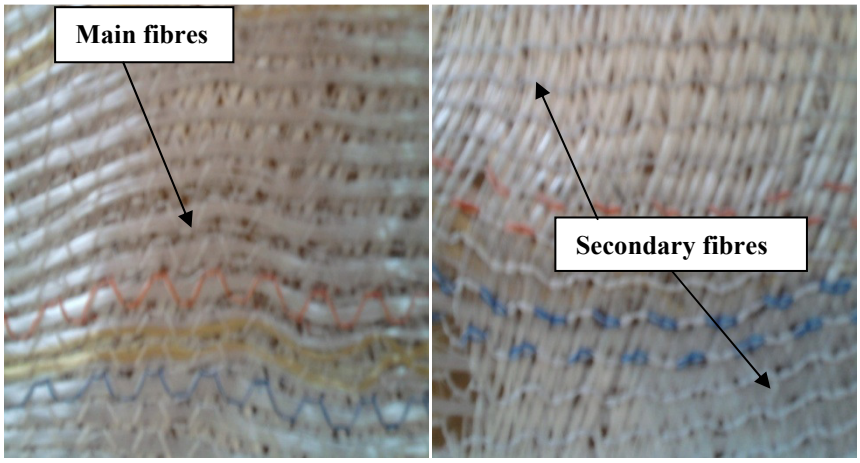

Figure 3.20 Three-axial lay-up of fibres in glass fabric sheet

The carbon fabric sheets were 1.1 mm thick by 1250 mm wide and 3 m long and were used to strengthen the end web panel of the specimen B3. The glass fabric sheets were 0.8 mm thick by 650 mm wide and 8.3 m long and were used to strengthen specimens B4 and B7. The properties of the carbon and the glass fabric sheets (with resin) as provided by the manufacturer are given in Table 3.7.

3.6.1.2 Technowrap-2K epoxy adhesive

A two-component epoxy, Technowrap-2K structural adhesive, comprising a resin and hardener was used to bond the carbon and glass fabric layers to the end web panels of the steel plate-girders. It was also manufactured and supplied by Walker Technical Resources Limited, Aberdeen, UK. The epoxy adhesive was prepared by mixing the resin and the hardener with a ratio of 5:1 by weight and stirred thoroughly for 2-3 minutes in accordance with the manufacturer's instructions. During mixing and the

application, the temperature of the adhesive mixture was kept between 25 to 50^{o}C. The adhesive mixture was applied within 10 minutes because it had very short setting time of 15 minutes; this is because it is generally used for repair works in the North Sea where accelerated curing is required. Properties of Technowrap-2K epoxy adhesive as provided by the manufacturer are given in Table 3.8.

Table 3.7 Properties of carbon and glass fabric sheets with resin (Technowrap 2K^{TM}, 2011) and (Technowrap^{TM} structural strengthening, 2011)

Name of property	**Carbon fabric**	**Glass fabric**
Tensile strength (MPa)	530	104
Tensile modulus (GPa)	36	13
Tensile strain at failure (%)	1.5	1.27
Shear modulus (GPa)	3.3	2
Poisson's ratio	0.32	0.27
Glass transition temperature T_g (^{o}C)	120	120

As supplied by the manufacturer

Table 3.8 Properties of Technowrap-2K epoxy adhesive (Technowrap-2K, 2011)

Tensile strength (MPa)	70
Modulus of Elasticity (GPa)	3.3
Density(Kg/m^3)	1050-1160
Elongation at failure (%)	2.1
Glass transition temperature T_g (^{o}C)	60
Colour	Resin: Light (or pale) yellow Hardener: Amber
Solubility	Soluble in water

As supplied by the manufacturer

3.6.1.3 Surface preparation

The preparation of the steel surface on one side of whole web in the end web panel was carried out in the same way as done in case of the G2 specimens.

3.6.1.4 Bonding

The adhesive mixture was spread on the prepared steel surface of the web in the test panel. The first layer of fabric sheet was placed keeping the direction of the main fabric fibres normal to the longitudinal axis of the plate-girder. For effective bonding, the layer was compressed with the help of a steel roller and the edges were compressed with a relatively small wooden roller, Figure 3.21. The second layer was applied keeping the direction of the main fibres parallel to the longitudinal axis of the plate-girder and rolled similarly. It was left for 45 to 60 minutes to become tacky before application of the next layer. The process was repeated for every two layers until the required number of layers had been applied. In specimens B3 and B4, the adhesive was also spread over the top surface of the final layer. In specimen B7, the top surface of the final layer was covered with a film and was compressed using a wooden board and steel clamps, Figure 3.22, for 72 hours while the epoxy cured.

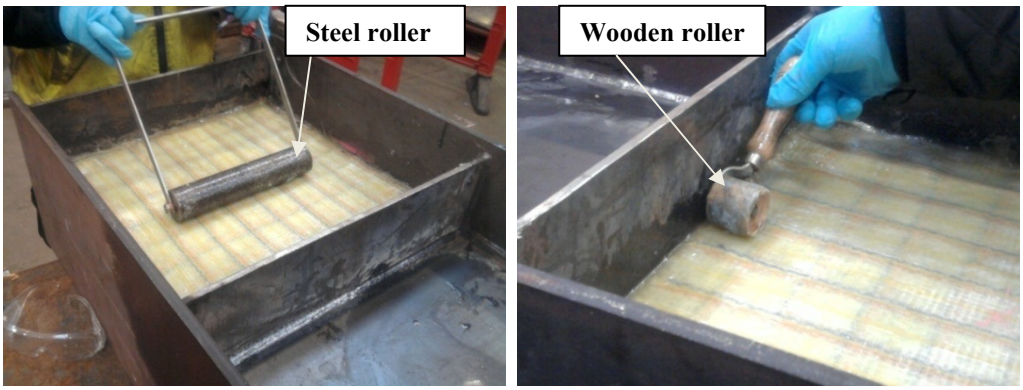

Figure 3.21 Compressing bonded layers of fabric sheets with steel and wooden rollers

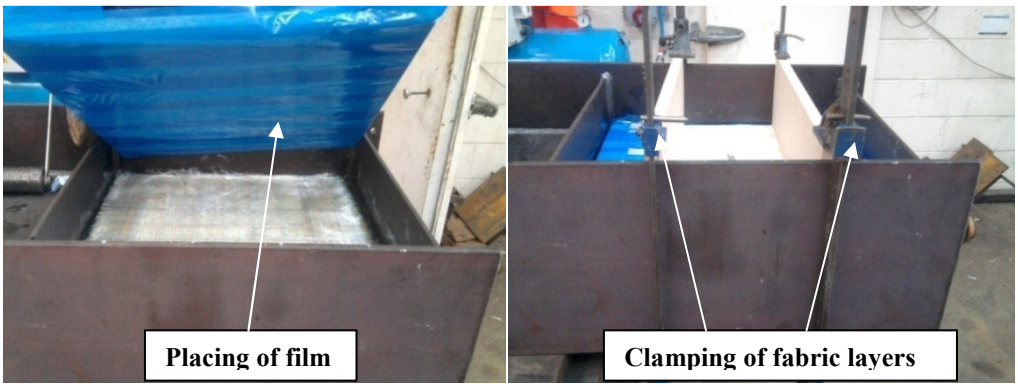

Figure 3.22 Placing film coating and clamping of glass fabric layers of specimen B7

3.6.2 Specimen B3 (4 layers of carbon fabric)

In specimen B3, four layers of the carbon fabric were applied to one side of the web in the end web panel of an S1 plate-girder, Figure 3.23. Each of the four applied layers was 480 mm x 480 mm in size and was cut from carbon fabric sheets, 3 m long and 1.1 mm thick by 1250 mm wide. The total thickness of the carbon fabric layers was approximately 6.2 mm.

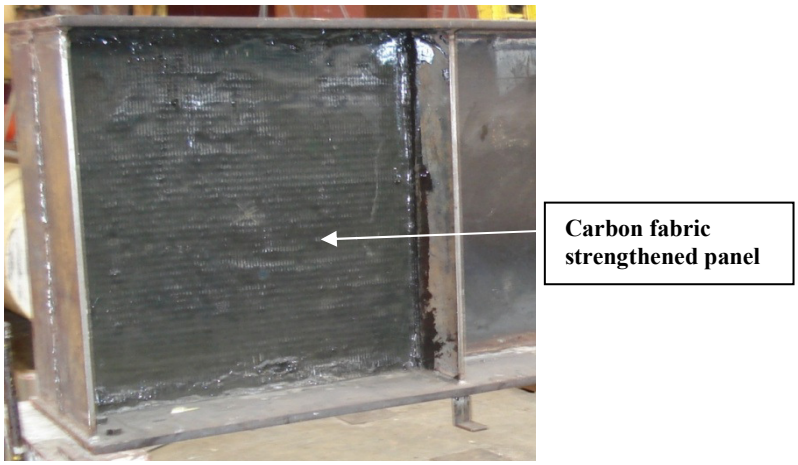

Figure 3.23 Carbon fabric-strengthened specimen B3

3.6.3 Specimen B4 (8 layers of glass fabric)

In specimen B4, eight layers of the glass fabric were applied to one side of the web in the end web panel of an S1 plate-girder, Figure 3.24. Since, it was less stiff than the carbon fabric, so eight layers of the glass fabric were used. Each layer was 480 mm x 480 mm in size and was cut from glass fabric sheets, 8.3 m long and 0.8 mm thick by 650 mm wide. The total thickness of the glass fabric layers was approximately 10.5 mm.

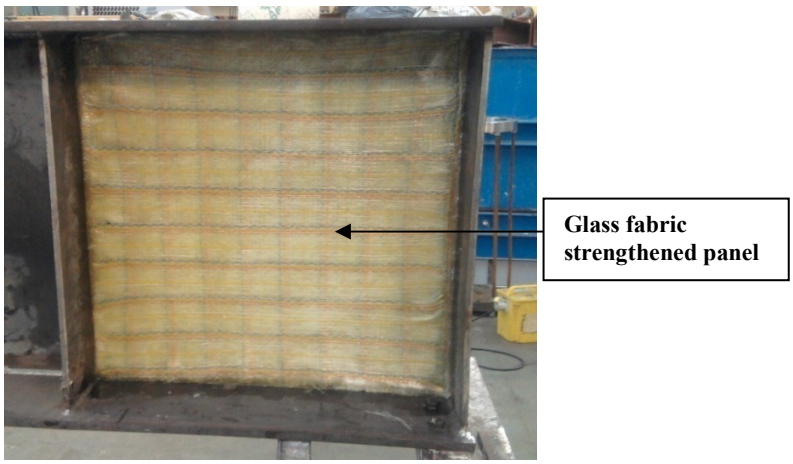

Figure 3.24 Glass fabric-strengthened specimen B4

3.6.4 Specimen B7 (4 layers of glass fabric)

Specimen B7 was strengthened using four layers of the glass fabric sheets which were applied to one side of the web in the end web panel of an S2 plate-girder, Figure 3.25. The objective of the test was to achieve an increase of approximately 30% in the ultimate load of the glass fabric-strengthened specimen, compared to that of the control specimen without a breakdown of the steel-fabric bond. Each of the four applied layers was 475 mm x 475 mm in size and was cut from 8.3 m long and 0.8 mm thick by 650 mm wide glass fabric sheets. The total thickness of the glass fabric layers was approximately 4 mm. Clamping of the fabric layers for 72 hours after their application was used to help in obtaining a better bond.

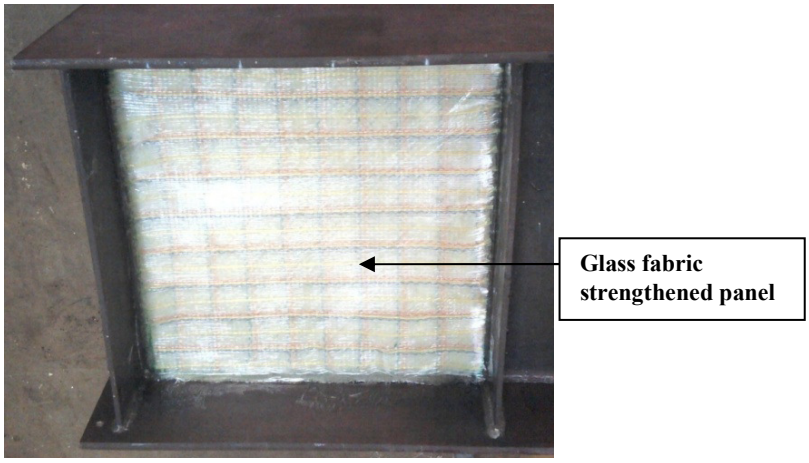

Figure 3.25 Glass fabric-strengthened specimen B7

3.7 Testing procedure

3.7.1 Test set up

All the specimens were tested in the same purpose built test rig, Figure 3.26. The load was measured using a 500 kN load cell which was reacted against a square box section steel girder, 250 x 250 x 12.5 mm in section and 750 mm long. The reaction was resisted by two steel Lee Macalloy bars, 2400 mm long and 35 mm in diameter with 450 mm threaded length on both ends. The top ends of the bars were bolted after passing through the box girder, while the bottom ends were bolted after passing through the 500 mm thick concrete strong floor.

The Lee Macalloy bars also passed through two 1000 mm long vertical circular steel hollow sections between the box girder and the concrete strong floor. The circular hollow sections were welded to a 2500 mm long horizontal steel U-girder, which was

bolted to the strong floor at its ends and at 500 mm from the each end. Inclined circular hollow sections were welded to the horizontal U-girder and top of the vertical circular hollow sections. This frame provided lateral support to the Macalloy bars to avoid sway which could cause the system to become unstable.

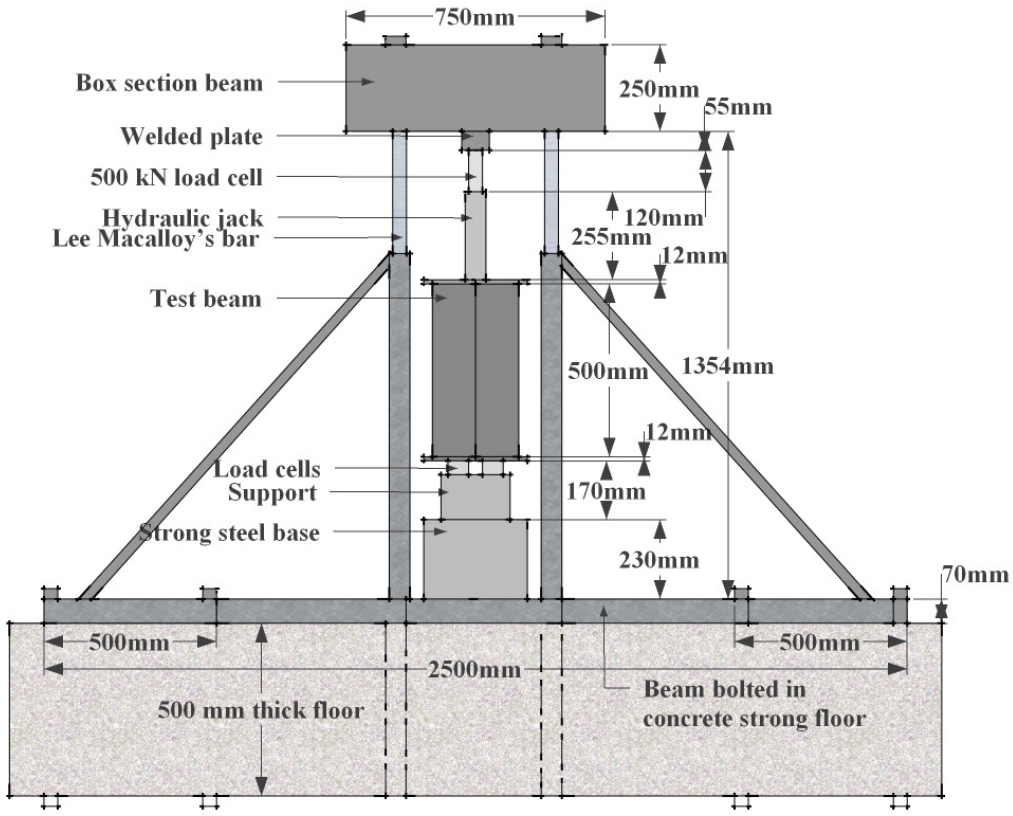

Figure 3.26 Test Rig

3.7.2 Loading and boundary conditions

The ends of the plate-girders were placed on two supports, Figure 3.27. The support near the test web panel was such that it restrained the girder vertically and horizontally, but was free to rotate. The other support restrained the girder vertically only and was therefore free to rotate and move horizontally. Both the supports rested on strong steel bases. Two 200 kN electronic load cells were placed between each of the supports and the girder to measure the end reactions. Use of two load cells was to avoid lateral instability of the girder.

In the tests of all specimens except B8, the load was applied to the plate-girder across its flange just above the second steel stiffeners in such a way that the test web panel was subjected to three times the load acting on rest of the girder. In the specimen B8, the

load was also applied at the same position just above GFRP stiffeners in a similar way. The load was applied incrementally at load intervals of approximately 20 to 50 kN. The duration of the loading for each test was between 2 to 4 hours. The load was cycled a few times to about half of the estimated ultimate load before finally loading the test specimen up to the ultimate load. The applied load and the end reactions were recorded at each load level.

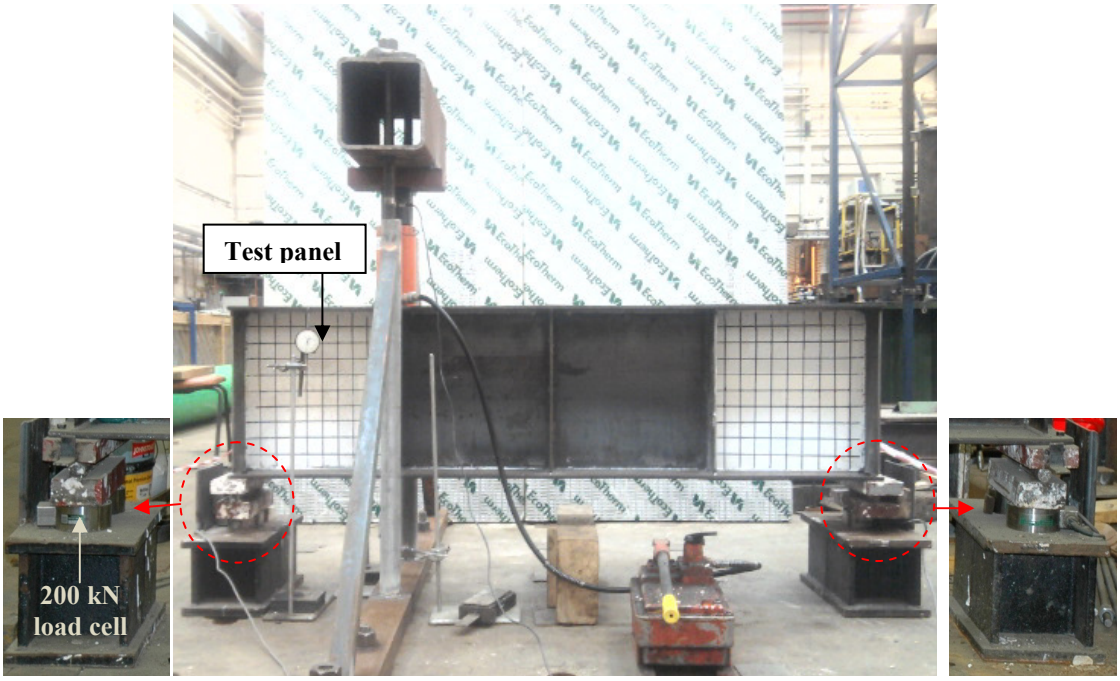

Figure 3.27 Loading and boundary conditions of control specimen

3.7.3 Instrumentation

The results to be obtained from the tests were the ultimate loads and load-deflection responses of specimens. Load cells and dial gauges were therefore used to measure the load increments and displacements (deflections) respectively without any installation of strain gauges. Four dial gauges were used to measure deflections of the control specimen B1, one at centre of the test web panel to measure lateral deflection of the web, one under the first internal steel stiffener to measure vertical deflection of the plate-girder and one under each of both ends, A and B, of the girder to measure vertical displacements, Figure 3.28. The vertical deflections of the girder ends were found, as expected, to be very small, less than 4 mm largely due to the settlement or bedding of the girder ends as shown in Figure 3.29. A Nobel digital readout was attached to the load cell placed on the hydraulic jack and an RDP transducer indicator E308 was attached to each of the four load cells beneath the girder ends to display the applied load and end reactions of the plate-girders respectively.

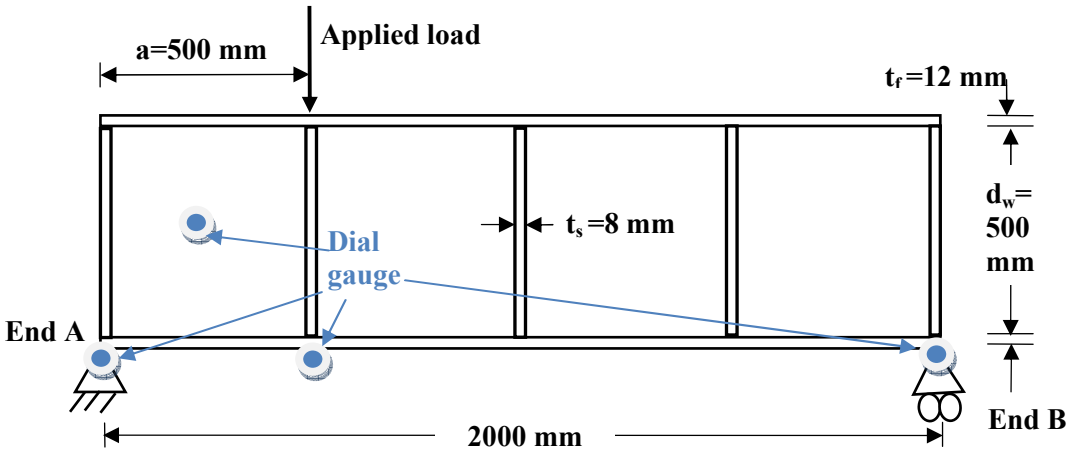

Figure 3.28 Positions of dial gauges in the test of control specimen B1

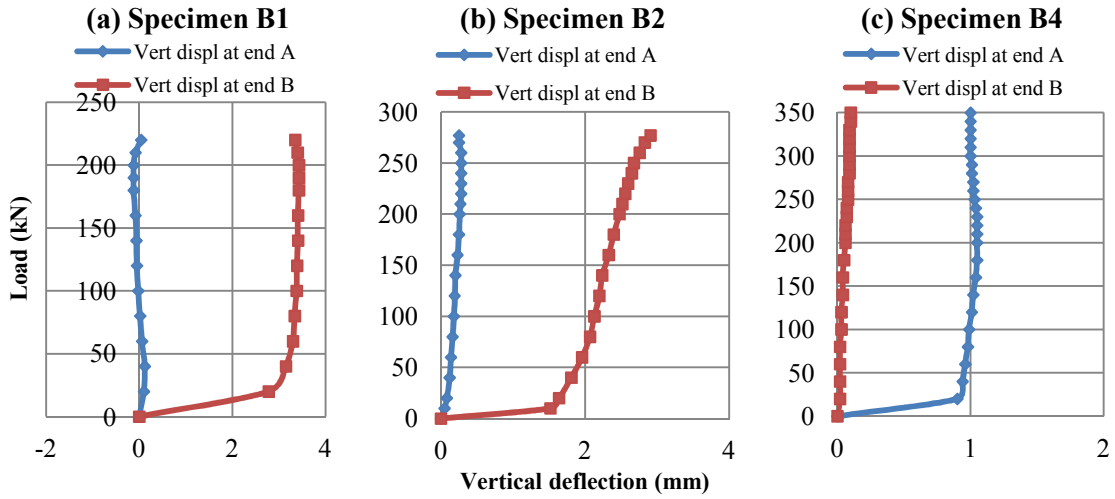

Figure 3.29 Loads vs vertical displacements of girder ends of specimens B1, B2 and B4

3.8 Specimen-wise results of tests

3.8.1 Control specimen B1

The load was cycled twice from zero to approximately 160 kN before finally applying the load to the failure of the specimen. The load was applied in increments of approximately 20 kN each up to 180 kN and then in 10 kN increments. Loads and dial gauge readings were recorded at each of these increments.

Figure 3.30 shows the finally applied load versus vertical deflection at the underside of the plate-girder beneath the loaded stiffeners and Figure 3.31 shows the load versus lateral deflection at the centre of the test panel of the specimen B1. The vertical and lateral deflections increased linearly with the applied load. After a load of approximately 180 kN, the vertical and lateral deflections however were observed to

undergo comparatively larger displacements at each load increment. The web of the end web panel, test panel, was observed to buckle out-of-plane diagonally between the applied loads of 180 to 200 kN. The plate-girder was finally able to carry an ultimate load of 230 kN and failed with an out-of-plane diagonal buckling of the web in the test panel followed by tension field action and development of four plastic hinges, two in the top flange and one each in the bottom flange and the external steel stiffeners, Figure 3.32. One plastic hinge in the top flange developed at the left end and the other at a distance of approximately 250 mm from it. The plastic hinge in the bottom flange developed at right end and that in the external stiffeners at distance of approximately 180 from the top corner of the girder.

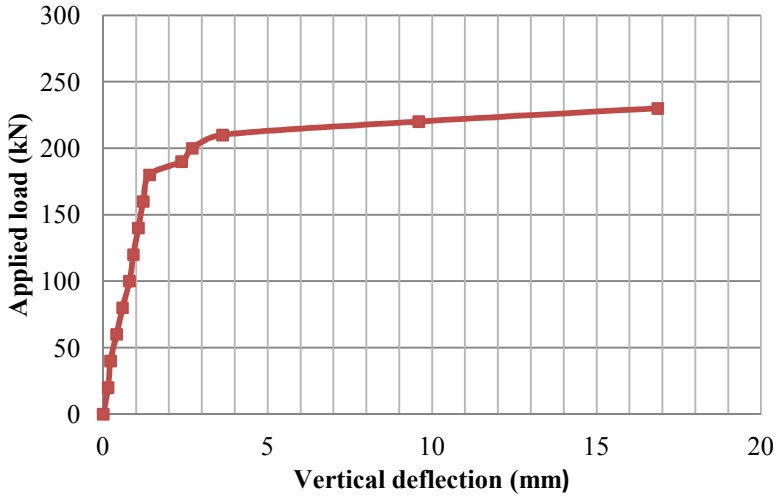

Figure 3.30 Load vs. vertical deflection at the underside of loaded stiffeners of control specimen B1

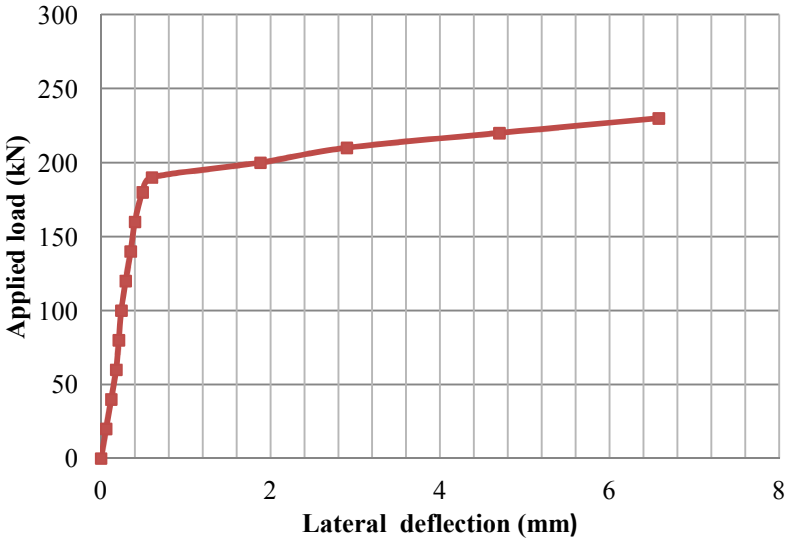

Figure 3.31 Load vs. lateral deflection at the centre of end web panel of specimen B1

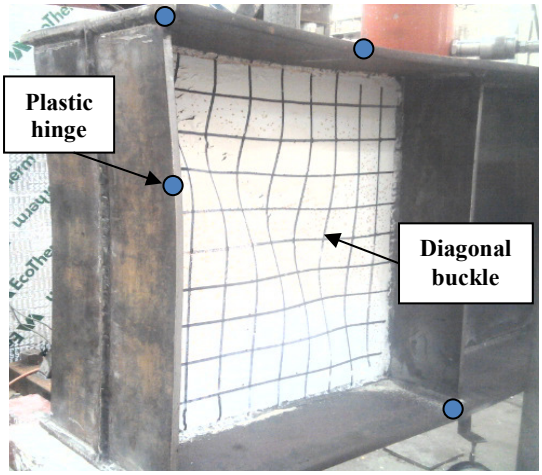

Figure 3.32 Control specimen B1 after failure

3.8.2 Control FE model B9

Figure 3.33 shows the applied load versus vertical deflection at the underside of the plate-girder beneath the loaded stiffeners and Figure 3.34 shows the load versus lateral deflection at the centre of the test panel of the model obtained from the FE analyses. It can be seen that the vertical deflections increased linearly with the applied load up to the ultimate load of 295 kN, then increased as the load dropped to approximately 278 kN and thereafter the vertical deflections increased without any increment in the applied load. The lateral deflections also increased with the applied load up to the ultimate load of 295 kN, but the relationship was not quite linear.

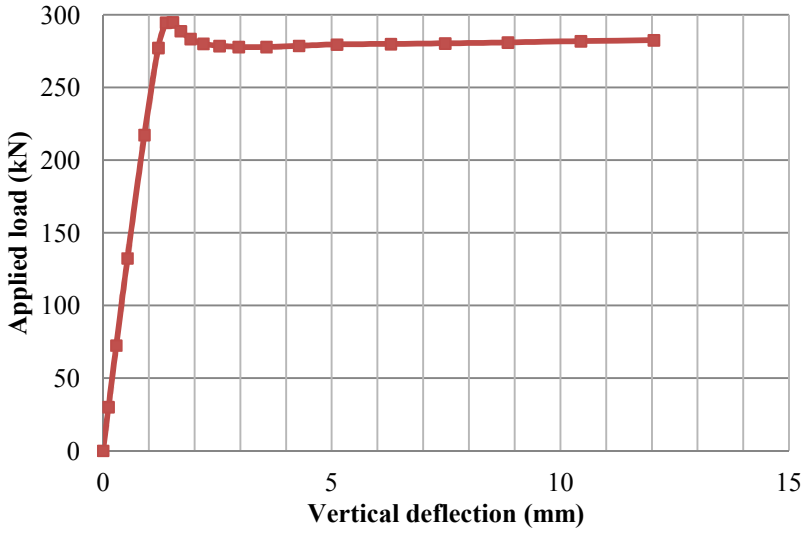

Figure 3.33 Load vs. vertical deflection at the underside of loaded stiffeners of control FE model B9

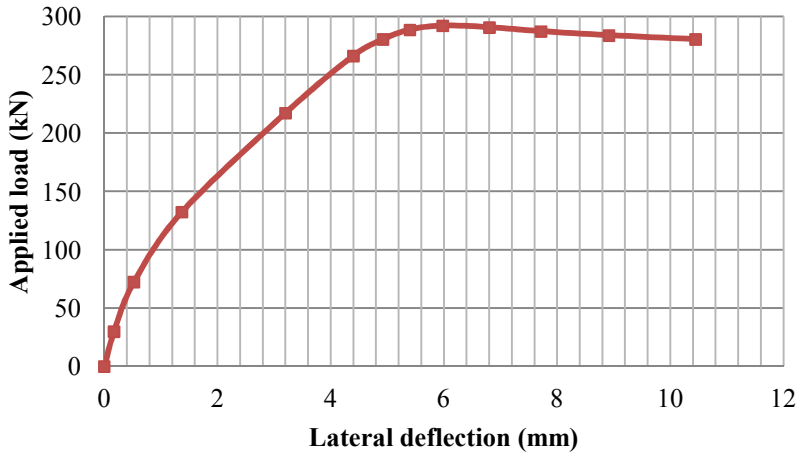

Figure 3.34 Load vs. lateral deflection at the centre of end web panel of FE mode B9

The model failed with an out-of-plane diagonal buckling of the web in the test panel and development of the four plastic hinges, two in the top flange and one each in the bottom flange and the external steel stiffeners, Figure 3.35, at similar positions as those in the specimen B1. The hinges in the external steel stiffeners and the top flange were at distances of approximately 190 mm and 250 mm respectively from the top corner of the plate-girder.

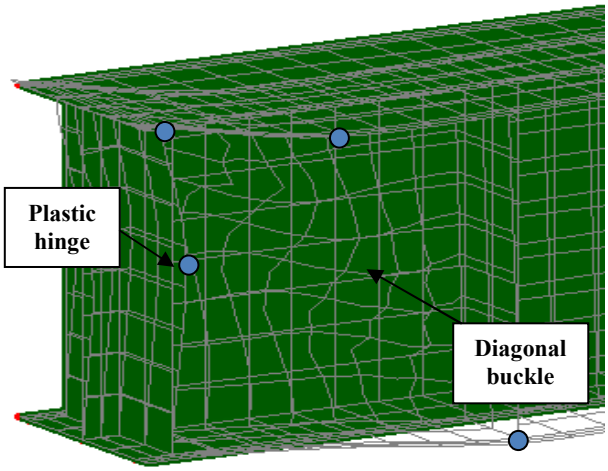

Figure 3.35 Control FE model B9 after failure

3.8.3 Specimen B2

The load was cycled twice from zero up to approximately 120 kN before finally applying the load up to the failure of the specimen. The load was applied in increments of approximately 20 kN each up to 200 kN and then in 10 kN increments.

Figure 3.36 shows the applied load versus vertical deflection at the underside of the plate-girder beneath the loaded stiffeners and Figure 3.37 shows the load versus lateral deflection at middle of the GFRP stiffener in the strengthened web panel of the test

specimen B2. The vertical deflections showed nearly linear behaviour with the applied load up to a load of approximately 270 kN. The test was stopped when the plate-girder was unable to carry further load beyond 277 kN, which was considered as the ultimate load.

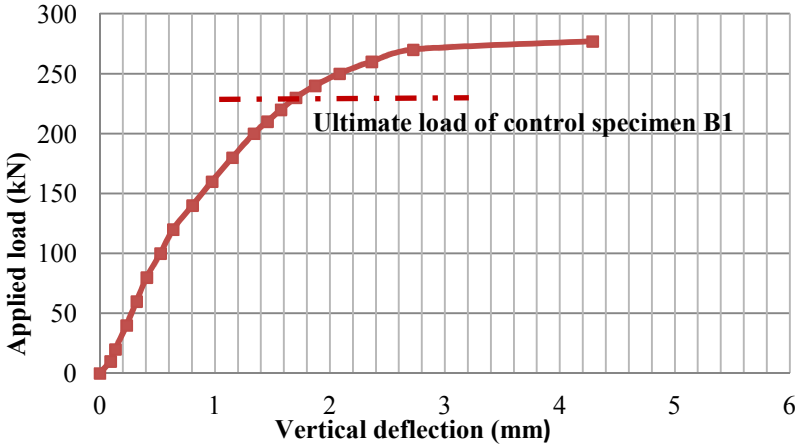

Figure 3.36 Load vs. vertical deflection at the underside of loaded stiffeners of specimen B2

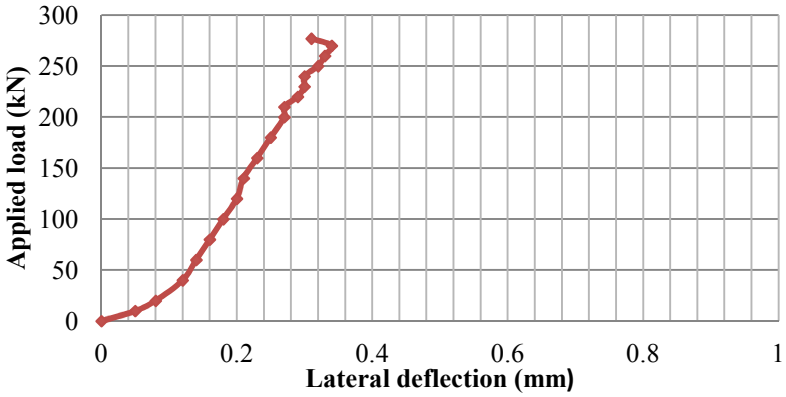

Figure 3.37 Load vs. lateral deflection at the middle of GFRP stiffener in the strengthened web panel of specimen B2

At the ultimate load, there were small out-of-plane diagonal buckles in the steel web on both sides of the GFRP stiffeners. The diagonal buckles in the web panel were not visible but could be felt by touching. Since the web panel was painted white, so one of the diagonal buckles also caused paint chipping, Figure 3.38. Four plastic hinges, two in the top flange and one each in the bottom flange and the external steel stiffeners, had developed, but were not visible. The hinges in the external steel stiffeners and the top flange were at distances of approximately 240 mm and 250 mm respectively from the top corner of the girder. No sign of any breakdown of the steel-GFRP bond or delamination of the GFRP was observed even at the ultimate load of the specimen.

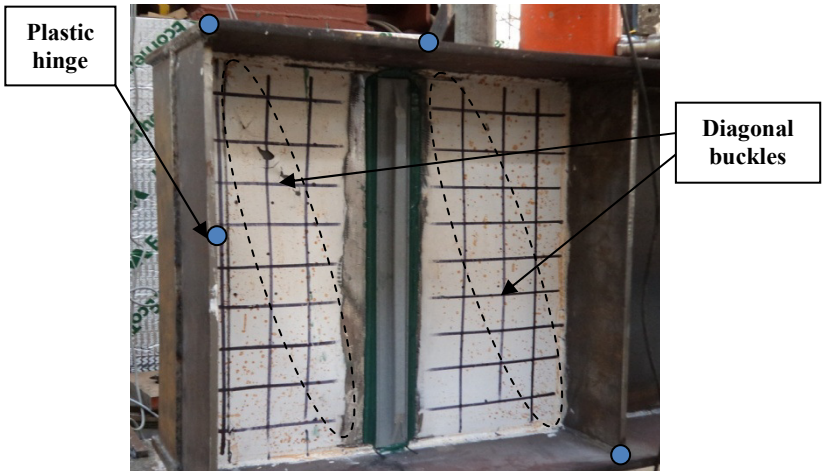

Figure 3.38 Specimen B2 after failure

3.8.4 Specimen B5

The load was cycled twice from zero up to 200 kN before finally applying the load up to the failure of the specimen. The load was applied in increments of approximately 50 kN up to 200 kN, then in 20 kN up to 300 kN and finally in 10 kN increments.

Figure 3.39 shows the applied load versus vertical deflection at the underside of the plate-girder beneath the loaded stiffeners of the test specimen B5. The vertical deflections showed nearly linear behaviour with the load up to a load of approximately 350 kN. Small out-of-plane diagonal buckles in the steel web on both sides of the GFRP stiffener were however observed between the loads of 280 and 300 kN. The diagonal buckles in the web panel were not visible but could be felt by touching. The specimen continued to carry the load up to approximately 380 kN. The diagonal buckles in the steel web then became visible. The applied load could not be increased beyond 380 kN. When an attempt was made to increase the load, the load started dropping and the specimen showed larger increments in vertical deflections, Figure 3.39.

During an attempt to increase the load, it went up to 374 kN, but then dropped to 362 kN and a loud noise, most likely due to a breakdown of the bond between the GFRP stiffener and the steel, was heard. When another attempt was made to increase the load, it went up to 367 kN and then dropped to 333 kN with an increase of approximately 1 mm in the vertical deflection and another loud noise of likely delamination within the GFRP was heard. The test was stopped because the load could not further be increased. The ultimate load of the specimen was considered to be 380 kN. Four plastic hinges, two in the top flange and one each in the bottom flange and the external steel stiffeners,

had developed, but were not visible. The hinges in the external steel stiffeners and the top flange were at distances of approximately 240 mm and 310 mm respectively from the top corner of the girder, Figure 3.40. After the test was stopped, the GFRP stiffener was carefully inspected and delamination of the GFRP layers in the flange of the stiffener at mid span was observed as shown in Figure 3.40.

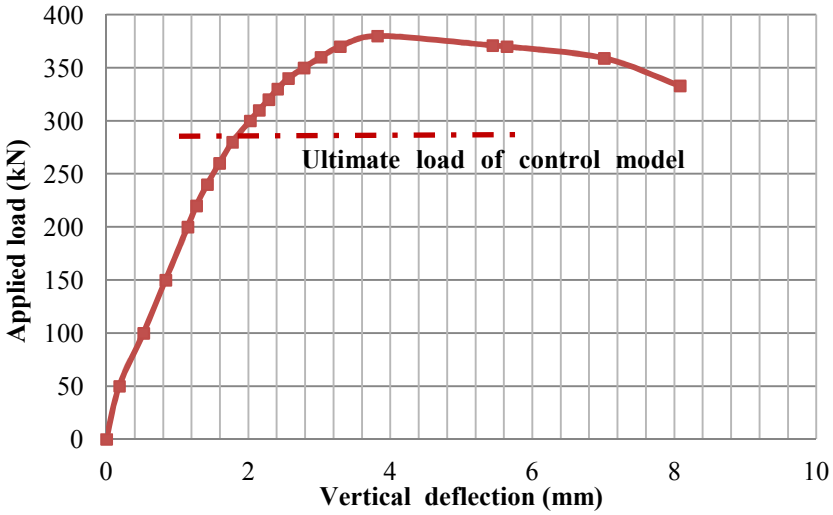

Figure 3.39 Load vs. vertical deflection at the underside of loaded stiffeners of specimen B5

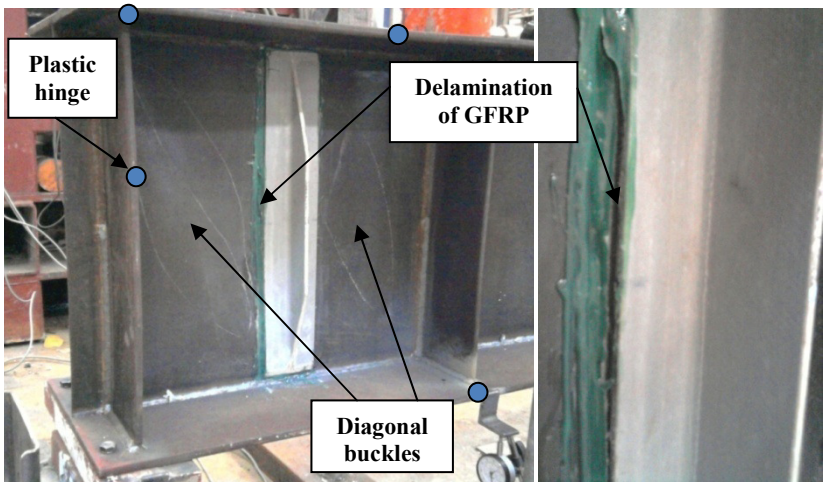

Figure 3.40 GFRP-strengthened specimen B5 after failure

3.8.5 Specimen B6

The load was cycled twice from zero up to 250 kN before finally applying the load up to the failure of the specimen. The load was applied in increments of approximately 50 kN up to 200 kN, then in 20 kN up to 400 kN and finally in 10 kN increments.

Figure 3.41 shows the applied load versus vertical deflection at the underside of the plate-girder beneath the loaded stiffeners and Figure 3.42 shows the load versus lateral deflection at middle of the diagonal GFRP stiffener in the strengthened web panel of the test specimen B6.

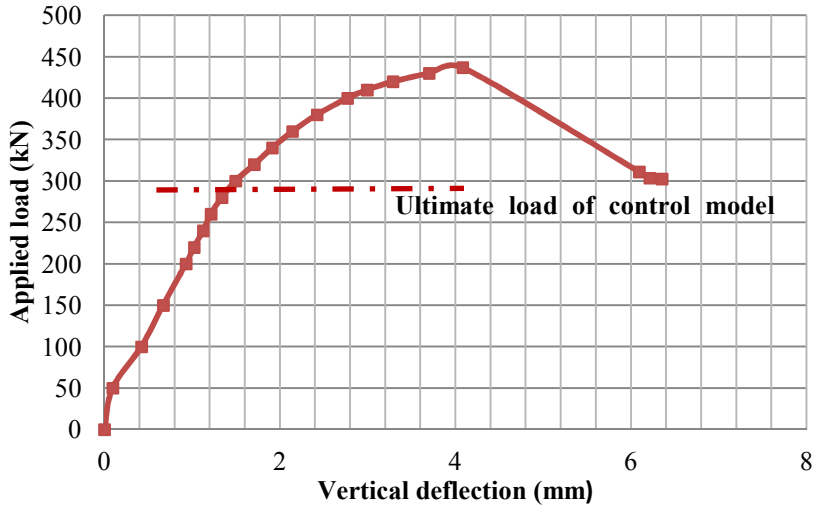

Figure 3.41 Load vs. vertical deflection at the underside of loaded stiffeners of specimen B6

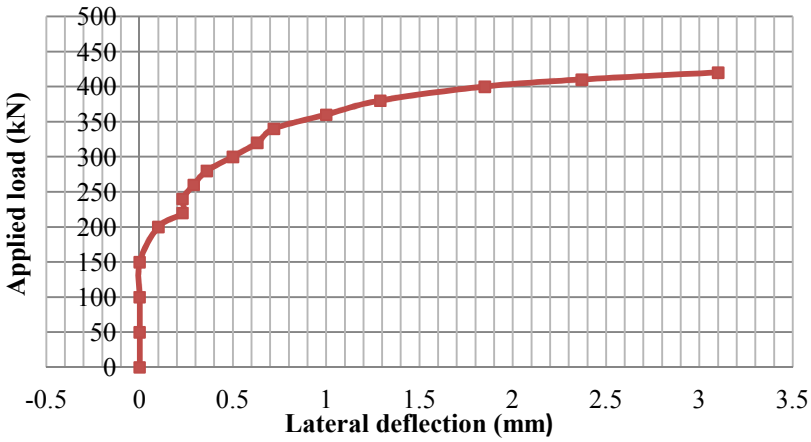

Figure 3.42 Load vs. lateral deflection at the middle of GFRP stiffener in the strengthened web panel of specimen B6

The vertical deflections showed nearly linear behaviour with the applied load up to a load of approximately 437 kN. The lateral deflections were negligible up to a load of 200 kN and then increased with the applied load up to a load of 340 kN. After a load of 340 kN, the lateral deflection was however observed to undergo comparatively large deflections and small diagonal buckles in the steel web on both sides of the GFRP stiffener were felt at this stage, but were not visible. Small noises, most likely due to a breakdown of the bond between the GFRP and the steel, were heard at loads of approximately 348 kN and 392 kN. The specimen continued to carry the load up to

approximately 437 kN. At this stage, a louder noise, most likely due to the bond breakdown within the GFRP, was heard and the load immediately dropped to approximately 317 kN with a large increase of about 2 mm in the vertical deflection. The load continued to drop gradually, finally fell to 295 kN and then remained constant, Figure 3.41. The test was stopped and the ultimate load of the specimen was considered to be 437 kN.

After the test was stopped, buckling of the diagonal GFRP stiffener together with delamination of the GFRP layers in its upper half-span and an out-of-plane diagonal buckle in the steel web normal to the GFRP stiffener were observed, Figure 3.43. Four plastic hinges, two in the top flange and one each in the bottom flange and the external steel stiffeners, had developed, but were not visible. The hinges in the external steel stiffeners and the top flange were at distances of approximately 240 mm and 310 mm respectively from the top corner of the girder, Figure 3.43.

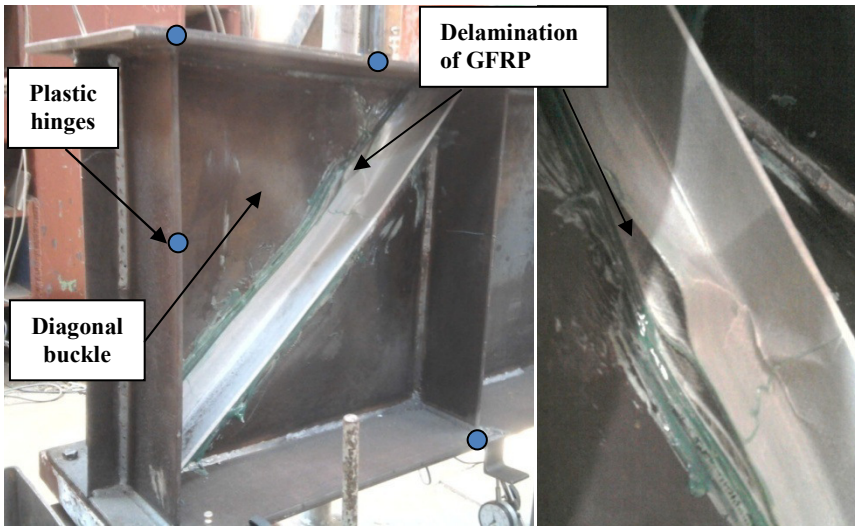

Figure 3.43 GFRP-strengthened specimen B6 after failure

Unlike the other GFRP strengthened specimens of group G2, the specimen B6 showed a brittle failure. At the ultimate load of 437 kN, the load dropped to 295 kN, which is about the ultimate load of the control model B9. It was considered that at the ultimate load, the diagonal GFRP stiffener could not resist the applied compressive load and buckled, but it was not detached from the web completely. The specimen then failed in a similar way to the control specimen which was the development of an out-of-plane buckling of the web panel followed by the formation of plastic hinges in the external steel stiffeners and the top and bottom flanges of the plate-girder.

3.8.6 Specimen B8

The load was cycled twice from zero up to approximately 120 kN before finally applying the load up to the failure of the specimen. The load was applied in increments of approximately 20 kN up to 200 kN and then in 10 kN increments.

Figure 3.44 shows the applied load versus vertical deflection at the underside of the plate-girder beneath the loaded stiffeners of the test specimen B8. The vertical deflections showed nearly linear behaviour with the applied load up to a load of 250 kN. The web of the test web panel was however observed to buckle out-of-plane diagonally between the applied loads of 220 to 230 kN. The specimen continued to carry further load and a loud noise, most likely due to bond breakdown between the GFRP and the steel, was heard at a load of 277 kN. The specimen was able to carry an ultimate load of approximately 285 kN. The test was stopped because the specimen was unable to carry any further load.

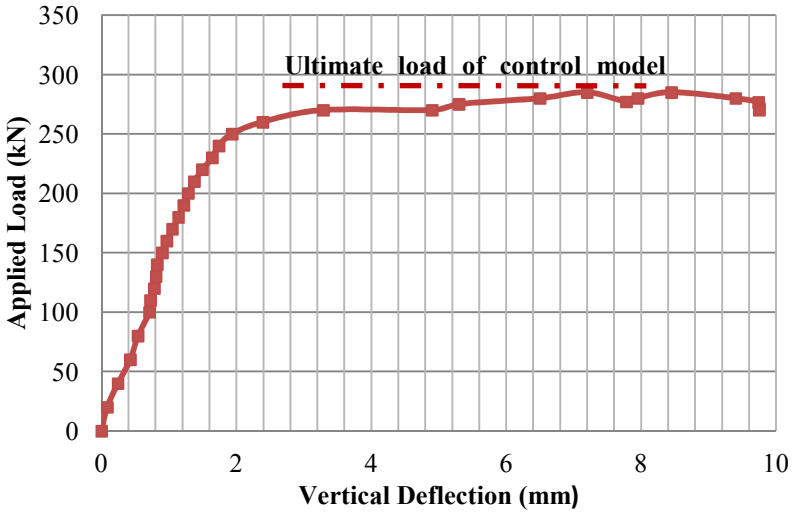

Figure 3.44 Load vs. vertical deflection at the underside of loaded stiffeners of specimen B8

At the ultimate load, four plastic hinges, two in the top flange and one each in the bottom flange and the external steel stiffeners, had developed, Figure 3.45. The hinges in the external steel stiffeners and the top flange were at distances of approximately 240 mm and 310 mm respectively from the top corner of the plate-girder. On inspection of the specimen after the test, the bond between the GFRP and the steel was found to be intact. However, delamination of the GFRP layers at lower end of the rear GFRP stiffener near the lower end of diagonal buckle in the steel web was observed as shown in Figure 3.46.

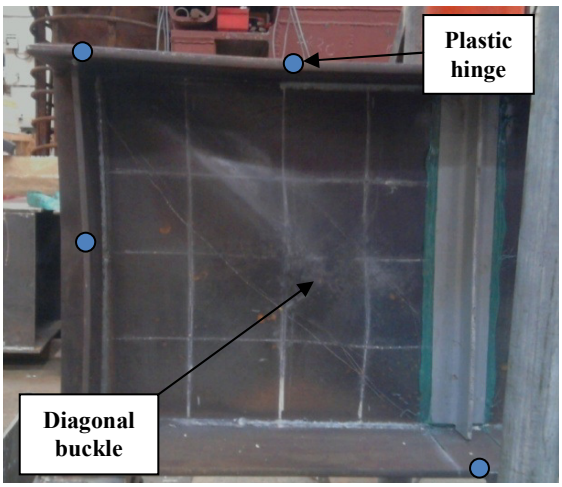

Figure 3.45 Specimen B8 after failure (front)

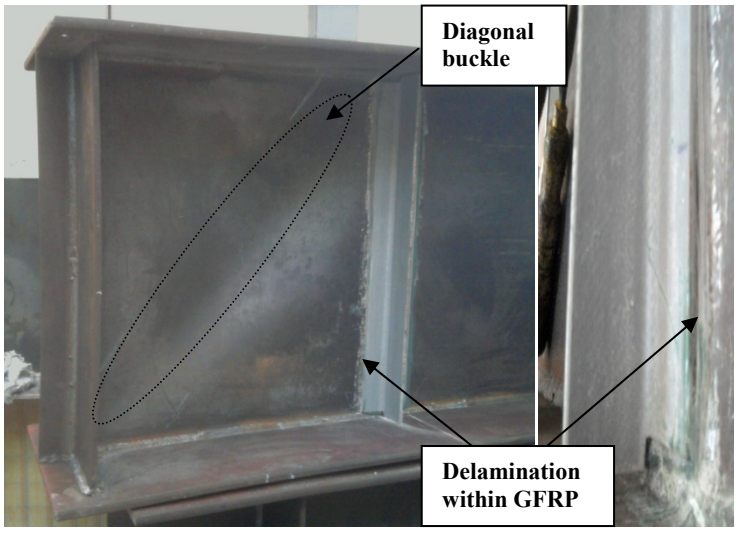

Figure 3.46 Delamination of GFRP in specimen B8 (back)

3.8.7 Specimen B3

The load was cycled twice from zero up to approximately 220 kN before being finally applied up to the ultimate load of the specimen. The load was applied in increments of approximately 20 kN up to 200 kN and then in 10 kN increments.

Figure 3.47 shows the applied load versus vertical deflection at the underside of the plate-girder beneath the loaded stiffeners and Figure 3.48 shows the load versus lateral deflection at the centre of the un-strengthened side of the end web panel of the test specimen B3. The vertical deflections increased nearly linearly with the applied load up to a load of approximately 260 kN. The lateral deflections were negligible up to a load of approximately 220 kN and started thereafter. A large increase of approximately 0.4 mm in the lateral deflection was recorded between the loads of 260 to 270 kN.

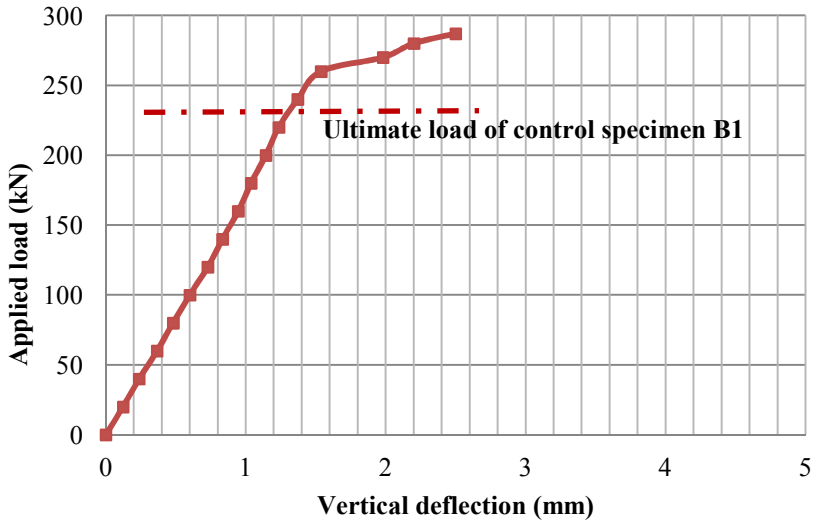

Figure 3.47 Load vs. vertical deflection at the underside of loaded stiffeners of specimen B3

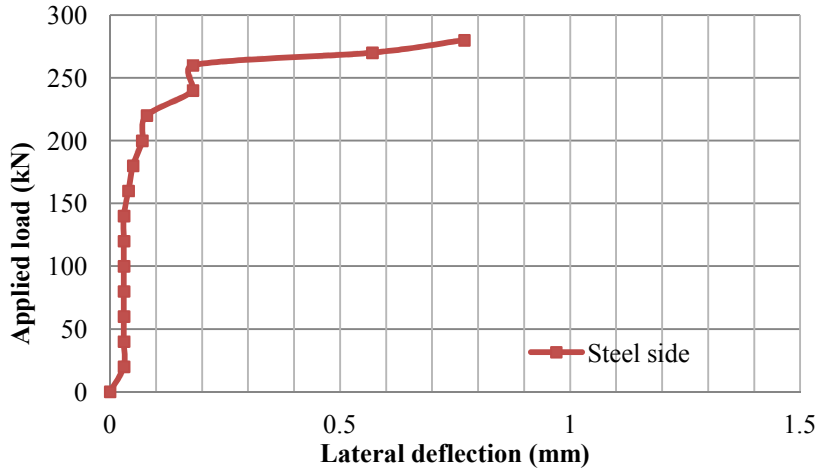

Figure 3.48 Load vs. lateral deflection at the centre of the strengthened web panel of specimen B3

A small noise, most likely due to the start of a breakdown of bond between the steel and carbon fabric, was heard at a load of approximately 240 kN and a further louder noise was heard at 270 kN. After a load of 270 kN, it was possible to increase the load but not to get an increment of 10 kN at each load step. Whenever an attempt to increase the load was made, it dropped but did not fall to the starting value of the load. At the load of 287 kN, a noise most likely of the bond breakdown, which was louder than the two earlier noises, was heard. The test was stopped because the specimen was unable carry further load. The failure of the specimen was considered to have been initiated by a breakdown of the fabric-steel bond. At this stage, the carbon fabric layers remained otherwise intact; there was no visible cracking at the surface of the top layer.

A small diagonal buckle on the un-strengthened steel side of the web in the test web panel, similar to that in the control specimen B1, developed which was not visible but could be felt by touching. Four plastic hinges, two in the top flange and one each in the bottom flange and the external steel stiffeners, had developed, Figure 3.49, but were not visible as those seen in specimens B1 and B8. The hinges in the external steel stiffeners and the top flange were at distances of approximately 280 mm and 250 mm respectively, from the top corner of the plate-girder. After the test was over, the specimen B3 was cut vertically along centre of the test panel, Figure 3.49, by sawing. It was confirmed that a breakdown of bond between the steel and carbon fabric surface had occurred without any bond breakdown within the fabric layers, Figure 3.50.

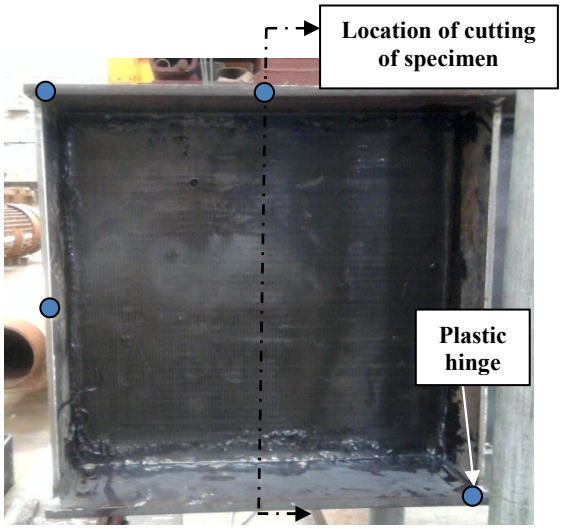

Figure 3.49 Specimen B3 after failure

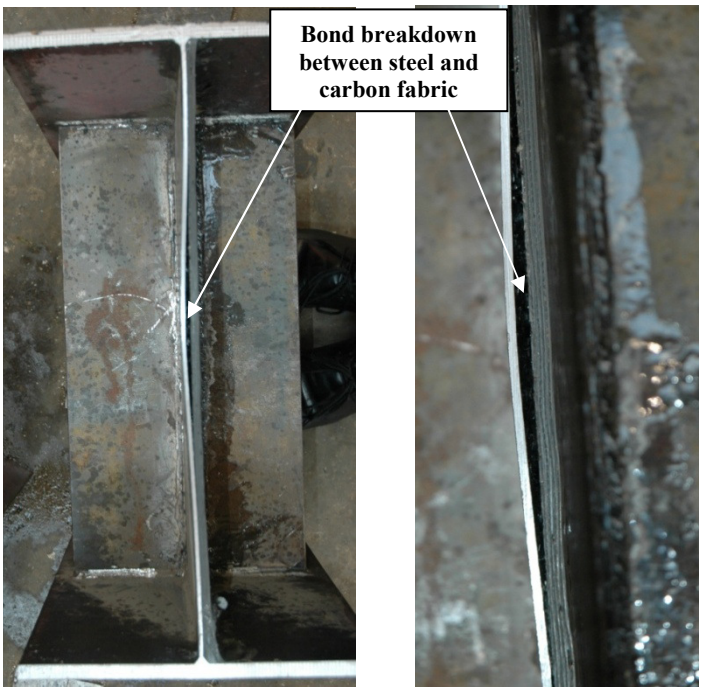

Figure 3.50 Bond breakdown between steel and carbon fabric in specimen B3

3.8.8 Specimen B4

The load was cycled twice from zero to approximately 180 kN. Following these load cycles it was necessary to remove and calibrate the load cells under the left end support of the plate-girder. The specimen was then loaded up to its ultimate load. The load was applied in increments of approximately 20 kN up to 200 kN and then in 10 kN increments.

Figure 3.51 shows the applied load versus vertical deflection at the underside of the plate-girder beneath the loaded stiffeners and Figure 3.52 shows the load versus lateral deflection at the centre of the test panel of the specimen B4. The vertical deflections increased nearly linearly with the applied load from a load of 20 kN up to 350 kN. A large increase of approximately 2 mm in the vertical deflection was recorded for the load increment from 350 to 354 kN, Figure 3.51. The lateral deflections also increased nearly linearly with load from 20 kN to 350 kN, but decreased significantly for the load increment from 350 to 354 kN.

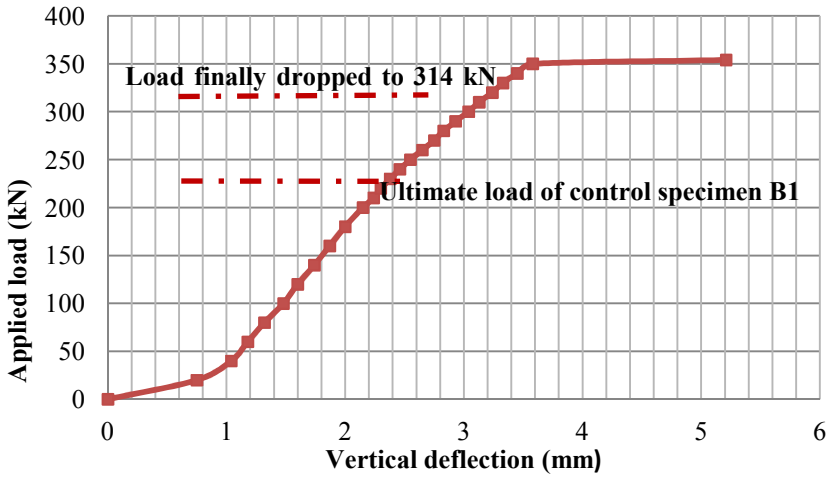

Figure 3.51 Load vs. vertical deflection at the underside of loaded stiffeners of specimen B4

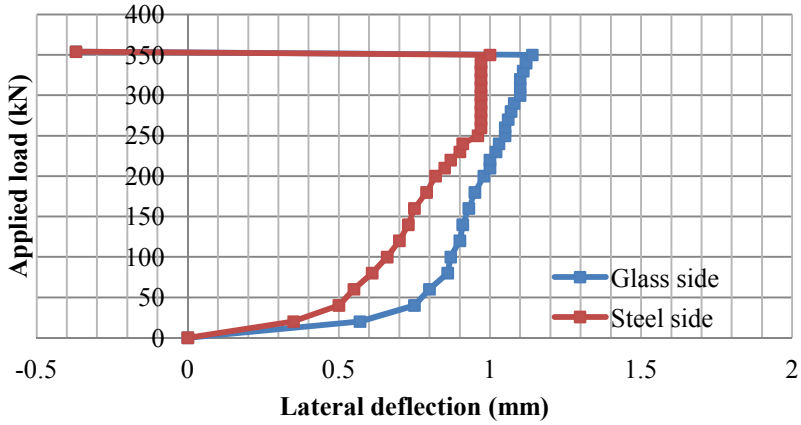

Figure 3.52 Load vs. lateral deflection at the centre of strengthened web panel of B4

A loud noise, most likely due to the breakdown of bond between the steel and glass fabric, was heard at the ultimate load of approximately 354 kN. The load then fell gradually to a load of 314 kN, which then remained constant. The test was stopped because the specimen was unable carry any further load beyond 354 kN. The failure of the specimen was considered to have been initiated by a breakdown of the fabric-steel bond. A small diagonal buckle on the un-strengthened steel side of the web in the test panel, similar to that in the control specimen B1, developed which was not visible but could be felt by touching. At the ultimate load, the glass fabric layers remained otherwise intact; there was no visible cracking at the surface of the top layer. Four plastic hinges, two in the top flange and one each in the bottom flange and the external steel stiffeners, had developed, Figure 3.53, but were not visible as those seen in specimens B1 and B8. The hinges in the external steel stiffeners and the top flange were at distances of approximately 280 mm and 250 mm respectively from the top corner of the plate-girder.

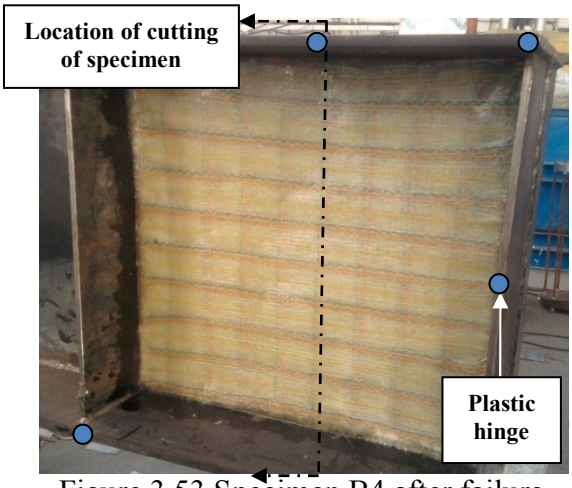

Figure 3.53 Specimen B4 after failure

As described earlier, the applied load was cycled twice before the final test. During the first load cycle, a residual vertical deflection of approximately 0.7 mm at the underside the plate-girder beneath the loaded stiffeners was recorded after removal of the applied load. The vertical deflection after removal of the applied load was almost negligible in the second load cycle. Following re-calibration of the load cells under the left end support, the load was then applied up to failure of the member. It can be seen from Figure 3.51 that an initial settling of the plate-girder of 0.7 mm occurred. Therefore, the vertical deflections have had a displacement of 0.7 mm deducted to account for settling down of the plate-girder. Figure 3.54 shows the applied load versus corrected vertical deflections at the underside of the plate-girder beneath the loaded steel stiffeners.

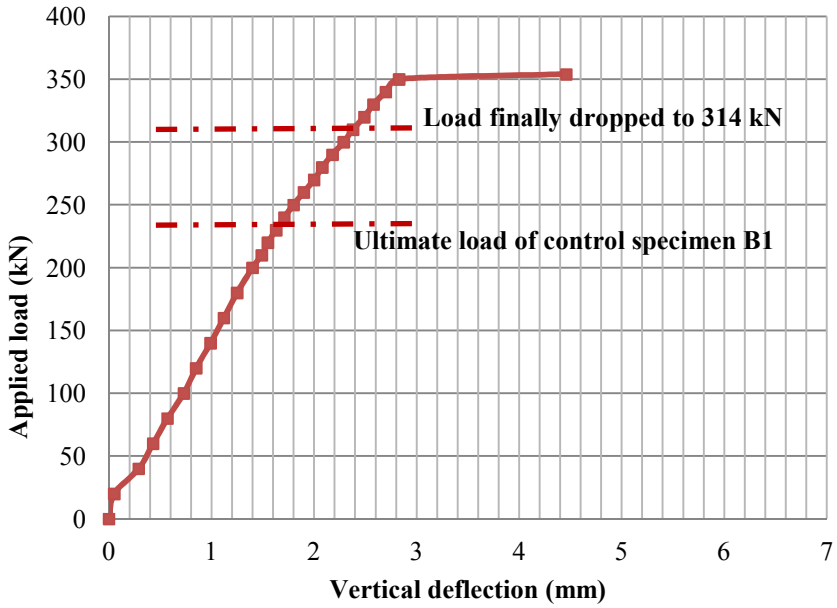

Figure 3.54 Load vs. corrected vertical deflection at the underside of loaded stiffeners of specimen B4

Similarly, Figure 3. 55 shows the load versus lateral deflection at the centre of the test panel of the specimen B4 after correcting the deflections on the steel and glass side due to initial settling of the plate-girder.

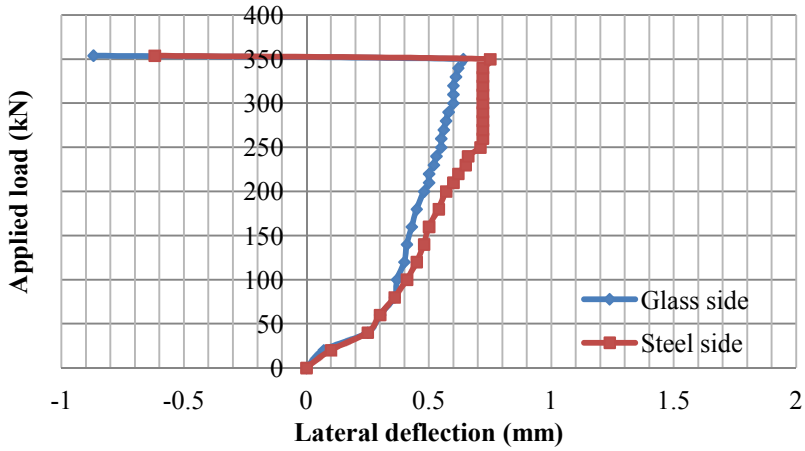

Figure 3. 55 Load vs. corrected lateral deflections at the centre of strengthened web panel of specimen B4

After the test was over, the specimen B4 was cut vertically along the centre of fabric-strengthened panel, Figure 3.53, by sawing. It was confirmed that a breakdown of bond between the steel and glass fabric surface had occurred without any bond breakdown within the fabric layers, Figure 3.56.

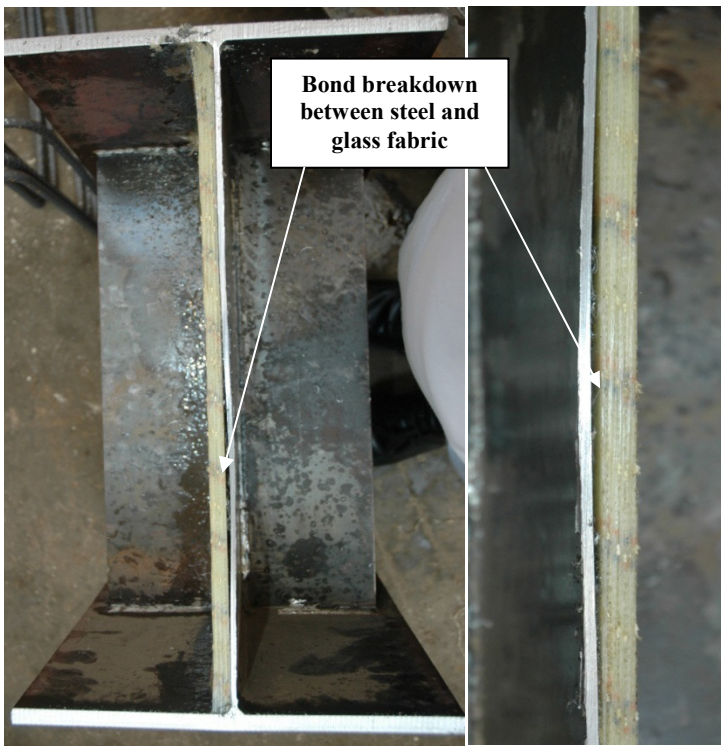

Figure 3.56 Bond breakdown between steel and glass fabric in specimen B4

3.8.9 Specimen B7

The load was cycled twice from zero to approximately 250 kN. The load was applied in increments of approximately 50 kN up to 250 kN, then in 20 kN up to 330 kN and finally in 10 kN increments.

Figure 3.57 shows the applied load versus vertical deflection at the underside of the plate-girder beneath the loaded stiffeners and Figure 3.58 shows the load versus lateral deflection at the centre of the test panel of the specimen B7. The vertical deflections increased nearly linearly with the applied load up to a load of 420 kN. The lateral deflections on the steel and the glass sides were negligible up to a load of 330 kN and were approximately 1.6 and 2.0 mm respectively at 420 kN. Between the loads of 420 to 428 kN, the lateral deflection on steel side increased significantly to approximately 14 mm and that on the glass side decreased to 0.8 mm.

A small noise, most likely due to the start of a breakdown of bond between the steel and glass fabric, was heard at a load of approximately 394 kN and a further louder noise was heard at 400 kN. The noises were then heard continuously with further increases in the load and stopped with the final and the loudest noise at the ultimate load of approximately 428 kN. At this stage, the load fell immediately to 278 kN and then

gradually to 265 kN, which is about the ultimate load of model of the control specimen B9. The test was stopped because the plate-girder was unable carry any further load. The failure of the specimen was considered to have been initiated by a breakdown of the fabric-steel bond. The glass fabric layers remained otherwise intact; there was no visible cracking at the surface of the top layer. The specimen B7 had a brittle failure like that of B6.

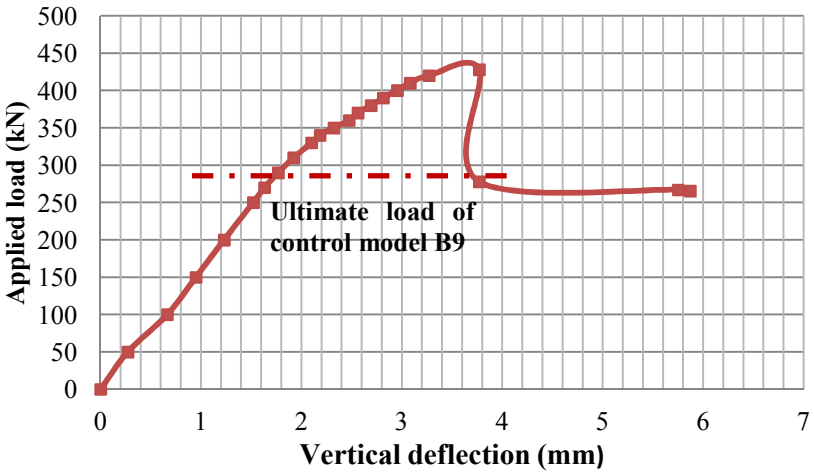

Figure 3.57 Load vs. vertical deflection at the underside of loaded stiffeners of specimen B7

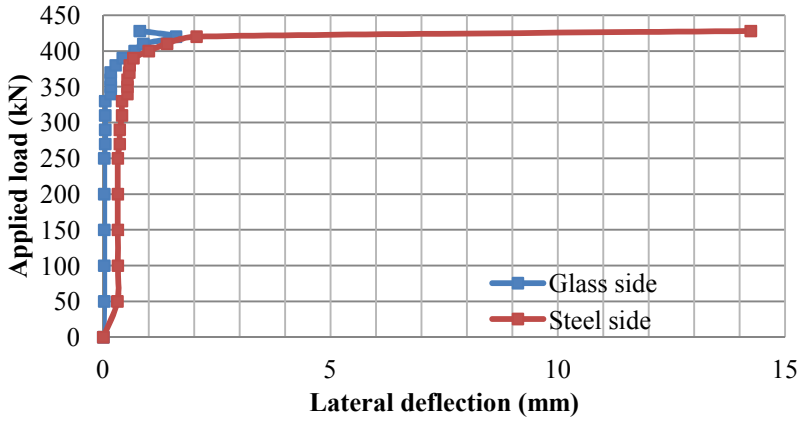

Figure 3.58 Load vs. lateral deflection at the centre of strengthened panel of specimen B7

After the test was over, an out-of-plane diagonal buckle on the un-strengthened steel side of the test panel, similar to that in the model B9, was observed, Figure 3.59, clearly indicating breakdown of the steel-fabric bond. Four plastic hinges, two in the top flange and one each in the bottom flange and the external steel stiffeners, had developed, Figure 3.59, but were not visible as those seen in specimens B1 and B8. The hinges in the external steel stiffeners and the top flange were at distances of approximately 310 mm and 240 mm respectively from the top corner of the plate-girder.

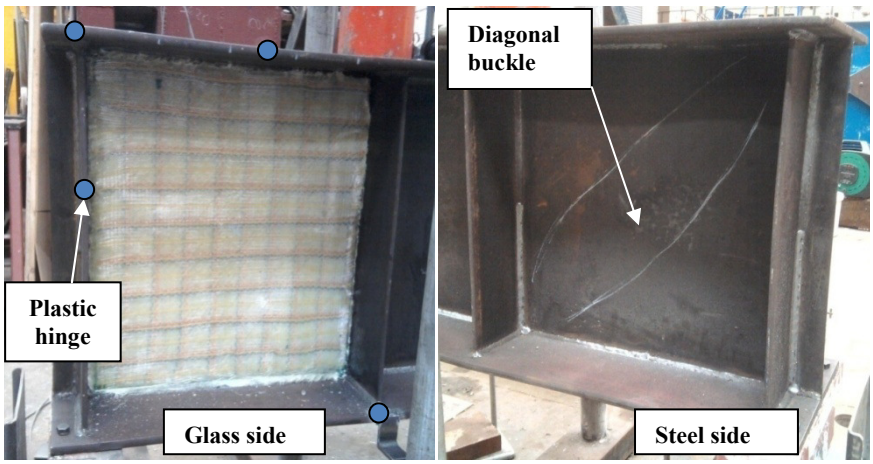

Figure 3.59 Specimen B7 after failure

3.9 Comparison of test results of specimens

3.9.1 Ultimate loads and modes of failure

Table 3.9 gives the ultimate loads and the modes of failure of the specimens of groups G1, G2 and G3. Ratios of the ultimate loads of the FRP-strengthened specimens to that of the respective un-strengthened specimen or FE model are also given.

3.9.2 Location of plastic hinges

At the failure of each specimen, plastic hinges developed in the top flange and the external steel stiffeners of all the specimens. To determine locations of the plastic hinges, the sections of the flanges and stiffeners were inspected along the length and kinks were encircled with chalk. The kinks were checked by putting a straight wooden plank along the length of the sections and distances were measured from the top corner of the test web panel. The hinge locations were within a variation range of ±10 mm at the points where the distances were measured from the top corner of the test panel.

Table 3.10 gives the locations of the plastic hinges developed in the top flange and the external steel stiffeners from the top corner of the test web panel using the nomenclature shown in Figure 3.60.

3.9.3 Load-deflection responses

Figure 3.61 and Figure 3.62 give the plots of the experimentally applied loads versus the vertical deflections at the underside of the plate-girder beneath the loaded stiffeners for the G2 and G3 test specimens respectively, compared to those of the G1 specimens.

Table 3.9 Ultimate loads and modes of failure of specimens B1 to B8 and model B9

Specimen No. (Girder series) & strengthening details	Ultimate load (kN)	Ratio of ult. load of str. to control	Mode of failure
Group G1: Un-strengthened control specimens			
B1 (S1) None	230	---	Out-of-plane diagonal buckling of web in test web panel
B9 (S2) None	295	---	Out-of-plane diagonal buckling of web in test web panel
Group G2: GFRP pultruded section strengthened specimens			
B2 (S1) 2 vertical GFRP stiffeners	277	1.20	Small out-of-plane diagonal buckles in steel web on both sides of the GFRP stiffeners
B5 (S2) 1 vertical GFRP stiffener	380	1.29	Out-of-plane diagonal buckles in steel web on both sides of the GFRP stiffener and delamination at mid of the GFRP stiffener
B6 (S2) 1 diagonal GFRP stiffener	437	1.48	Buckling of GFRP stiffener and delamination in its upper half and out-of-plane diagonal buckle in steel web normal to the diagonal GFRP stiffener
B8 (S2) 2 load-bearing GFRP stiffeners	285	0.97	Out-of-plane diagonal buckling of web in test panel and delamination at lower end of one GFRP stiffener
Group G3: FRP fabric strengthened specimens			
B3 (S1) 4 layers of carbon fabric	287	1.25	Breakdown of steel-fabric bond and small out-of-plane diagonal buckling of web in test panel on steel side
B4 (S1) 8 layers of glass fabric	354	1.54	Breakdown of steel-fabric bond and small out-of-plane diagonal buckling of web in test panel on steel side
B7 (S2) 4 layers of glass fabric	428	1.45	Breakdown of steel-fabric bond and out-of-plane diagonal buckling of web in test panel on steel side
Note: Four plastic hinges, two in the top flange and one each in the bottom flange and external steel stiffeners developed in all test specimens and FE model			

Table 3.10 Locations of plastic hinges developed in top flange and external steel stiffeners

Specimen/ Model No.	Distance of plastic hinge from top corner of test web panel (mm)	
	In top flange (A)	In end stiffener (B)
Group G1: Un-strengthened control specimens		
B1	250	180
B9	250	190
Group G2: GFRP pultruded section strengthened specimens		
B2	250	240
B5	260	240
B6	260	240
B8	260	240
Group G3: FRP fabric strengthened specimens		
B3	250	280
B4	250	280
B7	260	240

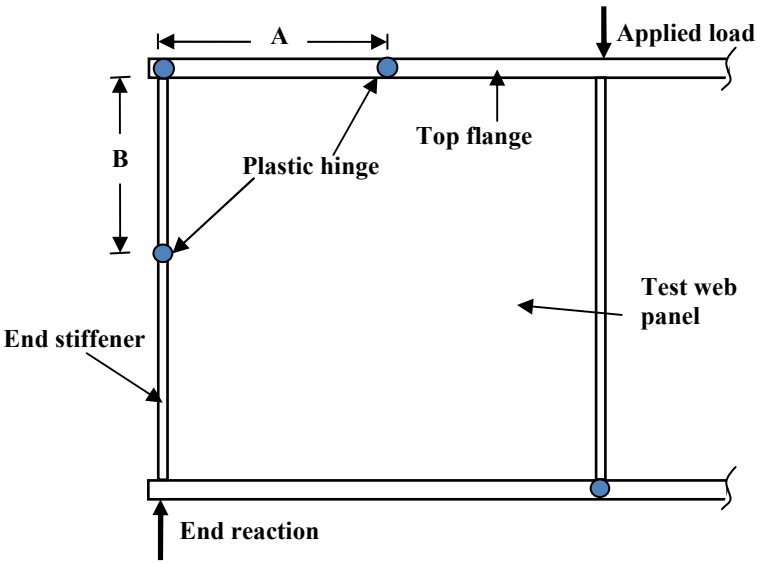

Figure 3.60 Distances of plastic hinges in top flange and external steel stiffeners

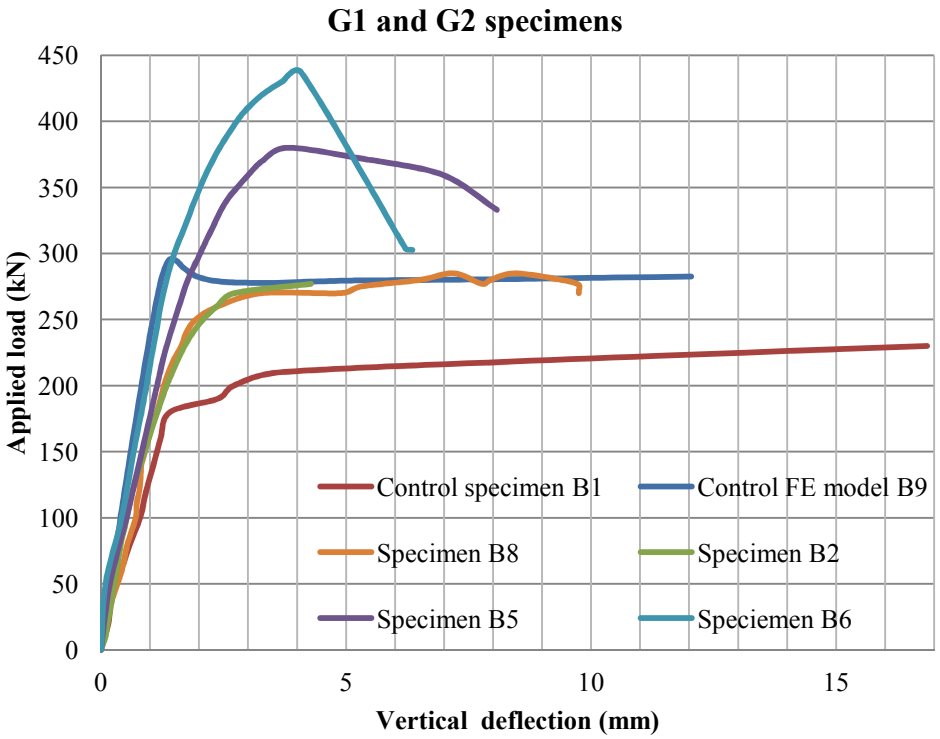

Figure 3.61 Load vs. vertical deflection at the underside of loaded stiffeners of G1 and G2 specimens

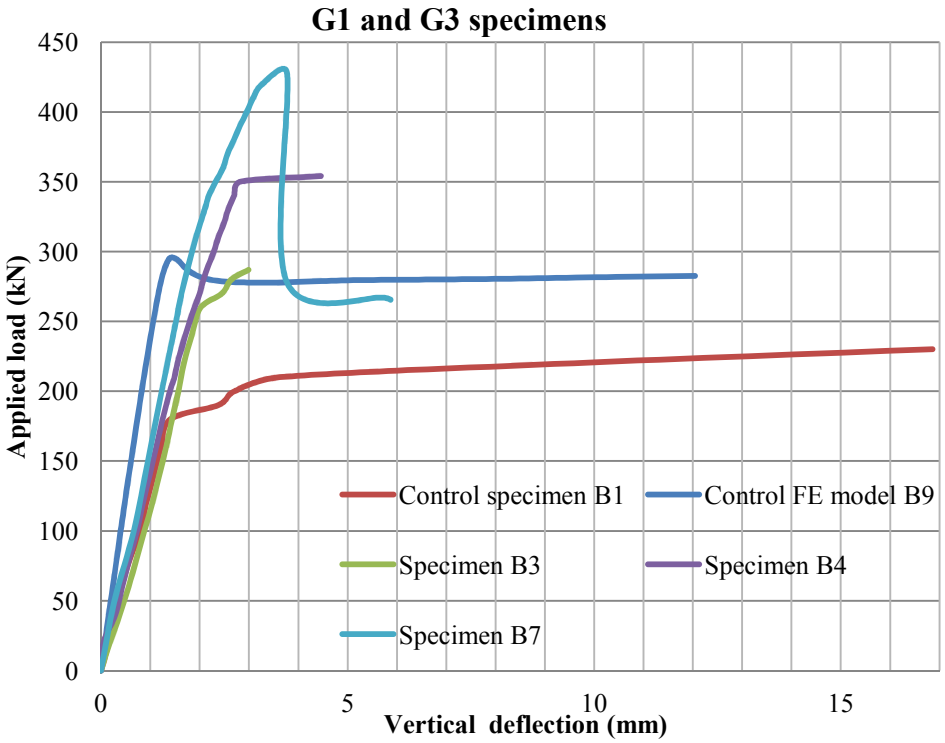

Figure 3.62 Load vs. vertical deflection at the underside of loaded stiffeners of G1 and G3 specimens

3.10 Discussion of results

3.10.1 Results of specimens of G1 and G2 groups

The results of the GFRP-strengthened specimens of group G2 are discussed and compared to those of the un-strengthened control specimens of group G1 as follows.

1. The ultimate loads of the specimens B2, B5 and B6 with GFRP pultruded section strengthening were increased by approximately 1.20, 1.29 and 1.48 times that of the respective control specimen, B1 or B9.

2. GFRP strengthening using vertical stiffeners delayed the initiation of out-of-plane buckling of the web in the end web panel of the specimens of group G2. In the tests, the out-of-plane diagonal buckling of the steel web on both sides of the GFRP stiffeners in the specimen B2 was observed at a load of 270 kN, which is 1.5 times of the 180 kN when the buckling was observed in the un-strengthened specimen B1. Similarly, the out-of-plane diagonal buckling of the steel web on both sides of the GFRP stiffener in the specimen B5 was observed at a load of 280 kN, which is 1.47 times of the 190 kN at which the first buckling mode occurred in eigenvalue FE analysis of model of the un-strengthened specimen B9.

3. Using a vertical GFRP stiffener on one side of the web in specimen B5 worked in a similar way to using two vertical stiffeners of similar stiffness on both sides of the web in specimen B2. The ultimate load of the specimen B2 was approximately 1.20 times that of the un-strengthened specimen B1 and the ultimate load of the specimen B5 was approximately 1.29 times that of the model of the un-strengthened specimen B9. The increase in the ultimate load of the specimen B5 was about 1.07 times that of the specimen B2. The stiffness, EI, of the GFRP stiffener used in B5 was about 1.30 times the combined stiffness of the two GFRP stiffeners used in B2, Appendix-A.

4. Use of a GFRP pultruded section stiffener on one side of the web, instead of two stiffeners of the similar stiffness on both sides, is a strengthening solution which can be used in situations when the strengthening on both sides of the web is either difficult or impossible.

5. Specimens B5 and B6 had a vertical and a diagonal GFRP stiffener of the same stiffness respectively on one side the web in the test web panel. The ultimate loads of B5 and B6 were 1.29 and 1.48 that of model of the un-strengthened specimen B9. The two specimens however had different failure modes. The failure of B5 was ductile and was initiated by the development of two out-of-plane diagonal buckles in the steel web on both sides of the GFRP stiffener with some delamination in the stiffener but no buckling. The failure of B6 was brittle and was initiated by buckling of GFRP stiffener followed by delamination in the stiffener and the development of an out-of-plane diagonal buckle in the steel web panel like that of the model B9.

6. The diagonal GFRP stiffener of the specimen B6 exhibited buckling followed by delamination of the fibre layers in the upper half at the ultimate load. There was no buckling and delamination in the vertical GFRP stiffeners of the specimen B2 at the ultimate load. The vertical GFRP stiffener of specimen B5 showed some delamination of the layers but no buckling at the ultimate load.

7. The ratio of the stiffnesses, EI, of each of the two load-bearing GFRP stiffeners used on both sides of the web beneath the applied load in the specimen B8 to that of each of the two load-bearing steel stiffeners at the same position in the FE model B9 was approximately 1:43, Appendix-A. Despite a significant variation in the stiffness, the GFRP stiffeners strengthened the web in a similar way to the steel stiffeners. The ultimate load, 285 kN, of B8 was 0.97 times that, 295 kN, of B9.

8. Preparation of the surfaces of the steel and GFRP pultruded section before bonding and clamping of the bonded GFRP stiffeners helped in ensuring a good steel-GFRP bond. No breakdown of the bond between the GFRP and the steel was observed in all the GFRP pultruded section strengthened specimens of group G2.

9. Tapering the ends of the GFRP pultruded section stiffeners to an angle of approximately 20 degrees in the specimens B2 and B5 proved to be successful in avoiding a breakdown of the bond between the steel and the GFRP at the ends of the GFRP stiffeners, even at the ultimate load of the specimens.

3.10.2 Results of specimens of G1 and G3 groups

The results of the FRP fabric-strengthened specimens of group G3 are discussed and compared to those of the un-strengthened control specimens of group G1 as follows.

1. The strengths of the specimens B3, B4 and B7 with FRP fabric strengthening were increased by approximately 1.25, 1.54 and 1.45 times that of the respective un-strengthened specimen, B1 or B9.

2. In the tests of the glass fabric strengthened specimens, the ultimate load of specimen B4 using eight layers of glass fabric was approximately 1.54 times that of the un-strengthened specimen B1. The ultimate load of specimen B7 using four layers of glass fabric was approximately 1.45 times that of model of the un-strengthened specimen B9. The increase in the ultimate load of B4 was about 1.05 times that of B7. The increases in the ultimate loads of the specimens B4 and B7 were not proportional to the number of the fabric layers applied to their end web panels.

3. Glass fabric exhibited a better bond with the steel surface than the carbon fabric. The breakdown of the bond between the glass fabric and the steel in the specimens B4 and B7 was considered to have occurred at the ultimate loads of 354 and 428 kN respectively, which were approximately 1.23 and 1.49 times that of specimen B3, with carbon fabric, which was 287 kN.

4. After breakdown of the bond between the steel and the fabric had occurred in the specimens B3, B4 and B7 of group G3, the fabric layers remained otherwise intact; there was not any visible delamination within the fabric layer or cracking at the surface of the top layer.

5. The ultimate loads of specimens B4 and B7 were 354 and 428 kN respectively. In both specimens, the glass fabric layers were applied and then compressed with the steel and wooden rollers in a similar way. In specimen B7, the glass fabric layers were also compressed using a wooden board and steel clamps after application and rolling of the final layer.

3.10.3 Results of specimens of G2 and G3 groups

The results of the GFRP-strengthened and FRP fabric-strengthened specimens of groups G2 and G3, respectively, are compared to each other as follows.

1. Failure in all three FRP fabric strengthened specimens, B3, B4 and B7, of group G3 was considered to have been initiated by a breakdown of the steel-fabric bond followed by an out-of-plane buckling of the web on the steel side. Failure in the three GFRP pultruded section strengthened specimens, B2, B5 and B8, of group G2 was initiated by the development of the out-of-plane diagonal buckling of the steel web without any breakdown of the steel-GFRP bond. The failure in the fourth specimen B6 of group G2 was initiated by buckling of GFRP stiffener followed by an out-of-plane diagonal buckling in the steel web without any breakdown of the steel-GFRP bond, but with delamination of the GFRP.

2. At failure, four plastic hinges, two in the top flange and one each in the bottom flange and end steel stiffeners, had developed in all the specimens of groups G1, G2 and G3. The locations where the hinges formed in the top flange and end steel stiffeners are given in Table 3.10.

3. The failure of all three specimens, B3, B4 and B7, of group G3 and of one specimen, B6, of group G2 was brittle. The failure of the two un-strengthened specimens, B1 and B9, of group G1 and of three specimens, B2, B5 and B8, of group G2 was ductile.

4. In the GFRP pultruded section strengthened web panels, the vertical stiffeners on one or both sides of the web divided the panel into two sub panels and increased its overall out-of-plane stiffness by decreasing the aspect ratios of the panels. In the FRP fabric strengthened panels, the application of fabric sheets increased the thickness of the web in the end web panel and increased its overall out-of-plane stiffness by reducing the slenderness ratio of the web.

5. The FRP fabric strengthening required a larger surface area of the steel to be prepared than that required in the GFRP pultruded section strengthening. The prepared area of the steel surface in the fabric strengthened specimens of group G3 was at least 4 times that required in the GFRP-strengthened specimens of group G2.

6. In the S1 and S2 plate-girders, the increase in the ultimate load of the un-strengthened control specimens was approximately proportional to the increase in the yield strength of the steel in the webs. The ultimate load, 295 kN, of the S2 control specimen B9 obtained from the FE analysis was about 1.28 times that, 230 kN, of the S1 control specimen B1 in the test. According to the results of the tensile tests, the yield strength of the steel in the web, 353 MPa, of the S2 plate-girders was approximately 1.30 times that, 274 MPa, of the S1 plate-girders.

3.11 Conclusions

Details and the results of tests on eight specimens have been presented in this Chapter. The tests were carried out on the un-strengthened or FRP-strengthened end web panels of steel plate-girders. The plate-girders were similar in construction and manufactured in two series, S1 and S2. The yield strength of the steel in web of the S2 plate-girders was 1.30 times that of the S1 plate-girders. Similarly, the ultimate load of the S2 control FE model B9 was about 1.28 times that of the S1 control test specimen B1.

The test results showed that the ultimate load of the un-strengthened specimen was increased by up to 1.48 times using GFRP pultruded section stiffeners to the end web panels. The use of a vertical GFRP stiffener on one side of the web in the specimen B5 worked in a similar way as two vertical GFRP stiffeners of similar stiffness used on both sides of the web in the specimen B2. The use of a diagonal GFRP stiffener on one side of the web in the end web panel in the specimen B6 gave about 1.15 times increase in the ultimate load of the specimen compared to the use of a vertical GFRP stiffener of the same stiffness in the specimen B5. The two specimens however had different failure modes. The failure of B5 was ductile and that of B6 was brittle. The load-bearing GFRP stiffeners in the specimen B8 strengthened the web in a similar way to the significantly more stiff load-bearing steel stiffeners in model of the control specimen B9. Failure in all GFRP strengthened specimens was initiated by out-of-plane diagonal buckling of the steel web without a breakdown of the steel-GFRP bond.

The use of carbon and glass fabric sheets to strengthen the end web panels of the steel plate-girders has also been investigated. The fabric strengthening increased the ultimate load of the un-strengthened specimen by up to 1.54 times before a breakdown of the steel-fabric bond. The bond breakdown caused a brittle failure in all the three fabric strengthened specimens B3, B4 and B7. The glass fabric in specimens B4 and B7 exhibited a better bond with the steel surface than the carbon fabric in the specimen B3. After application and rolling of each layer of the glass fabric in the specimens B4 and B7, the additional clamping of the layers in B7 helped in ensuring a better bond. The use of eight layers of the glass fabric to the end web panel of specimen B4 however only gave a small increase in the ultimate load compared to specimen B7 with four layers. At failure, four plastic hinges, two in the top flange and one each in the bottom flange and end steel stiffeners, had developed in all the un-strengthened and FRP-strengthened specimens.

Chapter 4 Validation of Finite Element Analyses

4.1 Introduction

Finite element, FE, modelling and analysis of specimens is a powerful tool to predict their behaviour in a physical test (Wonseok & Sotelino, 2006). In order to check the performance of the FE analyses, it is useful to carry out the FE validation studies of relatively simple models for which solutions already exist and previously tested specimens before the FE analyses of the specimens to be tested. This Chapter presents the details and results of the FE analyses carried out for nine models for which the solutions exist and thirty-eight test specimens for which the results were available using the LUSAS FE program, Version 14.3 (LUSAS, 2008). The objective was to validate the results of the FE analyses against the theoretical predictions of models and the test results of specimens.

The models chosen were a steel beam, a steel frame, steel plate and web panel, frame and web panel with diagonal stiffeners, glass fabric-strengthened plate and web panel and a steel plate-girder. The steel beam was subjected to pure bending, while the steel and fabric-strengthened plates were subjected to pure shear. The web panels were analysed in such a way that the webs were predominantly loaded in shear. The steel plate-girder was analysed in a similar way to that of un-strengthened control specimen B1 in the tests. The properties of the materials used in the models and the loading and boundary conditions employed are all described. The results of the FE analyses of models are discussed and compared to the theoretical predictions.

Thirty-five of the test specimens analysed were steel plate-girders tested by Rockey and Skaloud (1968 & 1972). The plate-girders mainly varied in the aspect ratio of the web panel, slenderness ratio of the web and thickness of the flanges. The remaining three specimens analysed were the plate-girders tested and analysed by Okeil et al (2009a & 2010). The plate-girders were similar to those tested by the author and included an un-strengthened specimen OB1 and two specimens OB2 and OB3 strengthened using glass FRP, GFRP, pultruded section stiffeners. The results of the FE analyses of all specimens are discussed and compared to those in the tests.

4.2 Validation models and specimens

FE validation studies of the following models and test specimens were carried out.

4.2.1 Models

1. Steel beam
2. Steel plate
3. Steel frame
4. Steel frame with a diagonal stiffener
5. Steel web panel
6. Steel web panel with diagonal stiffener(s)
7. Glass fabric-strengthened plate
8. Glass fabric-strengthened web panel
9. Steel plate-girder

4.2.2 Test specimens

1. Steel plate-girders tested by Rockey and Skaloud
2. Un-strengthened and GFRP-strengthened plate-girders tested by Okeil et al

4.2.3 Material modelling and properties

The steel, GFRP and glass fabric were modelled as isotropic and elastic-perfectly plastic materials in the theoretical predictions and FE analyses, respectively, using the properties given in Table 4.1.

Table 4.1 Properties of steel, GFRP and glass fabric

Property	Steel	GFRP	Glass fabric
Modulus of elasticity, E (GPa)	205	36	13
Yield strength, σ_y (MPa)	300	300	104
Shear modulus, G (GPa)	79	15.7	2.0
Poisson's Ratio, υ	0.3	0.15	0.27

4.2.4 Self-weight

The self weights of the models and specimens were about 1 to 2 % of the loads applied to them and were ignored in the theoretical predictions and the FE analyses.

4.3 Steel beam

Linear and nonlinear FE analyses of a steel beam were carried out and the results were compared to the theoretical predictions for validation. The parameters compared were the maximum longitudinal stress and maximum vertical displacement due to elastic bending and the ultimate plastic load of the beam.

4.3.1 Model geometry, loading and boundary conditions

Figure 4.1 shows the dimensions and the loading and boundary conditions of the beam. A uniformly distributed load, udl, was applied along the length of the beam. The beam was supported at both ends. The support at left end of the beam restrained the beam horizontally and vertically, but was free to rotate. The support at other end restrained the beam vertically, but was free to move horizontally and rotate.

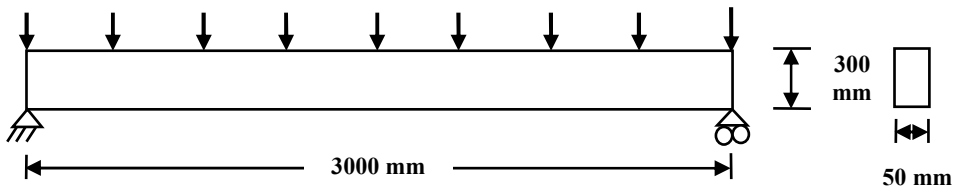

Figure 4.1 Dimensions, loading and boundary conditions of steel beam

4.3.2 Theoretical predictions

1. Maximum longitudinal stress due to elastic bending of the beam is given by Equation 4.1 and Equation 4.2.

$$\sigma_{b\,max} = My/I \qquad \text{Equation 4.1}$$

$$M = {}^{w\,L^2}/_{8} \qquad \text{Equation 4.2}$$

2. Maximum vertical displacement at mid-span of the beam was calculated using Equation 4.3.

$$\delta_{b\,max} = 5wL^4/384EI \qquad \text{Equation 4.3}$$

3. Ultimate plastic load is determined using the upper bound plastic analysis and is given by Equation 4.4 and Equation 4.5.

$$M_p = S_x\sigma_y \qquad \text{Equation 4.4}$$

$$W_c = 8M_p/L \qquad \text{Equation 4.5}$$

4.3.3 FE analyses

Two plane stress FE analyses were performed; a linear elastic analysis at a total load of 300 kN and a nonlinear analysis. Only material nonlinearity was modelled.

4.3.3.1 Element type

8-node semiloof curved thin shell element QSL8 and 8-node thick shell element QTS8 were used to model the steel beam in the FE analyses. The shell elements were used to check their applicability for in-plane bending effects of the steel beam.

4.3.3.2 Mesh convergence

Seven mesh sizes, 40x1, 40x2, 40x4, 40x6, 40x8, 40x10 and 40x12, were used to check the convergence of the solution for each of the QSL8 and QTS8 elements. Figure 4.2 shows the maximum longitudinal stresses due to elastic bending at mid-span of the beam versus the mesh sizes, obtained from linear FE analyses and their comparison with the theoretical predictions. A mesh of 40x8 was found to give converged results and was used in the FE analyses.

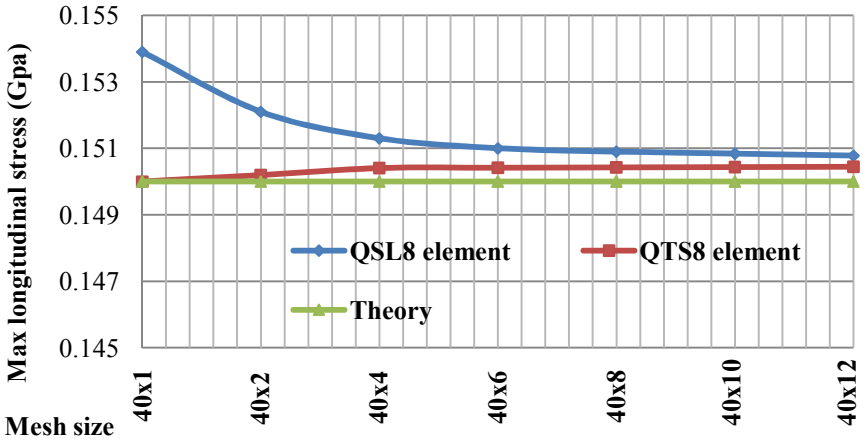

Figure 4.2 Maximum longitudinal stresses at mid-span of beam vs. mesh size

4.3.4 Theoretical predictions and FEA results

Table 4.2 shows a comparison of the theoretical predictions and FEA results of the elastic and elasto-plastic analyses of steel beam.

Table 4.2 Theoretical predictions and FEA results of steel beam

Type of analysis	Theory	FE analyses		QSL8/ Theory	QTS8/ Theory
		QSL8	QTS8		
Linear/ elastic analyses at load of 300 kN					
Max longitudinal stress at mid-span of beam (GPa)	0.15	0.151	0.1504	1.00	1.00
Max vertical displacement at mid-span of beam	4.573	4.775	4.777	1.04	1.04
Nonlinear/ plastic analyses					
Ultimate Plastic load of beam (kN) Mesh 40x8	900	860.1	860.1	0.96	0.96
Mesh 20x8	900	907	906	1.01	1.01

4.3.5 Discussion of results

1. The maximum longitudinal stresses at mid-span of the beam due to elastic bending obtained from linear FE analyses using each of the QSL8 and QTS8 elements were in good agreement with the theoretical predictions.

2. The FEA maximum elastic vertical displacement was 1.04 times larger than the theoretical displacement. The reason of this that the vertical displacement due to shear, being very small, was ignored in the theoretical prediction. The FEA displacement might also include the local displacements at the supports due to very large stresses which were also ignored in the theoretical prediction.

3. The ultimate plastic load, 900 kN, of the beam given by the upper bound plastic analysis was approximately 1.04 times that, 860 kN, obtained from the nonlinear FE analyses with a mesh of 40x8. This is because the longitudinal stresses became higher due to a finer mesh, 40x8, with 40 divisions along length of the beam and reached the value of the yield stress of the steel at a lower load. The two results however agreed for a coarser mesh, 20x8, with 20 divisions along the beam length.

4.4 Steel plate

Linear and nonlinear FE analyses of a simply supported steel plate were carried out and the results were compared to the theoretical predictions for validation. The parameters compared were the elastic critical load, maximum elastic vertical displacement and ultimate plastic load of the plate.

4.4.1 Model geometry, loading and boundary conditions

Figure 4.3 shows the dimensions and the loading and boundary conditions of the steel plate. A uniform edge load was applied along each edge of the plate in such a way that the plate was subjected to pure shear. The plate was supported at both corners on the left edge. The support at the bottom corner restrained the plate horizontally and vertically, but was free to rotate. The support at the top corner restrained the plate horizontally, but was free to move vertically and rotate. All four edges of the plate were restrained in the lateral direction.

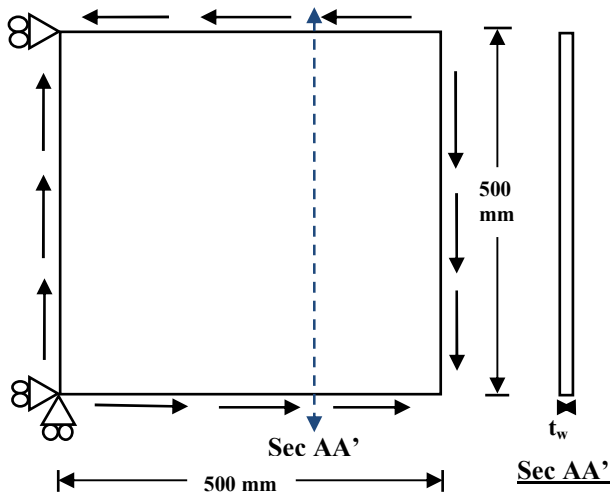

Figure 4.3 Dimensions, loading and boundary conditions of steel plate

4.4.2 Theoretical predictions

1. The maximum elastic vertical displacement of the plate at the un-supported bottom corner was determined using Equation 4.6.

$$\delta_{s\,max} = FL/\,AG \qquad \text{Equation 4.6}$$

2. The elastic shear buckling stress, τ_{cr}, of the simply supported steel plate is given by Equation 4.7 (Timoshenko & Krieger, 1959). The elastic critical load was obtained as the product of shear buckling stress and the area of cross section of the plate.

$$\tau_{cr} = \frac{\pi^2 KE}{12(1-\vartheta^2)}\frac{t_w^2}{d_w^2} \qquad \text{Equation 4.7}$$

Where 'K' is the shear buckling co-efficient and is given by:

$$K = 5.34 + \frac{4}{\left({}^{a}/_{d_w}\right)^2} \quad \text{for } {}^{a}/_{d_w} \geq 1.0 \quad \text{and} \quad K = 4 + \frac{5.34}{\left({}^{a}/_{d_w}\right)^2} \quad \text{for } {}^{a}/_{d_w} < 1.0$$

3. The ultimate plastic load in shear, V_p, of the plate with material nonlinearity, MNL, only was calculated using Equation 4.8 (Trahair et al, 2001).

$$V_p = \sigma_{yw} d_w t_w / \sqrt{3} \qquad \text{Equation 4.8}$$

4. The ultimate load of the plate with the material and geometric nonlinearities, MGNL, was estimated using the procedure in EC3 for estimation of the ultimate load of the web plate, $V_{bw,Rd}$, of a plate-girder and is given by Equation 4.9.

$$V_{bw,Rd} = \chi_w d_w t_w \sigma_{yw} / \sqrt{3} \gamma_{M1} \qquad \text{Equation 4.9}$$

4.4.3 Modes of buckling and failure

The simply supported thin steel plate subjected to pure shear tends to buckle out-of-plane along tensile diagonal and perpendicular to the compression diagonal (Trahair et al, 2001). The plate shall fail by yielding in the shear. The modes of the buckling and failure are shown in Figure 4.4.

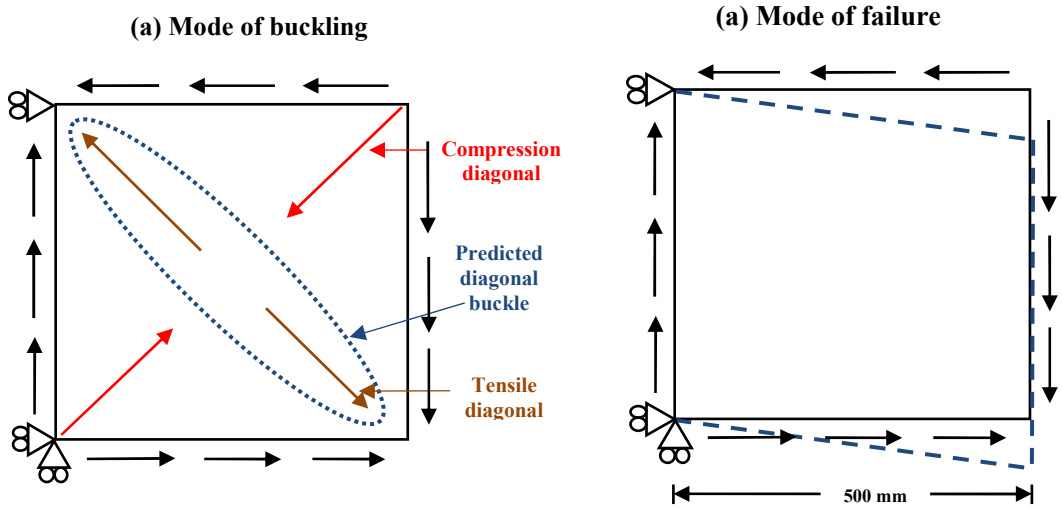

Figure 4.4 Predicted modes of (a) buckling and (b) failure of steel plate

4.4.4 FE analyses

The following FE analyses of the plate with a thickness of 3 mm were carried out.

1. Linear elastic analyses at an applied shear load of 80 kN to obtain the maximum vertical displacement at the un-supported bottom corner of the plate.
2. Linear eigenvalue analyses to obtain the elastic critical load.
3. Nonlinear analyses to obtain the ultimate plastic load. Initially, only material nonlinearity was modelled. Geometric nonlinearity was also then added by using the first buckling mode from eigenvalue analyses with a maximum lateral displacement of 1 mm in the plate.

Linear eigenvalue and nonlinear FE analyses of the plate with the thicknesses of 0.5, 1, 2, 3, 4, 5 and 6 mm were then carried out and the elastic critical and ultimate plastic loads were obtained.

4.4.4.1 Element type

The following five elements were used in the first stage of FE analyses.

1. 8-node semiloof curved thin shell element QSL8
2. 8-node thick shell element QTS8
3. 8-node solid continuum element HX8
4. 8-node solid continuum element HX8M with enhanced strains
5. 20-node solid continuum element HX20

The thin shell QSL8 element was only used for the second set of FE analyses.

4.4.4.2 Mesh convergence

Six uniform mesh sizes 4x4, 8x8, 12x12, 16x16, 20x20 and 40x40 were used to check the convergence of the results of the eigenvalue FE analyses. Figure 4.5 shows the elastic critical load plotted versus the six mesh sizes for each of QSL8, QTS8, HX8M and HX20 elements only. The results for the elastic critical load using the QSL8 element converged for a mesh of 8x8 and those using the QTS8 and HX20 elements converged for the meshes of 12x12 and 16x16 respectively. A mesh of 20x20 was found to give converged results for HX8M element. None of the six meshes used for HX8 element could give satisfactory results, Table 4.3; so are not plotted in Figure 4.5.

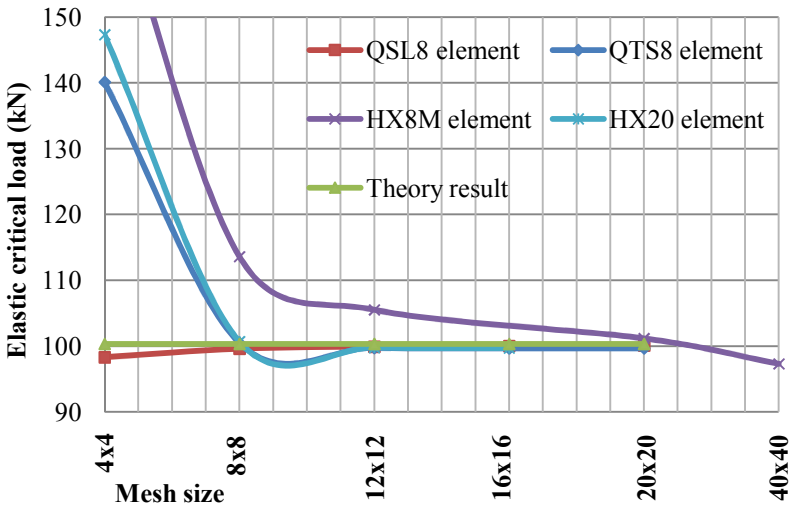

Figure 4.5 Elastic critical load of steel plate vs. mesh sizes

4.4.5 Theoretical predictions and FEA results

Table 4.3 gives a comparison of the results of the FE analyses and theoretical predictions of the 3 mm thick plate. Figure 4.6 shows the modes of buckling and failure of the 3 mm thick plate obtained from the FE analyses. The theory and FEA elastic critical and ultimate plastic loads of the plate with the thicknesses 0.5, 1, 2, 3, 4, 5 and 6 mm are given in Table 4.4 and also shown in Figure 4.7.

Table 4.3 Theoretical predictions and FEA results of steel plate

Type of analysis	**Theory**	**Element type and mesh size**				
		QSL8 8x8	**QTS8 16x16**	**HX8 40x40**	**HX8M 20x20**	**HX20 16x16**
Linear/ elastic analyses						
Max vertical displacement (mm) at a load of 80 kN	0.338	0.338	0.338	0.338	0.3378	0.341
Theory/ FEA	---	1.0	1.0	1.0	1.0	0.99
Eigenvalue/ buckling analyses						
Elastic critical load kN)	93.5	92.8	92.8	411	90.8	92.9
Theory/ FEA	---	1.02	1.02	0.23	1.04	1.02
Nonlinear analyses (material nonlinearity only)						
Ultimate plastic load (kN)	259.8	259.8	259.8	---	256.6	249.4
Theory/ FEA	---	1.0	1.0	---	1.01	1.04
Nonlinear analyses (material and geometric nonlinearities)						
Ultimate load (kN)	129.3	131.3	133.5	---	---	---
FEA/EC3	---	1.015	1.017	---	---	---

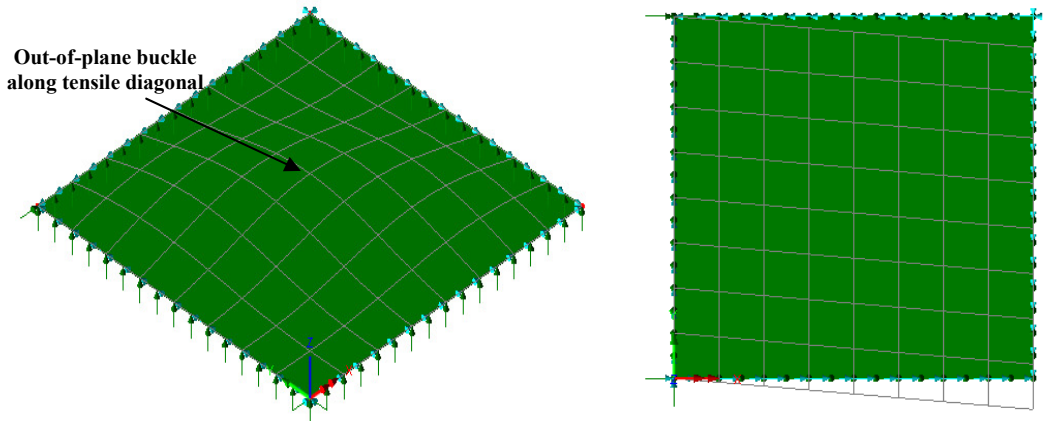

Figure 4.6 Modes of (a) first buckling and (b) failure steel plate (QSL8 element with 8x8 mesh)

Table 4.4 Theoretical and FEA elastic critical and ultimate loads of steel plate

Plate thickness t_w (mm)	Slenderness ratio (d_w/t_w)	Elastic critical load (kN)			Ultimate plastic load, MNL (kN)		
		Theory	FEA	Theory to FEA	Theory	FEA	Theory to FEA
0.5	1000	0.43	0.429	1.01	43.3	43.3	1.00
1.0	500	3.46	3.44	1.01	86.6	86.6	1.00
2.0	250	27.70	27.49	1.01	173.1	173.2	1.00
3.0	167	93.47	92.78	1.01	259.7	259.8	1.00
4.0	125	221.56	219.93	1.01	346.2	346.3	1.00
5.0	100	432.74	429.55	1.01	432.8	433.0	1.00
6.0	80	747.78	742.26	1.01	519.3	519.6	1.00

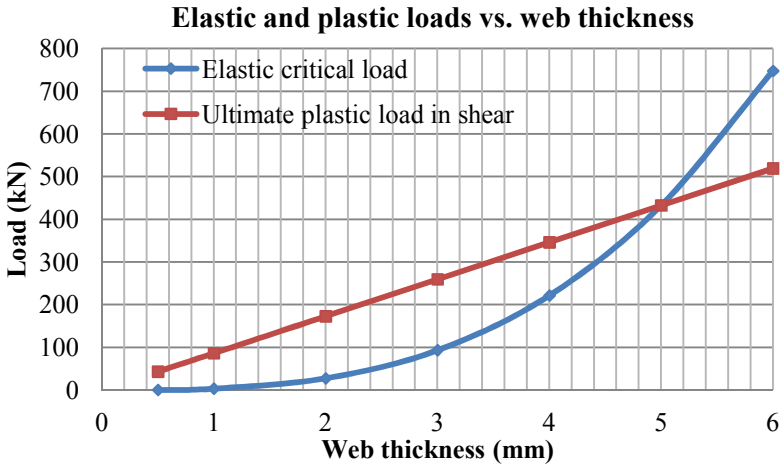

Figure 4.7 Elastic and plastic loads vs. thicknesses of steel plate

4.4.6 Discussion of results

1. At an applied shear load of 80 kN, the theoretical prediction for the maximum elastic vertical displacement at the un-supported bottom corner of the 3 mm thick plate was in very good agreement with those obtained from linear FE analyses using each of the QSL8, QTS8, HX8, HX8M and HX20 elements.

2. The theoretical elastic critical load of the 3 mm thick plate was also in very good agreement with the loads at the first buckling mode obtained from eigenvalue analyses using either of QSL8, QTS8, HX8M and HX20 elements.

3. The theoretical and FEA modes of the buckling and failure of the plate shown in Figure 4.4 and Figure 4.6 were in good agreement.

4. The theoretical ultimate plastic loads of 3 mm thick plate were in good agreement with those obtained from the FE analyses by modelling material nonlinearity only and using each of the QSL8, QTS8, HX8 and HX20 elements. At the ultimate plastic load of the plate in the FE analyses, the shear stresses, as expected, were uniform over whole area of the plate surface and were equal to the yield stress in shear, $\tau_{yw} = \sigma_{yw}/\sqrt{3} = 0.1732$ GPa, of the steel.

5. The ultimate loads of 3 mm plate obtained from the FE analyses by modelling the material and geometric nonlinearities and using QSL8 and QTS8 elements were in good agreement with that determined using the procedure in EC3.

6. In the mesh convergence using the linear FE analyses, none of the six meshes used for the HX8 element could give satisfactory results for the elastic critical load. The element was therefore not used in the nonlinear analyses.

7. The 16x16 and 20x20 meshes gave satisfactory results of for the solid elements HX20 and HX8M in the linear and nonlinear FE analyses. However, the analyses took at least three times the computing time required for the shell elements QSL8 and QTS8 with meshes of 8x8 and 12x12 respectively.

8. The theoretical and FEA elastic critical loads and ultimate plastic loads of the steel plates with the thicknesses of 0.5, 1, 2, 3, 4, 5 and 6 mm were in very good agreement.

4.5 Steel frame

Nonlinear FE analyses of a steel frame were carried out to compare the FEA ultimate plastic loads to those determined using the upper bound plastic analyses.

4.5.1 Model geometry, loading and boundary conditions

The steel frame comprised of the top and bottom flanges and two vertical stiffeners rigidly connected at the ends. Figure 4.8 shows the dimensions and the loading and boundary conditions of the frame.

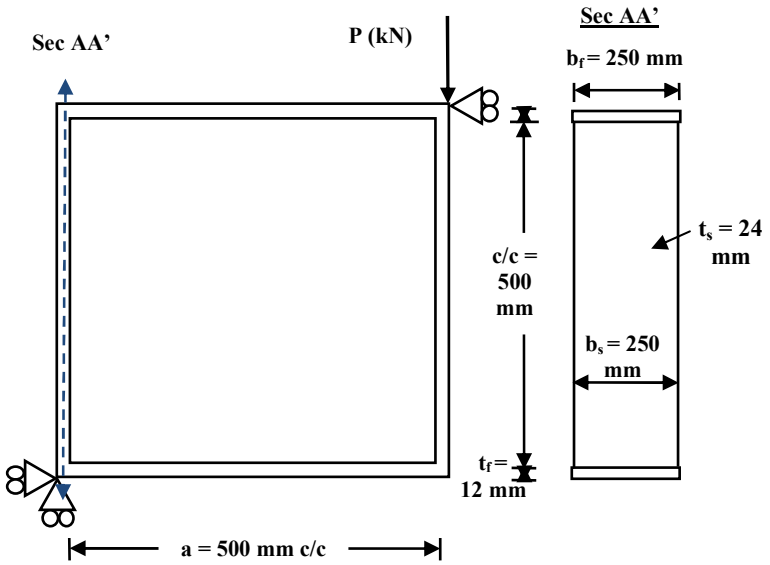

Figure 4.8 Dimensions, loading and boundary conditions of steel frame

4.5.2 Theoretical predictions

The ultimate plastic load, V_p, of the steel frame is estimated using the upper bound plastic analysis and is given by Equation 4.10.

$$V_p = \frac{b_f t_f^2 \sigma_{yf}}{a} \qquad \text{Equation 4.10}$$

4.5.3 Modes of failure

Assuming the vertical stiffeners were stiff enough to undergo any bending deformation, the steel frame would fail by the development of four plastic hinges in the top and bottom flanges, one each at four corners. The mode of the failure of the frame compared to that obtained from the FE analysis by modelling material nonlinearity only are shown in Figure 4.9.

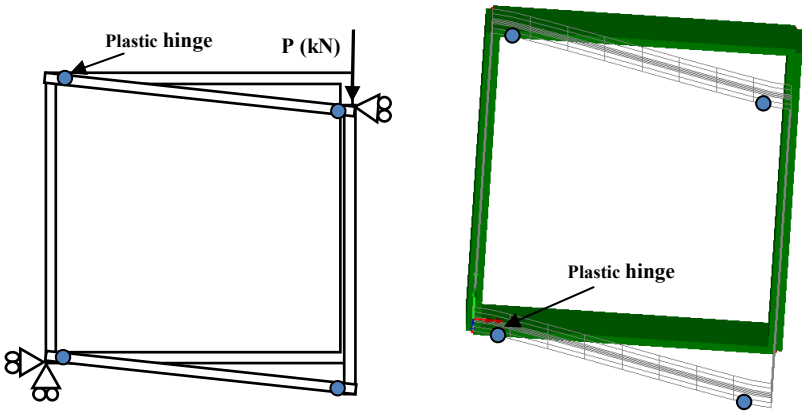

Figure 4.9 Predicted and FEA modes of failure of steel frame

4.5.4 FE analyses

Thin shell QSL8 and thick shell QTS8 element were used. Nonlinear FE analyses of the frame were carried out to obtain the ultimate plastic loads and modes of the failure. Initially, the material nonlinearity was only modelled. The geometric nonlinearity was also then added in the analyses.

4.5.5 Theoretical predictions and FEA results

Table 4.5 gives a comparison of the results of the upper bound and nonlinear FE analyses. Figure 4.10 shows the applied load versus vertical deflection at the un-supported bottom corner of the steel frame obtained from the FE analyses.

Table 4.5 Theoretical predictions and FEA results of steel frame

Analysis	**Ultimate load (kN)**		**Ratio of loads**		**Mode of failure**
	(1) MNL	(2) MGNL	UB/ FEA(1)	FEA(2)/ FEA(1)	
Upper bound	*21.6 **27.0	---	---	---	Four plastic hinges in flanges at corners
FEA (QSL8 element)	26.6	24.7	1.23 0.99	0.93	Four plastic hinges in flanges each at 50 mm (approx) from corner
FEA (QTS8 element)	26.4	24.58	1.22 0.98	0.93	Same as above

* assuming that hinges in the flanges form at corners (500 mm apart)
** assuming that hinges in the flanges form at 50 mm from corners (400 mm apart) i.e. 500/400 = 1.25

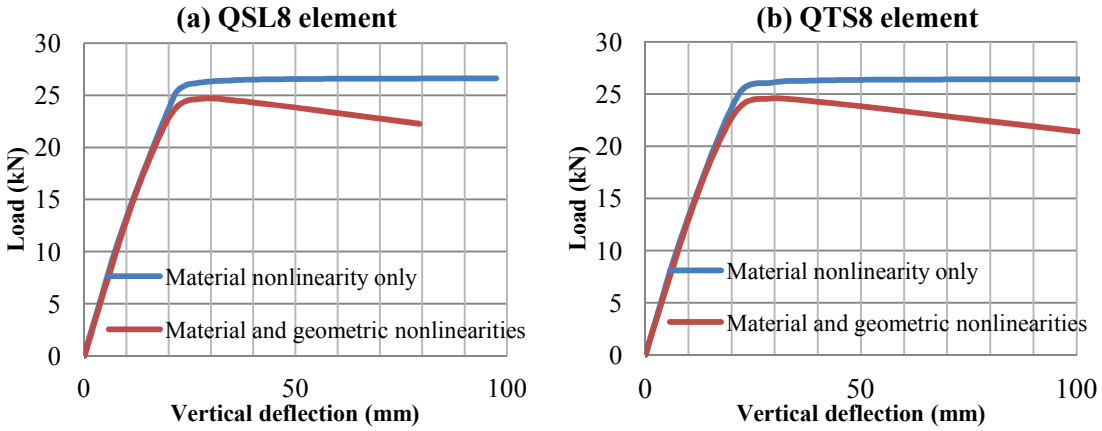

Figure 4.10 Load vs. vertical deflection of steel frame using (a) QSL8 and (b) QTS8 elements

4.5.6 Discussion of results

1. The ultimate plastic load of the steel frame given by the upper bound plastic analysis was in good agreement with those obtained from FE analyses by modelling the material nonlinearity only using either QSL8 or QTS8 element.

2. The predicted and FEA modes of the failure of the steel frame were similar; only difference being plastic hinges in the flanges, assumed to form at corners, were at a distance of approximately 50 mm from the corners.

3. The load-vertical deflection responses of the steel frame obtained from the nonlinear FE analyses using either QSL8 or QTS8 element were similar.

4.6 Steel frame with a diagonal stiffener

Nonlinear FE analyses of the steel frame with a diagonal steel and GFRP stiffener were carried out and the results were compared to those of the upper bound plastic analyses.

4.6.1 Model geometry, loading and boundary conditions

The dimensions and the loading and boundary conditions of the steel frame were same as shown in Figure 4.8. A diagonal stiffener, 50 mm wide by 3 mm thick, was added to the frame in such a way that its ends were connected to the loaded and supported joints of the frame.

4.6.2 Theoretical predictions

The ultimate plastic load, V_p, of the steel frame with a diagonal stiffener is estimated using the upper bound plastic analysis and is given by Equation 4.11. Euler load, F_e, of the diagonal stiffener is determined using Equation 4.12.

$$V_p = \frac{b_f t_f^2 \sigma_{yf}}{a} + \frac{t_s d_s \sigma_{ys}}{\sqrt{2}} \qquad \text{Equation 4.11}$$

$$F_e = \frac{\pi^2}{K L^2} EI \qquad \text{Equation 4.12}$$

4.6.3 Modes of failure

The model would fail by yielding of the diagonal stiffener and development of four plastic hinges in the top and bottom flanges, one each at four corners. The mode of the failure of the model compared to that obtained from the FE analysis by modelling the material nonlinearity only are shown in Figure 4.11.

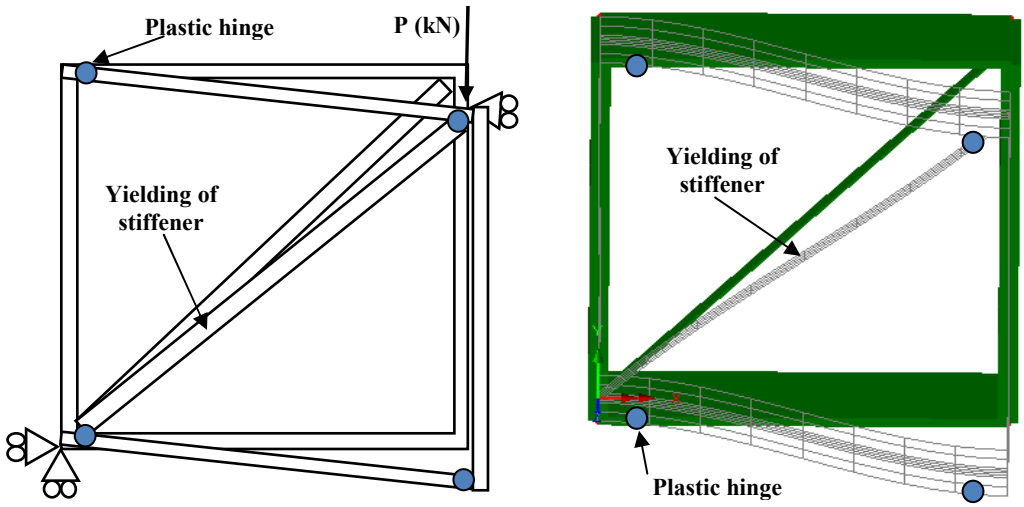

Figure 4.11 Predicted and FEA modes of failure of steel frame with a diagonal stiffener

4.6.4 FE analyses

The thin shell QSL8 element was used. Nonlinear FE analyses of the frame with a diagonal stiffener were carried out and the ultimate plastic load and mode of the failure were obtained. Initially, material nonlinearity was only modelled. The geometric nonlinearity was also added by using the first buckling mode from eigenvalue analyses.

4.6.5 Theoretical predictions and FEA results

Table 4.6 gives a comparison of the results of the upper bound and nonlinear FE analyses. Figure 4.12 shows the applied load versus vertical deflection at the un-supported bottom corner of the model obtained from the FE analyses.

Table 4.6 Theoretical predictions and FEA results of frames with a diagonal stiffener

Stiffener details	**Ultimate load, UL (kN)**			**Ratio of UL**		**Mode of failure in FE analyses**
	(1) Upper bound	(2) FEA (MNL)	(3) FEA (MGNL)	(2)/(1)	(3)/(2)	
Diagonal steel stiffener	53.4	58.5	25.3	1.09	0.43	Yielding of diagonal stiffener and hinges in flanges near four corners; in FEA with MGNL, the stiffener underwent buckling
Diagonal GFRP stiffener	53.4	58.5	24.8	1.09	0.42	Same as above

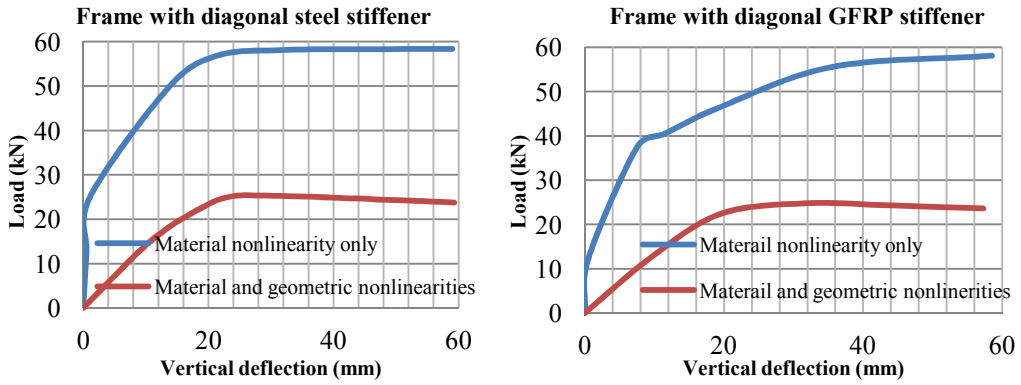

Figure 4.12 Load vs. vertical deflection of steel frame with a diagonal stiffener

4.6.6 Discussion of results

1. The ultimate plastic load of the steel frame with a diagonal steel or GFRP stiffener given by the upper bound plastic analysis was in good agreement with that obtained from FE analysis by modelling the material nonlinearity only. The predicted and FEA modes of the failure of the frame with a diagonal stiffener were also same.

2. In the FE analyses with the material and geometric nonlinearities, the diagonal stiffener underwent buckling and the frame failed like a bare steel frame with the development of four plastic hinges, two each in the top and bottom flanges near the corners.

3. Euler load of the diagonal stiffener with both ends fixed was approximately 2 kN. The sum of the Euler load of the diagonal stiffener and the ultimate plastic load, 21.6 kN, of the frame only given by the upper bound plastic analysis was 23.6 kN. This load was in close agreement with the FEA ultimate load, 25.3 kN, of the model with the material and geometric nonlinearities.

4.7 Steel web panel

Nonlinear FE analyses of the steel web panels were carried out and the results were compared to those given by the theoretical predictions.

4.7.1 Model geometry, loading and boundary conditions

The dimensions and the loading and boundary conditions of the steel frame surrounding the web plate were same as shown in Figure 4.8. The web plates were 0.5, 1, 2, 3, 4, 5 and 6 mm thick and were connected to the flanges and vertical stiffeners of the frame along the edges.

4.7.2 Theoretical predictions

The ultimate plastic load, V_p, of the web panel is estimated using the upper bound plastic analysis and is given by Equation 4.13. There is no formula to determine the ultimate load of the web panel with material and geometric nonlinearities. The design ultimate loads of the web panels are determined using the procedure in EC3 as given by Equation 4.9 and Equation 4.14 and compared to the ultimate loads obtained from the FE analyses. Details of the calculations are given in Appendix-B.

$$V_p = \frac{b_f t_f^2 \sigma_{yf}}{a} + \frac{t_w d_w \sigma_{yw}}{\sqrt{3}} \qquad \text{Equation 4.13}$$

$$V_{bf,Rd} = b_f t_f^2 \sigma_{yf} / c\gamma_{M0} \left[1 - \{M_{Ed}/M_{f,Rd}\}^2\right] \qquad \text{Equation 4.14}$$

4.7.3 Modes of failure

1. In the case of considering material nonlinearity only, the web panel would fail by yielding of the web plate and development of four plastic hinges, two in each of the top and bottom flanges at the corners.
2. If both material and geometric nonlinearities are considered, then according to the procedure assumed in EC3, the failure of the web panel would start with an out-of-plane diagonal buckling of the web followed by the diagonal yielding of the web in the tensile stress field and development of four plastic hinges, two in each of the top and bottom flanges.

4.7.4 FE analyses

The thin shell QSL8 element was used. Based upon the convergence study in Section 4.4.4.2, a mesh of 8x8 for the web plate was used. Nonlinear FE analyses of the web panel were carried out to obtain the ultimate loads and modes of the failure. Initially, material nonlinearity was only modelled. The geometric nonlinearity was also then added in the analyses by using the first buckling mode from eigenvalue analyses with maximum lateral displacements of $0.3t_w$ mm in the web plate.

4.7.5 Theoretical predictions and FEA results

Table 4.7 gives a comparison of the ultimate loads of the web panel given by the theoretical predictions and nonlinear FE analyses. Figure 4.13 shows the modes of the failure of the web panel obtained from FE analyses with (a) material nonlinearity only and (b) both material and geometric nonlinearities. Figure 4.14 shows the ultimate loads versus web thickness of the web panel obtained from the FE analyses.

Table 4.7 Theoretical and FEA ultimate loads of web panels

Web thickness t_w (mm)	Web slenderness	Ultimate load (MNL)			Ultimate load (MGNL)		
		Upper bound (UB)	FEA	UB to FEA	EC3	FEA	FEA to EC3
0.5	1000	65	70	0.93	34	56	1.64
1.0	500	108	113	0.96	59	83	1.41
2.0	250	195	200	0.98	116	134	1.16
3.0	167	281	285	0.99	193	181	0.94
4.0	125	368	371	0.99	293	282	0.96
5.0	100	455	456	1.00	417	389	0.93
6.0	80	541	542	1.00	564	494	0.88

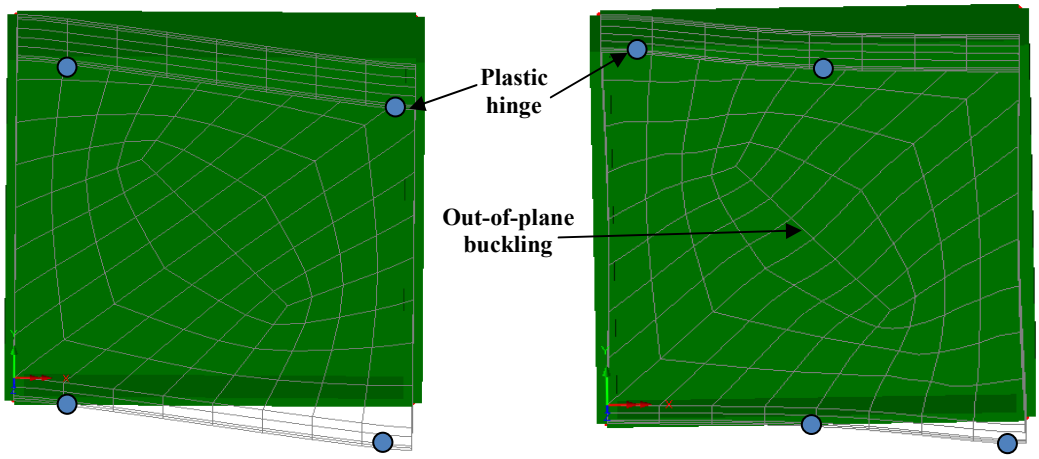

Figure 4.13 Modes of failure of web panel with a 3 mm thick web obtained from FE analyses with (a) MNL and (b) MGNL

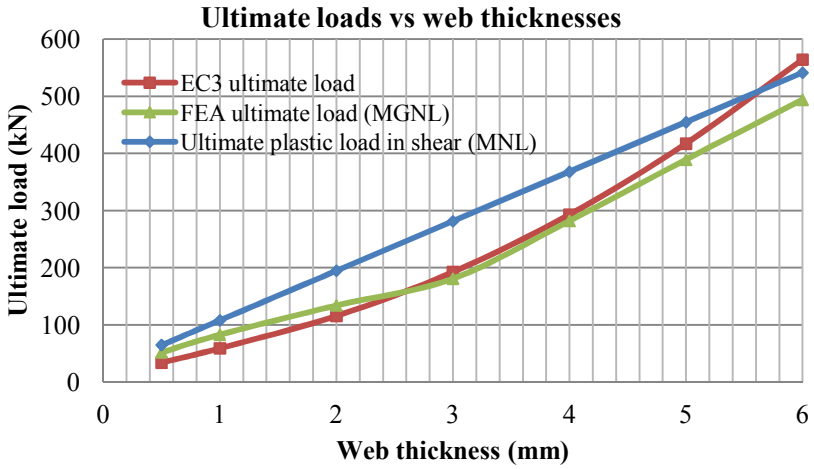

Figure 4.14 Ultimate load of steel web panel vs. web thickness

4.7.6 Discussion of results

1. The ultimate plastic loads of the web panels given by the upper bound plastic analyses were in good agreement with those obtained from FE analyses by modelling the material nonlinearity only.

2. The predicted and FEA modes of the failure of the web panel by modelling either the material nonlinearity only or both the material and geometric nonlinearities were in agreement.

3. Compared to the design ultimate loads given by the procedure in EC3, the FEA ultimate loads of the web panel were un-conservative for higher web slendernesses, $d_w/t_w > 167$, and conservative for lower web slendernesses, $d_w/t_w < 100$. In the intermediate range, the FEA and design ultimate loads of models were in agreement.

4. The design ultimate load, 564 kN, of the web panel with a 6 mm thick web given by the procedure in EC3 was greater that the ultimate plastic load of 541 kN. This is illogical and incorrect because the model cannot carry a load greater than its ultimate plastic load. It is therefore reasonable to limit that the design ultimate load of the web panel should be less than or equal to the ultimate plastic load in all cases.

4.8 Steel web panel with diagonal stiffeners

Nonlinear FE analyses of the steel web panels with diagonal steel or GFRP stiffeners on both sides of the web were carried and the results were compared to those determined from the upper bound plastic analyses. A web panel with a diagonal steel stiffener on one side of the web was also analysed to compare its behaviour to that with diagonal stiffeners of equivalent stiffness on both sides of the web.

4.8.1 Model geometry, loading and boundary conditions

The dimensions and the loading and boundary conditions of the steel frame surrounding the web plate were same as shown in Figure 4.8. A total of fifteen models with different thicknesses of the web were analysed. The web plate was strengthened with diagonal steel stiffeners, each 25 mm wide by 3 mm thick, on both sides of the web in the seven models and by the diagonal GFRP stiffeners of the same cross-section in another seven models. In the last model, a diagonal steel stiffener, 50 mm wide by 3 mm thick, was provided on one side of the web.

4.8.2 Theoretical predictions

The ultimate plastic load, V_p, of the with web panel with diagonal stiffener(s) is estimated using the upper bound plastic analysis and is given by Equation 4.15.

$$V_p = \frac{b_f t_f^2 \sigma_{yf}}{a} + \frac{t_w d_w \sigma_{yw}}{\sqrt{3}} + \frac{t_s d_s \sigma_{ys}}{\sqrt{2}} \qquad \text{Equation 4.15}$$

4.8.3 Modes of failure

The model would fail by yielding of the web and diagonal stiffener(s) and development of four plastic hinges in the top and bottom flanges, one each at four corners. The mode of the failure of the model compared to that obtained from the FE analysis by modelling material nonlinearity only are shown in Figure 4.15.

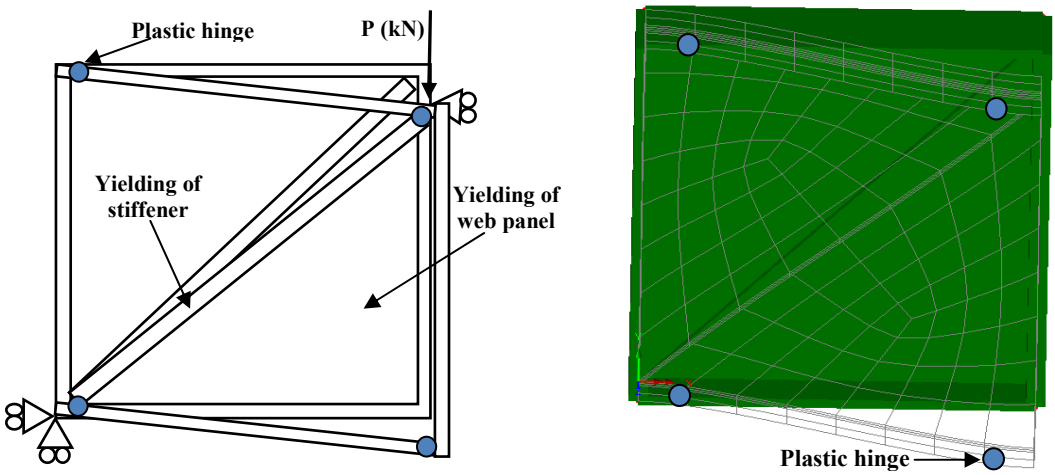

Figure 4.15 Predicted and FEA modes of failure of web panel with diagonal stiffeners

4.8.4 FE analyses

The thin shell QSL8 element was used. Nonlinear FE analyses of the web panel with diagonal stiffener(s) were carried out to obtain the ultimate loads and modes of the failure. Initially, only material nonlinearity was modelled. Geometric nonlinearity was also added by using the first buckling mode from eigenvalue analyses with maximum lateral displacements of $0.3t_w$ mm in the web plate.

4.8.5 Theoretical predictions and FEA results

Table 4.8 gives a comparison of the theoretical and FEA ultimate loads of models. Figure 4.16 shows the ratio of ultimate loads of the web panels with diagonal steel and GFRP stiffeners versus web thicknesses and Figure 4.17 shows the applied load versus vertical deflection of the web panels with the diagonal steel stiffener(s) on one and both sides of the web.

Table 4.8 Theoretical and FEA ultimate loads of web panels with diagonal stiffeners

Thickness of web t_w (mm)	(1) Theory (Upper bound)	Ultimate load (MNL) kN		Ultimate load (MGNL) kN		Ratio of ultimate loads		
		(2) Steel stiffeners	(3) GFRP stiffeners	(4) Steel stiffeners	(5) GFRP stiffeners	(1) /(2)	(4) /(2)	(5) /(3)
0.5	96.7	101.8	101.8	67.2	64.9	0.95	0.66	0.64
1.0	140.0	145.1	145.3	100.3	93.4	0.96	0.69	0.64
2.0	226.6	231.2	231.2	163.4	160.2	0.98	0.71	0.69
3.0	313.2	316.6	316.9	265.7	237.4	0.99	0.84	0.75
4.0	399.8	402.5	402.5	365.0	341.2	0.99	0.91	0.85
5.0	486.5	488.0	488.1	455.0	433.7	1.00	0.93	0.89
6.0	573.0	569.8	573.7	543.6	523.7	1.00	0.95	0.92

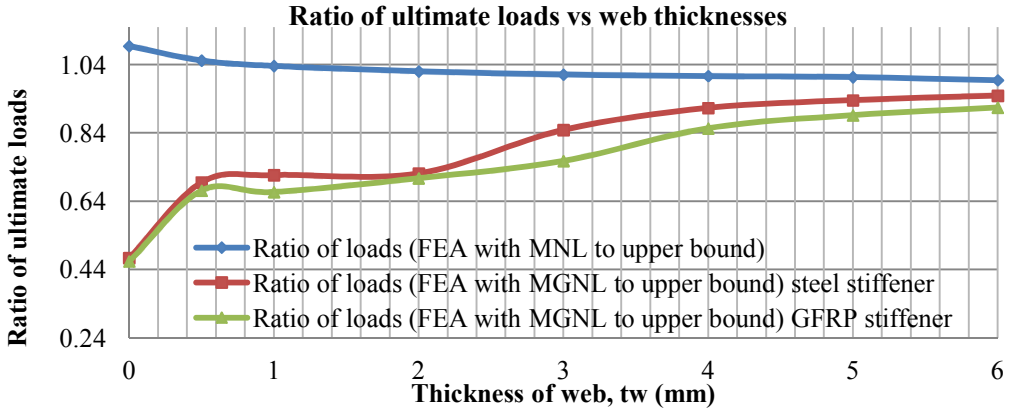

Figure 4.16 Ratio of ultimate loads of web panels with diagonal steel and GFRP stiffeners vs. web thicknesses

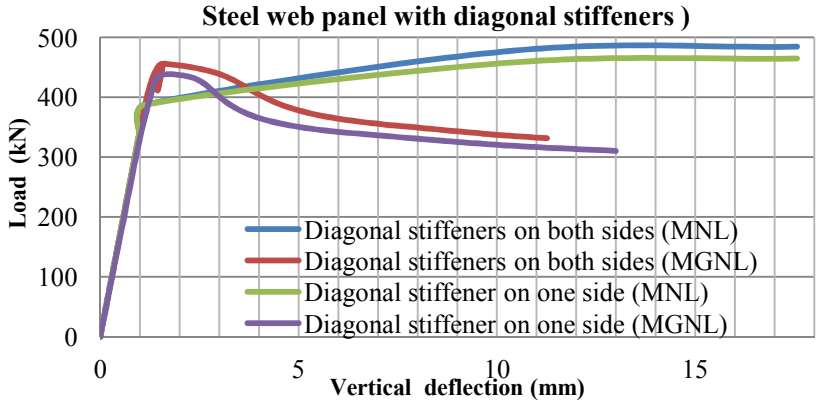

Figure 4.17 Load vs. vertical deflection of web panel with diagonal stiffener(s)

4.8.6 Discussion of results

1. The ultimate plastic loads of web panels either with the steel or GFRP diagonal stiffeners given by the upper bound plastic analyses were same because of the same yield strengths of the steel and GFRP.

2. The ultimate plastic loads of all web panels either with the steel or GFRP diagonal stiffeners given by the upper bound plastic analyses were in good agreement with those obtained from FE analyses by modelling the material nonlinearity only.

3. The predicted modes of the failure of all web panels with the diagonal stiffeners were similar to those obtained from the nonlinear FE analyses by modelling the material nonlinearity; only difference being plastic hinges in the flanges assumed to form at corners, were at a distance of approximately 50 mm from the corners.

4. The ultimate loads and load-deflection responses of the web panel with diagonal steel stiffener(s) on both sides of the web obtained from the FE analyses were in good agreement with those having the diagonal stiffener of equivalent stiffness on one side of the web, Figure 4.17.

5. The ultimate loads of the web panels with diagonal stiffeners on both sides of the web with a thin web, $\tau_{cr} < \tau_{yw}$, obtained from the FE analyses by modelling both material and geometric nonlinearities were approximately equal to the sum of the ultimate loads of the web panel given by EC3 and the ultimate plastic load of the diagonal stiffener(s). Similarly, the FEA ultimate loads of the models with a thick web, $\tau_{cr} \geq \tau_{yw}$, were approximately equal to the ultimate plastic load of the web panel only without the diagonal stiffeners.

4.9 Glass fabric-strengthened plate

Linear and nonlinear FE analyses of the steel plate strengthened using different thickness of glass fabric sheets were carried out and the results were compared to those given by the theoretical predictions. The parameters compared were elastic critical and ultimate loads of the glass fabric-strengthened plate. The fabric layers were assumed to be bonded perfectly to the steel and to act as homogenous material (i.e. no breakdown of bond within the fabric or delamination of the fabric layers).

4.9.1 Model geometry, loading and boundary conditions

Figure 4.18 shows the geometry and the loading and boundary conditions of the glass-fabric strengthened plate. 3, 6, 9, 12 and 15 mm thick layers of the glass fabric were applied to one side of the 3 mm thick steel plate over the whole area of surface of the plate.

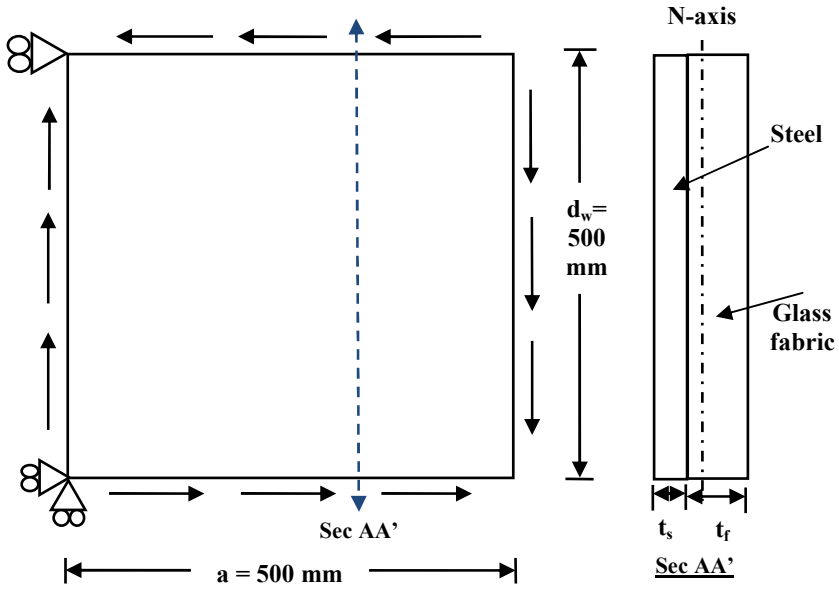

Figure 4.18 Dimensions, loading and boundary conditions of glass fabric-strengthened plate

4.9.2 Theoretical predictions

The elastic critical load of the composite plate was determined with the help of Equation 4.7 taking into account the equivalent steel thickness based on the flexure stiffness. The ultimate plastic load of the strengthened plate was estimated using the upper bound plastic analyses, Equation 4.8, as the ultimate plastic loads in shear of the steel and glass fabric sections. The ultimate load of the plate with material and geometric nonlinearities was estimated using the procedure in EC3, Equation 4.9. Further details and calculations are given in Appendix-B.

4.9.3 FE analyses

Linear eigenvalue FE analyses of the strengthened plate were carried out to obtain the elastic critical load. Nonlinear analyses were performed to obtain the ultimate load. Initially, the material nonlinearity was only modelled. The geometric nonlinearity was also then added in the analyses by using the first buckling mode from eigenvalue analyses with maximum lateral displacements of 1 mm in the plate.

4.9.3.1 Merge option

A merge option available in LUSAS to join the surfaces with different material properties was used for joining the steel and glass fabric sections. The merge option provides full interaction between two geometrical features being merged together. After merging, both the materials retain their properties, but act as the single feature.

4.9.3.2 Element and mesh

The thick shell QTS8 element with a uniform mesh of 12x12 was used in the FE analyses. The reason for using QTS8 was that the merge option was only available for that element.

4.9.4 Theoretical predictions and FEA results

Table 4.9 gives a comparison of the results of theoretical predictions and FE analyses of the glass fabric-strengthened plate. Figure 4.19 shows the ratio of the ultimate loads versus the thickness of glass fabric.

Table 4.9 Theoretical and FEA results of the glass fabric-strengthened plate

Thickness of section (mm)		**Elastic critical load (kN)**			**Ultimate load (MNL) kN**			**Ultimate load (MG NL) kN**		
Steel	**Glass fabric**	**Theory**	**FEA**	**Theory/ FEA**	**Theory (UB)**	**FEA**	**Theory/ FEA**	**EC3**	**FEA**	**EC3/ FEA**
3	0	93.5	92.8	1.01	259.7	259.8	1.00	129.2	134.0	0.96
3	3	165.6	164.9	1.00	349.7	349.8	1.00	210.6	190.9	1.10
3	6	422.4	419.2	1.01	439.7	439.9	1.00	361.8	290.1	1.25
3	9	963.9	949.8	1.01	529.7	530.0	1.00	530.0	473.3	1.12
3	12	1881	1831	1.03	619.7	610.6	1.01	619.7	608.4	1.02
3	15	3238	3119	1.04	709.7	688.6	1.03	709.7	700.7	1.01

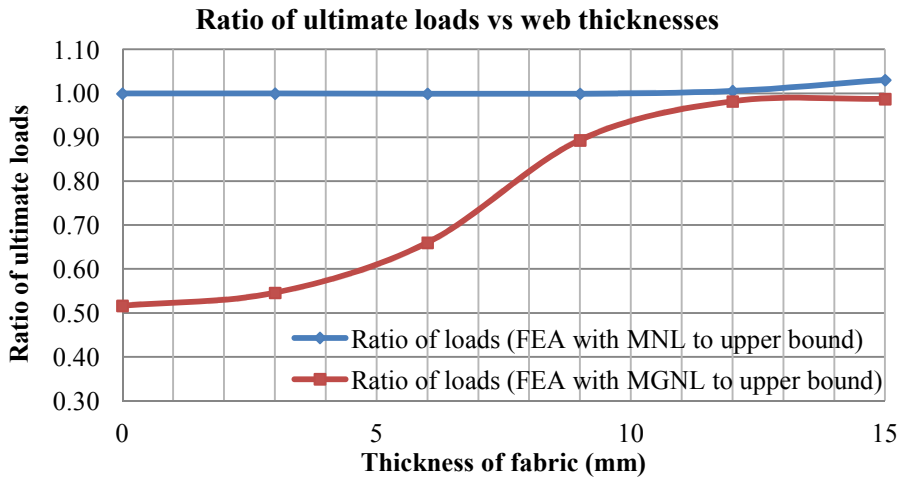

Figure 4.19 Ratio of ultimate loads of strengthened plate vs. thicknesses of glass fabric

4.9.5 Discussion of results

1. The theoretical elastic critical loads of the glass fabric-strengthened plate for all thicknesses of the fabric were in good agreement with those obtained from eigenvalue FE analyses. The theoretical loads, however, became slightly un-conservative as the thickness of the fabric increased. This is because that the eccentric effects of the applied load, which were ignored in the theoretical predictions, were accounted in the FE analyses.

2. For all thicknesses of the glass fabric, the ultimate plastic loads of the strengthened plate given by the upper bound plastic analyses were in very good agreement with those obtained from the nonlinear FE analyses by modelling the material nonlinearity only.

3. The ultimate loads of the strengthened plate given by the procedure in EC3 and those obtained from the nonlinear FE analyses by modelling the material and geometric nonlinearities were not in good agreement for all thicknesses of the glass fabric. The EC3 loads of the plate for the fabric thicknesses of 3 and 6 mm were 1.10 and 1.25 times greater than the FEA loads because of the increasing eccentric effects of the applied load. The EC3 load was then 1.12 times the FEA load for the fabric thickness of 9 mm because the elastic critical load became greater than the ultimate plastic load. For the fabric thicknesses of 12 and 15 mm, the EC3 and FEA loads of the plate were in good agreement and approximately equal to the ultimate plastic loads because the effect of the geometric nonlinearity then became almost negligible, Figure 4.19.

4.10 Glass fabric-strengthened web panel

Nonlinear FE analyses of the steel web panel strengthened using different thicknesses of glass fabric sheets to one side of the web were carried out and the results were compared to those of the theoretical predictions.

4.10.1 Model geometry, loading and boundary conditions

The geometry and the loading and boundary conditions of the frame surrounding the glass fabric-strengthened web plate were same as shown in Figure 4.8. Layers of the glass fabric were 3, 6, 9, 12 and 15 mm thick and were applied to one side of the 3 mm thick steel web plate over the whole area of surface of the plate.

4.10.2 Theoretical predictions

The ultimate plastic load of the glass fabric-strengthened web panel was estimated using the upper bound plastic analyses, Equation 4.13. The ultimate load by taking into account the material and geometric nonlinearities of the plate was determined using the procedure given in EC3. Further details and calculations are given in Appendix-B.

4.10.3 Modes of failure

1. In the case of considering material nonlinearity only, the model would fail by yielding of the strengthened web and development of four plastic hinges, two each in the top and bottom flanges at the corners.

2. If both material and geometric nonlinearities are considered, the failure of the model would occur by diagonal yielding of the strengthened web in the tensile stress field and development of four plastic hinges, two in each of the top and bottom flanges.

4.10.4 FE analyses

The thick shell QTS8 element with a merge option for joining the steel and glass fabric surfaces was used. Nonlinear FE analyses of the model were carried out to obtain the ultimate loads. Initially, only material nonlinearity was modelled. Geometric nonlinearity was also added in the analyses by using the first buckling mode from eigenvalue analyses with maximum lateral displacements of 1 mm in the web.

4.10.5 Theoretical predictions and FEA results

Table 4.10 gives a comparison of the theoretical and FEA ultimate loads of the glass fabric-strengthened web panel. Figure 4.20 shows the ratio of the ultimate loads versus the thickness of glass fabric.

Table 4.10 Theoretical and FEA results of glass fabric-strengthened web panel

Thickness (mm)		**Ultimate load (MNL) kN**			**Ultimate load (MG NL) kN**			**Failure mechanism in FE analyses**
Steel	**Glass fabric**	**Theory (UB)**	**FEA**	**Theory/ FEA**	**EC3**	**FEA**	**EC3/ FEA**	
3	0	281.4	284.3	0.99	192.4	186.0	1.03	Yielding of web and hinges in flanges near four corners; in FEA with MGNL, the hinges were 220 mm part
3	3	371.5	373.2	1.00	273.4	248.4	1.10	Same as above except that hinges were 230 mm apart
3	6	461.6	462.5	1.00	419.5	393.3	1.07	Same as above except that hinges were 250 mm apart
3	9	551.6	551.5	1.00	551.6	519.9	1.06	Same as above except that hinges were 270 mm apart
3	12	641.7	639.9	1.00	641.7	608.2	1.06	Same as above except that hinges were 320 mm apart
3	15	731.8	725.3	1.01	731.7	688.7	1.06	Same as above except that hinges were 400 mm apart

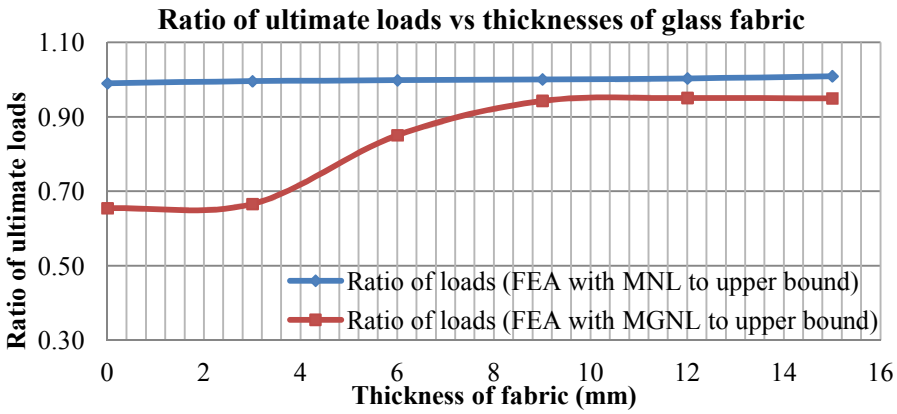

Figure 4.20 Ratio of ultimate loads of strengthened web panel vs. thicknesses of glass fabric

4.10.6 Discussion of results

1. For all thicknesses of the glass fabric, the ultimate plastic loads of the strengthened web panel given by the upper bound plastic analyses were in very good agreement with those obtained from the nonlinear FE analyses by modelling the material nonlinearity only.

2. The ultimate loads of the strengthened web panel given by the procedure in EC3 were un-conservative when compared to those obtained from the nonlinear FE analyses by modelling the material and geometric nonlinearities. This is due to the reason that the eccentric effects of the applied load, which were ignored in the theoretical predictions, were accounted in the FE analyses.

3. The EC3 ultimate loads of the strengthened web panel for the fabric thicknesses of 9, 12 and 15 mm were approximately equal to those given by the upper bound plastic analyses because the elastic critical loads of the strengthened web were greater than the ultimate plastic loads and the effect of the geometric nonlinearity became almost negligible.

4.11 Steel plate-girder

Nonlinear FE analyses of a steel plate-girder were carried out to compare its behaviour including the ultimate load and mode of the failure with those given by the existing design theories. The dimensions and the loading and boundary conditions applied to the plate-girder were same as those for the un-strengthened control specimen B1 in the tests. The properties of the steel used were as given in Table 4.1.

4.11.1 Model geometry, loading and boundary conditions

Figure 4.21 shows steel plate-girder together with the loading and boundary conditions. The load was applied to the plate-girder across its flange just above the second steel stiffeners. The plate-girder was supported at both ends. The support near the end web panel, test panel, was such that it restrained the girder vertically and horizontally, but was free to rotate. The support at the other end restrained the girder vertically only and was therefore free to rotate and move horizontally.

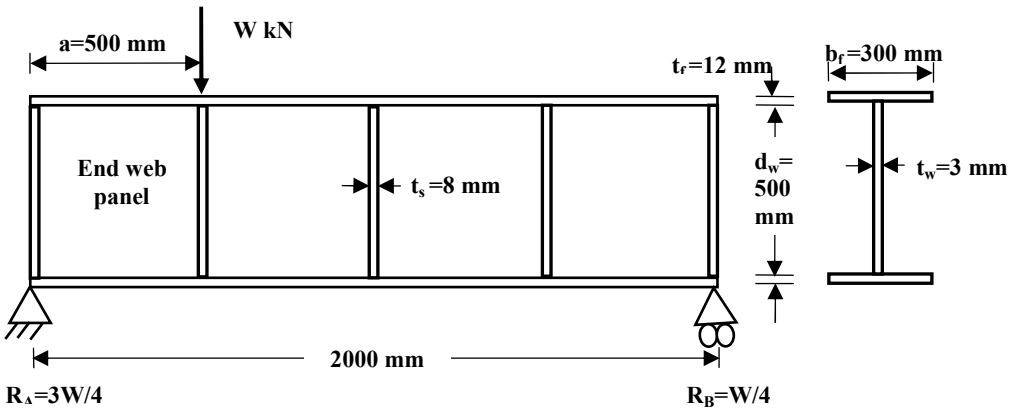

Figure 4.21 Dimensions, loading and boundary conditions of steel plate-girder

4.11.2 Theoretical predictions

The ultimate plastic load of the end web panel, test panel, of plate-girder was estimated using the upper bound plastic analysis, given by Equation 4.13. The ultimate plastic load of the plate-girder was obtained as 4/3rd that of the test panel. By considering the material and geometric nonlinearities, the ultimate load of the steel plate-girder was determined using the procedures given by (i) Basler (1969), (ii) Rockey et al (1978), (iii) Lee and Yoo (1999), (iv) British Standards 5950: Part1 (BS5950-I, 2000) and (v) Eurocode 3, EC3 (ENV3, 1997-1-5) and are given in Table 4.12. Details of calculations are given in Appendix-C.

4.11.3 Mode of failure

The steel plate-girder being investigated is subjected to high shear and low bending moment. In such plate-girders, shear buckling of thin web in the web panels occurs when the applied shear approaches the critical shear stress of the web. After buckling, the principal compressive stresses in the buckled web cease to increase, while the principal tensile stresses continue to increase. The additional load is then carried by a tensile membrane stress field and the flanges. The failure occurs when the web yields across the tensile stress field and four plastic hinges develop in the flanges (Rockey et al, 1978 and ENV 1993-1-5, 2006) as shown in Figure 4.22.

4.11.4 FE analyses

Nonlinear FE analyses of steel plate-girder were carried out to obtain the ultimate load and mode of the failure. Both the material and geometrical nonlinearities were modelled in the analyses. The loading and boundary conditions for the plate-girder in the analyses are shown in Figure 4.23.

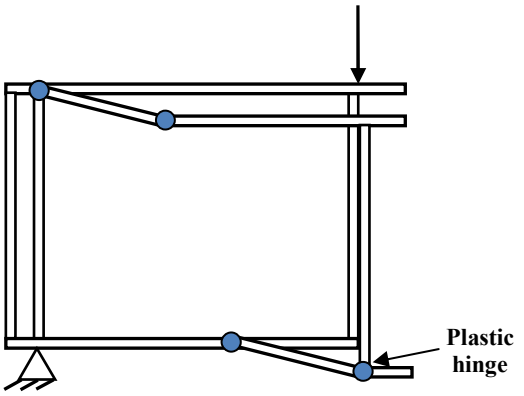

Figure 4.22 Failure mechanism of plate-girder (ENV 1993-1-5, 2006)

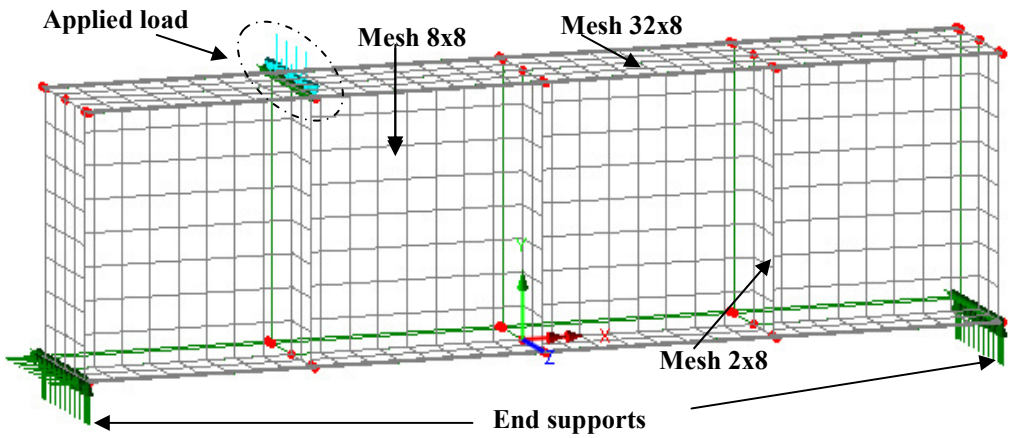

Figure 4.23 Model of steel plate-girder using QSL8 element

4.11.4.1 Element type

The thin shell element QSL8 and thick shell element QTS8 were used.

4.11.4.2 Mesh convergence

To check the convergence of the solutions, four uniform mesh sizes 4x4, 8x8, 12x12 and 16x16 were used to model the web in panels between the stiffeners for each of the QSL8 and QTS8 elements. Eigenvalue and nonlinear FE analyses of the plate-girder were carried out using each of the QSL8 and QTS8 elements. The elastic critical and the ultimate loads of the plate-girder obtained from the FE analyses were plotted against each of the four mesh sizes for both the elements, Figure 4.24. The results of the QSL8 and QTS8 elements were found to converge for 8x8 and 12x12 meshes respectively and were used for the web in each panel of the steel plate-girder. For the flanges and stiffeners, relatively coarse meshes were used; details are given in Table 4.11 and shown in Figure 4.23.

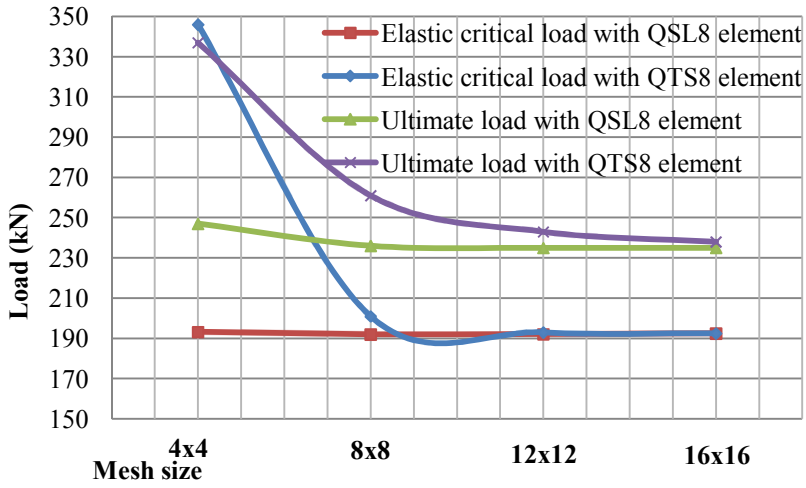

Figure 4.24 Elastic critical and ultimate loads of plate-girder vs. mesh sizes

Table 4.11 Mesh sizes used in models of steel plate-girder

Element	**Mesh size**		
	Web in panel	Flange	Stiffener
QSL8	8x8	32x8	2x8
QTS8	12x12	48x8	2x12

4.11.4.3 Imperfections

A lateral imperfection of 1 mm in the web of the plate-girder was assumed. It was included in the nonlinear FE analyses by using the first buckling mode from eigenvalue analysis with a maximum lateral displacement of 1 mm in the web.

4.11.5 Theoretical predictions and FEA results

4.11.5.1 Ultimate loads

Table 4.12 gives a comparison of the theory and FEA ultimate loads of the steel plate-girder.

4.11.5.2 Load-deflection responses

Figure 4.25 shows the applied load versus vertical deflection responses at the underside of the plate-girder beneath the loaded steel stiffeners obtained from nonlinear FE analyses for each of the QSL8 and QTS8 elements.

Table 4.12 Theory and FEA ultimate loads of steel plate-girder

Name of procedure	Ultimate load (kN)	Theory /QSL8	Theory /QTS8
Ultimate plastic load (material nonlinearity only)			
QSL8 element	381	---	---
QTS8 element	380	1.0	1.0
Theory (upper bound)	381	1.0	1.0
Ultimate load (material and geometric nonlinearities)			
QSL8 element	242	---	---
QTS8 element	246	---	---
Basler	260	1.07	1.05
Rockey et al	263	1.09	1.07
Lee and Yoo	216	0.89	0.88
British standards BS 5950	277	1.14	1.13
Eurocode 3, EC3	270	1.11	1.10

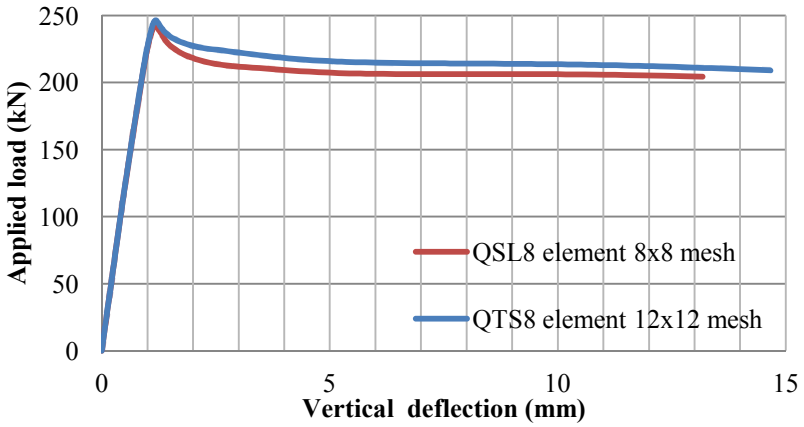

Figure 4.25 Load vs. vertical deflection at the underside of loaded steel stiffeners

4.11.5.3 Modes of buckling and failure

Figure 4.26 shows the first buckling mode of the plate-girder obtained from an eigenvalue analysis. Figure 4.27 shows modes of the failure of the plate-girder obtained from the nonlinear FE analyses using each of the QSL8 and QTS8 elements. The failure was initiated by out-of-plane diagonal buckling of the web in the end web panel, test panel, followed by diagonal yielding of the web and development of four plastic hinges, two in the top flange and one each in the bottom flange and the external stiffeners. The hinges in the top flange and external stiffeners were at distances of approximately 250 mm and 190 mm, respectively, from the top corner of the plate-girder.

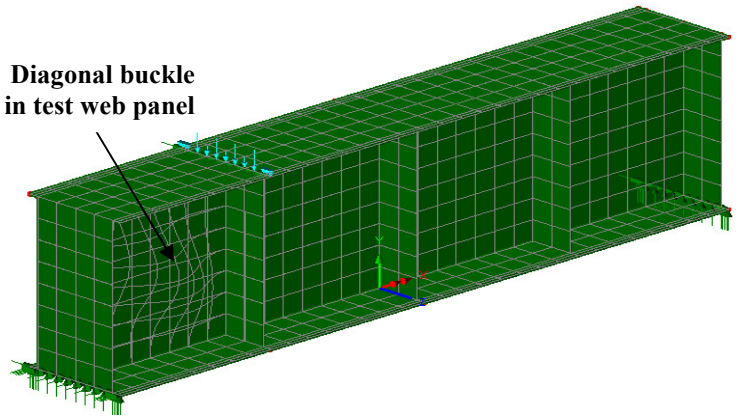

Figure 4.26 First buckling mode of steel plate-girder (QSL8 element)

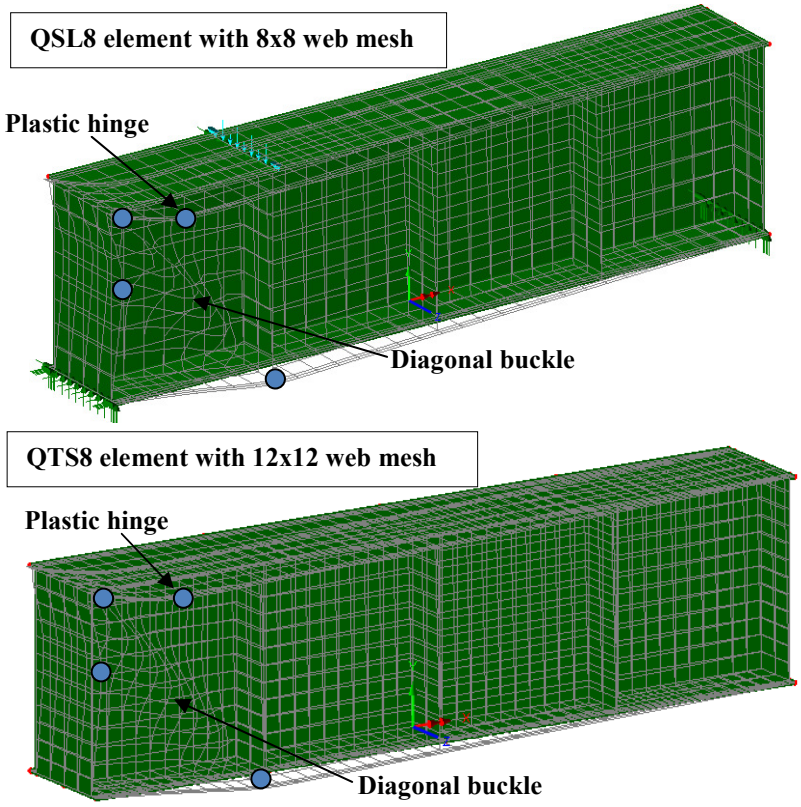

Figure 4.27 FEA modes of failure of steel plate-girder (QSL8 and QTS8 elements)

4.11.5.4 Distributions of stresses

1. At the ultimate load of 242 kN in the nonlinear FE analysis using QSL8 element, the values of the major (tensile) and minor (compressive) principal stresses, S_1 and S_3, in the web of end panel were 0.204 and -0.1235 GPa respectively, Figure 4.28(a) and (b). The maximum equivalent stress based on von-Mises yield criterion 'S_E', 0.31 GPa, in the tensile stress field of the web in the end panel, being a combined effect of the major and minor principal stresses, was approximately equal to the yield strength, 0.30 GPa, of the steel in the web, Figure 4.29.

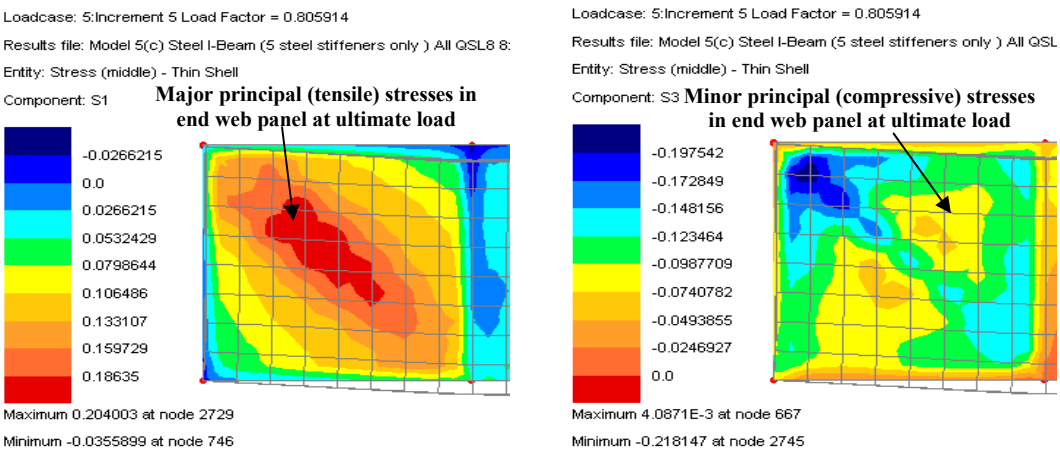

Figure 4.28 Major and minor principal stresses in end panel at ultimate load of girder

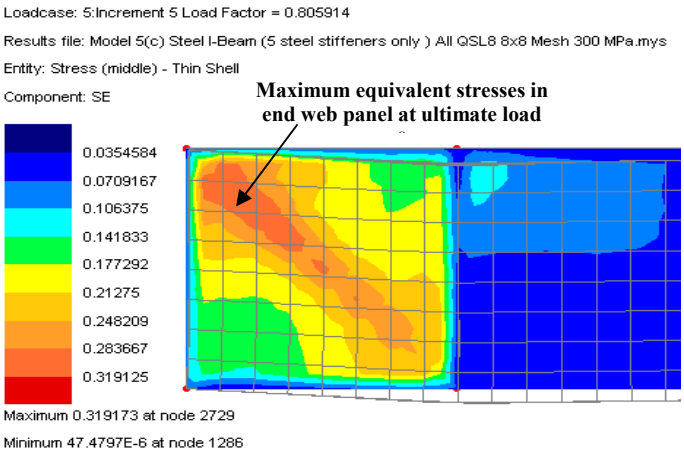

Figure 4.29 Equivalent stresses in end web panel at ultimate load of plate-girder

2. At the ultimate load of the plate-girder, the longitudinal stresses in the flanges and the external stiffeners were in the elastic range. After diagonal yielding of the web in the end panel, the longitudinal stresses in the flanges and the external stiffeners increased significantly and became approximately equal to the yield strength of the steel at the places where plastic hinges were formed, Figure 4.27.

3. After yielding of the web in end panel and development of plastic hinges in the top and bottom flanges and the external steel stiffeners, the plate-girder could not carry any further load and was assumed to have failed.

4.11.6 Discussion of results

1. The ultimate plastic load, 381 kN, of steel plate-girder given by the upper bound plastic analysis was in good agreement with that, 380 kN, obtained from the nonlinear FE analyses by modelling material nonlinearity only, Table 4.12.

2. The mode of the failure of the plate-girder obtained from the nonlinear FE analyses was different from that assumed in the design theories. The design theories assume the external stiffeners to remain rigid and the four plastic hinges to occur only in the top and bottom flanges, Figure 4.22. In the FE analyses, four plastic hinges, two in the top flange and one each in the bottom flange and the external stiffeners, were formed, Figure 4.27.

3. The ultimate load, 242 kN, of the steel plate-girder obtained from the nonlinear FE analysis by modelling both material and geometric nonlinearities was compared to those determined using the equations of five design theories. The ultimate loads given by the four design theories, except Lee and Yoo, were un-conservative due to the different failure modes assumed in the procedures and obtained from the FE analyses. Among them, the ultimate load, 260 kN, given by Basler's theory was less un-conservative and that, 277 kN, given by British Standards theory was more un-conservative.

4. Rockey and Skaloud's theory predicted the plastic hinge in the top flange to occur at a distance of approximately 237.5 mm from top corner of the end web panel which was in a reasonable agreement with the FEA prediction which indicated its occurrence at approximately 250 mm from top corner of the end web panel.

5. The distribution of stresses in the nonlinear FE analyses shows that at the ultimate load of the plate-girder, the maximum equivalent stress based on von-Mises yield criterion, being a combined erffect of the major and minor principal stresses, in the web of end panel was approximately equal to the yield strength of the steel in the web.

6. At the ultimate load of plate-girder, the longitudinal stresses in the flanges and the external stiffeners in the FE analysis were in the elastic range. After yielding of the web in the end panel, the longitudinal stresses in the flanges and the external stiffeners increased significantly and were approximately equal to the yield strength of the steel at the places where the plastic hinges were formed.

7. The load-vertical deflection responses of the plate-girder obtained from nonlinear FE analyses using either QSL8 or QTS8 element were in agreement, Figure 4.25.

4.12 Steel plate-girders of Rockey and Skaloud

Nonlinear FE analyses of the steel plate-girders tested by Rockey and Skaloud (1968 & 1972) were carried out. The ultimate loads and modes of the failure were obtained from the FE analyses and were compared to those in the tests.

4.12.1 Tests

Rockey and Skaloud (1968 & 1972) carried out the tests on thirty-five steel plate-girders. The plate-girders were manufactured in two series I and II and varied mainly in the aspect ratio of the web panels, slenderness ratio of the web and thickness of the flanges. Figure 4.30 shows the plate-girders and their loading and boundry conditions. Table 4.13 gives the dimensions of the plate-girders and the yield strengths of the steel used in the web.

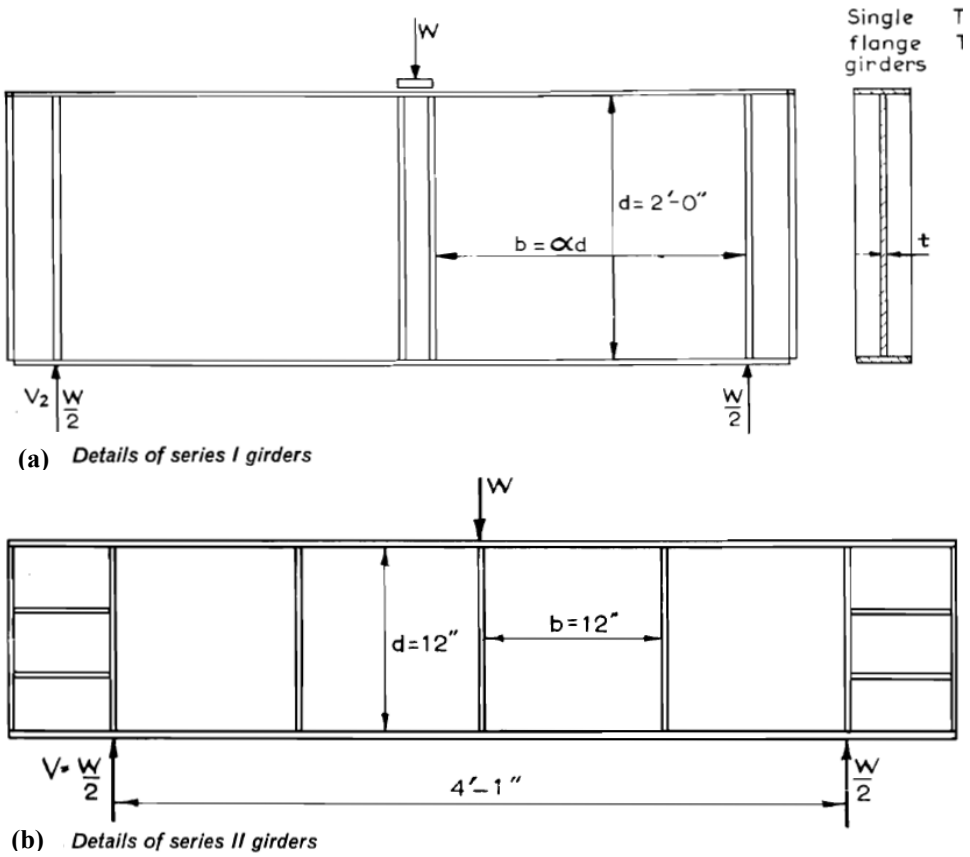

Figure 4.30 Details of series I and II steel plate-girders (Rockey & Skaloud, 1972)

Table 4.13 Dimensions and properties of steel plate-girders (Rockey & Skaloud, 1972)

Plate-girder No.	Aspect ratio a/d_w	Web			Length of web panel a (mm)	Flange(s)	
		Thickness t_w (mm)	Depth d_w (mm)	Lower yield strength (MPa)		Width b_f (mm)	Thickness t_f (mm)
Series I plate-girders							
TG1	1.0	2.72	609.6	253	609.6	101.6	4.7
TG1a	1.0	2.72	609.6	239	609.6	101.6	4.75
TG2	1.0	2.72	609.6	238	609.6	101.6	6.55
TG2a	1.0	2.72	609.6	243	609.6	101.6	6.43
TG3	1.0	2.74	609.6	252	609.6	101.6	12.57
TG3a	1.0	2.74	609.6	233	609.6	101.6	12.62
TG4	1.0	2.72	609.6	229	609.6	101.6	15.88
TG4a	1.0	2.72	609.6	259	609.6	101.6	15.82
TG13	1.0	2.62	609.6	271	609.6	101.6	25.32
TG5	1.5	2.62	609.6	291	914.4	203.2	9.52
TG5a	1.5	2.62	609.6	263	914.4	203.2	9.5
TG6	1.5	2.62	609.6	298	914.4	203.2	16.36
TG6a	1.5	2.62	609.6	252	914.4	203.2	16.13
TG7	1.5	2.62	609.6	287	914.4	203.2	25.91
TG7a	1.5	2.62	609.6	293	914.4	203.2	25.83
TG8	1.5	2.62	609.6	297	914.4	203.2	31.98
TG8a	1.5	2.62	609.6	297	914.4	203.2	28.72
TG9	2	2.62	609.6	266	1219.2	203.2	9.85
TG9a	2	2.62	609.6	289	1219.2	203.2	9.85
TG10	2	2.62	609.6	266	1219.2	203.2	16.26
TG11	2	2.62	609.6	295	1219.2	203.2	32.13
TG12	2	2.62	609.6	264	1219.2	203.2	47.98
TG12a	2	2.62	609.6	275	1219.2	203.2	48.2
Series II plate-girders							
TG14	1.0	0.965	304.8	219	304.8	76.2	3.12
TG15	1.0	0.965	304.8	219	304.8	76.2	5.0
TG16	1.0	0.965	304.8	219	304.8	76.2	6.45
TG17	1.0	0.965	304.8	219	304.8	76.2	9.32
TG18	1.0	0.965	304.8	219	304.8	76.2	12.95
TG19	1.0	0.965	304.8	219	304.8	76.2	15.52
TG20	1.0	2.03	304.8	229	304.8	76.2	3.25
TG21	1.0	2.03	304.8	229	304.8	76.2	4.88
TG22	1.0	2.03	304.8	229	304.8	76.2	6.48
TG23	1.0	2.03	304.8	229	304.8	76.2	9.22
TG24	1.0	2.03	304.8	229	304.8	76.2	12.95
TG25	1.0	2.03	304.8	229	304.8	76.2	15.54

4.12.2 FE analyses

Nonlinear FE analyses of all the thirty-five test steel plate-girders were carried using the LUSAS (LUSAS, 2008). Both the material and geometrical nonlinearities were modelled in the analyses.

4.12.2.1 Assumptions

The following assumptions were made in the FE analyses.

1. The yield strengths of the steel in the web, flanges and stiffeners were used as given in Table 4.14.

Table 4.14 Yield strengths of steel used in FE models of plate-girders

Plate-girder series	**Yield strength of steel (MPa)**		
	Web	**Flange**	**Stiffener**
Series I	*Given lower yield strength was used	Assumed as 300 MPa	Assumed as 300 MPa
Series II	*Given lower yield strength was used	**Given lower yield strength was used	Assumed as 300 MPa

*Given in Table 4.13 **Given in Rockey & Skaloud (1972)

2. The thicknesses of the internal stiffeners and end posts of all plate-girders and the web length between the internal steel stiffeners beneath the applied load of the series I plate-girders were not given. The thickness of the each end post was taken as 15 mm and that of the internal stiffener taken as 10 mm. The web length between the internal steel stiffeners of the series I plate-girders was assumed to be 50 mm.

3. No information about the initial geometrical imperfections in the web was provided by Rockey & Skaloud (1972). A lateral imperfection of 1 mm in the web of the plate-girders was assumed. The imperfection was included in the nonlinear FE analyses by using the first buckling modes from eigenvalue analyses with a maximum lateral displacement of 1 mm in the web.

4.12.2.2 Material modelling

The steel was modelled as an isotropic and elastic-perfectly plastic material. The modulus of elasticity was taken as 205 GPa and the Poisson ratio taken as 0.3. The values of the yield strength of the steel in the webs, flanges and stiffeners were used as given in Table 4.13 and Table 4.14.

4.12.2.3 Loading and boundary conditions

The loading and boundary conditions were same for all the plate-girders; those for the plate-girder TG4 are shown in Figure 4.31.

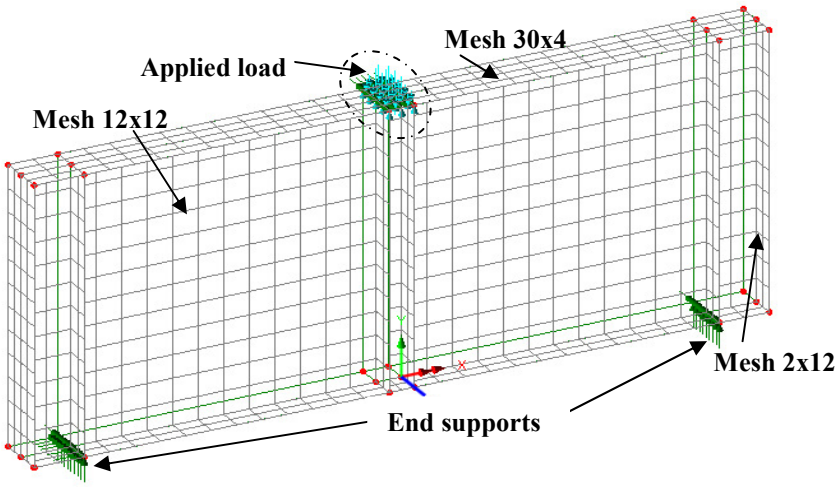

Figure 4.31 Model of steel plate-girder TG4

4.12.2.4 Element type and mesh size

The thin shell QSL8 element was used in the FE analyses of all plate-girders. Using the results of mesh studies described in section 4.11.4.2, a mesh for the web in the each web panel was taken to have a square element size of approximately 50 mm. The mesh sizes of the flanges and stiffeners were taken to adjust them with that of the web. Table 4.15 gives and Figure 4.31 shows the mesh sizes used for the webs, flanges and stiffeners of the steel plate-girders.

Table 4.15 Mesh sizes used in models of steel plate-girders

Plate-girder No.	**Mesh size**		
	Web in panel	Flange	Stiffener
Series I plate girders			
TG1 to TG4a & TG13	12x12	30x4	2x12
TG5 to TG8a	18x12	42x4	2x12
TG9 to TG12a	24x12	54x4	2x12
Series II plate girders			
TG14 to TG25	12x12	54x8	4x12

4.12.3 Results of tests and FE analyses

4.12.3.1 Ultimate loads

Table 4.16 gives the comparisons of the ultimate loads of the plate-girders, respectively, in the tests and the FE analyses.

Table 4.16 Test and FEA ultimate loads of series I and II steel plate-girders

Plate-girder No.	Slenderness ratio, d_w/t_w	Ultimate load (kN)		
		Test	FEA	Test/FEA
Series I plate-girders				
TG1	224	225	282.2	0.797
TG1a	224	239	279.7	0.854
TG2	224	251	300.7	0.835
TG2a	224	234	284.5	0.822
TG3	224	284	314.4	0.903
TG3a	224	269	297.4	0.904
TG4	224	317	301.5	1.051
TG4a	224	302	332.3	0.909
TG5	233	233	283.7	0.913
TG5a	233	259	261.9	0.890
TG6	233	283	328.0	0.863
TG6a	233	266	278.1	0.957
TG7	233	354	410.5	0.862
TG7a	233	385	425.4	0.905
TG8	233	402	496.3	0.810
TG8a	233	413	501.3	0.824
TG9	233	245	249.7	0.981
TG9a	233	240	264.6	0.907
TG10	233	256	261.1	0.980
TG11	233	354	405	0.874
TG12	233	455	496.0	0.917
TG12a	233	490	508.6	0.963
TG13	233	415	419.4	0.99
Mean = 0.901 and Standard Deviation =0.068				
Series II plate-girders				
TG14	316	50.7	46.5	1.089
TG15	316	58.7	51.6	1.137
TG16	316	62.6	54.2	1.154
TG17	316	77.9	62.1	1.254
TG18	316	101	72.9	1.386
TG19	316	109	86.2	1.264
TG20	150	102	111.0	0.919
TG21	150	142	121.4	1.170
TG22	150	157	125.8	1.248
TG23	150	162	132.7	1.221
TG24	150	192	139.6	1.376
TG25	150	207	151.1	1.370
Mean = 1.216 and Standard Deviation =0.129				
Overall Mean = 1.009 **Overall Standard Deviation =0.179**				

Figure 4.32 shows the FEA and test ultimate loads of plate-girder specimens and Figure 4.33 shows ratios of the ultimate loads versus flange thicknesses of specimens for the different web slenderness ratios.

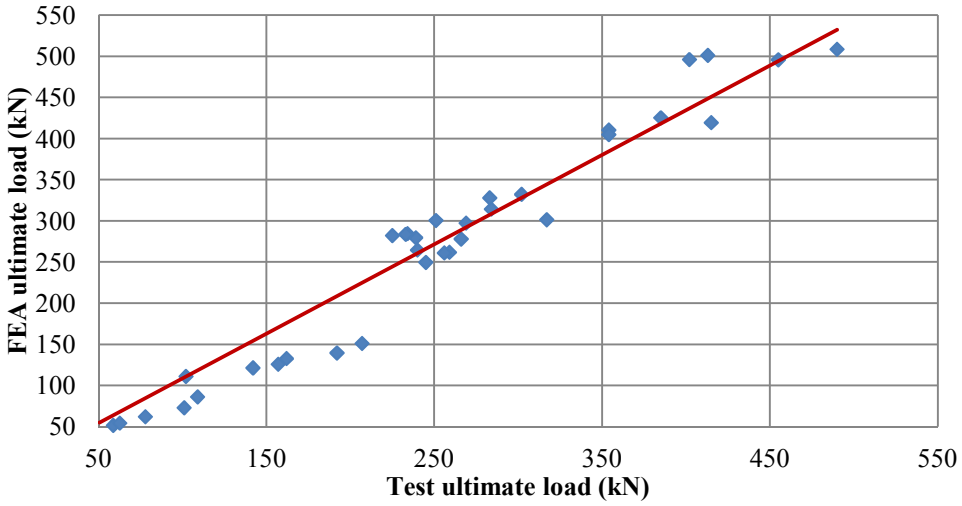

Figure 4.32 FEA and test ultimate loads of 35 plate-girders (specimens TG1-TG25)

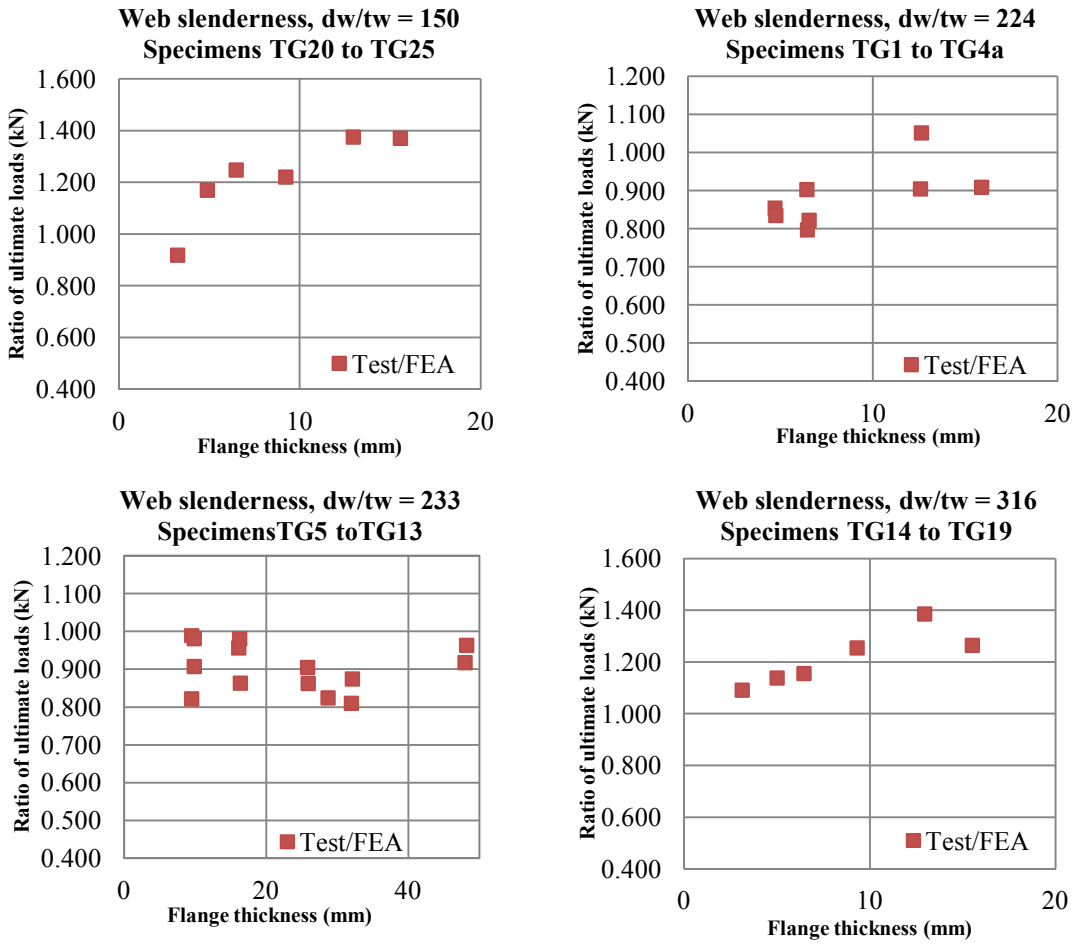

Figure 4.33 Ratios of ultimate loads versus flange thicknesses of plate-girders (specimens TG1 to TG25) for different web slendernesses

4.12.3.2 Modes of failure

Figure 4.34 to Figure 4.36 show modes of the failure of three plate-girders TG4, TG5 and TG19 in the tests and the FE analyses.

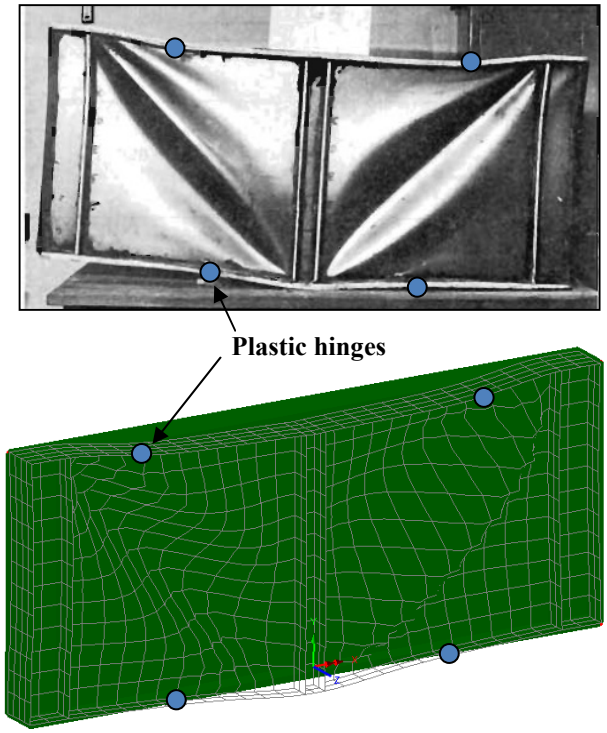

Figure 4.34 Test and FEA modes of failure of specimen TG4 (Rockey & Skaloud, 1972)

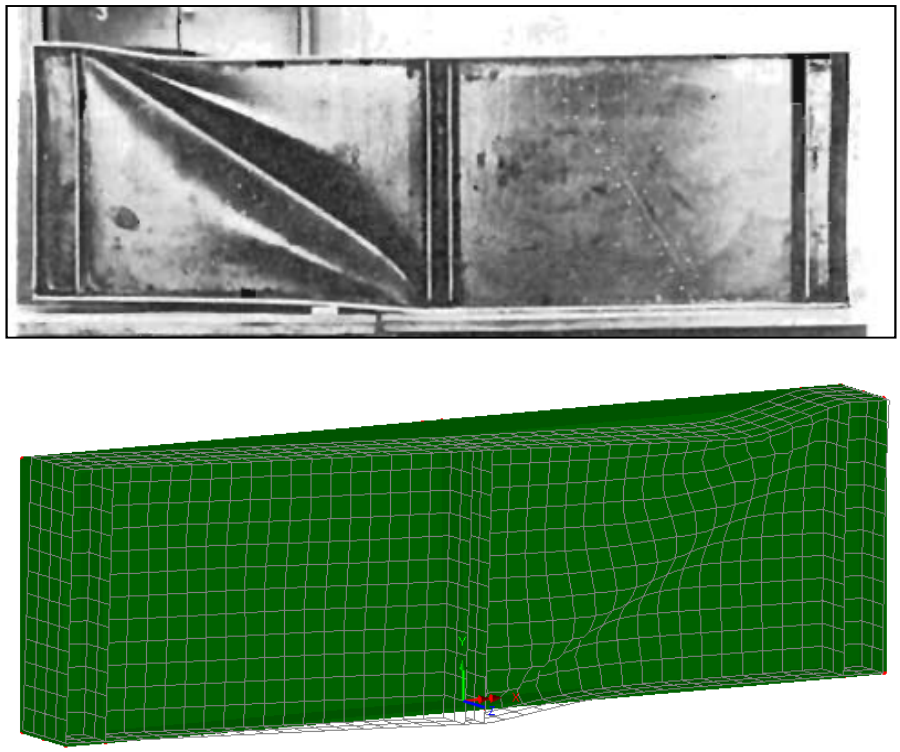

Figure 4.35 Test and FEA modes of failure of specimen TG5 (Rockey & Skaloud, 1972)

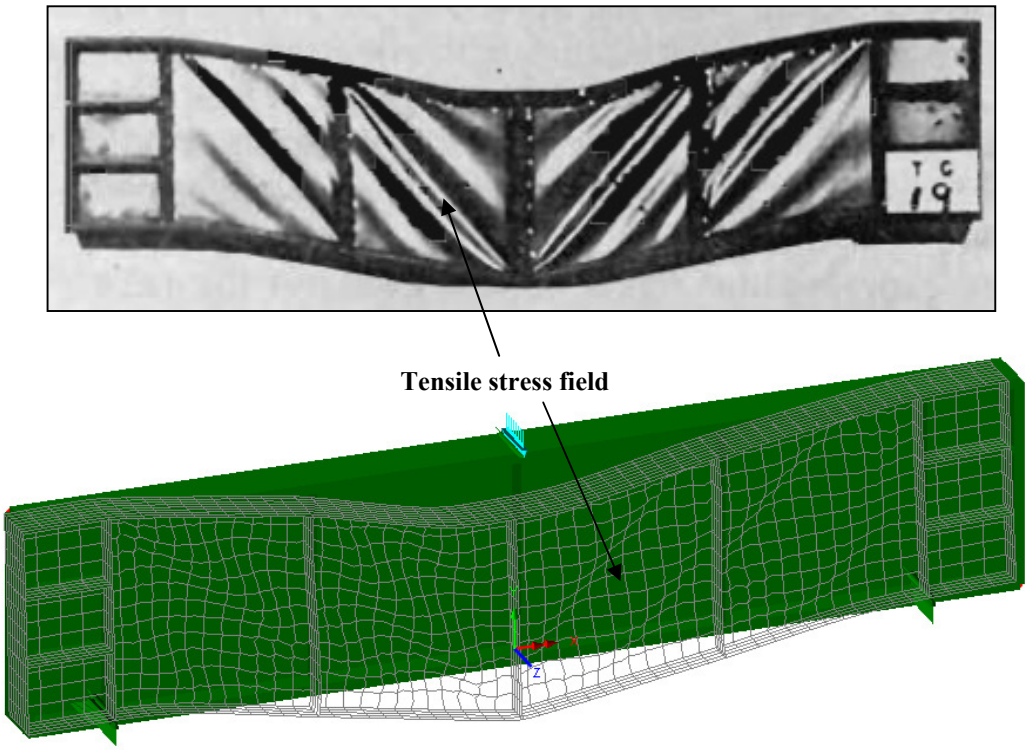

Figure 4.36 Test and FEA modes of failure of specimen TG19 (Rockey & Skaloud, 1972)

4.12.4 Discussion of results

1. The ultimate loads of 22 of 23 series I plate-girders, except TG4, in the tests were lower, up to 0.80 times, than those obtained from the FE analyses. The mean of ratios of the test to FEA ultimate loads is 0.901 with a standard deviation of 0.068.

2. The ultimate loads of 11 of 12 series II plate-girders, except TG20, in the tests were greater, up to 1.38 times, than those obtained from the FE analyses. The mean of ratios of the test to FEA ultimate loads is 1.216 with a standard deviation of 0.129.

3. Compared to the test ultimate loads, the ultimate loads of plate-girders obtained from the FE analyses were generally conservative for the higher and lower web slendernesses, d_w/t_w = 316 and 150. The FEA ultimate loads were un-conservative for the intermediate slendernesses, d_w/t_w = 224 and 233 which increased with the increases in flange thicknesses.

4. The difference between the test and FEA ultimate loads of the plate-girders could also be attributed to the missing data, particularly the thicknesses of the end posts and the geometrical imperfections in the web for which uniform values have been assumed for all plate-girders in the FE analyses.

5. The test failure modes of three plate-girders, TG4 and TG5 of series I and TG19 of the series II, were available and were in good agreement with those obtained from the nonlinear FE analyses.
6. Well-defined plastic hinges formed in the flanges of plate-girder TG1 in the test have been correctly predicted by the FE analysis, Figure 4.34.

7. In the test of plate-girder TG5, one web panel had failed while the other panel remained undistorted. The same failure mode has been predicted by the FE analysis, Figure 4.35.

8. At failure, plate-girder TG19 had well-developed tensile membrane stress field in the test, which has also been predicted by the FEA failure mode, Figure 4.36.

9. Discrepancies have been found in the test ultimate loads of five pairs of the series I plate girders. It can be observed from Table 4.17 and Figure 4.37 that ratios of the test ultimate loads of the five pairs are not proportional to the ratios of the yield strengths of the steel in the web. The dimensions and properties of the steel of the each pair of the plate-girders were almost the same except the yield strength of the steel in the web. The ratios of the FEA ultimate loads of these pairs are however proportional to the ratios of the yield strengths of the steel in the web.

Table 4.17 Ratios of test and FEA ultimate loads of five pairs of plate-girders

Plate-girder pair	**Yield strength of web steel (MPa)**	**Ratio of yield strengths (e.g.TG1/TG1a)**	**Ultimate load of plate-girder (kN)**		**Ratio of ultimate loads of pair (e.g.TG1/TG1a)**	
			Test	**FEA**	**Test**	**FEA**
TG1	253	1.06	225	290.5	0.94	1.01
TG1a	239		239	280.4		
TG2	238	0.98	251	287.5	1.07	0.96
TG2a	243		234	290.5		
TG4	229	0.88	317	301.5	1.05	0.90
TG4a	259		302	332.3		
TG5	291	1.10	233	283.7	0.90	1.09
TG5a	263		259	261.9		
TG9	266	0.92	245	264.6	1.02	0.94
TG9a	289		240	249.7		

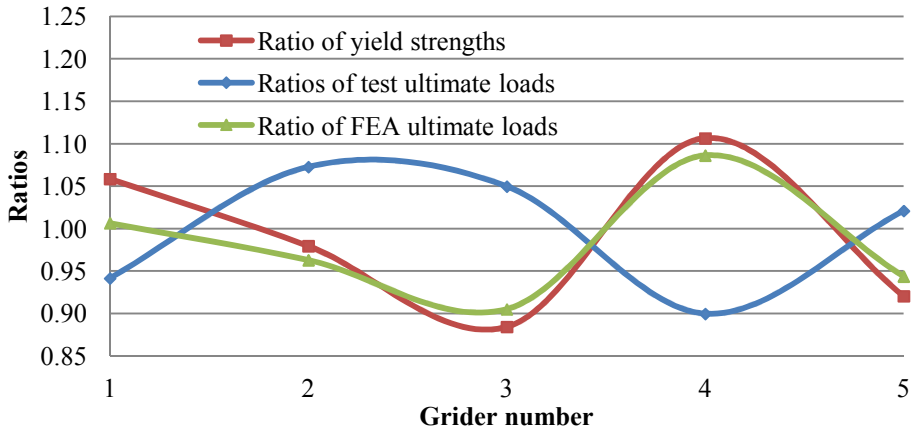

Figure 4.37 Ratios of test and FEA ultimate loads of five pairs of plate-girders

10. Good agreement between the test and FEA modes of the failure of three plate-girders and a reasonable agreement between the test and FEA ultimate loads of all plate-girders give confidence about the accuracy of the FEA results of the specimens.

4.13 Steel plate-girders of Okeil et al

Nonlinear FE analyses of three steel plate-girders, specimens OB1, OB2 and OB3, tested and analysed by Okeil et al (2009a & 2010) were carried out using the LUSAS. The ultimate loads and modes of the failure obtained from the FE analyses were compared to those in the tests. The specimens OB1, OB2 and OB3 were analysed because of their similarity with the specimens B1, B2 and B6 tested and analysed by the author.

4.13.1 Tests and FE analyses by Okeil et al

Details of the tests and FE analyses of three plate-girders, specimens OB1, OB2 and OB3, carried out by Okeil et al (2009a, 2010 & 2011) have been given in Chapter 2. Test specimens OB1, OB2 and OB3 were the end web panels, test panels, of the steel plate-girders, Figure 4.38. The specimen OB1 was a control plate-girder without any FRP-strengthening in the end web panel. The end web panels of specimens OB2 and OB3 were strengthened using two vertical and one diagonal GFRP pultruded section stiffeners respectively. Nonlinear FE analyses of specimens OB1 and OB2 were also carried out by Okeil et al using 8-node solid elements in the ANSYS FE program.

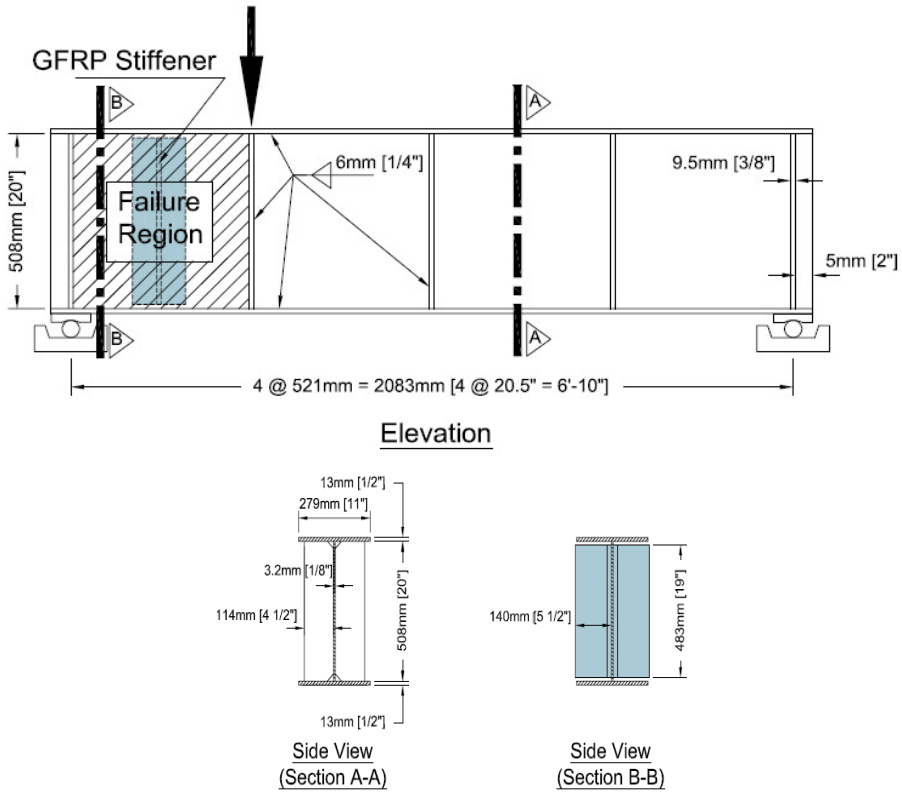

Figure 4.38 Details of control and GFRP-strengthened specimens OB1 and OB2 (Okeil et al, 2009a)

4.13.2 FE analyses by author

Nonlinear FE analyses of all three specimens OB1, OB2 and OB3 were carried out by modelling both the material and geometrical nonlinearities.

4.13.2.1 Material modelling

The steel and GFRP were modelled as isotropic and elastic-perfectly plastic materials; the properties used are given in Table 4.18. The yield strengths of the steel in the flanges and stiffeners were not given and were assumed the same as that of the steel in the web.

Table 4.18 Properties of steel and GFRP (Okeil et al, 2009a & 2011)

Property	Steel	GFRP
Modulus of elasticity (GPa)	205	17.2
Yield strength in web (MPa)	310	150*
Poisson's Ratio	0.3	0.27

* Assumed by author

4.13.2.2 Loading and boundary conditions

The loading and boundary conditions were same for all the specimens; those for the control specimen OB1 are shown in Figure 4.39.

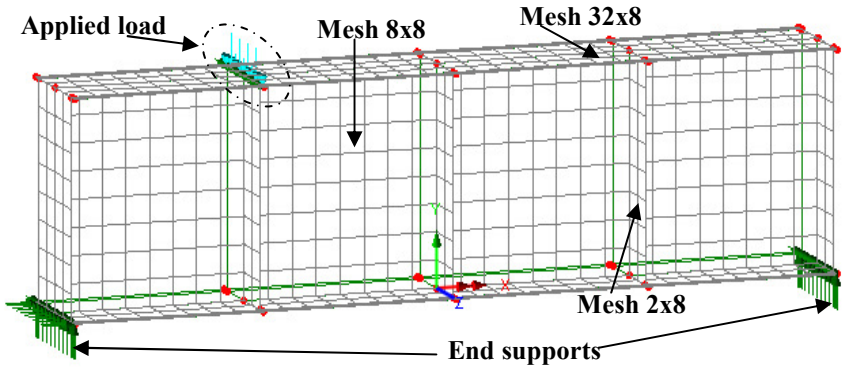

Figure 4.39 Loading and boundary conditions of model of control specimen OB1

4.13.2.3 Element type and mesh size

The thin shell QSL8 element was used in the FE analyses of all three specimens. Using the results of mesh studies described in section 4.11.4.2, an 8x8 mesh size was used for the web in each panel, Figure 4.39. The mesh sizes of 32x8 and 2x8 were used for the flanges and stiffeners in order to adjust them with that of the web panels.

4.13.2.4 Imperfections

No information about the initial geometrical imperfections in the web was provided by Okeil et al (2009a, 2009b & 2010). A lateral imperfection of 1 mm in the web was assumed. The imperfection was included in the nonlinear FE analyses using the first buckling mode from eigenvalue analyses with a maximum lateral displacement of 1 mm in the web.

4.13.3 Results of tests and FE analyses

4.13.3.1 Ultimate loads

Table 4.19 shows a comparison of the ultimate loads of the specimens in the tests and the FE analyses.

Table 4.19 Test and FEA ultimate loads of test specimens OB1, OB2 and OB3

Specimen No.	Ultimate load (kN)			Ratio of ultimate loads	
	Test	FEA (ANSYS)	FEA (LUSAS)	LUSAS/ Test	LUSAS/ ANSYS
OB1	278	278	276	0.99	0.99
OB2	389	403	361	0.93	0.90
OB3	435	---	427	0.98	---

4.13.3.2 Modes of failure

Figure 4.40 to Figure 4.42 show the modes of the failure of three specimens OB1, OB2 and OB3 in the tests and the FE analyses using LUSAS.

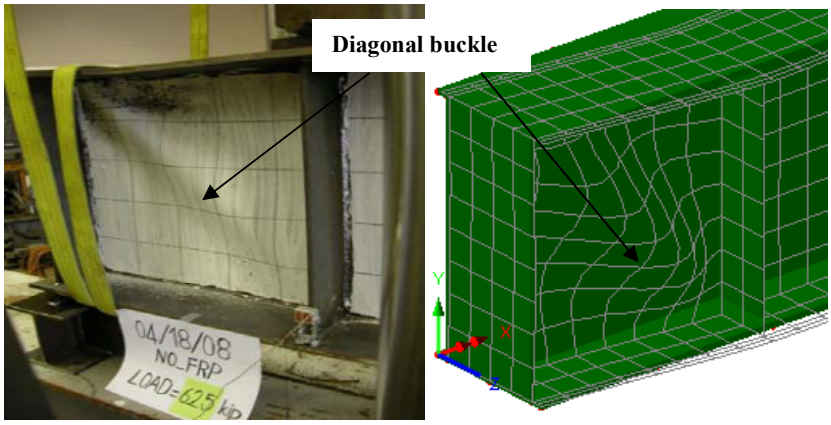

Figure 4.40 Test and FEA (LUSAS) modes of failure of specimen OB1 (Okeil et al, 2010)

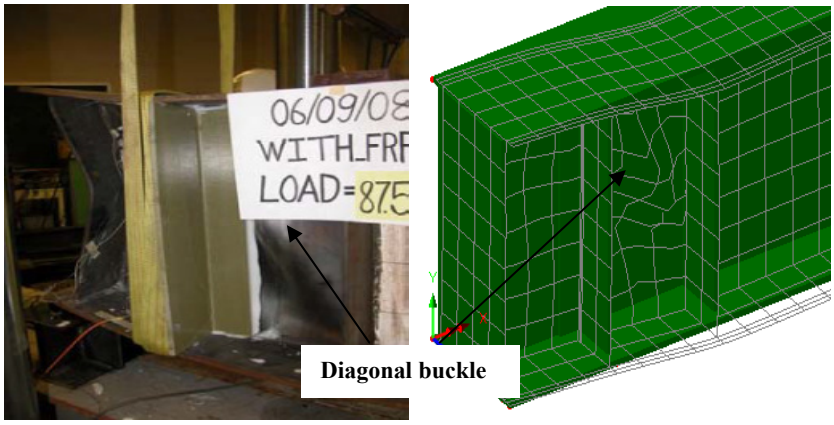

Figure 4.41 Test and FEA (LUSAS) modes of failure of specimen OB2 (Okeil et al, 2010)

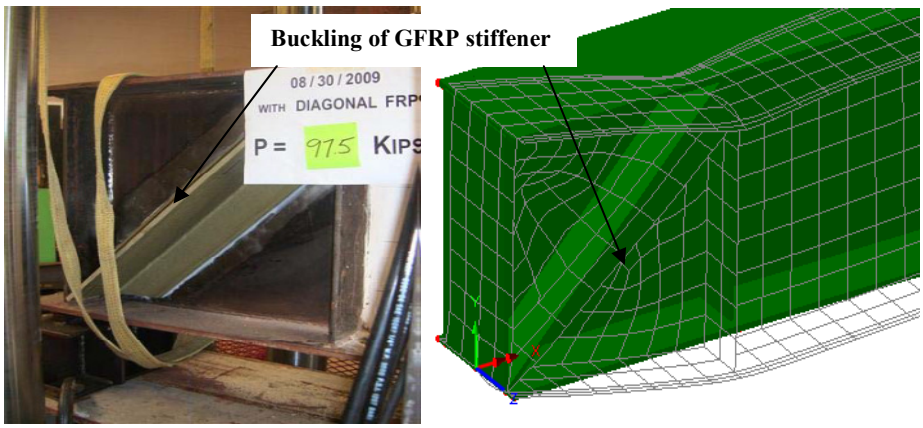

Figure 4.42 Test and FEA (LUSAS) modes of failure of specimen OB3 (Okeil et al, 2010)

4.13.4 Discussion of test and FEA results

1. The ultimate loads of the three test specimens OB1, OB2 and OB3 obtained from FE analyses using LUSAS were in good agreement with those in the tests and FE analyses using the ANSYS.

2. The modes of the failure of all the three specimens obtained from the nonlinear FE analyses using LUSAS were in agreement with those in the tests.

4.14 Conclusions

This Chapter has described FE analyses of nine models and thirty-eight test specimens using LUSAS. The models were a steel beam, a steel frame, steel plate and web panel, frame and web panel with diagonal stiffeners, glass fabric-strengthened plate and web panel and a steel plate-girder. The specimens were steel plate-girders tested by Rockey and Skaloud (1968 & 1972) and Okeil et al (2009a & 2010).

The ultimate plastic loads and modes of the failure of all models given by the upper bound plastic analyses were in good agreement with those obtained from the FE analyses by modelling material nonlinearity only. The ultimate loads of the steel and glass fabric-strengthened plates or web panels given by the procedure in Eurocode 3 were in good agreement with those obtained from the FE analyses by modelling both the material and geometric nonlinearities. The shell elements, QSL8 with a coarse mesh and QTS8 with a relatively finer mesh, were found to give satisfactory results in the FE analyses of the beam, plates, web panels and plate-girder. Of the three solid elements HX8, HX8M and HX20 used in the FE analyses of the steel plate, only the two

elements, HX8M and HX20, could give satisfactory results, but they took at least 3 times the computing time required for the shell elements. The merge option for joining of two surfaces with the dissimilar properties has been found suitable to be used for the glass fabric-strengthened plates and web panels. The ultimate loads of the steel plate-girder determined using the procedures given by Basler, Rockey, Eurocode 3 and British standards were un-conservative compared to those obtained from the nonlinear FE analyses by modelling both the material and geometric nonlinearities because of the different failure mechanisms. The design procedures assume plastic hinges to occur in the top and bottom flanges only, while the hinges were also formed in the external stiffeners in the FE analyses.

The FEA ultimate loads of thirty-five steel plate-girders, TG1 to TG25, of Rockey and Skaloud (1968 & 1972) were in a reasonable agreement with those in the tests. The test modes of the failure of three plate-girders were available and were correctly predicted by the FE analyses. The FEA and test ultimate loads and modes of the failure of three specimens OB1, OB2 and OB3 of Okeil et al (2009a & 2010) were in good agreement. After validation studies, the FE analyses of specimens B1 to B8, to be tested, can be carried out to predict their behaviour in the tests with a reasonable good accuracy.

Chapter 5 Finite Element Analyses of Test Specimens

5.1 Introduction

This Chapter presents the details of finite element, FE, analyses carried out of models of the eight test specimens using the LUSAS FE program, Version 14.3 (LUSAS, 2008). The specimens included one un-strengthened specimen B1 and the seven fibre reinforced polymer, FRP, strengthened specimens B2 to B8. Before carrying out the FE analyses of the test specimens, the validation studies described in Chapter 4 were carried out.

FE models of the eight test specimens, B1 to B8, were analysed to predict the behaviour of the specimens in the tests. Because of good agreement between the test and FEA results of control specimen B1 for the S1 plate-girders, a model of the un-strengthened specimen B9 was also analysed and used as the control for the test specimens and models using the S2 plate-girders. The details of the element, mesh size and material properties used and the loading and boundary conditions applied are described in this Chapter. The results obtained from the FE analyses of the models are presented and discussed. The results of the FE analyses are then compared to those of specimens in the tests for validation.

5.2 Finite element analyses

Nonlinear FE analyses of all the models were carried out to obtain the ultimate loads, modes of failure and load-deflection responses of the test specimens. Both the material and geometrical nonlinearities were modelled.

5.2.1 Objectives

The objectives of carrying out the FE analyses of the test specimens are given below.

1. To predict the behaviour of the test specimens up to failure before testing.

2. To compare the ultimate loads, modes of the failure, load-deflection responses and locations of the plastic hinges of the FE models with those of the test specimens.

3. To check more details about the distribution of stresses because the FE analyses can give the detailed information of the stresses throughout the entire loading.

5.2.2 Assumptions

The following assumptions were made in the FE analyses.

1. Perfect bond was assumed between the steel and pultruded GFRP surfaces in all the strengthened models of groups G2.

2. Delamination of the FRP composite materials was considered not to occur.

3. No breakdown of the bond between the steel and FRP fabric surfaces was assumed to occur in the strengthened models of groups G3.

5.2.3 FE models

A total of nine FE models were analysed. As mentioned earlier, eight models B1 to B8 represented as accurately as possible the eight test specimens. Ninth model of the un-strengthened specimen B9 was used as control for comparison with the results of S2 specimens. The FE models were divided into three groups G1, G2 and G3 as for the test specimens. Table 5.1 gives the group-wise details of the nine FE models.

Table 5.1 Grouping and strengthening of FE models B1 to B9

Model No.	Girder series	Details of FRP-strengthening
Models of G1 specimens (Un-strengthened control)		
B1	S1	None
B9	S2	None
Models of G2 specimens (GFRP pultruded section strengthened)		
B2	S1	2 vertical GFRP pultruded section stiffeners, one on each side of the web
B5	S2	1 vertical GFRP pultruded section stiffener on one side of the web only
B6	S2	1 diagonal GFRP pultruded section stiffener on one side of the web only
B8	S2	2 vertical load-bearing GFRP pultruded section stiffeners in place of load-bearing steel stiffeners in model B9
Models of G3 specimens (FRP fabric strengthened)		
B3	S1	4 layers of carbon fabric on one side of the web only
B4	S1	8 layers of glass fabric on one side of the web only
B7	S2	4 layers of glass fabric on one side of the web only

5.2.4 Loading and boundary conditions

All nine models were analysed under the same the loading and boundary conditions. Figure 5.1and Figure 5.2 show the loading and boundary conditions of the models B1 and B3, respectively, for the FE analyses. A uniformly distributed line load acting vertically downwards in the y-direction was applied across full width, 300 mm, of the flange of the plate-girder model. Self-weight, 1.5 kN, of the plate-girder was very small compared to the applied load and was ignored in the analyses. The model was supported at both ends. The line support near the test web panel restrained the model vertically and horizontally, but was free to rotate. The support at the other end restrained it vertically, but was free to rotate and move horizontally.

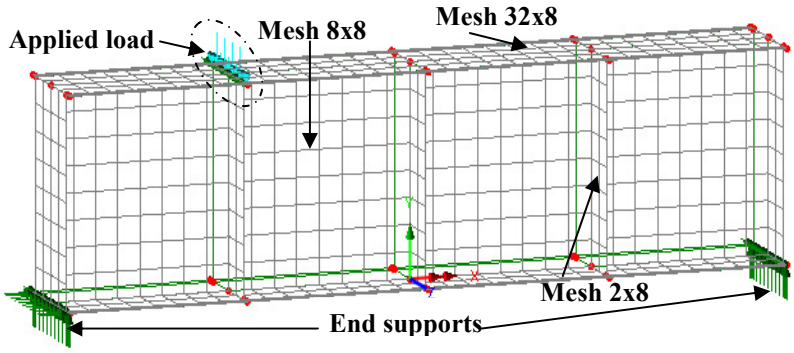

Figure 5.1 Model of specimen B1 (QSL8 element)

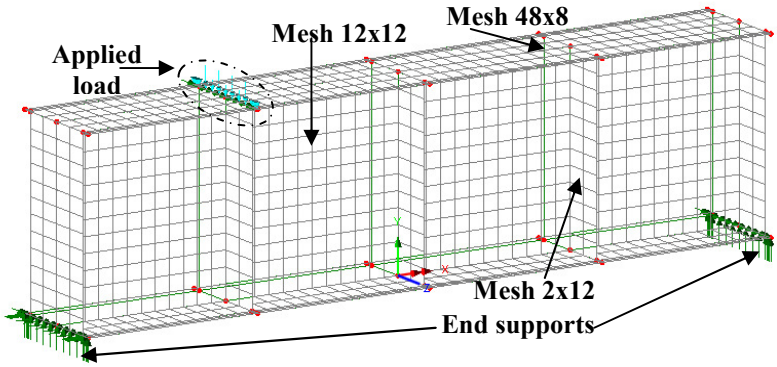

Figure 5.2 Model of specimen B3 (QTS8 element)

5.2.5 Material modelling

The steel was modelled as an isotropic and elastic-perfectly plastic material. The GFRP pultruded sections and the carbon and glass fabrics were also modelled as the isotropic and elastic-perfectly plastic materials because the stresses in FRP were well within the elastic range. Plastic properties were assigned to see if the stresses in any portion of the FRP were beyond the elastic range. The material properties used in the FE analyses were same as those measured or supplied in the tests and are given in Table 5.2.

Table 5.2 Properties of steel, GFRP pultruded sections and carbon and glass fabrics

Name of material		Modulus of elasticity (GPa)	Poisson's Ratio	Yield strength (MPa)	Ultimate strength (MPa)
S1 plate-girders	Flange	*205	*0.3	**322	**446
	Web	*205	*0.3	**274	**375
	Stiffener	*205	*0.3	**308	**463
S2 plate-girders	Flange	*205	*0.3	**330	**440
	Web	*205	*0.3	**353	**473
	Stiffener	*205	*0.3	**334	**450
GFRP pultruded sections	Tensile	**36	*0.15	---	**350
	Compressive	---	---	---	**250
Carbon fabric		**36	*0.32	---	*530
Glass fabric		*13	*0.27	---	*104

* Value supplied by manufacturer ** Test value obtained by author

5.2.6 Element type

1. 8-node semiloof curved thin shell QSL8 element was used for the models of the un-strengthened specimens and GFRP pultruded section strengthened specimens.

2. 8-node thick shell QTS8 element was used for the models of the FRP fabric strengthened specimens. The reason for this is that the QTS8 element is provided with a merge option to allow two surfaces with different properties to be joined. This option was not available for the QSL8 element.

5.2.7 Mesh

Mesh convergence studies described in Section 4.11.4.2 were used, following which an 8x8 mesh, Figure 5.1, for the QSL8 element and 12x12 mesh, Figure 5.2, for the QTS8 element were used for the web in each web panel of the plate-girders. The mesh sizes of for the flanges and stiffeners were used to adjust them with that of the web. Table 5.3 gives the mesh sizes for each of the QSL8 and QTS8 elements.

Table 5.3 Mesh sizes used in models of steel plate-girders

Element	Mesh size		
	Web in panel	Flange	Stiffener
QSL8	8x8	32x8	2x8
QTS8	12x12	48x8	2x12

5.2.8 Merge option

A merge option available in LUSAS was used to join the steel and FRP fabric surfaces in the models of FRP fabric strengthened specimens of group G2 in the same way as described in Chapter 4.

5.2.9 Imperfections

A lateral imperfection of 1 mm was measured at the centre of the web in the end web panel of an S2 plate-girder. The imperfection was included in the analyses of all specimens by using the first buckling mode from eigenvalue analyses with a maximum lateral displacement of 1 mm in the web.

Eurocode 3, EC3 (ENV 1993-1-5, 2006) describes lateral imperfections in the web to be taken as 'a/200' to include the web buckling of plate-girders in FE analyses, which comes as 2.5 mm for a = 500mm. In order to study the effect of lateral imperfections in the web, nonlinear FE analyses of the control specimen B1 first with no imperfection and then with the imperfections of 1, 2, 3, 4 and 5 mm in the web were carried out.

5.3 Model-wise results of FE analyses

5.3.1 Model B1

Figure 5.3 shows the applied load versus vertical deflection at the underside of the loaded stiffeners and Figure 5.4 shows the load versus lateral deflection at the centre of the web in the end web panel for the initial lateral imperfections of 0, 1, 2, 3, 4 and 5 mm in the web obtained from the FE analyses.

It can be seen that the vertical and lateral deflections increases linearly with the applied load up to the ultimate load. It can also been seen that the load-deflection responses with no initial imperfection in the web, as expected, are different from those with the imperfections. The load-deflection responses with the imperfections from 1 to 5 mm are not significantly different from each other. The ultimate load, 242 kN, of the model with the smallest imperfection of 1 mm is approximately 1.08 times greater than that, 223 kN, with the largest imperfection of 5 mm. The effect of these imperfections on the ultimate load compared to that, 2.5 mm, determined according to EC3 is within a range of ± 4%.

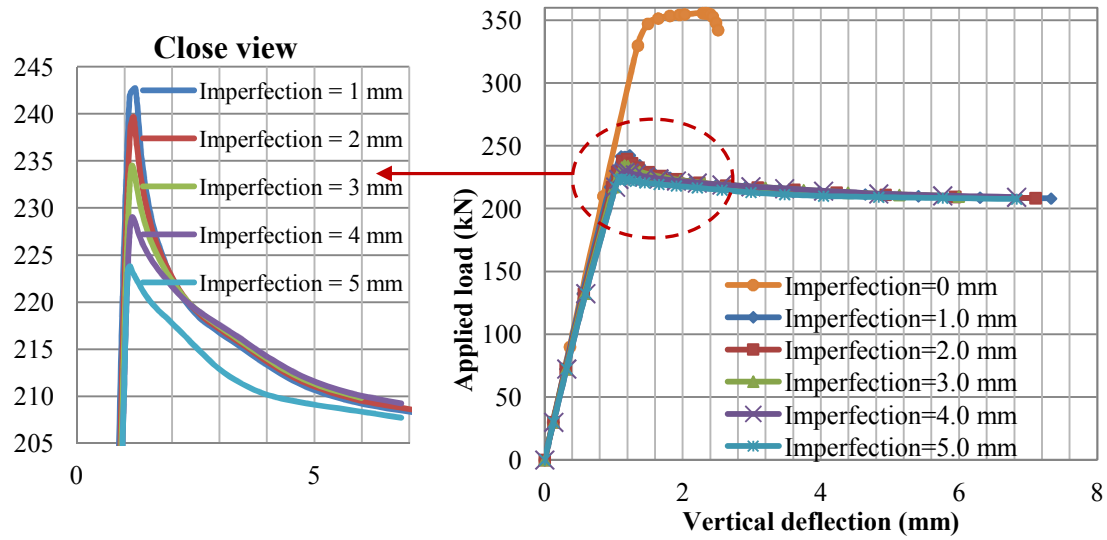

Figure 5.3 Load vs. vertical deflection at the underside of loaded stiffeners of model B1

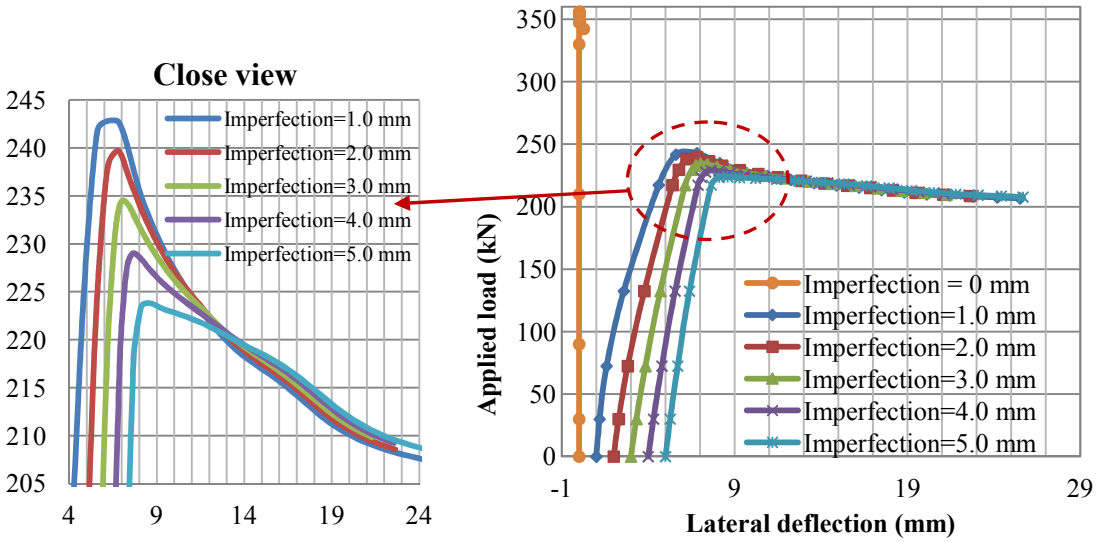

Figure 5.4 Load vs. lateral deflection at the centre of end web panel of model B1

The model failed with out-of-plane diagonal buckling of the web in the end panel followed by its diagonal yielding and development of four plastic hinges, two in the top flange and one each in the bottom flange and the external steel stiffeners, Figure 5.5. One plastic hinge in the top flange developed near the left corner of the end web panel and the other at a distance of approximately 250 mm from it. The plastic hinge in the bottom flange developed near right corner of the end web panel and that in the external stiffeners at distance of approximately 190 from the top corner of the plate-girder.

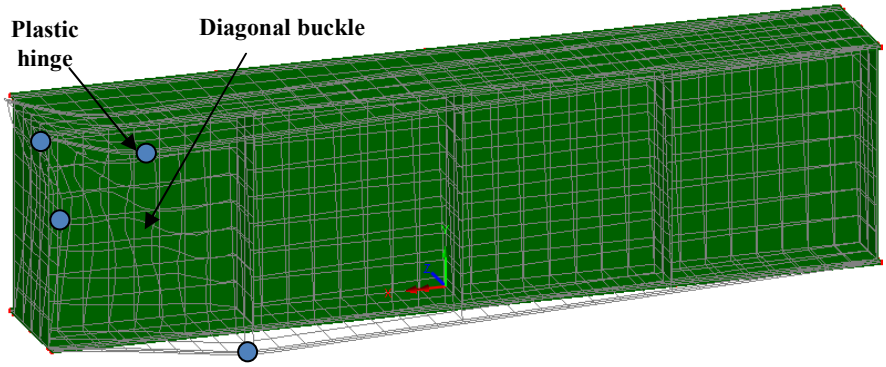

Figure 5.5 Mode of failure of model B1

The ditrsibution of stresses in the nonlinear FE analyses of the model B1 was similar to that of the analysed steel plate-girder described in Chapter 4. At the ultimate load of the model B1, the major (tensile) and minor (compressive) principal stresses, S_1 and S_3, in the web of the end panel were 0.198 and -0.114 GPa respectively, Figure 5.6. The maximum equivalent stress based on von-Mises yield criterion 'S_E', 0.287 GPa, in the tensile stress field of the end web panel, being a combined effect of the major and minor principal stresses, was 1.04 times the yield strength, 0.274 GPa, of the steel in the web, Figure 5.7.

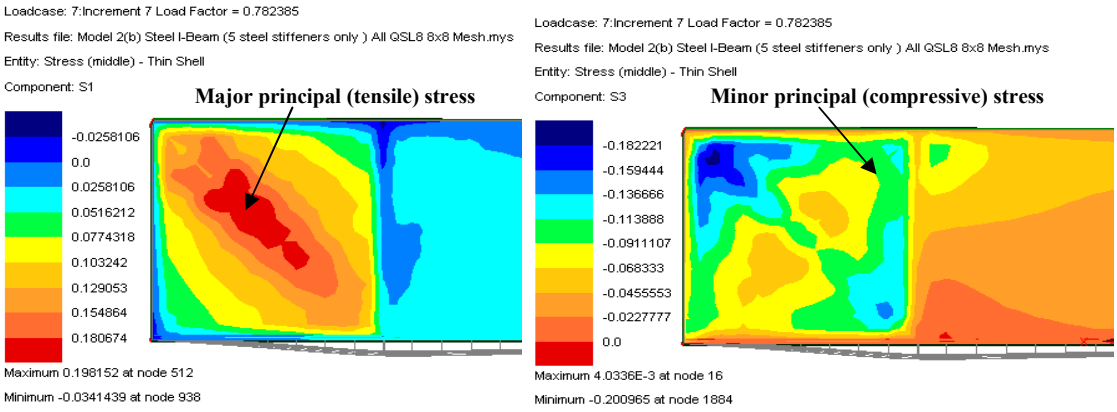

Figure 5.6 Major and minor principal stresses in web of end panel at ultimate load of B1

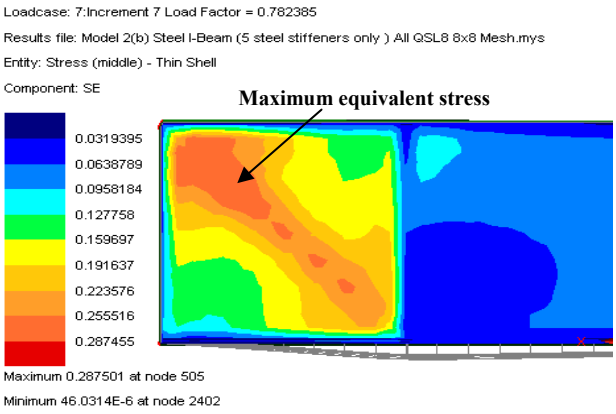

Figure 5.7 Distribution of equivalent stresses in web of end panel at ultimate load of B1

5.3.2 Model B9

Figure 5.8 shows the applied load versus vertical deflection at the underside of the loaded stiffeners and Figure 5.9 shows the load versus lateral deflection at the centre of the web in the end web panel obtained from the FE analyses. The vertical deflection increases linearly with the applied load up to the ultimate load of 295 kN, then increases as the load drops to approximately 278 kN and thereafter the vertical deflection increases without any change in the applied load. The lateral deflection also increases with the applied load up to the ultimate load of 295 kN, but the relationship is not linear.

The model failed with out-of-plane diagonal buckling of the web in the end panel followed by its diagonal yielding and development of four plastic hinges, two in the top flange and one each in the bottom flange and the external steel stiffeners, Figure 5.10, at the similar positions as those seen in the model B1. The plastic hinges in the external steel stiffeners and the top flange were at distances of approximately 190 mm and 300 mm respectively from the top corner of the plate-girder.

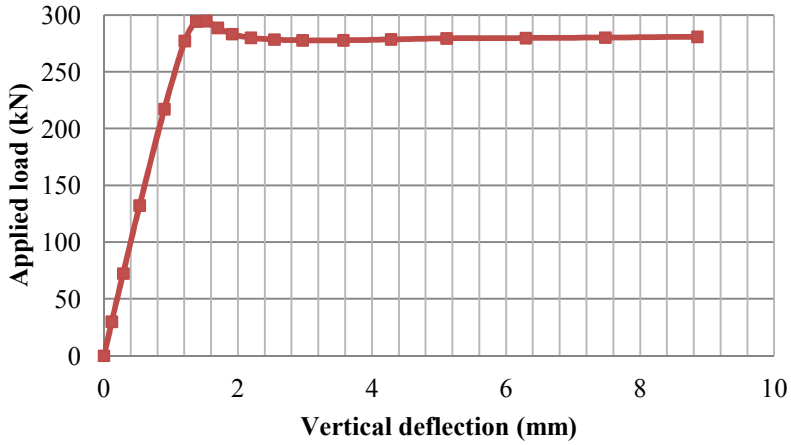

Figure 5.8 Load vs. vertical deflection at the underside of loaded stiffeners of model B9

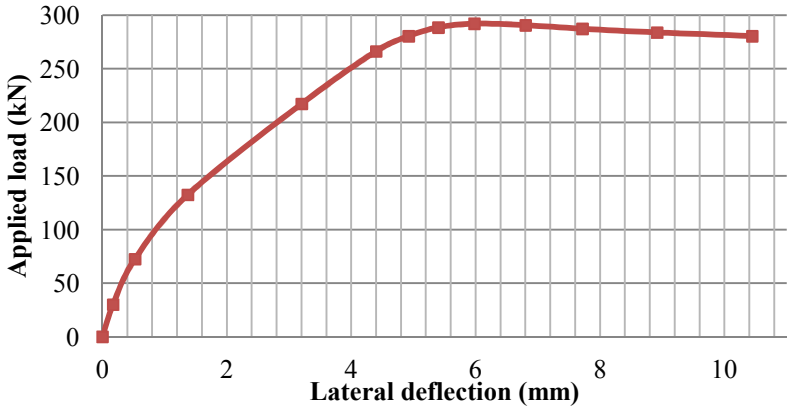

Figure 5.9 Load vs. lateral deflection at the centre of end web panel of model B9

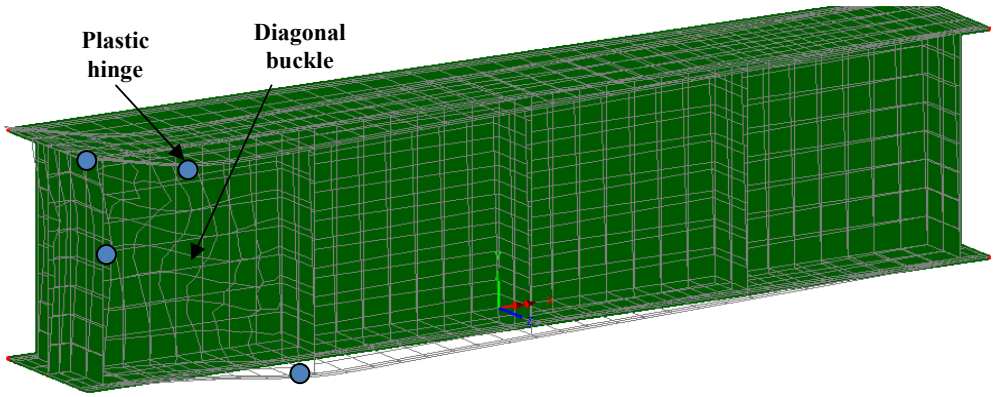

Figure 5.10 Mode of failure of model B9

The distribution of stresses in the un-strengthened FE model B9 was very similar to that of the model B1. At the ultimate load of the model B9, the values of the major (tensile) and minor (compressive) principal stresses, S_1 and S_3, in the web of end panel were 0.2625 and -0.144 GPa respectively, Figure 5.11. The maximum equivalent stress based on von-Mises yield criterion 'S_E', 0.371 GPa, in the tensile stress field of the end web panel was 1.05 times the yield strength, 0.353 GPa, of the steel in the web, Figure 5.12.

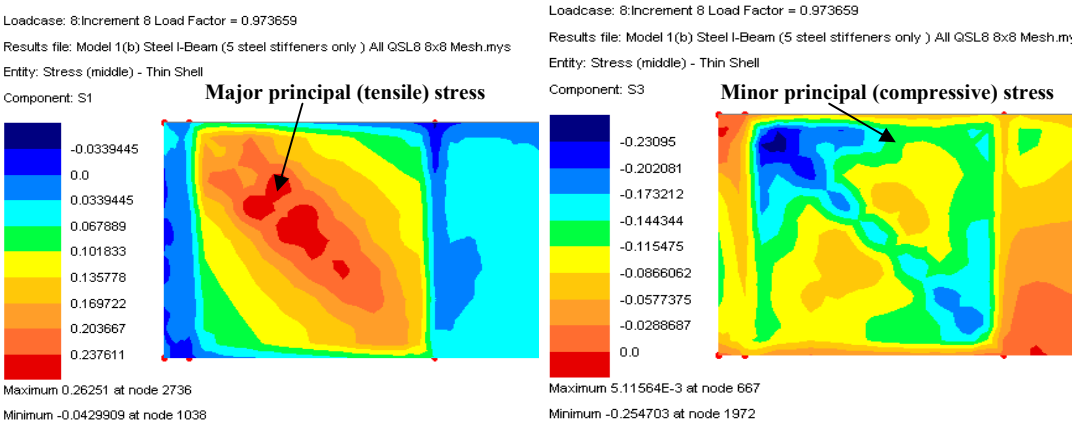

Figure 5.11 Major and minor principal stresses in web of end panel at ultimate load of B9

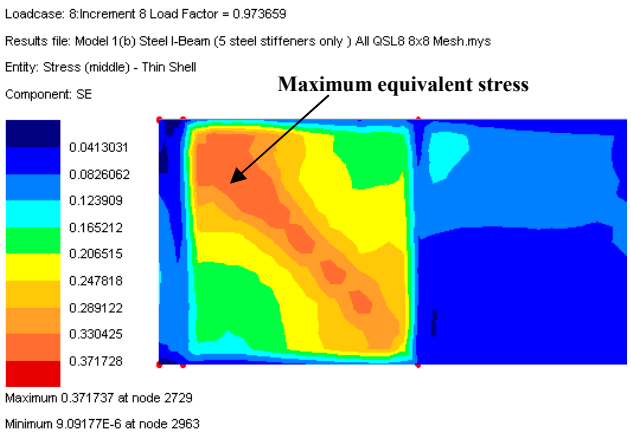

Figure 5.12 Distribution of equivalent stresses in web of end panel at ultimate load of B9

5.3.3 Model B2

Figure 5.13 shows the applied load versus vertical deflection at underside of the loaded stiffeners and Figure 5.14 shows the load versus lateral deflection at middle of the GFRP stiffener in the strengthened web panel obtained from the FE analyses. The vertical deflection increases linearly with the applied load up to the ultimate load of 287 kN, then increases as the load drops to approximately 250 kN and thereafter the vertical deflection increases without any change in the applied load. The lateral deflection increases nearly linearly with the applied load up to the ultimate load of 287 kN and then increases as the load drops to approximately 250 kN.

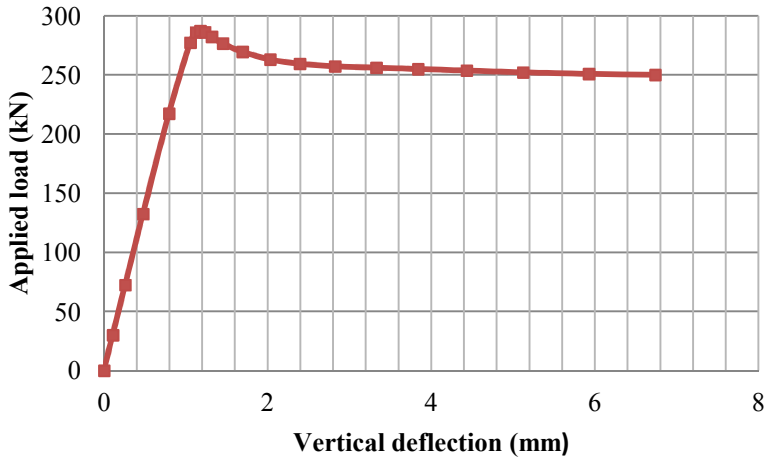

Figure 5.13 Load vs. vertical deflection at the underside of loaded stiffeners of model B2

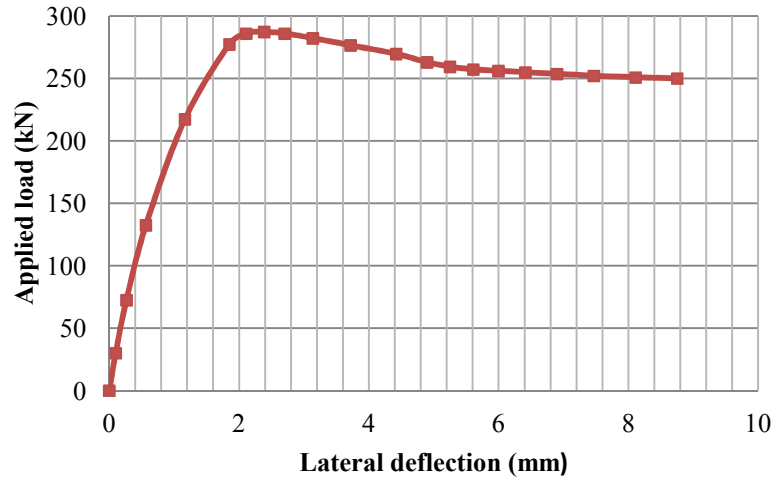

Figure 5.14 Load vs. lateral deflections at the centre of FRP-strengthened web panel of B2

The model failed with development of two out-of-plane diagonal buckles in the steel web on both sides of the GFRP stiffener together with buckling of the stiffener and

development of four plastic hinges, two in the top flange and one each in the bottom flange and the external steel stiffeners, Figure 5.15. The plastic hinges in the external steel stiffeners and the top flange were at distances of approximately 220 mm and 250 mm respectively from the top corner of the plate-girder.

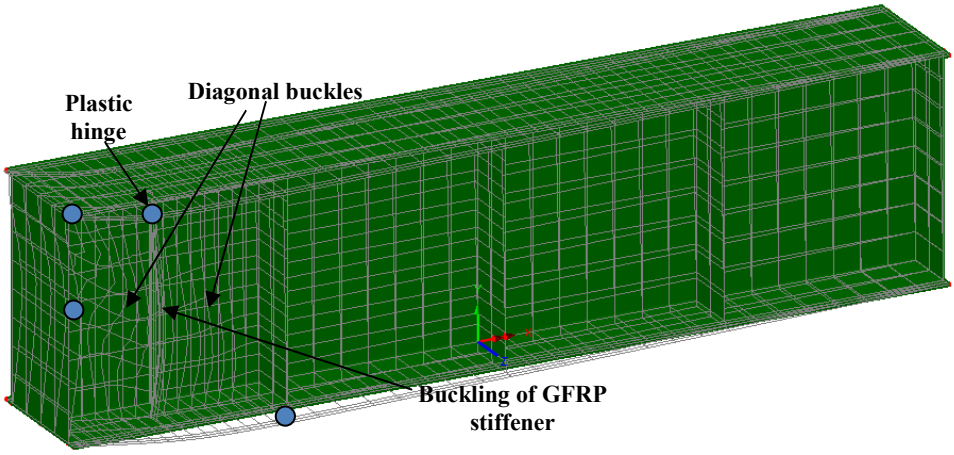

Figure 5.15 Mode of failure of model B2

At the ultimate load of 287 kN, the maximum equivalent stress 'S_E', 0.285 GPa, in the web of each of the two sub-panels of the FRP-strengthened web panel was 1.04 times the yield strength, 0.274 GPa, of the steel in the web, Figure 5.16.

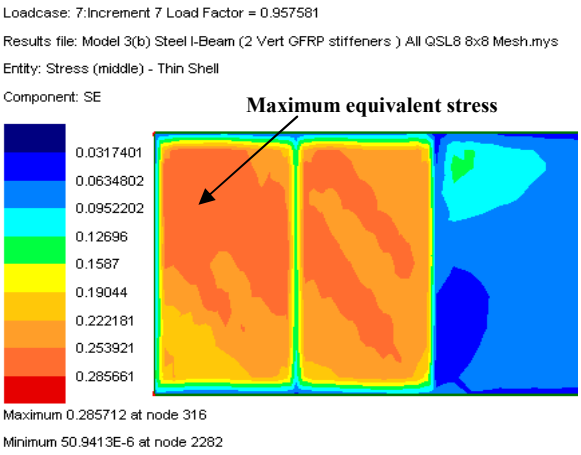

Figure 5.16 Distribution of equivalent stresses in web of end panel at ultimate load of B2

5.3.4 Model B5

Figure 5.17 shows the applied load versus vertical deflection at underside of the loaded stiffeners and Figure 5.18 shows the load versus lateral deflection at middle of the GFRP stiffener in the strengthened panel obtained from the FE analyses.

The vertical deflection increases linearly with the applied load up to the ultimate load of 368 kN, then increases as the load drops to approximately 333 kN and thereafter the vertical deflection increases without any change in the applied load. The lateral deflection is negligible up to a load of 150 kN, then has a very small increase of approximately 0.25 mm up to the ultimate load and thereafter increases as the load drops to 333 kN.

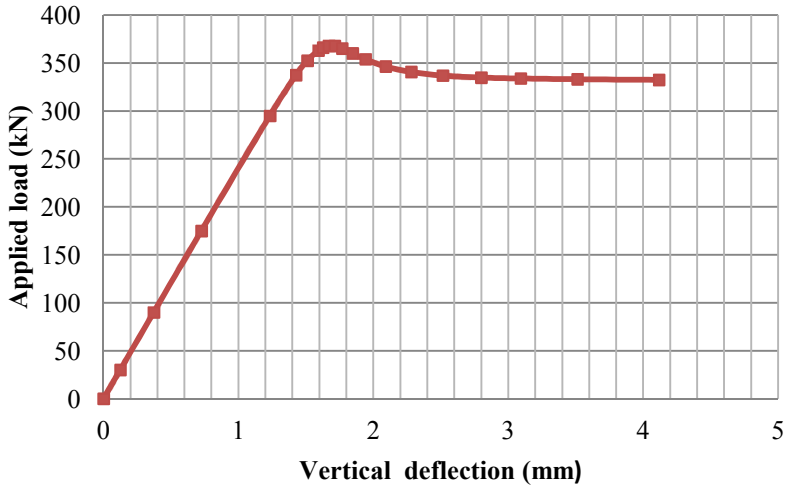

Figure 5.17 Load vs. vertical deflection at the underside of loaded stiffeners of model B5

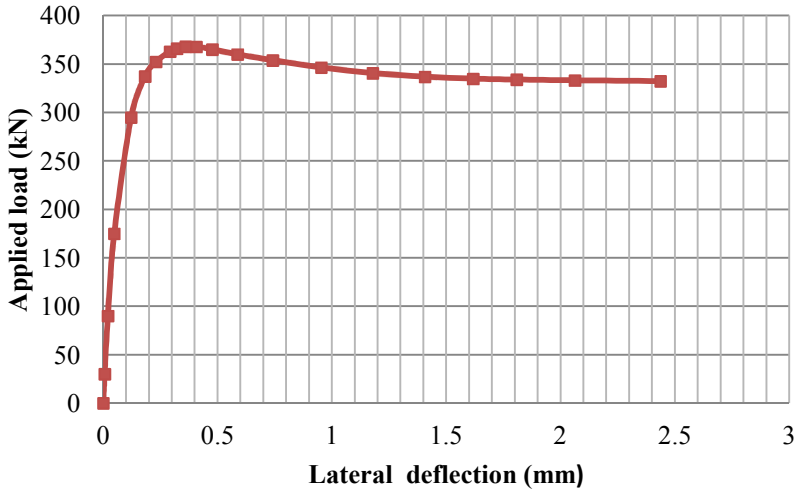

Figure 5.18 Load vs. lateral deflection at the centre of FRP-strengthened web panel of B5

The model failed with development of two out-of-plane diagonal buckles in the steel web on both sides of the GFRP stiffener and four plastic hinges, two in the top flange and one each in the bottom flange and external steel stiffeners, Figure 5.19. The plastic hinges in the external steel stiffeners and top flange were at distances of approximately 250 mm and 300 mm respectively from the top corner of the plate-girder.

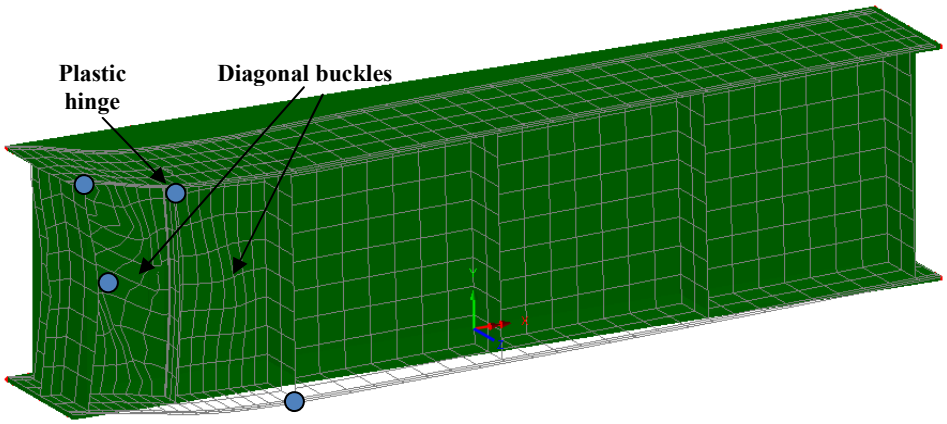

Figure 5.19 Mode of failure of model B5

At the ultimate load of 368 kN, the maximum equivalent stress 'S_E', 0.361 GPa, in the web of each of the two sub-panels of the FRP-strengthened web panel was 1.02 times the yield strength, 0.353 GPa, of the steel in the web, Figure 5.20.

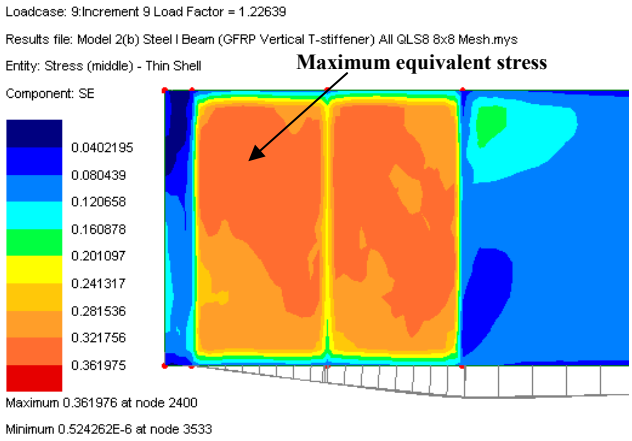

Figure 5.20 Distribution of equivalent stresses in web of end panel at ultimate load of B5

5.3.5 Model B6

Figure 5.21 shows the applied load versus vertical deflection at the underside of the loaded stiffeners and Figure 5.22 shows the load versus lateral deflection at middle of the GFRP stiffener in the strengthened web panel obtained from the FE analyses. The vertical and lateral deflections increase linearly with the applied load up to a load of approximately 410 kN. The increases in the two deflections continue up to the ultimate load of 456 kN, but the relationships are not linear. Both the deflections finally decrease with a sharp drop in the load to approximately 300 kN.

The model showed a relatively brittle failure, which was initiated with buckling of the GFRP stiffener and development of an out-of-plane diagonal buckle in the steel web in the end panel similar to that of the model B9. Four plastic hinges, two in the top flange and one each in the bottom flange and the external steel stiffeners, Figure 5.23, had developed. The hinges in the external steel stiffeners and top flange were at distances of approximately 220 mm and 300 mm respectively from the top corner of the plate-girder.

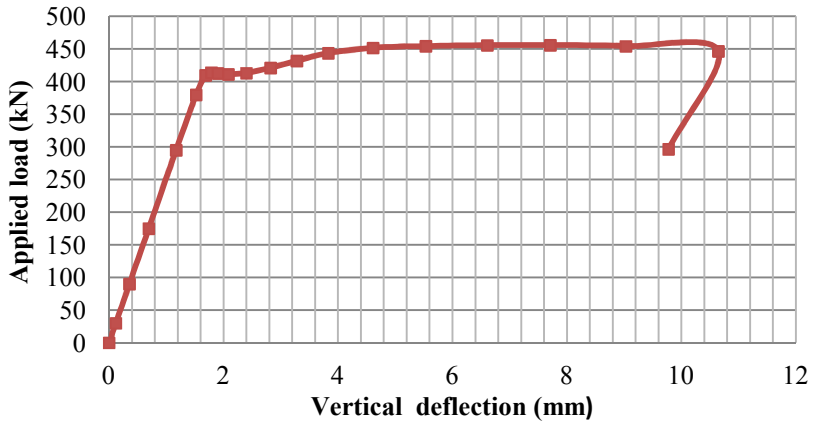

Figure 5.21 Load vs. vertical deflection at the underside of loaded stiffeners of model B6

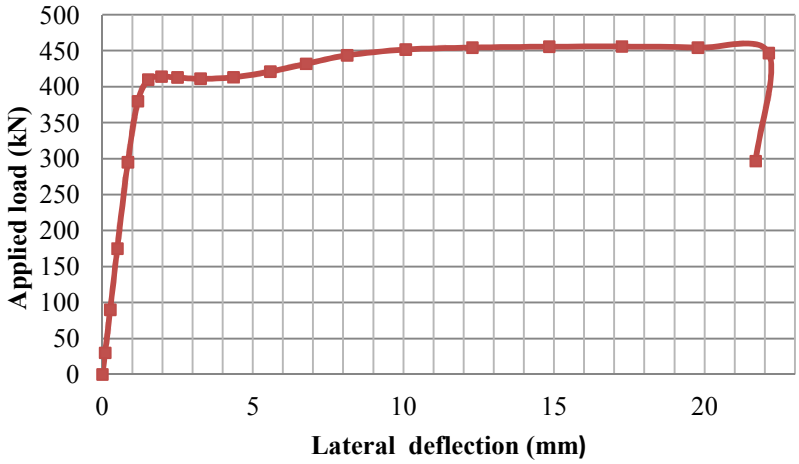

Figure 5.22 Load vs. lateral deflection at the centre of strengthened web panel of B6

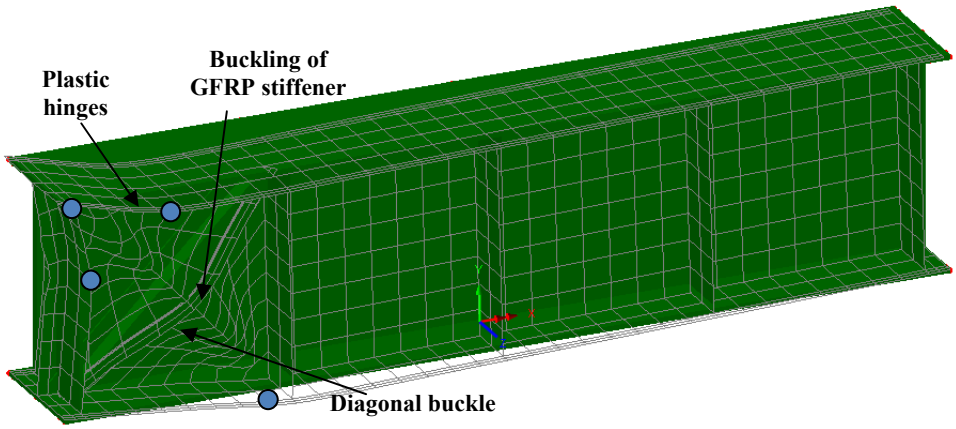

Figure 5.23 Mode of failure of model B6

At the ultimate load of 456 kN, the maximum equivalent stress 'S_E', 0.377 GPa, in the web of each of the two sub-panels of the FRP-strengthened web panel was 1.06 times the yield strength, 0.353 GPa, of the steel in the web, Figure 5.24.

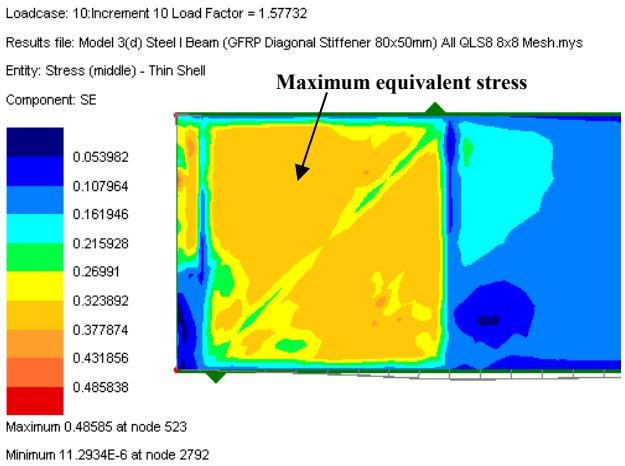

Figure 5.24 Distribution of equivalent stresses in web of end panel at ultimate load of B6

5.3.6 Model B8

Figure 5.25 shows the applied load versus vertical deflection at the underside of the loaded stiffeners and Figure 5.26 shows the load versus lateral deflection at the centre of the web in the end web panel obtained from the FE analyses. The vertical deflection increases linearly with the applied load up to the ultimate load of 284 kN, then increases as the load dropped to approximately 265 kN and thereafter the vertical deflection increases without any change in the applied load. The lateral deflection also increases with the applied load up to the ultimate load of 284 kN, but the relationship is not linear.

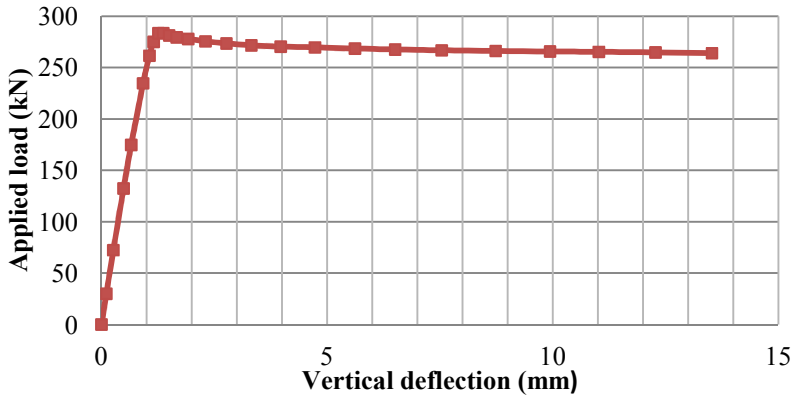

Figure 5.25 Load vs. vertical deflection at the underside of loaded stiffeners of model B8

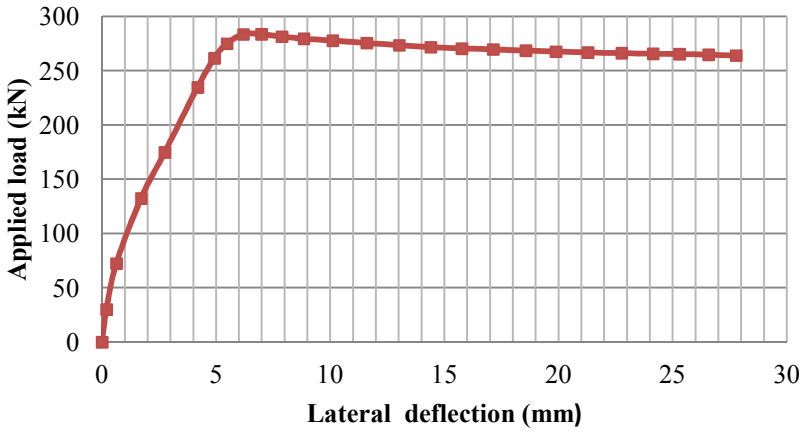

Figure 5.26 Load vs. lateral deflection at the centre of end panel of model B8

The model failed with out-of-plane diagonal buckling of the web in the end panel followed by its diagonal yielding and development of four plastic hinges, two in the top flange and one each in the bottom flange and the external steel stiffeners, Figure 5.27, at the similar positions as those seen in models B1 and B9. The plastic hinges in the external steel stiffeners and the top flange were at distances of approximately 200 mm and 300 mm respectively from the top corner of the plate-girder.

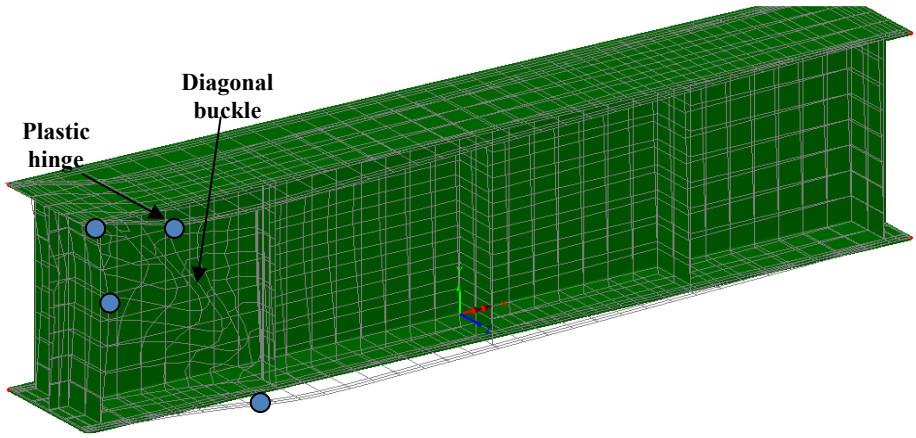

Figure 5.27 Mode of failure of model B8

At the ultimate load of 284 kN, the maximum equivalent stress 'S_E', 0.375 GPa, in the tensile stress field of the end web panel was 1.06 times the yield strength, 0.353 GPa, of the steel in the web, Figure 5.28.

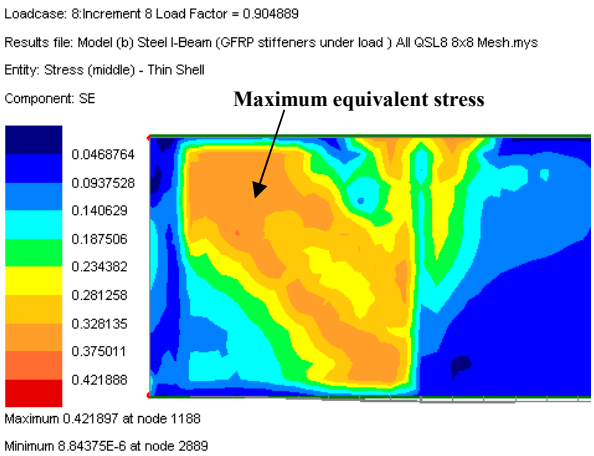

Figure 5.28 Distribution of equivalent stresses in web of end panel at ultimate load of B8

5.3.7 Model B3

Figure 5.29 shows the applied load versus vertical deflection at underside of the loaded stiffeners and Figure 5.30 shows the load versus lateral deflections at centres of the first and second web panels obtained from the FE analyses. The vertical deflection and the lateral deflection at the centre of the second web panel increase with the applied load up to the ultimate load of 705 kN. The lateral deflection at the centre of the first web panel, strengthened panel, is negligible up to a load of 400 kN and has a very small increase of approximately 0.3 mm in the backward direction between the loads 400 to 705 kN.

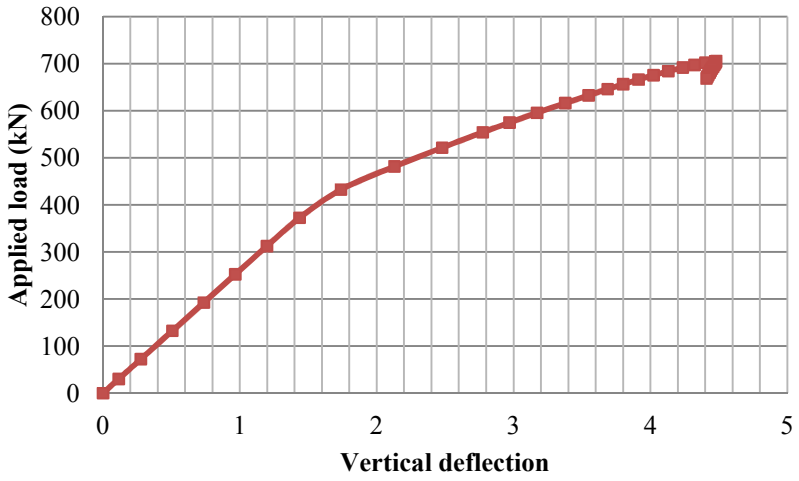

Figure 5.29 Load vs. vertical deflection at the underside of loaded stiffeners of model B3

The model failed with the out-of-plane buckling of the un-strengthened web in the three web panels except the strengthened panel, yielding of the web in the second and fourth web panels, yielding of the loaded stiffeners near the applied load and the formation of four plastic hinges, two in the top flange and one each in the loaded stiffeners and

bottom flange, Figure 5.31. The buckling of the web initially started in the second web panel, adjacent to the strengthened panel, and was observed in the third and fourth panels when the applied load exceeded 520 kN.

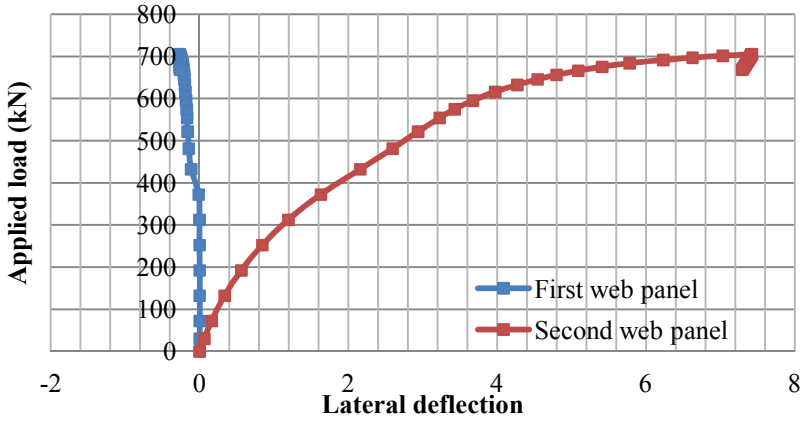

Figure 5.30 Load vs. lateral deflections at centres of first and second web panels of B3

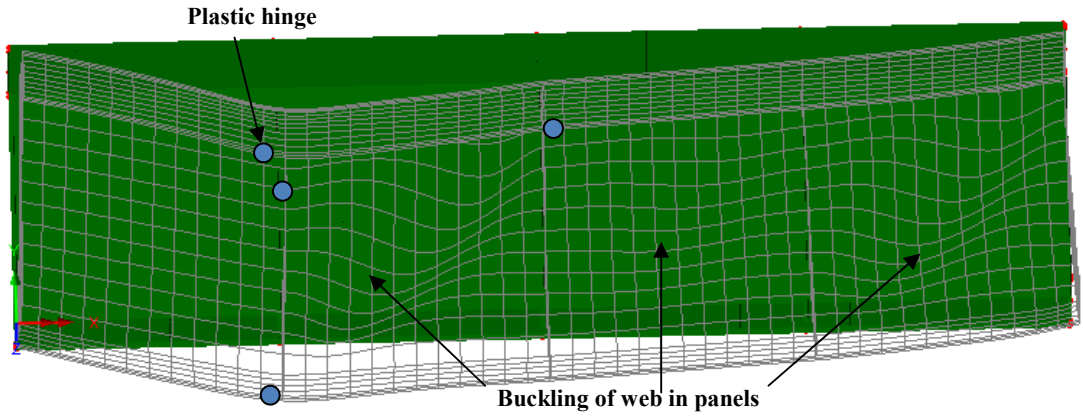

Figure 5.31 Mode of failure of model B3

At the ultimate load of 705 kN, the maximum equivalent stress 'S_E', 0.274 GPa, in the webs of the second and fourth web panels was equal to the yield strength, 0.274 GPa, of the steel in the web, Figure 5.32.

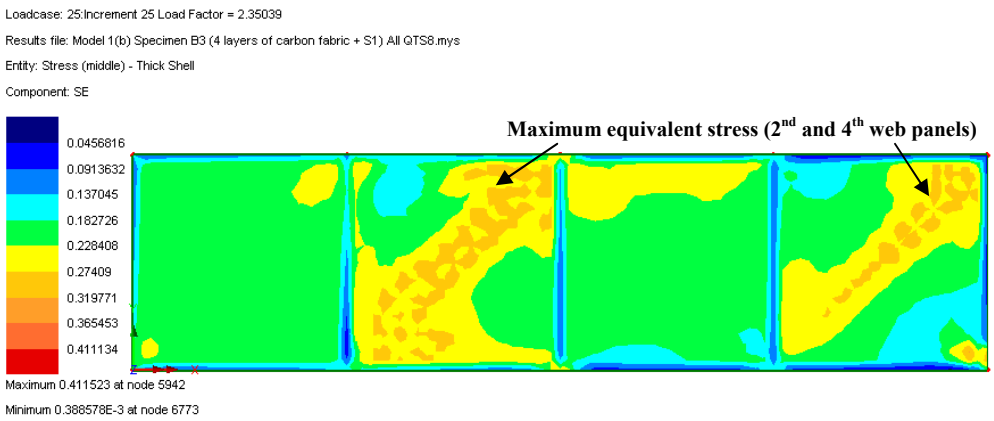

Figure 5.32 Distribution of equivalent stresses in web of end panel at ultimate load of B3

5.3.8 Model B4

Figure 5.33 shows the applied load versus vertical deflection at underside of the loaded stiffeners and Figure 5.34 shows the load versus lateral deflections at the centres of the first and second web panels obtained from the FE analyses. The vertical deflection and the lateral deflection at the centre of the second web panel increase with the applied load up to the ultimate load of 706 kN. The lateral deflection at the centre of the first web panel, strengthened panel, is however negligible up to the ultimate load.

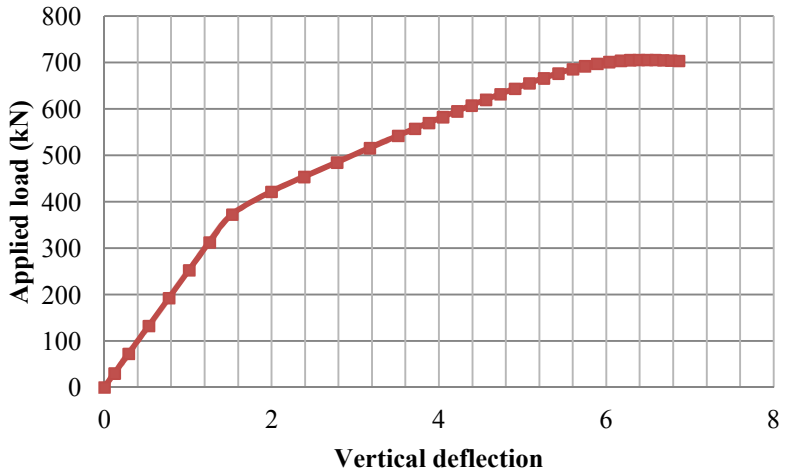

Figure 5.33 Load vs. vertical deflection at the underside of loaded stiffeners of B4

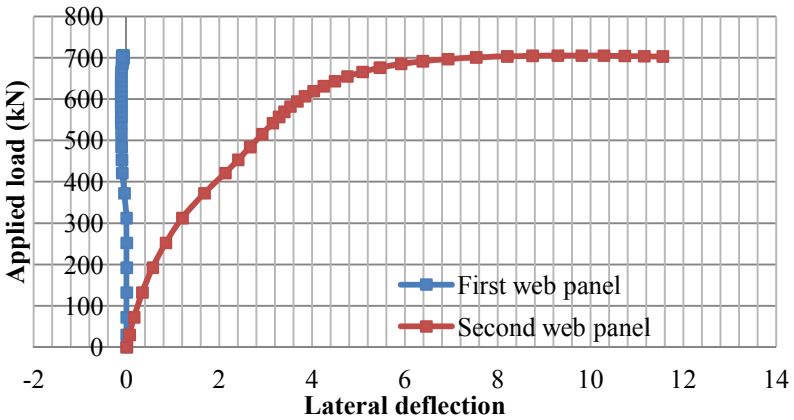

Figure 5.34 Load vs. lateral deflections at centres of first and second web panels of B4

The model B4 failed in a same way to the model B3 which was initiated by the out-of-plane buckling of the un-strengthened web in the three web panels except the strengthened panel and followed by yielding of the web in the second and fourth web panels, yielding of the loaded stiffeners near the applied load and the formation of four plastic hinges, two in the top flange and one each in the loaded stiffeners and bottom flange, Figure 5.35. The buckling of the web initially started in the second web panel,

adjacent to the strengthened panel, and was observed in the third and fourth panels when the applied load exceeded 520 kN.

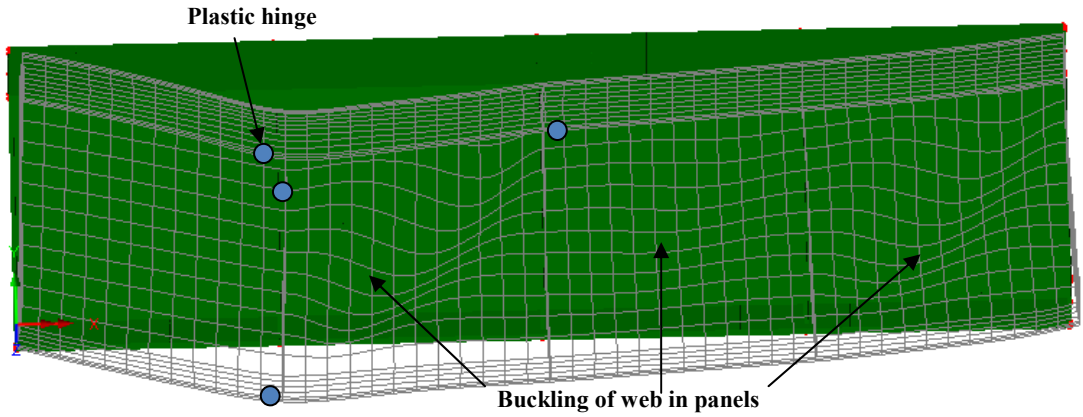

Figure 5.35 Mode of failure of model B4

At the ultimate load of 706 kN, the maximum equivalent stress 'S_E', 0.283 GPa, in the webs of the second and fourth web panels was 1.03 times the yield strength, 0.274 GPa, of the steel in the web, Figure 5.36.

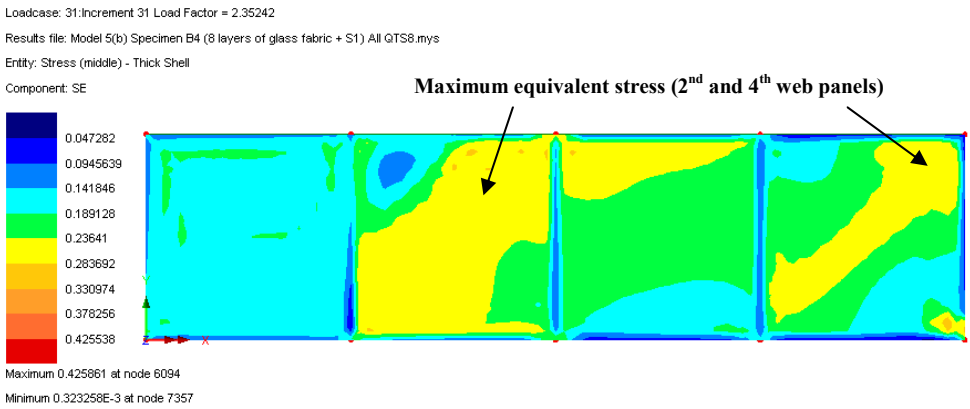

Figure 5.36 Distribution of equivalent stresses in web of end panel at ultimate load of B4

5.3.9 Model B7

Figure 5.37 shows the applied load versus vertical deflection at underside of the loaded stiffeners and Figure 5.38 shows the load versus lateral deflections at centres of the first and second web panels obtained from the FE analyses. The vertical deflection increases linearly with the applied load up to a load of approximately 420 kN and continues to increase up to the ultimate load of 439 kN, but the relationship then is not linear. After the ultimate load, it also increases with decrease in the applied load. The lateral deflection at the centre of the first web panel increases with applied load up to the ultimate load and that at the centre of the second panel is negligible during the entire loading.

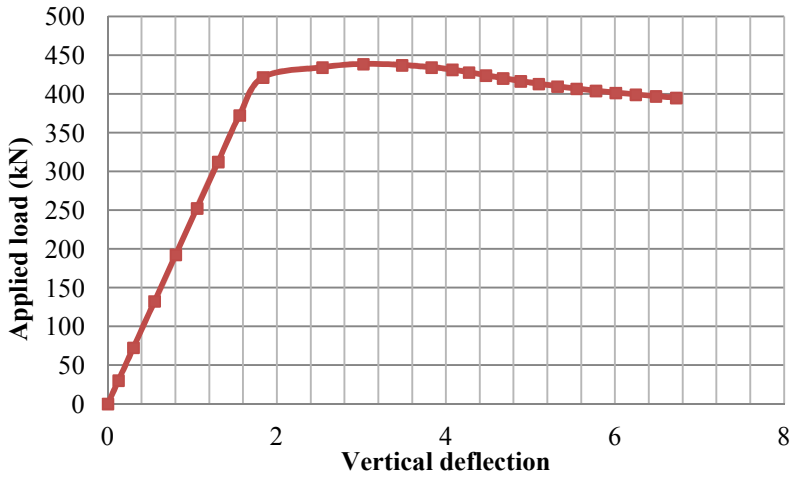

Figure 5.37 Load vs. vertical deflection at the underside of loaded stiffeners of model B7

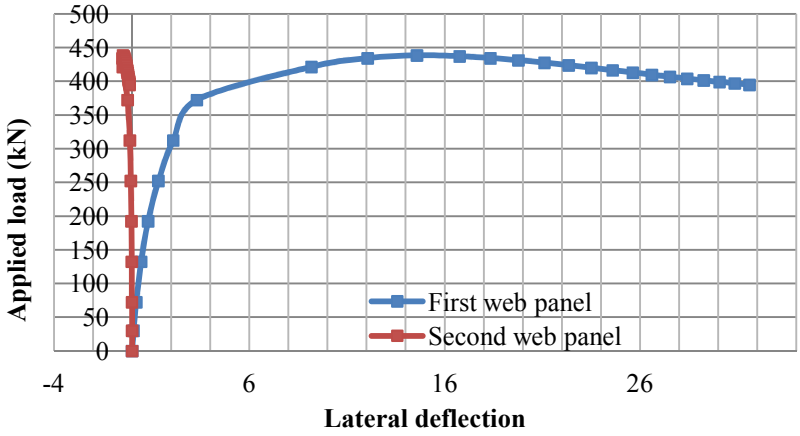

Figure 5.38 Load vs. lateral deflection at centres of first and second web panels of B7

The model failed with the out-of-plane diagonal buckling of the web in the strengthened web panel and development of four plastic hinges, two in the top flange and one each in the external steel stiffeners and bottom flange, Figure 5.39. The hinges in the external stiffeners and top flange were at distances of approximately 290 mm and 270 mm from the top corner of the plate-girder. At the ultimate load of 439 kN, the maximum equivalent stress 'S_E' in the web of the end web panel is shown in Figure 5.40.

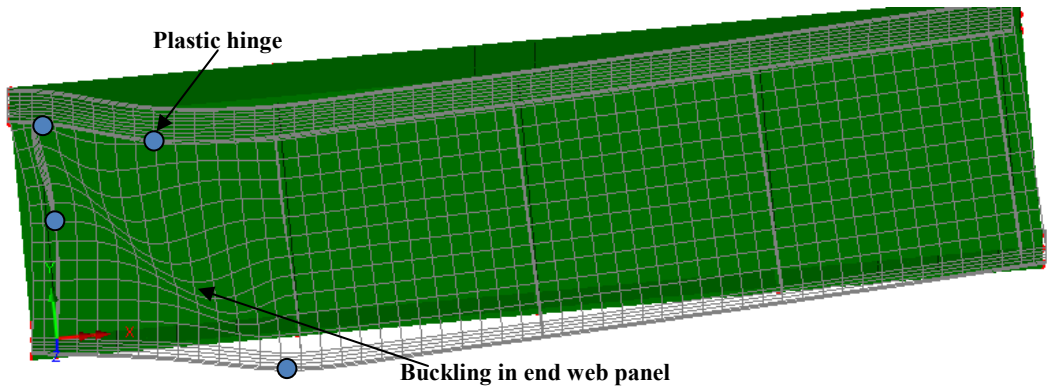

Figure 5.39 Mode of failure in model B7

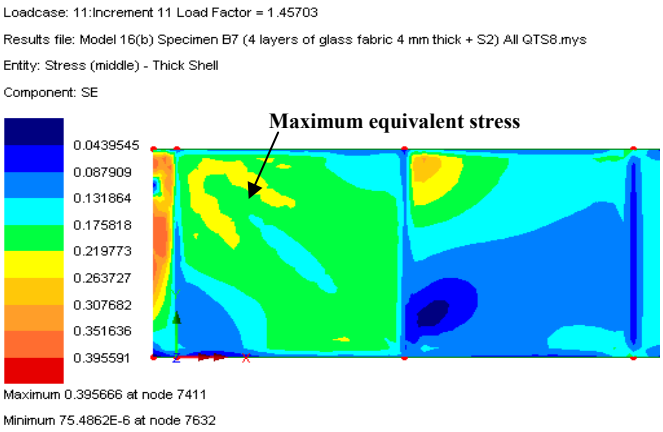

Figure 5.40 Distribution of equivalent stresses in web of end panel at ultimate load of B7

5.4 FEA and test results of specimens

5.4.1 Ultimate loads

Table 5.4 gives a comparison of the ultimate loads of specimens in the tests and FE analyses.

Table 5.4 Test and FEA ultimate loads of test specimens and FE models

Specimen No. (Plate-girder series)	Ultimate load (kN)		Ultimate load of FRP-str. to control		FEA to test ultimate loads
	FEA	Test	FEA	Test	
Group G1: Un-strengthened control specimens					
B1 (S1)	235	230	---	---	1.02
B9 (S2)	295	--	---	---	---
Group G2: GFRP pultruded section strengthened specimens					
B2 (S1)	287	277	1.22	1.20	1.03
B5 (S2)	368	380	1.25	1.29	0.97
B6 (S2)	456	437	1.54	1.48	1.04
B8 (S2)	284	285	0.96	0.97	1.00
Group G3: FRP fabric strengthened specimens					
B3 (S1)	705	287	3.0	1.25	2.45
B4 (S1)	706	354	3.0	1.54	1.99
B7 (S2)	439	428	1.49	1.45	1.03

5.4.2 Location of plastic hinges

Table 5.5 gives the locations where the plastic hinges were formed in the top flange and the external steel stiffeners of the specimens in the tests and the FE analyses. The distances of the plastic hinges are taken from the left top corner of the test panel.

Table 5.5 Locations of plastic hinges developed in test specimens and FE models

Specimen No. (Girder series)	Distance of plastic hinge from top corner of test web panel			
	Top flange (mm)		Ext steel stiffeners (mm)	
	FEA	Test	FEA	Test
B1 (S1)	250	250	190	180
B9 (S2)	250	---	200	---
B2 (S1)	250	250	220	240
B5 (S2)	250	260	250	240
B6 (S2)	250	260	250	240
B8 (S2)	250	260	200	240
B3 (S1)	---	250	---	280
B4 (S1)	---	250	---	280
B7 (S2)	220	260	290	240

5.4.3 Modes of failure

Figure 5.41 to Figure 5.48 show the test and FEA failure modes of specimens B1 to B8.

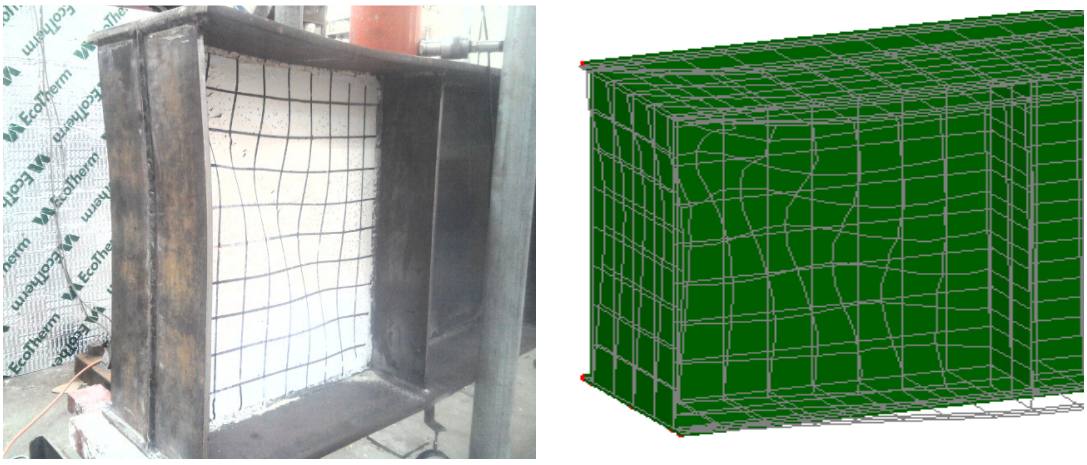

Figure 5.41 Test and FEA modes of failure of un-strengthened specimen B1

Figure 5.42 Test and FEA modes of failure of GFRP-strengthened specimen B2

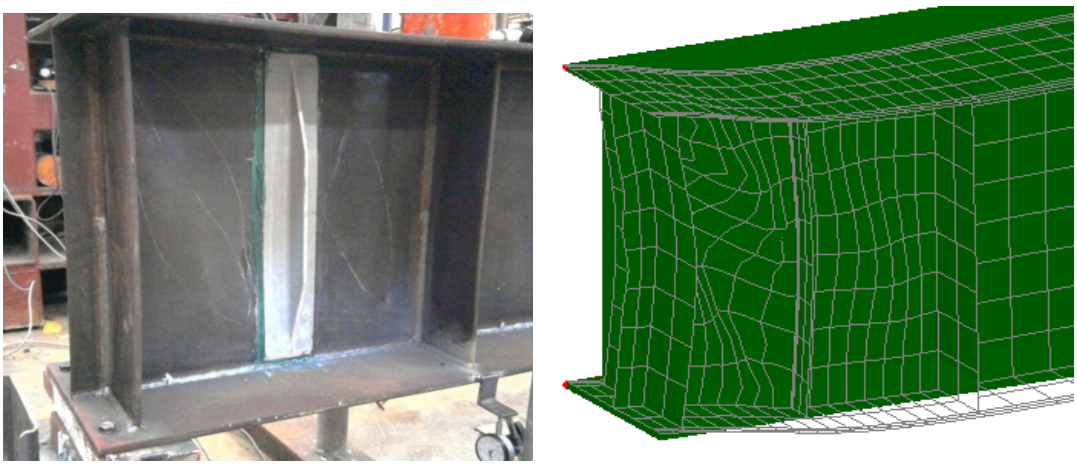

Figure 5.43 Test and FEA modes of failure of GFRP-strengthened specimen B5

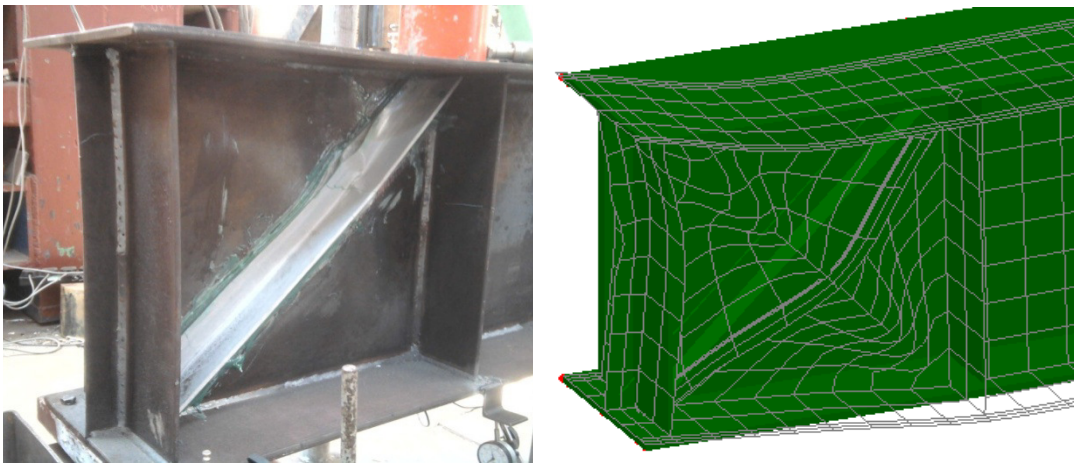

Figure 5.44 Test and FEA modes of failure of GFRP-strengthened specimen B6

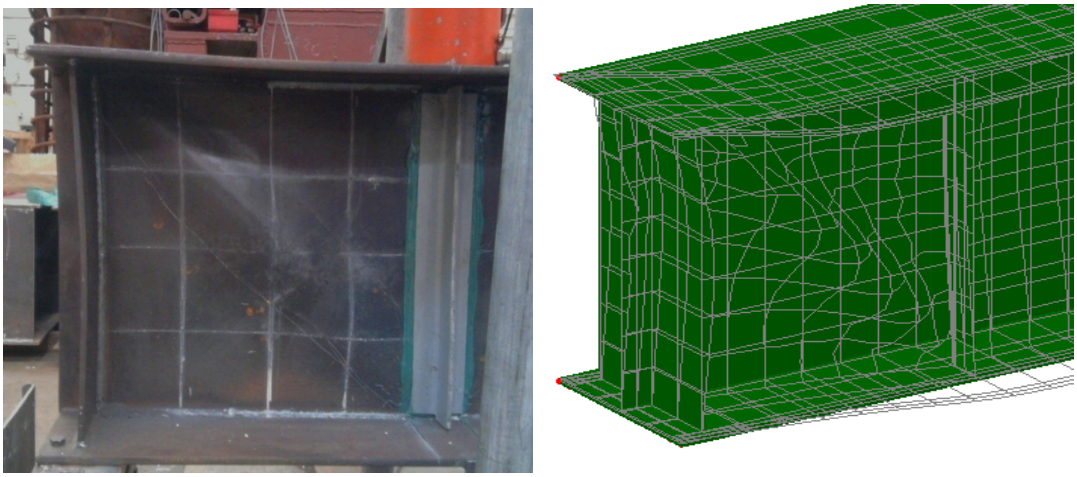

Figure 5.45 Test and FEA modes of failure of specimen B8 with GFRP stiffeners under load

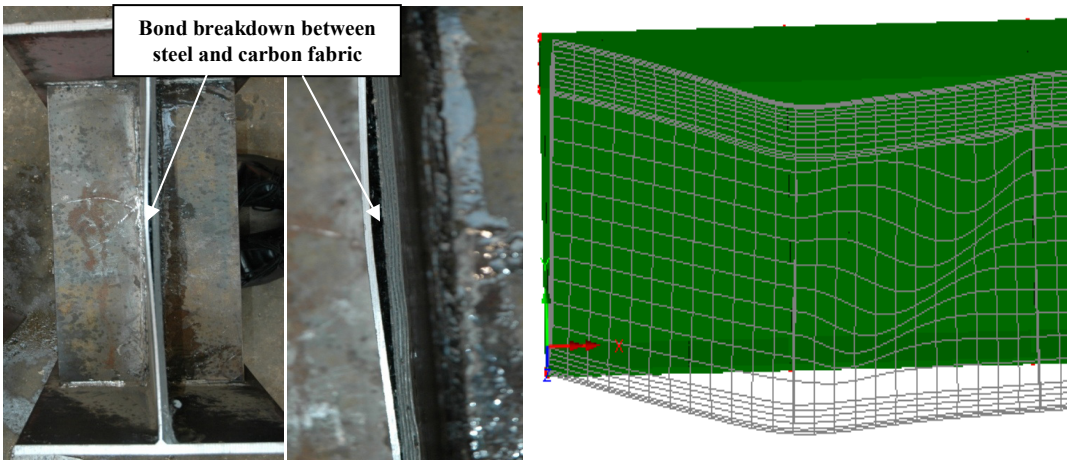

Figure 5.46 Test and FEA modes of failure of carbon fabric-strengthened specimen B3

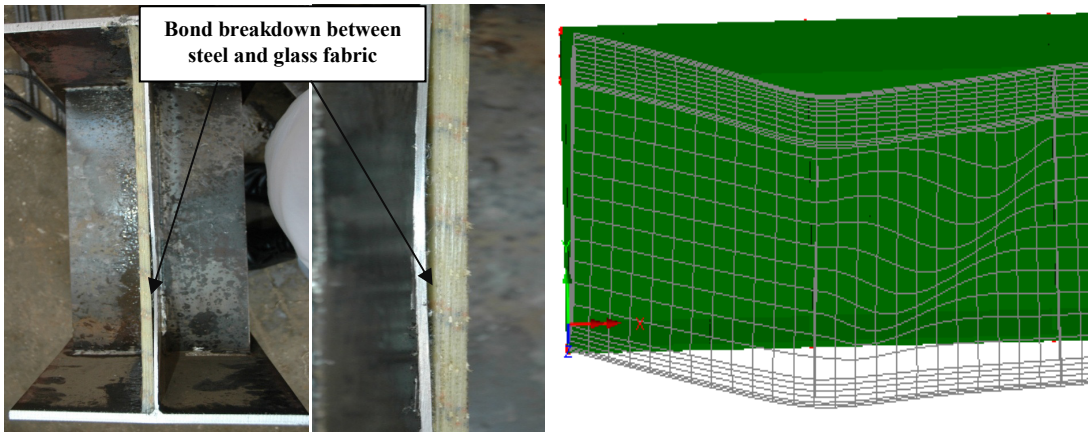

Figure 5.47 Test and FEA modes of failure of glass fabric-strengthened specimen B4

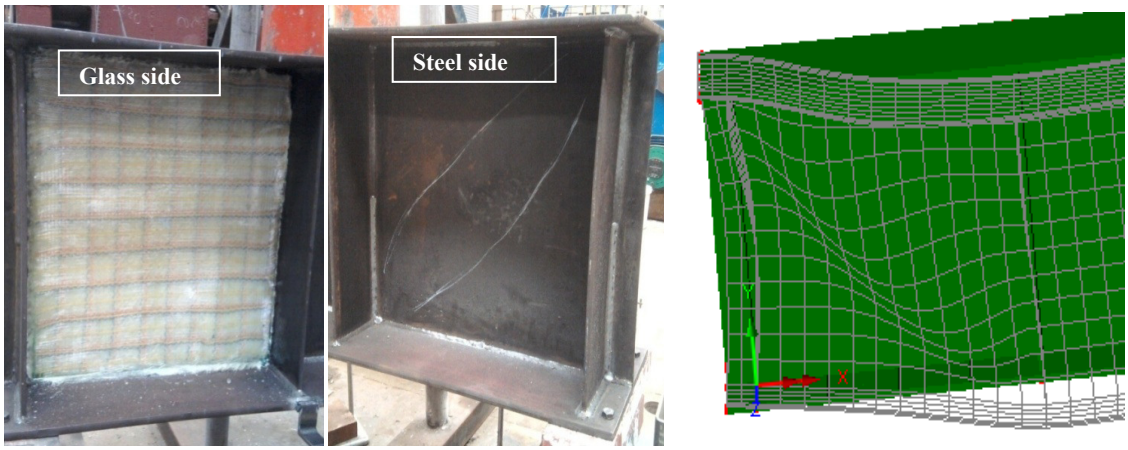

Figure 5.48 Test and FEA modes of failure of glass fabric-strengthened specimen B7

5.4.4 Load-vertical deflection responses

Figure 5.49 to Figure 5.56 show responses of the applied load versus vertical deflection at the underside of plate-girder beneath the loaded stiffeners of specimens B1 to B8 in the tests and the FE analyses.

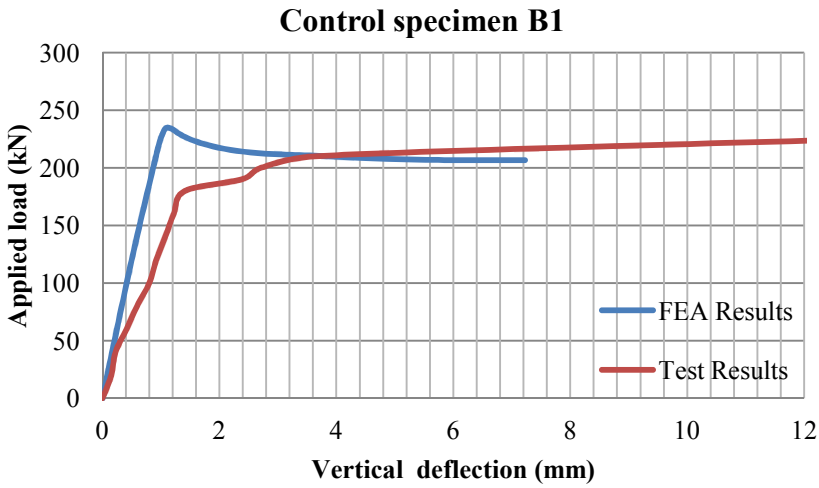

Figure 5.49 Load versus vertical deflection at the underside of loaded stiffeners of B1

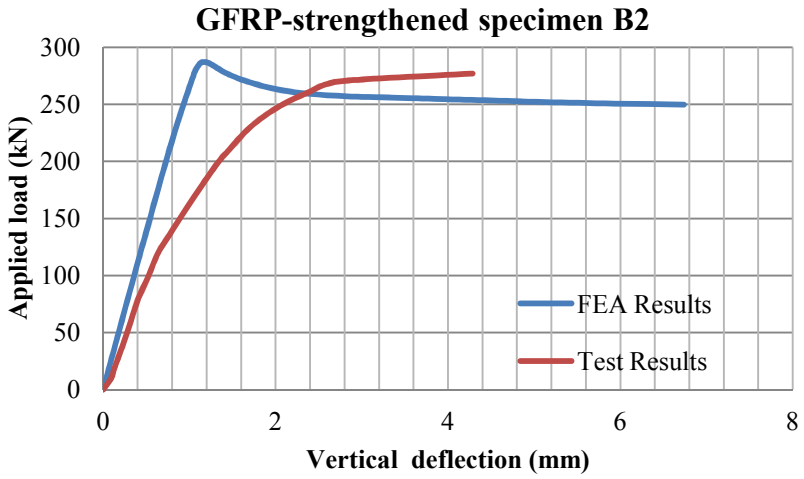

Figure 5.50 Load versus vertical deflection at the underside of loaded stiffeners of B2

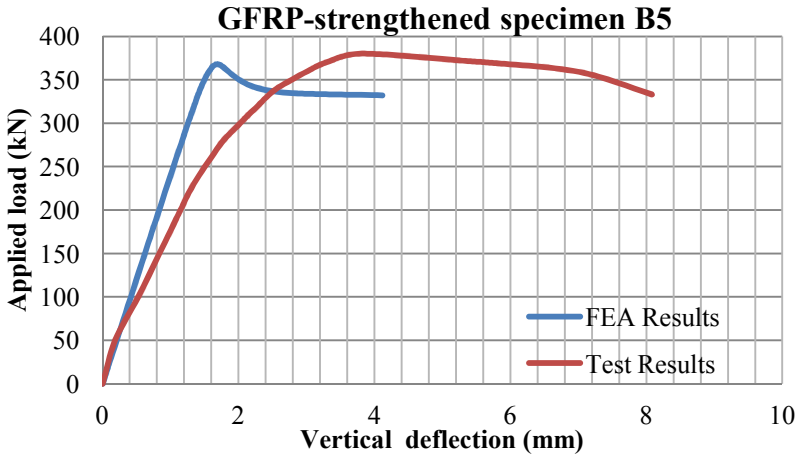

Figure 5.51 Load versus vertical deflection at the underside of loaded stiffeners of B5

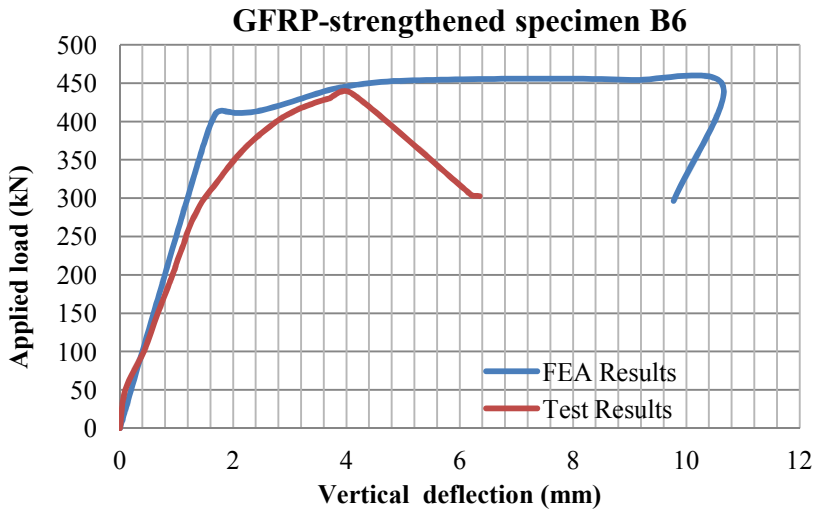

Figure 5.52 Load versus vertical deflection at the underside of loaded stiffeners of B6

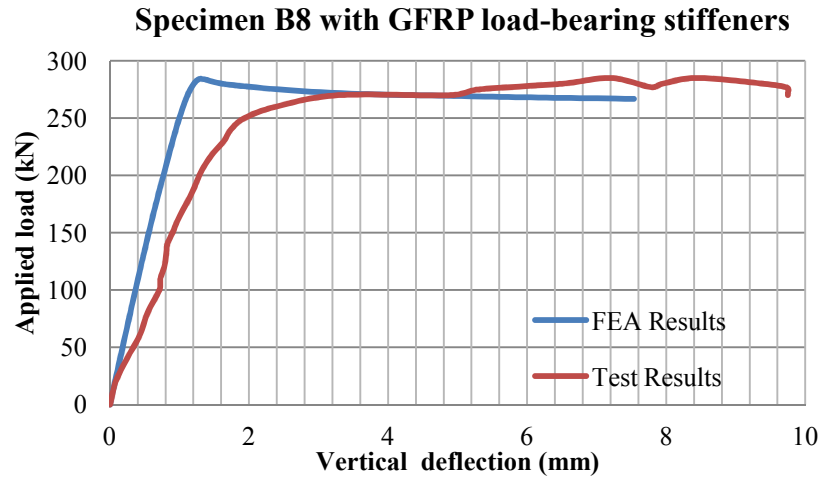

Figure 5.53 Load versus vertical deflection at the underside of loaded stiffeners of B8

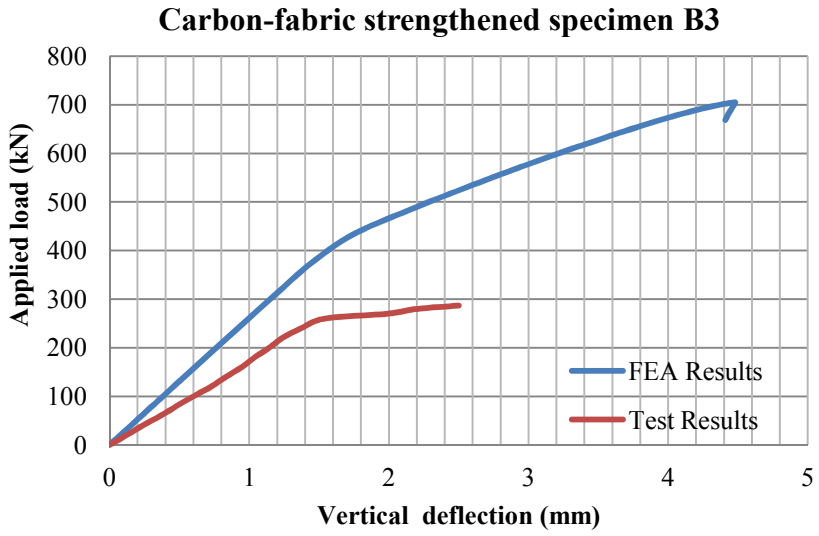

Figure 5.54 Load versus vertical deflection at the underside of loaded stiffeners of B3

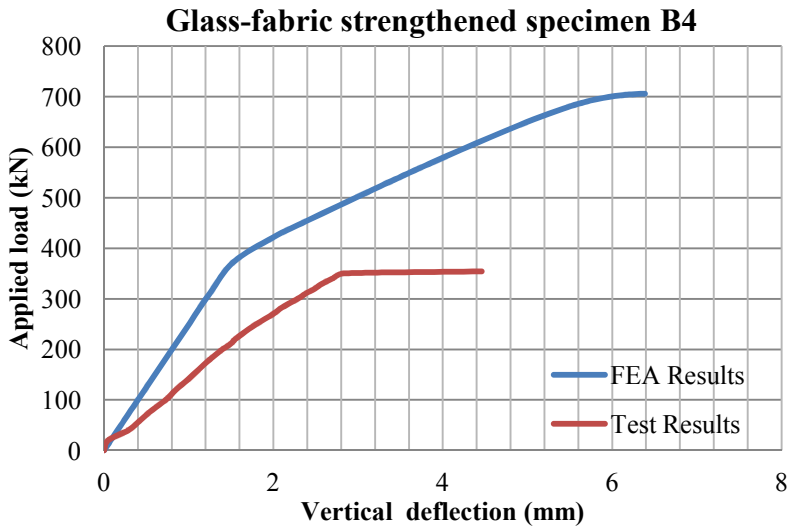

Figure 5.55 Load versus vertical deflection at the underside of loaded stiffeners of B4

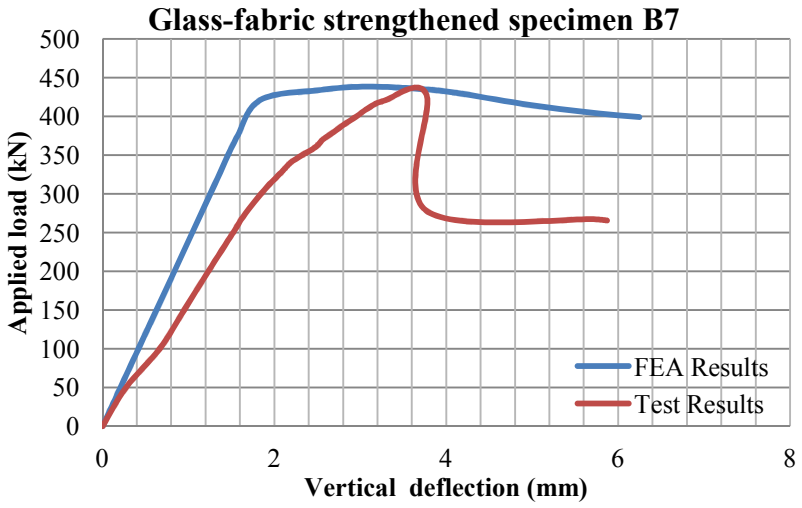

Figure 5.56 Load versus vertical deflection at the underside of loaded stiffeners of B7

5.5 Discussions of results

5.5.1 Results of FE analyses

The results of the FE analyses of the FRP-strengthened models are discussed and compared to those of the un-strengthened models as follows.

1. The ultimate loads of the GFRP pultruded section strengthened models B2, B5 and B6 were increased by approximately 1.22, 1.25 and 1.54 times, compared to those of the respective models of the un-strengthened specimen, B1 or B9.

2. The failure of models B2 and B5 with vertical GFRP stiffeners was ductile and was initiated by the development of two out-of-plane diagonal buckles in the steel web on either side of the stiffener. The failure of the model B6 with a diagonal GFRP

stiffener was relatively brittle and was initiated by buckling of the GFRP stiffener followed by an out-of-plane diagonal buckling of the steel web in the end panel.

3. Using a vertical GFRP stiffener on one side of the web panel in the model B5 strengthened the member in a similar way to using two vertical stiffeners of similar stiffness, one on each side of the panel in the model B2. The ultimate loads of models B2 and B5 were approximately 1.22 and 1.25 times that of the respective models of un-strengthened specimen, B1 or B9. The use of GFRP stiffener on one side of the web is preferable over the use of GFRP stiffeners on both sides of the web because not only the increase in the ultimate load has a small difference, but the use of the stiffener on one side of the web is also easier in practice.

4. The effect of lateral imperfections in the web were studied by carrying out nonlinear FE analyses of the control specimen B1 first with no imperfection and then with the imperfections of 1, 2, 3, 4 and 5 mm. The load-deflection responses with no initial imperfection in the web, as expected, were different from those with the imperfections. The load-deflection responses with the imperfections of 1 to 5 mm were not significantly different from each other. The ultimate load, 242 kN, of the model with the smallest imperfection of 1 mm was approximately 1.08 times greater than that, 223 kN, with the largest imperfection of 5 mm. The effect of these imperfections on the ultimate load compared to that, 2.5 mm, determined according to EC3 was within a range of ± 4%. Since such effect would be even less in the FRP-strengthened specimens, so similar studies were not carried for the other specimens.

5. The ultimate load, 284 kN, of FE model B8 with the load-bearing GFRP stiffeners was approximately 0.96 times that, 295 kN, of the model B9 with the load-bearing steel stiffeners.

6. The ultimate loads of the FRP fabric-strengthened models B3, B4 and B7 were approximately 3.0, 3.0 and 1.49 times those of the respective models of the un-strengthened specimen, B1 or B9.

7. In the two FRP fabric-strengthened models B3 and B4, the out-of-plane diagonal buckling of the web initially started in the second web panel, adjacent to the strengthened panel. The buckling of the web was also observed in the third and fourth web panels when the applied load exceeded 520 kN. In the third fabric-strengthened model B7, the buckling of the web was only observed in the strengthened panel.

8. The distribution of stresses in FE analyses showed that at the ultimate load of specimens, the maximum equivalent stress based on von-Mises yield criterion 'S_E' in the tensile stress field of the web in the yielded web panel, being a combined effect of the major (tensile) and minor (compressive) principal stresses, was approximately equal to the yield strength of the steel in the web.

5.5.2 Results of tests and FE analyses

A comparison of the test and FEA results of specimens is given as follows.

1. The test and FEA results for the ultimate loads, modes of the failure and load-vertical deflection responses for the un-strengthened specimen B1 and GFRP-strengthened specimens B2, B5, B6 and B8 were in good agreement.

2. In the tests, the failure of the un-strengthened specimens B1 was initiated by out-of-plane diagonal buckling of the test web panel. The failure in the three GFRP-specimens B2, B5 and B8 was also initiated by the development of out-of-plane diagonal buckle(s) in the steel web without any breakdown of the steel-GFRP bond, while that in the fourth specimen B6 was initiated by buckling of the GFRP stiffener followed by an out-of-plane diagonal buckling in the steel web without any breakdown of the steel-GFRP bond. Four plastic hinges, two in the top flange and one each in the external steel stiffeners and bottom flange, had developed in all the five test specimens. The same modes of failure of these specimens have been predicted by the FE analyses.

3. The test and FEA load-deflection responses for the fabric-strengthened specimens B3, B4 and B7 were in agreement up to breakdown of the bond between the fabric and the steel that occurred in the tests, but was not modelled in the FE analyses.

4. Specimens B3, B4 and B7 had different modes of the failure in the tests and the FE analyses. In the tests, the failure of all three specimens was initiated by a breakdown of the steel-fabric bond followed by an out-of-plane buckling of the web in the strengthened web panel on the steel side and formation of the four plastic hinges, two in the top flange and one each in the external steel stiffeners and bottom flange. In the FE analyses, the failure of two specimens B3 and B4 was initiated by the out-of-plane buckling of the un-strengthened web in the three web panels except the strengthened panel, yielding of the web in the second and fourth web panels, yielding of the loaded stiffeners near the applied load and the formation of four plastic hinges, two in the top flange and one each in the loaded stiffeners and bottom flange. The failure of the third specimen B7 was initiated by the buckling of web in the strengthened panel followed by the yielding of the strengthened web and formation of four plastic hinges, two in the top flange and one each in the external steel stiffeners and bottom flange.

5. The FE analyses also predicted approximately the correct locations at which plastic hinges developed in the top and bottom flanges and the external steel stiffeners of the six test specimens B1, B2, B5, B6, B7 and B8.

6. The small differences in the test and the FEA load-deflection responses of the specimens, Figure 5.49 to Figure 5.56, have been observed. At the ultimate loads of specimens, the FEA vertical deflections at the underside of the loaded stiffeners are also smaller than those in the tests. This can possibly be attributed to presence of residual stresses, strain hardening of the steel and geometrical imperfections in the webs of the test specimens. In the FE analyses, the residual stresses were not included, while the lateral geometrical imperfections in the web were assumed to be the same in all models. Also in the FEA analyses, the steel and FRP composites were modelled as elastic perfectly plastic materials by ignoring any strain hardening.

5.6 Conclusions

This Chapter has presented finite element, FE, analyses and the results of the two un-strengthened specimens, B1 and B9, and seven FRP-strengthened specimens, B2 to B8, using the LUSAS FE program. The QSL8 element with an 8x8 mesh for the web of each panel has been used in the FE analyses of models of the un-strengthened and GFRP-strengthened specimens. In the FE analyses of models of the FRP fabric-strengthened specimens, the QTS8 element with a mesh 12x12 was used because it could use a merge option for joining and full interaction of two surfaces with the different properties.

The FEA results show that ultimate loads of three models B2, B5 and B6 with the GFRP pultruded section stiffeners were increased by up to 1.54 times, compared to those of the models of un-strengthened specimen, B1 or B9. In the fourth model B8, the load-bearing GFRP stiffeners strengthened the web in a similar way to the load-bearing steel stiffeners in the model B9. The ultimate loads of the FRP fabric-strengthened models B3, B4 and B7 were increased by up to 3.0 times, compared to those of the models of un-strengthened specimen, B1 or B9.

Finally, comparisons of the test and FEA results of specimens have been presented in this Chapter. The ultimate loads, modes of the failure and load-vertical deflection responses of the un-strengthened specimen B1, and the four GFRP-strengthened specimens B2, B5, B6 and B8 in the tests and FE analyses were in good agreement. The test and FEA load-vertical deflection responses of the FRP fabric-strengthened specimens, B3, B4 and B7, were in agreement up to breakdown of the bond between the fabric and the steel. The breakdown of the fabric-steel bond that occurred in the tests of B3, B4 and B7 was not modelled in the FE analyses. The FE analyses also predicted approximately correct locations at which plastic hinges developed in the top and bottom flanges and the external steel stiffeners of the six specimens B1, B2, B5, B6, B7 and B8.

Chapter 6 Design Guidance

6.1 Introduction

This Chapter presents details of design procedures developed for steel plate-girders with the web in web panels strengthened using GFRP pultruded sections as web stiffeners or with layers of FRP composite fabrics. The design procedures, to be described, can be used to estimate the ultimate load of FRP-strengthened plate-girders and determine the suitable cross-sections of GFRP pultruded section stiffeners. The procedures in Eurocode 3, EC3 (ENV 1993-1-5, 2006) have been used to develop the design procedures.

The design procedures have been used to estimate the ultimate loads of FRP-strengthened plate-girders, specimens B2 to B8. The ultimate loads of the un-strengthened specimens B1 and B9 are estimated using the procedure in EC3. The design ultimate loads of specimens B1 to B9 are compared to those in the tests and FE analyses. The failure mechanism of the plate-girders in the tests and obtained from the FE analyses was different from that assumed in the design procedure in EC3. The failure mechanism of the steel plate-girders in EC3 assumes the end posts to remain rigid and plastic hinges to form in the top and bottom flanges only. The plate-girders used in the tests and FE analyses had non-rigid end posts and the hinge also formed in the end posts. The FE analyses of the specimens with the rigid end posts were carried out. The design ultimate loads of specimens are then compared to the FEA ultimate loads for validation. The design procedures for the plate-girders with diagonal GFRP stiffeners and layers of FRP fabric sheets have also been validated using an FE study of thirty-five models. The cross-sections of GFRP stiffeners required for the specimens B2, B5, B6 and B8 are determined using the design procedures and are compared to those used in the test specimens.

The design procedures have also been used to estimate the ultimate loads of specimens OB2 and OB3 tested and analysed by Okeil et al (2009a, 2010 & 2011). The cross-sections of the two vertical GFRP stiffeners of specimen OB2 and a diagonal GFRP stiffener of specimen OB3 are also determined using the design procedures. The ultimate loads of specimens and the cross-sections of the GFRP stiffeners given by the design procedures are compared to those in the tests and FE analyses.

6.2 Background

Guidelines for FRP-strengthening of steel structures were made available in 2004 in a report published by the Construction Industry Research and Information Association (CIRIA), United Kingdom (Cadie et al, 2004). The CIRIA report provided guidance for the use, structural design, implementation, quality control, inspection and future maintenance of FRP-strengthened steel structures. The report focused on strengthening of steel members in order to increase their axial and flexural strengths. No guidance was given in the report for the FRP-strengthening of thin-walled steel members where the failure is initiated due to buckling of the members. The report, however, recommended carrying out more research in the area in order to develop design guidelines.

A review of the available literature described in Chapter 2 has revealed that little attention has been given to the use of FRP composites to strengthen thin-walled members, such as the webs of steel plate-girders. Okeil et al (2009a & 2010) carried out some experimental and analytical work to strengthen the webs of two plate-girders using GFRP pultruded sections. The GFRP pultruded sections were used as intermediate web stiffeners in the one plate-girder and as the diagonal web stiffener in the other plate-girder. The design guidelines for the FRP-strengthened plate-girders, however, were not developed.

Eurocode 3, EC3 (ENV 1993-1-5, 2006) describes simple procedures to estimate the ultimate load of steel plate-girders and to determine the suitable cross-sections of steel web stiffeners. The procedures in EC3 have therefore been used to develop the design procedures for the FRP-strengthened plate-girders. The results of the tests and FE analyses of the un-strengthened and FRP-strengthened plate-girders given in Chapters 3 and 5 have been used to validate the procedures. The failure mechanism of the plate-girders observed in the tests and FE analyses of specimens B1 to B9 was different from that described in EC3. In order to understand the difference, a brief of the two failure mechanisms is given as follows.

6.3 Failure mechanisms of plate-girders

6.3.1 Failure mechanism in Eurocode 3

The failure mechanism of a steel plate-girder subjected to high shear and low bending moment assumed in EC3 is based upon Hoglund's Theory (Hoglund, 1973). The theory assumes that failure occurs when the web plate yields under the joint action of the initial shear buckling stress and the post-buckling tensile membrane stress and plastic hinges that form in the top and bottom flanges, Figure 6.1(b). The end posts or end stiffeners are assumed to be strong enough that no hinge forms in the end posts.

6.3.2 Failure mechanism in tests and FE analyses

The failure mechanism of the un-strengthened and FRP-strengthened plate-girders, specimens B1 to B9, observed in the tests and FE analyses was different to that assumed in EC3. In addition to plastic hinges formed in the flanges, the hinge also formed in the end posts of the test specimens and FE models, Figure 6.1(b).

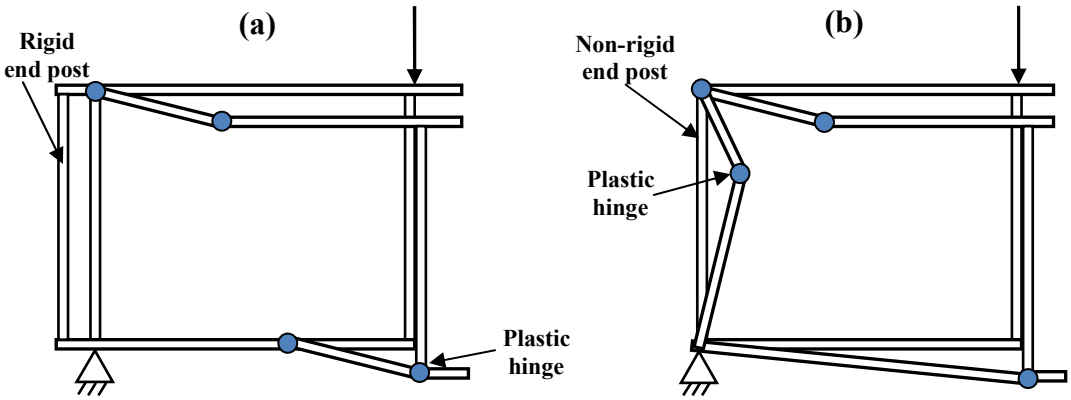

Figure 6.1 Failure mechanism of plate-girder in (a) EC3 (ENV 1993-1-5, 2006) and (b) tests and FE analyses

6.3.3 FE analyses of specimens with rigid end posts

FE analyses of all test specimens, B1 to B8, with non-rigid end posts were carried out and are described in Chapter 5. The test and FEA ultimate loads and modes of the failure of five specimens B1, B2, B5, B6 and B6 were in good agreement. All the test specimens have therefore been modelled with the rigid end posts and FE analyses were carried out. The ultimate loads and modes of the failure obtained from the analyses were compared to those given by the design procedure for validation.

6.4 Ultimate load of un-strengthened plate-girder

To estimate the shear strength/ ultimate load, $V_{b,Rd}$, of a steel plate-girder with bare steel webs in the web panels, the following procedure given in EC3 (ENV 1993-1-5, 2006) has been used.

1. The ultimate load of the web panel is taken as the sum of the ultimate load contributions of the web, $V_{bw,Rd}$, and the flanges, $V_{bf,Rd}$, in the web panel.

$$V_{b,Rd} = V_{bw,Rd} + V_{bf,Rd} \leq \frac{\eta d_w t_w \sigma_{yw}}{\sqrt{3}\gamma_{M1}} \qquad \text{Equation 6.1}$$

2. The contributions of the ultimate loads of the web, $V_{bw,Rd}$, and the flanges, $V_{bf,Rd}$, in the web panel are given by:

$$V_{bw,Rd} = \chi_w d_w t_w \sigma_{yw}/\sqrt{3}\gamma_{M1} \qquad \text{Equation 6.2}$$

$$V_{bf,Rd} = b_f t_f^2 \sigma_{yf}/c\gamma_{M0}\left[1 - \{M_{Ed}/M_{f,Rd}\}^2\right] \qquad \text{Equation 6.3}$$

3. The web slenderness, λ_w, of the web panel and the reduction factor for shear buckling, χ_w, for ultimate load of the web with non-rigid end posts are given by:

$$\lambda_w = 0.76\sqrt{\sigma_{yw}/\tau_{cr}} \qquad \text{Equation 6.4}$$

$$\chi_w = 0.83/\lambda_w \qquad \text{Equation 6.5}$$

4. Assuming the web in the web panel to be simply supported along all the four edges, the critical shear stress, τ_{cr}, of the web is given by:

$$\tau_{cr} = \frac{\pi^2 KE}{12(1-\upsilon^2)}\frac{t_w^2}{d_w^2} \qquad \text{Equation 6.6}$$

5. The distance between the plastic hinges 'c' in the flanges is given by:

$$c = a\left[0.25 + \frac{1.6 b_f t_f^2 \sigma_{yf}}{d_w 2 t_w \sigma_{yw}}\right] \qquad \text{Equation 6.7}$$

Where,

η = co-efficient that includes the increase of shear strength/ ultimate load at smaller web slendernesses (1.2 for S235 to S460 grades of steel)

γ_{M0}, γ_{M1} = partial safety factors for the resistance to instability (taken as unity)

χ_w = reduction factor for the ultimate load of web depending on λ_w

λ_w = web slenderness of shear web panel

τ_{cr} = elastic shear buckling stress

b_f = width of flange

d_w = depth of web plate

t_f = thickness of flange

t_w = thickness of web plate

K = shear buckling co-efficient of the web in a web panel

M_{Ed} = maximum elastic bending moment

$M_{f,Rd}$ = plastic moment of the flanges only ($M_{Ed} < M_{f,Rd}$) = $A_f.h_f.\sigma_{yf}$

The above procedure has been used to estimate the ultimate loads of the un-strengthened plate-girders, specimens B1 and B9. The ultimate load of the end web panel, test panel, of the plate-girder has been estimated. The ultimate load of the steel plate-girder is then taken as 4/3 times that of the test panel, Figure 6.2.

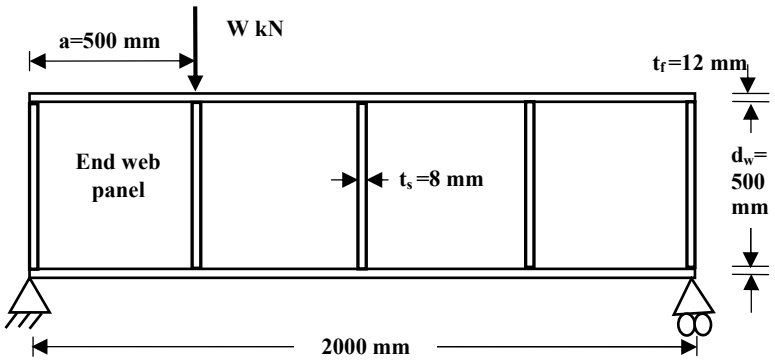

Figure 6.2 Loading and boundary conditions of steel plate-girder, specimen B1

6.5 Design procedures

The following design procedures have been developed for the steel plate-girders with the webs in web panels strengthened using either GFRP pultruded section stiffeners or layers of FRP composite fabrics.

1. Design of plate-girders with intermediate GFRP stiffeners
2. Design of plate-girders with load-bearing GFRP stiffeners
3. Design of plate-girders with diagonal GFRP stiffeners
4. Design of plate-girders with layers of FRP fabric sheets

6.5.1 Assumptions

The following assumptions were made for all design procedures.

1. Perfect bond is assumed between the surfaces of the steel and FRP composites, both pultruded sections and composite fabrics.
2. Breakdown of the bond within the FRP or delamination of the FRP composites does not occur.

6.5.2 Limitations

All design procedures shall be subject to the following limitations.

1. The ultimate load of the un-strengthened or FRP-strengthened plate-girder given by a design procedure or the procedure in EC3 shall not be greater than the ultimate plastic load of the plate-girder given by the upper bound plastic analysis.
2. The width-to-thickness ratio, b_s/t_s, of a steel plate stiffener or of the web of a GFRP pultruded T-section stiffener should be less than '$0.55\sqrt{(E/\sigma_{ys})}$' in order to avoid local buckling of the stiffener (Hoglund, 1973).

6.6 Design of plate-girders with intermediate GFRP stiffeners

6.6.1 Assumptions

1. The intermediate web stiffener does not resist the applied load alone, but works with the web to resist the loads. Therefore in determining and checking the cross-section of either the steel or GFRP stiffener(s), the effective section of the stiffener(s) should be taken as gross area of the cross-section comprising the stiffener(s) and a width of the web plate equal to '$15\varepsilon t$' on both the sides, but not more than the actual dimension available on each side of the stiffener, see clause 9.1.2 of EC3 and Figure 6.3, where $\varepsilon = \sqrt{(235/\sigma_{yw}}$ in MPa).

2. When a GFRP pultruded T-section is used as a vertical web stiffener in the plate-girder, the flange of the T-section is used mainly to bond the GFRP section to the steel surface and contributes a little to its overall stiffness. Thus, it is reasonable to assume that the flange of GFRP T-section does not contribute to its stiffness and can be ignored. Therefore only the web of the GFRP stiffener should be used to determine its second moment of area, I, and the stiffness, EI.

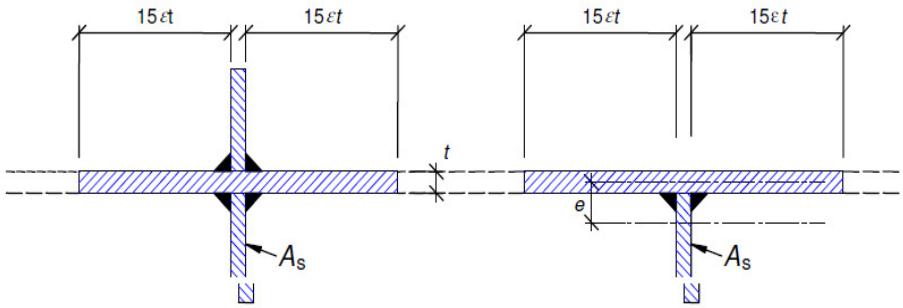

Figure 6.3 Effective cross-section of stiffener (ENV 1993-1-5, 2006)

6.6.2 Cross-section of GFRP stiffener

The cross-section of the intermediate GFRP stiffeners is determined as follows.

1. Minimum second moment of area, $I_{s\ min}$, and the minimum stiffness, $EI_{s\ min}$, required for an effective section of rigid steel intermediate stiffener(s) are determined with help of the following equations contained in clause 9.3.3 of EC3.

   For $a/d_w < \sqrt{2}$ $\quad I_{s\ min} \geq 1.5\ d_w^3\ t_w^3\ /a^2$ Equation 6.8

   For $a/d_w \geq \sqrt{2}$ $\quad I_{s\ min} \geq 0.75\ d_w\ t_w^3$ Equation 6.9

2. The required cross-section of rigid flat steel plate stiffener(s) is determined by satisfying the 'minimum stiffness requirement, $EI_{s\ min}$'.

3. The cross-section of the flat GFRP pultruded section stiffeners is determined by making its stiffness, EI, equal to that of the flat steel stiffener.

4. The stiffness requirement of the GFRP pultruded section is satisfied by making that of the effective section equal to the minimum required stiffness, $EI_{s\ min}$.

6.6.3 Ultimate load

The stiffness, EI, of the intermediate GFRP pultruded section stiffeners is determined and compared to the stiffness requirement, $EI_{s\ min}$, contained in clause 9.3.3 of EC3. If the stiffness requirement of EC3 is satisfied, the GFRP stiffeners are treated as 'rigid'; otherwise as 'non-rigid'. The ultimate load of the web panel with intermediate GFRP stiffeners is determined as the sum of the ultimate load contributions of the web and the flanges using the procedure given in EC3. The value of the shear buckling coefficient, K, and the critical shear stress, τ_{cr}, of the web in the web panel with rigid or non-rigid intermediate GFRP stiffeners are determined as follows.

6.6.3.1 Rigid intermediate stiffeners

Rigid intermediate GFRP stiffeners divide a web panel into two sub-panels. Assuming the webs in each of the two sub-panels to be simply supported along all the four edges, the shear buckling coefficient, K, and the critical shear stress, τ_{cr}, of the web are determined.

6.6.3.2 Non-rigid intermediate stiffeners

The two procedures are given in clause 5.3.3 of EC3 to determine the shear buckling coefficient, K, of a web in the panel with non-rigid intermediate stiffener(s) and are described as follows.

1. The buckling coefficient, K, may be taken as the minimum of the values from the web between any two transverse stiffeners (e.g. a_2 x h_w and a_3 x h_w in Figure 6.4) and that between two rigid stiffeners containing non-rigid transverse stiffeners (e.g. a_4 x h_w in Figure 6.4).

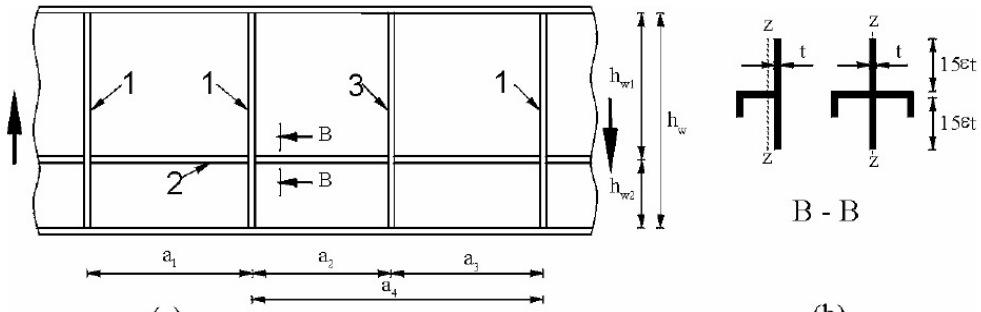

1 Rigid transverse stiffener
2 Longitudinal stiffener
3 Non-rigid transverse stiffener

Figure 6.4 Web with transverse and longitudinal stiffeners (ENV 1993-1-5, 2006)

2. By assuming rigid boundaries for the web in panels bordered by the flanges and rigid transverse stiffeners, the value of 'K' may be obtained from the web buckling analysis of a combination of two adjacent web panels with one flexible (non-rigid) transverse stiffener.

The above procedure has been used to estimate the ultimate loads of specimens B2 and B5 and to determine the cross-sections of the intermediate GFRP stiffeners required for the specimens B2 and B5.

6.7 Design of plate-girders with load-bearing GFRP stiffeners

6.7.1 Assumptions

1. Only the web of the GFRP T-section stiffener is used to determine its minimum stiffness, $EI_{s\,min}$, the same as given in section 6.6.1.

2. In determining and checking the cross-section of either the steel or GFRP stiffeners, the effective section of the stiffeners should be used, see clause 9.1.2 of EC3 and Figure 6.3 given in section 6.6.1.

3. Both the 'strength and stiffness requirements' of the stiffener have to be satisfied for the design of load-bearing GFRP stiffeners. The reason is that the load-bearing transverse stiffeners increase not only the out-of-plane stiffness of the web by resisting the lateral load due to web deflection, but also should not buckle or yield due to the axially applied load.

6.7.2 Cross-section of GFRP stiffener

The cross-section of the load-bearing GFRP stiffeners is determined as follows.

1. The required cross-section of a flat steel plate for the load-bearing transverse stiffeners is determined by satisfying the 'stiffness requirement, $EI_{s\,min}$' in the same way as for the intermediate stiffeners.

2. The 'strength requirement' is satisfied by ensuring that the Euler load and the squash load of the steel stiffeners are greater than the load applied to the stiffeners.

3. The cross-section of the flat GFRP pultruded section is determined by making its stiffness, $EI_{s\,min}$, equal to that of the flat steel stiffeners. The 'strength requirement' is satisfied in the same way for the steel stiffeners.

6.7.3 Ultimate load

If the load-bearing GFRP stiffeners satisfy the 'strength and stiffness requirements' of the design procedure, they are treated as rigid stiffeners. The ultimate load of a plate-girder with the rigid load-bearing GFRP stiffeners is determined as the sum of the ultimate load contributions of the web and the flanges using the procedure in EC3.

The above design procedure has been used to estimate the ultimate load of specimen B8 and to determine the cross-section of load-bearing GFRP stiffeners required for the specimen B8.

6.8 Design of plate-girders with diagonal GFRP stiffeners

Review of the available literature described in Chapter 2 reveals that neither EC3 nor any other design code has a procedure for determining the ultimate load of a plate-girder with the web having a diagonal stiffener. The procedure in EC3 has been used to develop this design procedure together with the FE validation studies described in Chapter 4.

6.8.1 Assumptions

1. The diagonal stiffener acts as a compression strut in a frame comprising the flanges and stiffeners surrounding the web in a web panel.

2. The load applied to the web panel with diagonal stiffener(s) is jointly carried by the frame, web and the diagonal stiffener(s).

3. The failure of the web panel with a diagonal stiffener occurs when the web yields with or without buckling, the diagonal stiffener buckles elastically or squashed plastically and plastic hinges develop in the flanges of the frame.

6.8.2 Cross-section of diagonal stiffener

The cross-section of the diagonal stiffener is determined as follows.

1. The cross-section of diagonal GFRP or steel stiffener has to be such that the Euler load and the squash load of the GFRP stiffener are greater than the additional load required by the strengthened web panel over that of the un-strengthened web panel.

2. However, in case of a GFRP T-section diagonal stiffener, the effects of local buckling of the web of stiffener should be considered. In order to avoid the effects of the local buckling, the width-to-thickness ratio, b_s/t_s, of a steel plate stiffener or of the web of a GFRP pultruded T-section stiffener should be less than '$0.55\sqrt{(E/\sigma_{ys})}$' (Hoglund, 1973).

6.8.3 Ultimate load

The ultimate load of the frame or web panel of a steel plate-girder strengthened with diagonal stiffener(s) is determined as follows.

1. For a frame comprising the flanges and stiffeners or web panel without a web, the ultimate load is given by the ultimate plastic load of the frame and the minimum of the Sinθ times ultimate plastic load and Sinθ times Euler load of the diagonal stiffener, Figure 6.5.

2. For a web panel with a thin web, i.e. $\tau_{cr} < \tau_{yw}$, the ultimate load is given by the ultimate load of the un-strengthened web panel estimated using the procedure in EC3 and the Sinθ times ultimate plastic load of the diagonal stiffener(s).

3. For a web panel with a thick web, i.e $\tau_{cr} \geq \tau_{yw}$, the ultimate load is given by the ultimate plastic load of the un-strengthened web panel and the Sinθ times ultimate plastic load of the diagonal stiffener(s).

Where,

τ_{cr} = shear buckling stress of the un-strengthened web

τ_{yw} = yield stress in shear of the steel web $=\sigma_{yw}/\sqrt{3}$

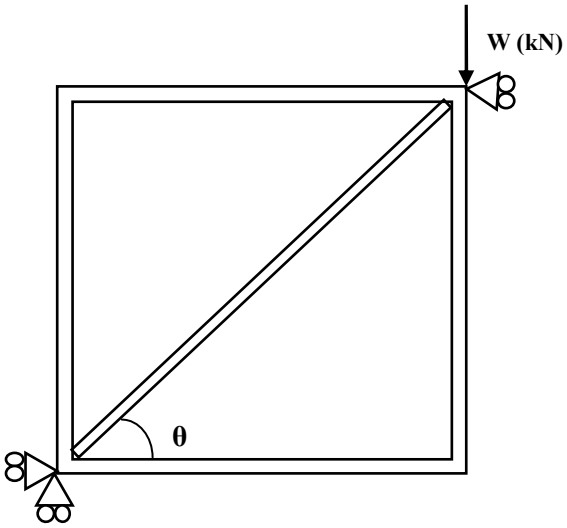

Figure 6.5 Web panel of steel plate-girder with a diagonal stiffener

The procedure has been used to estimate the ultimate load of specimen B6 and to determine the cross-section of diagonal GFRP stiffener required for the specimen B6.

6.9 Design of plate-girders with layers of FRP fabric sheets

Neither EC3 nor any other design code has a procedure for determining the ultimate load of a plate-girder with the web strengthened using layers of the composite fabric sheets. The procedure in EC3 has been used to develop this design procedure together with the FE validation studies described in Chapter 4.

6.9.1 Ultimate load

The ultimate load of the web panel of a steel plate-girder with the web strengthened with layers of the composite fabric is determined as follows.

1. The elastic critical load, V_{cr}, of the fabric-strengthened web in the web panel is determined using the equivalent steel thicknesses based on the flexural stiffness.

2. The ultimate plastic load in shear, V_p, of the fabric-strengthened web in the web panel is given by the ultimate plastic loads in shear of the steel and fabric sections.

3. If $V_{cr} < V_p$ for the fabric-strengthened web, the ultimate load of the fabric-strengthened web panel is determined using the procedure in EC3 using the elastic critical load, V_{cr}, of the equivalent steel web.

4. If $V_{cr} \geq V_p$ for the fabric-strengthened web, the ultimate load of the fabric-strengthened web panel is determined as the ultimate plastic load of the frame and the ultimate plastic load in shear of the steel and fabric sections.

The design procedure has been used to estimate the ultimate loads of the specimens B3, B4 and B7 with four and eight and four layers of the carbon and glass fabric sheets respectively.

6.10 Validation of design procedures using test and FEA results of specimens B1 to B9

6.10.1 Ultimate load of specimens

The design procedures, described above, have been used to estimate the ultimate loads of the FRP-strengthened specimens B2 to B8 and the procedure in EC3 to estimate the ultimate loads of the un-strengthened specimens B1 and B9. For all the specimens, the ultimate load of the end web panel is determined and is then multiplied by 4/3 to give the ultimate load of the plate-girder specimen. Measured values of the material properties of the steel and GFRP are used and the partial safety factors are taken as unity. The test and FEA ultimate loads of specimens B1 to B9 are given in Chapters 3 and 5 respectively. Table 6.1 gives a comparision of the design, test and FEA ultimate loads of all specimens. Details of the design calculations are given in Appendix-D.

Table 6.1 Design, test and FEA ultimate loads of specimens B1 to B9

Specimen No.	Ultimate load (kN)			Ratio of ultimate loads	
	Design	Test	FEA	Design/ test	Design/ FEA
Group G1: Un-strengthened specimens					
B1	265	230	235	1.15	1.13
B9	296	--	295	---	1.00
Group G2: GFRP pultruded section-strengthened specimens					
B2*	*369	277	287	1.33	1.29
B2**	**344	277	287	1.24	1.20
B5	413	380	368	1.09	1.12
B6	482	437	456	1.10	1.06
B8	296	285	284	1.04	1.04
Group G3: FRP fabric-strengthened specimens					
B3	1007	287	705	3.50	1.42
B4	773	354	706	2.18	1.09
B7	461	428	439	1.08	1.05

* GFRP stiffeners assumed to satisfy the 'stiffness requirement' of design procedure

** First buckling mode from eigenvalue analysis used in design procedure

6.10.2 Cross-sections of GFRP stiffeners

Suitable cross-sections of GFRP stiffeners required for specimens B2, B5, B6 and B8 to achieve the test ultimate loads of specimens have been determined using the design procedures. The depth of the web of GFRP stiffeners were determined by keeping thicknesses of the flange and web and width of the flange the same as those in the GFRP stiffeners used in test specimens. Table 6.2 gives a comparison of cross-sections of the GFRP stiffeners used in the test specimens and those required by the design procedures. Details of the design calculations are given in Appendix-E.

Table 6.2 Cross-sections of GFRP stiffeners used in test specimens B2, B5, B6 and B8 and those required by design procedures

Specimen No	**Cross-section of stiffener(s) (flange width x overall depth x web/flange thickness)**		
	Test	**Eurocode 3 (steel stiffeners)**	**Design procedure**
B2	**40 x 25 x 5mm** 2 GFRP stiffeners used	**20 x 4 mm** 2 steel stiffeners required	**40 x 33 x 5 mm** 2 GFRP stiffeners required
Remark: The depth of web of GFRP stiffeners used in the test specimen is smaller than that required to satisfy the 'stiffness requirement' of design procedure			
B5	**80 x 50 x 6.4mm** 1 GFRP stiffener used	**30 x 4 mm** 1 steel stiffener required	**80 x 40 x 6.4 mm** 1 GFRP stiffener required
Remark: The depth of web of GFRP stiffener used in the test specimen is greater than that required to satisfy the 'stiffness requirement' of design procedure			
B6	**80 x 50 x 6.4mm** 1 GFRP stiffener used	---	**80 x 48 x 6.4 mm** 1 GFRP stiffener required
Remark: The depth of web of GFRP stiffener used in the test specimen satisfies the 'design requirement'			
B8	**80 x 50 x 6.4mm** 2 GFRP stiffeners used	**65 x 5 mm** 2 steel stiffeners required	**80 x 40 x 6.4 mm** 2 GFRP stiffeners required
Remark: The depth of web of GFRP stiffeners used in the test specimen is greater than that required to satisfy the 'strength and stiffness requirements' of design procedure			

6.10.3 Discussion of results

The ultimate loads of specimens B1 to B9 given by the design procedures are discussed and compared to those in the tests and FE analyses as follows.

1. The design ultimate load, 265 kN, of the un-strengthened specimen B1 is 1.15 and 1.13 times greater than the test and FEA ultimate loads of 230 and 235 kN respectively.

2. The design ultimate load, 296 kN, of FE model of the un-strengthened specimen B9 is approximately equal to the FEA ultimate load of 295 kN.

3. The design ultimate load of specimen B2 has been determined using two approaches. In the first approach assuming the GFRP stiffeners to be 'rigid', the design ultimate load, 369 kN, is 1.33 and 1.29 times greater than the test and FEA ultimate loads of 277 and 287 kN respectively. In the second approach assuming the GFRP stiffeners to be 'non-rigid', the design ultimate load is 344 kN. This is also 1.24 and 1.20 times greater than the test and FEA ultimate loads.

4. The design ultimate load, 413 kN, of specimen B5 strengthened using a vertical GFRP intermediate stiffener in the end web panel is also 1.09 and 1.12 times greater than the test and FEA ultimate loads of 380 and 368 kN respectively.

5. The design ultimate load, 296 kN, of specimen B8 with the load-bearing GFRP web stiffeners is 1.04 times greater than the test and FEA ultimate loads of 285 and 284 kN respectively.

6. The design ultimate load, 482 kN, of specimen B6 with a diagonal GFRP stiffener is 1.10 and 1.06 times greater than the test and FEA ultimate loads of 437 and 456 kN respectively.

7. The design ultimate loads, 1007, 773 and 461 kN, of the FRP fabric-strengthened specimens B3, B4 and B7 are 1.42, 1.09 and 1.05 times greater than the FEA ultimate loads of 705, 706 and 439 kN respectively.

8. The design ultimate loads of specimens B3 and B4 are significantly greater, 3.50 and 2.18 times, than the test ultimate loads of 287 and 354 kN respectively. This is because the breakdown of the steel-fabric bond that occurred in the tests of these specimens was not included in the design procedure or modelled in the FE analyses.

9. Despite a bond breakdown in the test, the design ultimate load, 461 kN, of the fabric-strengthened specimen B7 is 1.08 times the test ultimate load, 428 kN. It appears that breakdown of the bond in the test occurred at a load which was close to its ultimate strength.

10. The depth of web of the intermediate GFRP stiffeners used in test specimen B2 is smaller and that of the specimen B5 is greater than those required to satisfy the design requirement.

11. The depth of web of the diagonal GFRP stiffener used in test specimen B6 is greater than that required to satisfy the design requirement.

12. The depth of web of each of the load-bearing GFRP pultruded section stiffeners of the test specimen B8 is greater than that required to satisfy the design requirement.

6.11 Validation of design procedures using FE analyses of specimens B1 to B9 with rigid end posts

The design ultimate loads of un-strengthened specimen B1 and GFRP-strengthened specimens B2, B5, B6 and B8 are 1.04 to 1.24 times greater than the test and FEA ultimate loads and those of the fabric-strengthened specimens B3, B4 and B7 are 1.05 to 1.42 times greater than the FEA ultimate loads of specimens with non-rigid end posts, Table 6.1. Since the measured values of the properties of the steel and FRP were used, so the design ultimate loads of specimens should be less than or approximately equal to the test and FEA ultimate loads. It has already been discussed that the design procedures were based on those in EC3 in which the end posts of plate-girder are assumed to be remain rigid and plastic hinges to form in the top and bottom flanges only, while in both the tests and FE analyses of the test specimens, the hinges formed in the flanges and the end posts.

6.11.1 FE modelling of specimens with rigid end posts

In order to validate the design procedures, the modes of failure of the test specimens B1 to B9 in the FE analyses need to be same as the models used in the design procedure. It has also been discussed in Chapter 5 that the test and FEA ultimate loads as well as modes of the failure of specimens B1, B2, B5, B6 and B8 were in good agreement. Therefore, models of all test specimens were built with the rigid end posts. Details of the models are as follows.

1. Models of the S1 and S2 plate-girders used for test specimens B1 to B9 had double stiffeners, each 12 mm thick, at both ends of the plate-girders, Figure 6.6. In the models of the fabric-strengthened plate-girders, specimens B3, B4 and B7, the thickness of the load-bearing steel stiffeners was also increased to 12 mm to avoid development of the plastic hinges in the stiffeners and thickness of the webs in the un-strengthened web panels was increased to 6 mm to obtain the failure in the fabric-strengthened panels.

2. The remaining dimensions of the S1 and S2 plate-girders, the properties of the steel and FRP composites and the loading and boundary conditions were the same as in test specimens.

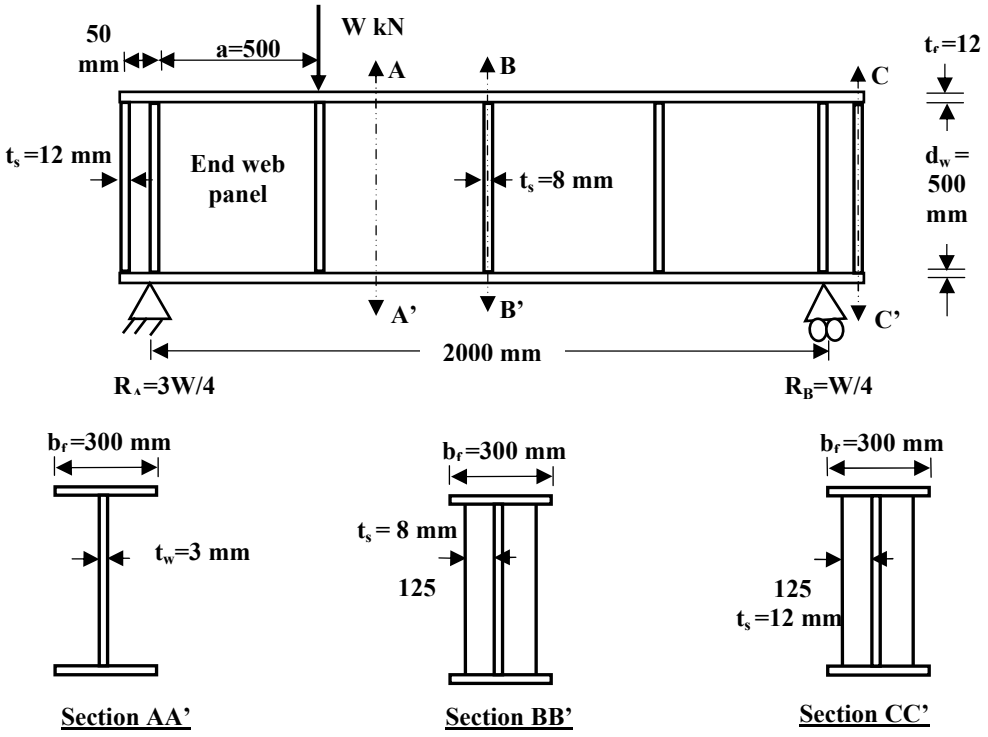

Figure 6.6 Dimensions of S1 and S2 steel plate-girders with rigid end stiffeners (posts)

3. Nonlinear FE analyses of all the models with rigid end posts by modelling both material and geometric nonlinearities were carried out in the same way as those for the specimens with non-rigid end posts described in Chapter 5.

6.11.2 Ultimate loads of specimens

Table 6.3 gives the design ultimate loads of specimens B1 to B9 and FEA ultimate loads the speciemns with rigid and non-rigid end posts.

Table 6.3 Design and FEA ultimate loads of B1 to B9 with rigid and non-rigid end posts

Specimen No.	Ultimate load (kN)			Ratio of ultimate loads	
	Design	FEA 1 (Non-rigid end posts)	FEA 2 (Rigid end posts)	Design/ FEA 1	Design/ FEA 2
Group G1: Un-strengthened specimens					
B1	265	235	269	1.13	0.99
B9	296	295	323	1.00	0.92
Group G2: GFRP pultruded section-strengthened specimens					
B2	344	287	331	1.20	1.04
B5	413	368	394	1.12	1.05
B6	482	456	507	1.06	0.95
B8	296	284	295	1.04	1.00
Group G3: FRP fabric-strengthened specimens					
B3	1007	705	934	1.42	1.08
B4	773	706	758	1.09	1.02
B7	461	439	470	1.05	0.98

6.11.3 Modes of failure

Figure 6.7(a) to (i) show the modes of failure of specimens, B1 to B9, with rigid end posts obtained from FE analyses.

6.11.4 Load-deflection responses

Figure 6.8(a) to (i) show the load versus vertical deflection at the underside of loaded stiffeners of specimens, B1 to B9, with rigid and non-rigid end posts obtained from FE analyses.

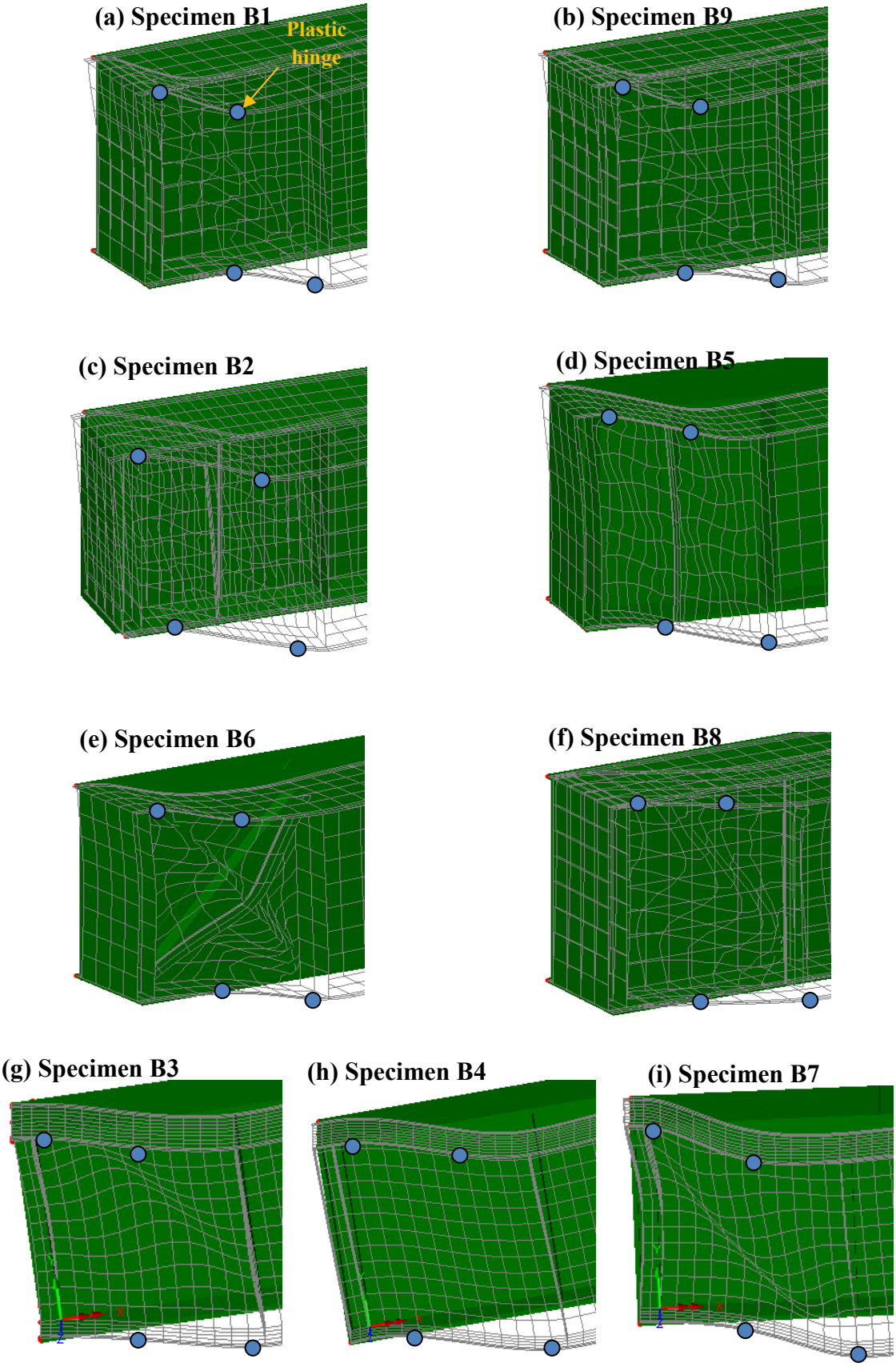

Figure 6.7 FEA modes of failure of specimens, B1 to B9, with rigid end posts

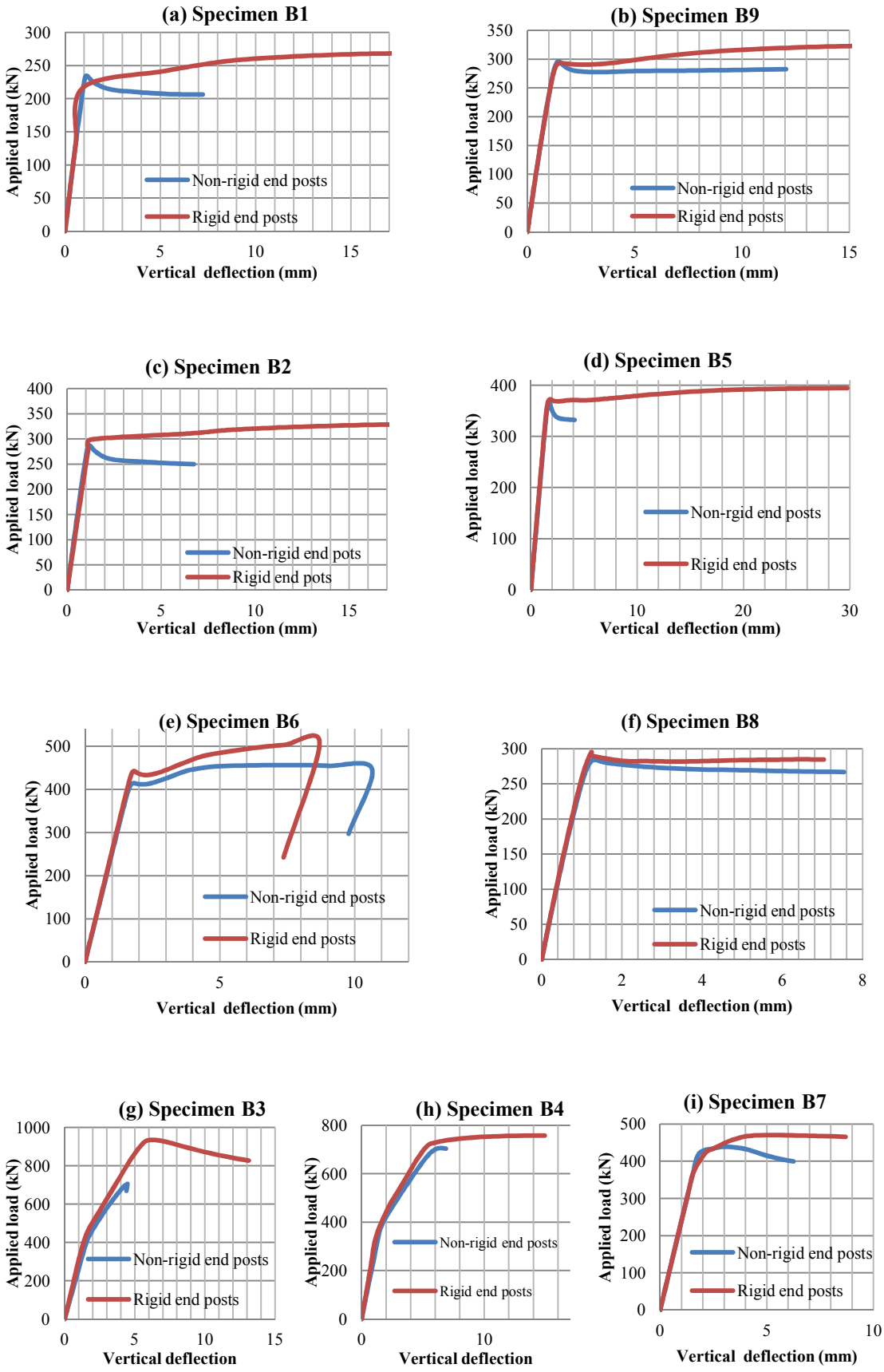

Figure 6.8 Load-vertical deflection responses of specimens, B1 to B9, with rigid and non-rigid end posts

6.11.5 Discussion of results

1. The design ultimate loads of all nine specimens B1 to B9, Table 6.3, are in good agreement with the FEA ultimate loads of the specimens with rigid end posts.

2. It can be seen from Figure 6.7(a) to (i) that the plastic hinges causing the failure of specimens are formed in the top and bottom flanges with no hinges in the stiffeners of end posts. The failure mechanism of the specimens is the same as that assumed in the EC3.

3. The load-vertical deflection responses of specimens, B1 to B9, with rigid and non-rigid end posts show that the elastic response of the specimens with rigid and non-rigid end posts is same, but the platsic response of the speciemns is different due to the addition of rigid end posts.

4. It can be seen from Figure 6.8(a) to (i) that the ultimate load of a plate-girder with non-rigid end posts is incresaed by by providing the rigid end posts.

5. The test ultimate loads of the fabric-strengthened specimens B3, B4 and B7 were increased by 1.25, 1.54 and 1.45 times before a breakdown of the steel-fabric bond, compared to those of the respective un-strengthened specimen, B1 or B9. The least increase in the ultimate load of specimen obtained is 25% for the test specimen B3. Since a breakdown of the bond is not included in the design procedure for fabric-strengthened plate-girders, so for the use in practice the procedure should be limited to a safe increase in the ultimate load, say up to 20%, compared to the un-strengthened plate-girder.

6.12 Validation of design procedures using test and FEA results of specimens OB1 to OB3

Details of the tests and FE analyses of three plate-girders, specimens OB1, OB2 and OB3, carried out by Okeil et al (2009a, 2010 & 2011) have been given in Chapter 2. Control specimen OB1 was a steel plate-girder with an un-strengthened end web panel. The end web panel of the specimen OB2 was strengthened using two vertical GFRP stiffeners one on each side of the web and that of OB3 strengthened using a diagonal GFRP stiffener on one side of the web.

6.12.1 Ultimate loads of specimens

The design procedures, described earlier, have been used to estimate the ultimate loads of GFRP-strengthened specimens OB2 and OB3. Since the web of the diagonal GFRP T-section stiffener used in test specimen OB3 was very slender, so a depth of the web of the GFRP stiffener equal to 10 times of its thickness has been considered to estimate the design ultimate load. The ultimate load of the un-strengthened specimen OB1 is given by the procedure in EC3.

Table 6.4 gives a comparison of the design, test and FEA ultimate loads of specimens OB1, OB2 and OB3. Details of the design calculations are given in Appendix-F.

Table 6.4 Design, test and FEA ultimate loads of specimens OB1, OB2 and OB3 (Okeil et al, 2009a, 2010 & 2011)

Specimen No.	**Ultimate load (kN)**			**Ratio of ultimate loads**	
	Design	**Test**	**FEA**	**Design/ test**	**Design/ FEA**
OB1	304	278	276	1.09	1.10
OB2	429	389	361	1.10	1.19
OB3	520	435	427	1.20	1.22

6.12.2 Cross-sections of GFRP stiffeners

Suitable cross-sections of GFRP stiffener(s) required for specimens OB2 and OB3 to achieve the test ultimate loads of specimens have been determined using the design procedures. The depth of the web of GFRP stiffeners were determined by assuming thicknesses of the flange and web as 8 mm. Table 6.5 gives a comparison of cross-sections of the GFRP stiffeners used in the test specimens and those required by the design procedures. Details of the calculations are given in Appendix-G.

Table 6.5 Cross-sections of GFRP stiffeners used in test specimens OB2 and OB3 and those required by design procedures (Okeil et al, 2009 & 2010)

Specimen No	**Cross-section of stiffener(s) (flange width x overall depth x web/flange thickness)**		
	Test	**Eurocode 3**	**Design procedure**
OB2	**140 x 128 x 9.5 mm** 2 GFRP stiffeners used	**20 x 5 mm** 2 steel stiffeners required	**60 x 40 x 8 mm** 2 GFRP stiffeners required
Remark: The depth and thickness of the web of GFRP stiffeners used in the test specimen are greater than those required to satisfy the 'stiffness requirement' of the design procedure			
OB3	**140 x 128 x 9.5 mm** 1 GFRP stiffener used	---	**80 x 60 x 9 mm** 1 GFRP stiffener required
Remark: The depth and thickness of the web of GFRP stiffener in the test specimen are greater than those required to satisfy the 'design requirement'			

6.12.3 FE analyses of specimens with rigid end posts

The design ultimate loads of specimens OB1, OB2 and OB3 are 1.09 to 1.22 times greater than the test and FEA ultimate loads because the modes of failure of the plate-girders in the tests and FE analyses were different from that assumed in the design procedures. In order to validate the design procedures, the modes of failure of the test specimens in the FE analyses need to be same as the models used in the design procedure. The models of test specimens OB1, OB2 and OB3 were therefore built with rigid end posts by providing double stiffeners, each 13 mm thick, at both ends of the plate-girders. The remaining dimensions of the plate-girders, the properties of the steel and GFRP and the loading and boundary conditions were the same as in test specimens. Nonlinear FE analyses of all the models with rigid end posts were carried out in the same way as those for the specimens with non-rigid end posts as described in Chapter 4.

6.12.4 Ultimate loads of specimens

Table 6.6 gives a comparision of the ultimate loads of specimens given by the design procedures and those obtained from FE analyses for the speciemns with rigid and non-rigid end posts.

Table 6.6 Design and FEA ultimate loads of OB1 to OB3 with rigid and non-rigid end posts

Specimen No.	Ultimate load (kN)			Ratio of ultimate loads	
	Design	FEA 1 (Rigid end posts)	FEA 2 (Non-rigid end posts)	Design/ FEA 1	Design/ FEA 2
OB1	304	276	310	1.10	0.98
OB2	429	361	386	1.19	1.11
OB3	520	427	486	1.22	1.07

6.12.5 Modes of failure

Figure 6.9(a) to (c) show the modes of the failure of specimens, OB1 to OB3, with rigid end posts obtained from the FE analyses.

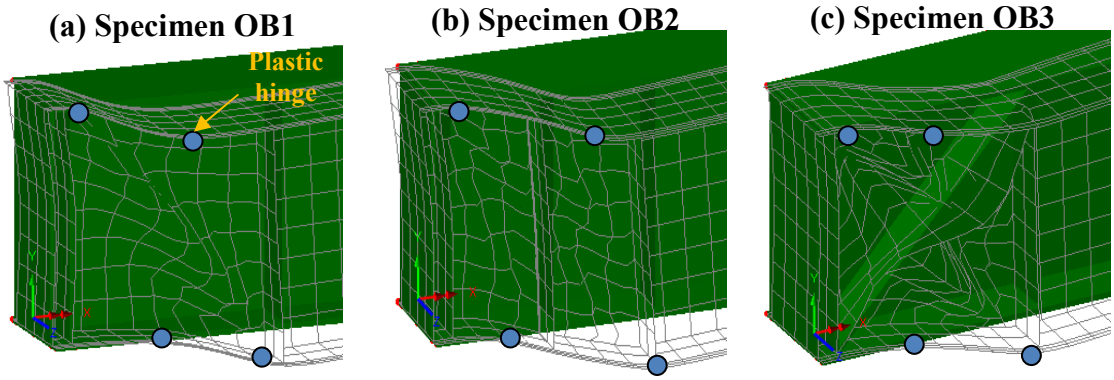

Figure 6.9 FEA modes of failure of specimens, OB1 to OB3, with rigid end posts

6.12.6 Load-deflection responses

Figure 6.10(a) to (c) show the load versus vertical deflection at the underside of loaded stiffeners of specimens, OB1 to OB3, with rigid and non-rigid end posts obtained from the FE analyses.

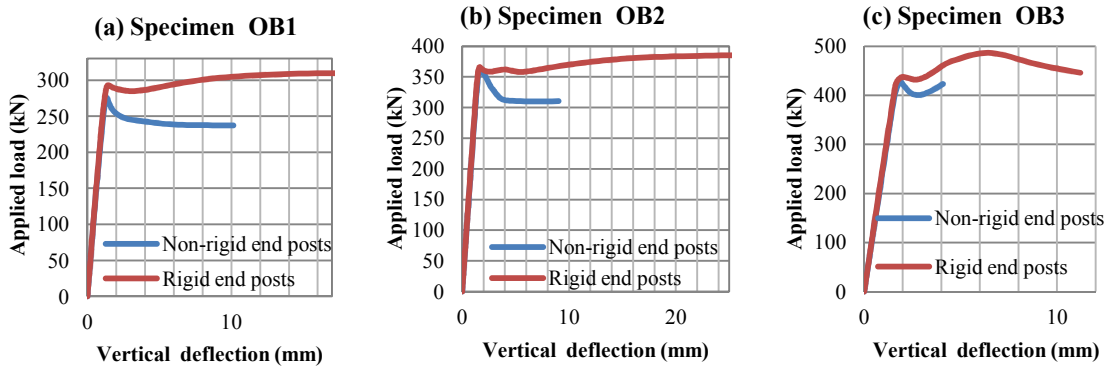

Figure 6.10 Load-deflection responses of OB1 to OB3 with rigid and non-rigid end posts

6.12.7 Discussion of results

1. The design ultimate load, 304 kN, of the un-strengthened specimen OB1 is 1.09 and 1.10 times greater than the test and FE ultimate loads, 278 and 276 kN respectively, of the specimen with non-rigid end posts. The design ultimate load is, however, in good agreement with the FEA ultimate load, 310 kN, of the specimen OB1 with rigid end posts.

2. The design ultimate load, 428 kN, of specimen OB2 is 1.10 and 1.19 times greater than the test and FEA ultimate loads, 389 and 361 kN respectively, of the specimen with non-rigid end posts. The design ultimate load is still 1.11 times the FEA ultimate load, 386 kN, of the specimen OB2 with rigid end posts. The reason of this may be that the GFRP stiffeners were treated as 'rigid' because they satisfied the stiffness requirement of the design procedure. The GFRP stiffeners, however, buckled together with the web in the FE analyses.

3. The design ultimate load, 520 kN, of specimen OB3 is 1.20 and 1.22 times greater than the test and FEA ultimate loads, 435 and 427 kN respectively, of the specimen with non- rigid end posts. The design ultimate is still greater, 1.07 times, than the FEA ultimate load, 486 kN, of the specimen OB3 with the rigid end posts because the local buckling of the web of the diagonal GFRP stiffener was observed in the FE analysis, Figure 6.9(c), but was ignored in the design procedure.

4. In models of the specimens OB1, OB2 and OB3 with rigid end posts, the plastic hinges causing the failure are formed in the top and bottom flanges with no hinges forming in the end posts. The failure mechanism of the specimens is the same as that assumed in the EC3.

5. The load-vertical deflection responses of specimens, Figure 6.10(a) to (c), with rigid and non-rigid end posts show that the elastic response of the specimens with rigid and non-rigid end posts is same, but the platsic response of the speciemns is different due to the addition of rigid end posts.

6. The depths and thicknesses of the webs of intermediate and diagonal GFRP stiffeners of test specimens OB2 and OB3 are greater than those required to satisfy the design requirements.

6.13 Parametric studies for validation of design procedures

As described earlier, the design procedures for determining the ultimate load of a plate-girder with the web strengthened using (a) diagonal GFRP stiffeners and (b) layers of the composite fabric sheets have been developed using the procedure in EC3 together with the FE validation studies described in Chapter 4. Only the ultimate load of one test specimen B6 with a diagonal GFRP stiffener was available to validate the design procedure of plate-girder with diagonal stiffeners. The design procedure of plate-girder with layers of fabric sheets could only be validated against the FEA results of specimens B3, B4 and B7 because of a breakdown of the steel-fabric bond in the tests. The two design procedures have therefore further been validated using the FE studies of thirty-five models. The geometry and the loading and the boundary conditions of the web panel used in the FE studies are shown in Figure 6.11. The properties of the steel, GFRP and the carbon and glass fabrics used in the FE studies of the models are given in Table 6.7.

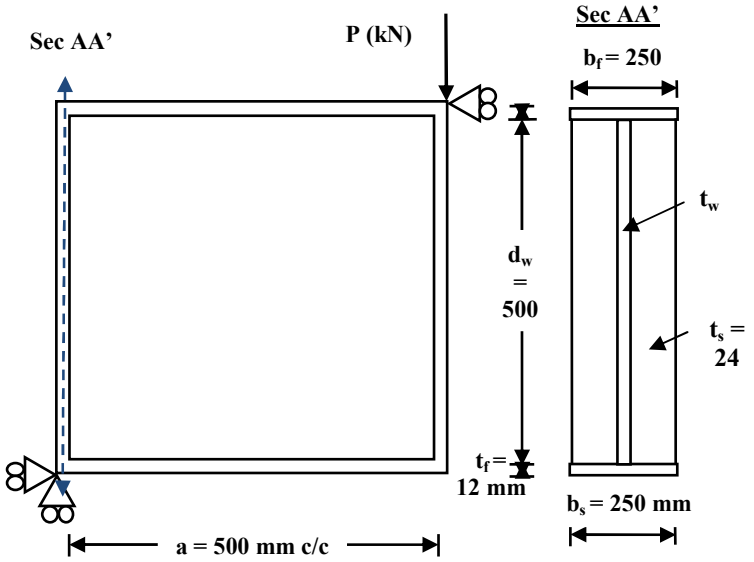

Figure 6.11 Dimensions, loading and boundary conditions of steel web panel (not to scale)

Table 6.7 Properties of steel, GFRP and glass fabric

Property	Steel	GFRP	Carbon fabric	Glass fabric
Modulus of elasticity, E (GPa)	205	36	36	13
Yield strength, σ_y (MPa)	300	300	274	104
Shear modulus, G (GPa)	79	15.7	3.3	2.0
Poisson's Ratio, υ	0.3	0.15	0.32	0.27

6.13.1 Parametric studies for design procedure of plate-girder with diagonal stiffeners

Two parametric studies each comprising nonlinear FE analyses of the steel web panels with diagonal stiffeners were carried out, details of which are given in Chapter 4. The design procedure was used to estimate ultimate loads of the models.

6.13.1.1 First study

The first study comprised the FE analyses of sixteen models of the web panel with diagonal stiffeners on both sides of the web. Eight models had diagonal steel stiffeners and the remaining eight had diagonal GFRP stiffeners. Both the steel and GFRP stiffeners were of same cross-sections, each 25 mm wide by 3 mm thick. Two of the models had no web, while the web thickness was varied from 0.5 to 6 mm in the remaining fourteen models. The design and FEA ultimate loads of the models are given in Table 6.8. Details of the calculations are given in Appendix-H.

Table 6.8 FEA and design ultimate loads of models with diagonal stiffeners (First study)

Thickness of web t_w (mm)	**FEA ultimate load**		***Design ultimate load (kN)**	**Design to FEA ultimate loads**	
	Steel stiffeners	GFRP stiffeners	Steel & GFRP stiffeners	Steel stiffeners	GFRP stiffeners
0	25.3	24.8	22.1	0.87	0.89
0.5	67.2	64.9	65.8	0.98	1.01
1.0	100.3	93.4	90.8	0.91	0.97
2.0	163.4	160.3	148	0.91	0.92
3.0	265.7	237.4	225	0.85	0.95
4.0	365	341.2	325	0.89	0.95
5.0	455	433.7	449	0.99	1.03
6.0	544	523.8	572	1.05	1.09

*Design ultimate loads of models with steel and GFRP stiffeners are same because of the same yield strength of the steel and GFRP

6.13.1.2 Second study

In the second study, the FE analyses of eleven models of the web panel with diagonal stiffeners on the one or both sides of the web were carried out. The models varied both in the web thicknesses and the cross-section of the diagonal stiffeners. The design and FEA ultimate loads of the models are given in Table 6.9, details given in Appendix-H.

Table 6.9 FEA and design ultimate loads of models with diagonal stiffeners (Second study)

Diagonal steel stiffener			Web thickness t_w (mm)	Ultimate load (kN)		
Depth d_s (mm)	Thickness t_s (mm)	One or both sides		Design	FEA	Design to FEA
100	12	Both	0.5	543	534	1.02
100	12	Both	1.0	568	559	1.02
100	12	Both	2.0	625	636	0.98
100	12	Both	3.0	702	746	0.94
100	3	Both	3.0	320	311	1.03
25	12	Both	3.0	320	360	0.89
25	3	Both	3.0	225	264	0.85
100	12	One	3.0	448	485	0.92
100	3	One	3.0	257	281	0.91
25	12	One	3.0	257	282	0.91
25	3	One	3.0	209	235	0.89

6.13.2 Parametric studies for design procedure of plate-girder with layers of composite fabric sheets

Two parametric studies each comprising nonlinear FE analyses of the fabric-strengthened web panels were carried out, details of which are given in Chapter 4. The design procedure was used to estimate ultimate loads of the models.

6.13.2.1 First study

The first study comprised the FE analyses of five models of the glass fabric-strengthened web panel. 3 mm thick steel web of the models was strengthened using 3, 6, 9, 12 and 15 mm thick layers of the glass fabric, respectively, on one side of the web. The thickness of the fabric-strengthened section of the each model was converted to equivalent steel thickness based on the flexural stiffness and the ultimate load was estimated using the design procedure. The design and FEA ultimate loads of the models are given in Table 6.10. Details of the calculations are given in Appendix-H.

Table 6.10 Design and FEA ultimate loads of glass fabric-strengthened models

Web thickness (mm)			Ultimate load (kN)		
Steel	**Glass fabric**	***Equivalent**	**Design**	**FEA**	**Design to FEA**
3	3	3.63	273.4	248.4	1.10
3	6	4.96	419.5	393.3	1.07
3	9	6.53	551.6	519.9	1.06
3	12	8.16	641.7	608.2	1.06
3	15	9.78	731.7	688.7	1.06

* Equivalent steel thickness based on flexural stiffness

6.13.2.2 Second study

As mentioned earlier, the design procedure for fabric-strengthened plate-girders, for the use in practice, has been limited to obtain an increase of 20% in the ultimate loads of an un-strengthened plate-girder. In this parametric study, the thicknesses of the carbon and glass fabric sheets required to obtain at least 20% increase in the design ultimate loads of specimens B3, B4 and B7 were determined using the design procedure. Using the determined thicknesses of the fabric layers, the FE analyses of the specimens with rigid end posts were carried out and the ultimate loads were obtained. The design and FEA ultimate loads of the specimens are given in Table 6.11. Details of the calculations are given in Appendix-H.

Table 6.11 Design and FEA ultimate loads of specimens B3, B4 and B7

Specimen No. & fabric thickness	**No. of fabric layers required**	**Design ultimate load (kN)**		**Ultimate load (kN)**		
		Control specimen	**Strengthened to control**	**Design**	**FEA**	**Design to FEA**
B3 (1.5 mm)	1 layer of carbon fabric	265 (B1)	1.46	389	372	1.05
B4 (2.5 mm)	2 layers of glass fabric	265 (B1)	1.37	364	346	1.05
B7 (2.5 mm)	2 layers of glass fabric	296 (B9)	1.31	389	401	0.97

6.13.3 Discussion of results of parametric studies

1. The design ultimate loads of the sixteen models with the diagonal steel and GFRP stiffeners are in reasonable agreement with the FEA ultimate loads of models. The design loads for the model without a web panel is conservative and that of the model with the thickest web is un-conservative. This is because the diagonal stiffener in the frame without a web undergoes buckling and contributes a little to the ultimate load. In case of a very thick web, the role of geometric nonlinearity is almost negligible and the diagonal stiffener also contributes a little to the ultimate load because of a smaller cross-section compared to that of the web.

2. The design ultimate loads of the eleven models with the diagonal steel stiffeners are also in reasonable agreement with the FEA ultimate loads of models.

3. The increase in the ultimate load of the model using the diagonal stiffeners, 25 mm wide by 12 mm thick, on both sides of the 3 mm thick web is approximately twice that using the stiffener of the same cross-section on one side of the web.

4. The 100 mm wide by 3 mm thick and 25 mm wide by 12 mm thick diagonal stiffeners have the same areas of cross-section. The design ultimate loads of the models using the two cross-sections of diagonal stiffener on both side of the web are same, while the FEA ultimate loads of the two models differ by 15%. This is because that the effects of local buckling of the stiffener, 100 mm wide by 3 mm thick, have been accounted in the FE analyses, but are ignored in the design procedure.

5. The design ultimate loads of the five glass fabric-strengthened models are in agreement with the FEA ultimate loads of models. The design ultimate loads, however, are un-conservative in all cases. The reason of this that the nonlinear geometric effects are accounted in the FE analyses even when the elastic critical load, V_{cr}, of the fabric-strengthened web is equal to or greater than the ultimate plastic load in shear, V_p.

6. The design ultimate loads of specimens B3, B4 and B7 with the rigid end posts using one layer of the carbon fabric and two layers each of the glass fabric, respectively, are in good agreement.

6.14 Conclusions

This Chapter has presented design procedures for the estimation of the ultimate load of FRP-strengthened plate-girders and for the design of suitable cross-sections of GFRP pultruded sections as intermediate, load-bearing and diagonal web stiffeners. The design procedures have been used to estimate the ultimate loads of FRP-strengthened plate-girders, specimens B2 to B8, and to determine suitable cross-sections of the GFRP stiffeners of specimens B2, B5, B6 and B8. The procedure in EC3 has been used to estimate the ultimate loads of the un-strengthened plate-girders, specimens B1 and B9.

The design ultimate loads of the un-strengthened and GFRP-strengthened specimens B1, B2, B5, B6, B8 and B9 were greater, up to 1.24 times, than those in the tests and the FE analyses of the test specimens. The design ultimate loads of the FRP fabric-strengthened specimens B3, B4 and B7 were significantly greater, up to 3.50 times, than the test ultimate loads because in the tests a breakdown of the steel-fabric bond occurred which was not modelled in the design procedure. The failure mechanism of the plate-girders in the tests and FE analyses was different from that assumed in EC3. The design procedures based on those in EC3 assumed plastic hinges to occur in the top and bottom flanges only, while in the tests and FE analyses, the hinges were also formed in the end posts. The design ultimate loads and modes of the failure of the specimens were, however, in good agreement with those obtained from the FE analyses of specimens with the rigid end posts. The depths of the webs of GFRP stiffeners were determined by keeping thicknesses of the flange and web and width of the flange the same as those in the GFRP stiffeners used in test specimens. The depths of the webs of GFRP stiffeners used in test specimens B5, B6 and B8 have been found greater than those required by the design procedures. The depth of the web of GFRP stiffeners used in test specimen B2 was, however, smaller than the design requirement.

Compared to the un-strengthened specimen, the least increase in the ultimate loads of the fabric-strengthened specimens obtained was 25% for test specimen B3. The design procedure for the fabric-strengthened plate-girders, for the use in practice, has therefore been limited up to an increase of 20% in the ultimate load. It has also been found that one layer of the carbon fabric in specimen B3 and two layers each of the glass fabric in specimens B4 and B7 with rigid end posts, respectively, were sufficient

to obtain the least increase of 20% in the design ultimate loads compared to those of the respective un-strengthened specimens, B1 and B9.

A further validation of the design procedures for the plate-girders with diagonal GFRP stiffeners and layers of FRP fabric sheets has been carried out using FE analyses of thirty-five models. The design and FEA ultimate loads of all models were found be in reasonable agreement. The design procedures have also been validated against the test and FEA results of an un-strengthened specimen OB1 and two GFRP-strengthened specimens OB2 and OB3 of Okeil et al (2009a & 2010). The design ultimate loads of specimens were in reasonable agreement with those obtained from the FE analyses of specimens with the rigid end posts. The depth and thickness of the web of the intermediate and diagonal GFRP stiffeners used in specimens OB2 and OB3, however, were greater than those required by the design procedures.

The proposed design procedures for FRP-strengthened plate-girders have been validated using the results of the tests and FE analyses of nine specimens, B2 to B8, OB2 and OB3, and those of the FE analyses of thirty-five models. The design procedures can therefore be used in practice to estimate of the ultimate loads of FRP-strengthened plate-girders and to determine suitable cross-sections of GFRP pultruded sections as intermediate, load-bearing and diagonal web stiffeners.

Chapter 7 Conclusions

7.1 Overview of research

The details and the results of an investigation into the use of carbon and glass fibre-reinforced polymer, FRP, composites to strengthen the webs of steel plate-girders have been presented in the thesis. The investigation comprised tests of eight specimens, B1 to B8, and finite element analyses, FEA, of nine models of the specimens, B1 to B9. The objective was to obtain a minimum increase of 20% in the ultimate load of the FRP-strengthened specimens compared to that of the un-strengthened specimen. Design procedures for strengthening using the FRP composites have been developed. The results of the tests and FE analyses of the test specimens B1 to B9 have been used to validate the design procedures. The design procedures have also been validated using the results of the tests and FE analyses of the three test specimens, OB1 to OB3, of Okeil et al (2009a & 2010) and those of the FE analyses of thirty-five models.

7.2 Tests of specimens

The tests of one un-strengthened control specimen, B1, and the seven FRP-strengthened specimens, B2 to B8, were carried out on end web panels of steel plate-girders. Four plate-girders each comprising two specimens were tested. The plate-girders, two in each of series S1 and S2, were manufactured using S275 grade of steel. The S1 and S2 plate-girders were similar in construction; but the steel in the web had different yield and ultimate tensile strengths. The end web panels of three specimens B2, B5 and B6 were strengthened using GFRP pultruded section stiffeners and those of the other three specimens B3, B4 and B7 with layers of the carbon and glass fabrics. In specimen B8, the load-bearing GFRP stiffeners were used in place of the load-bearing steel stiffeners. Further details are given in Chapter 3.

7.2.1 Results of tests

The results of the tests of specimens B1 to B8 show that.

1. The ultimate loads of the specimens B2, B5 and B6 with GFRP pultruded section strengthening were increased by approximately 1.20, 1.29 and 1.48 times that of the respective un-strengthened specimen, B1 or B9.

2. The ultimate load of specimen B8 with the load-bearing GFRP stiffeners was 0.97 times that of FE model B9 with the load-bearing steel stiffeners.

3. Using a vertical GFRP stiffener on one side of the web in the web panel, specimen B5, strengthened the panel in a similar way to using two vertical stiffeners of similar stiffness one on each side of the web, specimen B2. The ultimate loads of specimens B2 and B5 were approximately 1.20 and 1.29 times that of the respective un-strengthened specimen, B1 or B9.

4. The failure of specimens B2 and B5 with vertical GFRP stiffeners was ductile and was initiated by the development of two out-of-plane diagonal buckles in the steel web on either side of the stiffener. The failure of the specimen B6 with a diagonal GFRP stiffener was brittle and was initiated by buckling of the GFRP stiffener followed by delamination in the stiffener and the development of an out-of-plane diagonal buckle in the steel web of the end web panel

5. Tapering the ends of the GFRP pultruded section stiffeners to an angle of approximately 20 degrees in the specimens B2 and B5 proved to be successful in avoiding a breakdown of the bond between the steel and the GFRP at the ends of the GFRP stiffeners, even at the ultimate load of the specimens.

6. The strengths of specimens B3, B4 and B7 with FRP fabric strengthening were increased by approximately 1.25, 1.54 and 1.45 times that of the respective un-strengthened specimen, B1 or B9.

7. Failure in all three FRP fabric strengthened specimens, B3, B4 and B7, was brittle and was initiated by a breakdown of the steel-fabric bond followed by an out-of-plane buckling in the strengthened web on the steel side.

8. Glass fabric exhibited a better bond with the steel surface than the carbon fabric. The breakdown of the bond between the glass fabric and the steel in the specimens B4 and B7 was considered to have occurred at the ultimate loads of 354 and 428 kN respectively, which were approximately 1.23 and 1.49 times that of specimen B3, with carbon fabric, which was 287 kN.

9. In the tests of the glass fabric strengthened specimens, the ultimate load of specimen B4 using eight layers of glass fabric was approximately 1.54 times that of the un-strengthened specimen B1. The ultimate load of specimen B7 using four layers of glass fabric was approximately 1.45 times that of the model of un-strengthened specimen B9. The increase in the ultimate load of B4 was about 1.05 times that of B7. The increases in the ultimate loads of the specimens B4 and B7 were not proportional to the number of the fabric layers applied to their end web panels.

10. Four plastic hinges, two in the top flange and one each in the bottom flange and external stiffeners or end posts, developed in all the test specimens B1 to B8.

7.3 FE analyses of specimens

Before testing, finite element, FE, analyses were carried out on models of the test specimens B1 to B8 using the LUSAS FE program, Version 14.3 (LUSAS, 2008). Eight models were built to represent the eight specimens B1 to B8. Because of good agreement between the test and FEA results of specimen B1, an FE model of the un-strengthened specimen B9 was analysed and used as the control for the test specimens and models using the S2 plate-girders. Both material and geometric nonlinearities were modelled. The lateral imperfections in the web were included in the analyses of all specimens by using the first buckling mode from eigenvalue analyses with a maximum lateral displacement of 1 mm in the web, Chapter 5. Before carrying out the FE analyses of the test specimens, validation studies were carried out using nine models and thirty-eight specimens tested by others, Chapter 4.

7.3.1 Results of tests and FE analyses

A comparison of the results of the tests and FE analyses of the un-strengthened and FRP-strengthened specimens shows that.

1. The test and FEA ultimate loads, modes of the failure and load-deflection responses for the un-strengthened specimen B1 and GFRP pultruded section strengthened specimens B2, B5, B6 and B8 were in good agreement.

2. The test and FEA load-deflection responses for the fabric-strengthened specimens B3, B4 and B7 were in agreement up to breakdown of the bond between the fabric and the steel that occurred in the tests, but was not modelled in the FE analyses.

3. Specimens B3, B4 and B7 had different modes of the failure in the tests and the FE analyses. In the tests, the failure of all three specimens was initiated by a breakdown of the steel-fabric bond followed by an out-of-plane buckling of the web in the strengthened web panel on the steel side and formation of the four plastic hinges, two in the top flange and one each in the external steel stiffeners and bottom flange. In the FE analyses, the failure of two specimen B3 and B4 was initiated by the out-of-plane buckling of the un-strengthened web in the three web panels except the strengthened panel, yielding of the web in the second and fourth web panels, yielding of the loaded stiffeners near the applied load and the formation of four plastic hinges, two in the top flange and one each in the loaded stiffeners and bottom flange. The failure of the third specimen B7 was initiated by the buckling of web in the strengthened panel followed by the yielding of the strengthened web and formation of four plastic hinges, two in the top flange and one each in the external steel stiffeners and bottom flange

4. The small differences in the test and the FEA load-deflection responses of the specimens have been observed. At the ultimate loads of specimens, the FEA vertical deflections at the underside of the loaded stiffeners are also smaller than those in the tests. This can possibly be attributed to presence of residual stresses, strain hardening of the steel and geometrical imperfections in the webs of the test specimens. In the FE analyses, the residual stresses were not included, while the lateral geometrical imperfections in the web were assumed to be the same in all models. Also in the FEA analyses, the steel and FRP composites were modelled as elastic perfectly plastic materials by ignoring any strain hardening.

5. The FE analyses also predicted approximately the correct locations at which plastic hinges developed in the top and bottom flanges and the external stiffeners of the six test specimens B1, B2, B5, B6, B7 and B8.

6. The distribution of stresses in FE analyses showed that at the ultimate load of specimens, the maximum equivalent stress based on von-Mises yield criterion 'S_E' in the tensile stress field of the web in the yielded web panel, being a combined effect of the major tensile and minor compressive principal stresses, was approximately equal to the yield strength of the steel in the web.

7.4 Design procedures for FRP-strengthened plate-girders

The design procedures for steel plate-girders with the webs in web panels strengthened using GFRP pultruded section stiffeners or with layers of FRP composite fabrics have been developed from those in Eurocode 3, EC3 (ENV 1993-1-5, 2006). The design procedures can be used to estimate the ultimate load of FRP-strengthened plate-girders and determine suitable cross-sections of the GFRP pultruded section stiffeners. The design procedures are subject to the following limitations.

1. The ultimate load of the un-strengthened or FRP-strengthened plate-girder given by a design procedure or the procedure in EC3 shall not be greater than the ultimate plastic of the plate-girder given by the upper bound plastic analysis.

2. The width-to-thickness ratio, b_s/t_s, of a steel plate stiffener or of the web of a GFRP pultruded T-section stiffener should be less than '$0.55\sqrt{(E/\sigma_{ys})}$' in order to avoid local buckling of the stiffener (Hoglund, 1973).

The design procedures have been used to estimate the ultimate loads of specimens B2 to B8 and to determine suitable cross-sections of the GFRP stiffeners required for specimens B2, B5, B6 and B8. The procedure in EC3 has been used to estimate the ultimate loads of the un-strengthened specimens B1 and B9. It has, however, been observed that the failure mechanism of the plate-girders in the tests and FE analyses was different from that assumed in the procedure in EC3. EC3 assumes the end posts to remain rigid and plastic hinges to form in the top and bottom flanges only, while in both the tests and FE analyses of the test specimens, the hinges were also formed in the end posts. In order to validate the design procedures, the modes of failure of the test specimens B1 to B9 in the FE analyses need to be same as the models used in the design procedure. Therefore, the FE analyses of the specimens with the rigid end posts were carried out.

7.4.1 Validation of` design procedures

The design procedures have been validated using the results of the test and FE analyses of specimens B1 to B9. The results of the specimens tested and analysed by Okeil et al (2009a & 2010) and those of two parametric studies have also been used to validate the design procedures. The results of the validation are given as follows.

1. The design ultimate loads of un-strengthened specimens B1 and B9 and GFRP-strengthened specimens B2, B5, B6 and B8 were 1.04 to 1.24 times greater than the test and FEA ultimate loads of specimens with non-rigid end posts.

2. The design ultimate loads of the FRP fabric-strengthened specimens B3, B4 and B7 were 1.42, 1.09 and 1.08 times greater than the FEA ultimate loads of specimens with non-rigid end posts.

3. The design ultimate loads of the two fabric-strengthened specimens B3 and B4 were significantly greater, 3.50 and 2.18 times, than the test ultimate loads of specimens with non-rigid end posts. This was because the breakdown of the steel-fabric bond that occurred in the tests of these specimens was not included in the design procedure. Despite a breakdown of the bond, the design ultimate load of the third specimen B7 was 1.08 times the test ultimate load of the specimen with non-rigid end posts.

4. The depths of the webs of GFRP stiffeners were determined by keeping thicknesses of the flange and web and width of the flange the same as those in the GFRP stiffeners used in test specimens. The depths of the webs of GFRP stiffeners used in test specimens B5, B6 and B8 were greater than those required by the design procedures. The depth of the web of GFRP stiffeners used in the specimen B2 was, however, smaller than the design requirement.

5. The FEA ultimate loads of all plate-girders, speciemns B1 to B9, with non-rigid end posts were incresaed by by providing the rigid end posts.

6. The design ultimate loads of all nine specimens B1 to B9 were in good agreement with the ultimate loads obtained from the FE analyses of the specimens with rigid end posts.

7. In the FE analyses of specimens with rigid end posts, the plastic hinges causing the failure of specimens formed in the top and bottom flanges with no hinges formed in the of end posts. The failure mechanism of the specimens was the same as that assumed in the procedure in EC3.

8. The load-vertical deflection responses of specimens B1 to B9 show that the elastic response of the specimens with rigid and non-rigid end posts was same. The platsic response of the speciemns with the rigid end posts was, however, different from that with the non-rigid end posts.

9. Before a breakdown of the steel-fabric bond, the test ultimate loads of the fabric-strengthened specimens B3, B4 and B7 were increased by 1.25, 1.54 and 1.45 times compared to that of the respective un-strengthened specimen, B1 or B9. The least increase in the ultimate load of specimen obtained was 25% for the test specimen B3. Therefore for the use in practice, the procedure has been limited up to an increase of 20% in the ultimate load of fabric-strengthened plate-girders compared to that of the un-strengthened plate-girder because a breakdown of the bond is not included in the design procedure.

10. It has been found that one layer of the carbon fabric in specimen B3 and two layers each of the glass fabric in specimens B4 and B7 with rigid end posts, respectively, were sufficient to obtain the least increase of 20% in the design ultimate loads compared to that of the respective un-strengthened specimen, B1 or B9.

11. The design ultimate loads of specimens B3, B4 and B7 using one layer of the carbon fabric and two layers of each the glass fabric, respectively, were in good agreement with those obtained from the FE analyses of specimens with the rigid end posts.

12. The design ultimate loads of the twenty-seven models with the diagonal steel and GFRP stiffeners and the five models with glass fabric-strengthened webs were in reasonable agreement with the FEA ultimate loads of the models.

13. The design ultimate loads of specimens OB1, OB2 and OB3 of Okeil et al (2009a & 2010) were in reasonable agreement with those obtained from the FE analyses of specimens with the rigid end posts.

14. The depth and thickness of the webs of intermediate and diagonal GFRP stiffeners used in specimens OB2 and OB3 were greater than those required by the design procedures.

15. After validation of the proposed design procedures for FRP-strengthened plate-girders using the results of the tests and FE analyses of nine specimens and those of FE analyses of thirty-five models, the design procedures can be used in practice.

7.5 Major contributions from the reserach

Following are the major contributions from the reserach work.

1. The tests of the un-strengthened and FRP-strengthened steel plate-girders have been carried out and results are presented. The test results show increases in the ultimate loads of the plate-girders by up to 54% due to FRP-strengthening.

2. Finite element, FE, modelling tecniques have been developed for the analyses of the un-strengthened and FRP-strengthened test plate-girder speciemens. The FE modelling techniques have been valiated against the test results for the ultimate loads, modes of the failure and load-deflection responses of specimens. The modelling techniques and the results of their validation are presented.

3. Design procedures for FRP-strengthened steel plate-girders have been developed. The procedures can be used in practice (a) to estimate the ultimate load of FRP-strengthened plate-girders and (b) to determine suitable cross-sections for the GFRP pultruded section stiffeners.

7.6 Future work

In view of the findings of the present study, further research is required to be carried out in the following areas.

1. The behaviour of the bond between the steel and FRP composites has been found to be the most critical issue in the FRP-strengthened plate-girders either using GFRP pultruded section or the carbon and glass fabrics. The increase in the strength of an FRP-strengthened plate-girder largely depends upon the strength and durability of the steel-FRP bond. The behaviour of the steel-FRP bond needs a comprehensive study with the help of the tests and FE modelling. Once the bond behaviour is understood properly, it would be easier to avoid a breakdown of the bond and to obtain optimum strength of the FRP-strengthened plate-girders.

2. In the design procedures for FRP-strengthened steel plate-girders, a perfect bond has been assumed between the steel and FRP composites. A breakdown of the steel-FRP bond occurred in the tests of three out of the seven FRP-strengthened plate-girders. Once the bond behaviour is understood properly, it may possible to amend the design procedures in such a way that the optimum design ultimate load can be estimated before a breakdown of the bond.

3. Numerous experimental and numerical investigations have been carried to study the strength of adhesively bonded joints subjected to the tensile loads. The investigations are required to be carried out to study the bond strength of composite sections subjected to the shear loads.

4. Using the design procedure and FE analyses, it has been found that one layer of the carbon fabric in specimen B3 and two layers each of the glass fabric in specimens B4 and B7 with rigid end posts, respectively, were sufficient to obtain the least increase of 20% in the design ultimate loads compared to that of the respective un-strengthened specimen, B1 or B9. The breakdown of the steel-fabric bond was neither included in the design procedure nor modelled in the FE analyses. It would therefore be useful to carry out the tests of the strengthened specimens to verify if such increase in the ultimate load of the specimens can be obtained without a bond breakdown.

5. The tests and FE analyses of the un-strengthened and FRP-strengthened plate-girders with non-rigid end posts have been carried out. The FE analyses of the plate-girders with rigid end posts have also been carried out. It is suggested that the tests of two randomly chosen FRP-strengthened plate-girders with rigid end posts be carried out to validate the results of the FE analyses.

6. The tests and FE analyses of the un-strengthened and FRP-strengthened steel plate-girders subjected to static loads have been carried out. Similar FE analyses of the plate-girders subject to cyclic loads are to be carried out to study the comparative behaviour. It will also be useful to carry out one or two tests of the plate-girders subject to the cyclic loading for validation purposes as well as understanding their behaviour in a physical test

7. The effectiveness of using GFRP pultruded sections as vertical and diagonal web stiffeners in steel plate-girders have been studied using the tests and FE analyses. In order to study the effectiveness of using GFRP pultruded sections as longitudinal web stiffeners in plate-girders, it is suggested to carry out the FE analyses of the plate-girders with the longitudinal GFRP stiffeners together with a few validation tests.

Appendices

Appendix A Stiffness, EI, of stiffeners used in specimens B2, B5 and B8 and FE model B9

A.1 GFRP stiffeners of specimen B2

Since the flanges of two GFRP stiffeners, Figure 8.1(a), were used mainly to bond the stiffeners to the steel surfaces and do not contribute much to their stiffness, EI. Therefore only the webs of the GFRP stiffeners, Figure 8.1(b), have been used to calculate the second moment of area, I, and the stiffness, EI, as under.

$I = bd^3/12 = [5 \times (50)^3]/12 = 52{,}083 \text{ mm}^4$

$EI = 52{,}083 \times 36 = 1{,}875{,}000 \text{ kN-mm}^2$

A.2 GFRP stiffener of specimen B5 and B8

The web of the GFRP stiffener, Figure 8.2, of specimens B5 and B8 has only been used to calculate the second moment of area, I, and the stiffness, EI, in the same way as for the GFRP stiffeners of B2.

$I = bd^3/12 = [6.4 \times (50)^3]/12 = 66{,}667\text{mm}^4$

$EI = 66{,}667 \times 36 = 2{,}400{,}000 \text{ kN-mm}^2$

A.3 Steel stiffeners of FE model B9

The second moment of area, I, and the stiffness, EI, of each of the two of the steel stiffeners, Figure 8.3, used in the control FE model B9 has been calculated as under.

$I = bd^3/12 = [3.1 \times (125)^3]/12 = 504{,}557.29 \text{ mm}^4$

$EI = 504{,}557.29 \times 205 = 103{,}434{,}244.8 \text{ kN-mm}^2$

1. Ratio of EI of GFRP stiffener of B5 to those of B2

   $= 2{,}400{,}000/1{,}875{,}000 = 1.28 \approx 1.30$

2. Ratio of EI of steel stiffener of B9 to GFRP stiffener of B8

   $= 103{,}434{,}244.8/ 2{,}400{,}000 = 43.08 \approx 43$

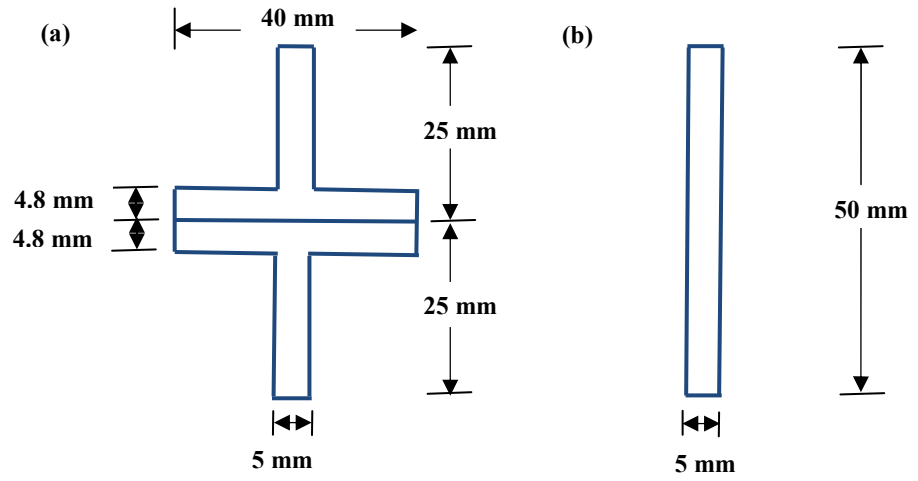

Figure 8.1 (a) Dimensions of (a) GFRP stiffeners and (b) webs of GFRP stiffeners of specimen B2

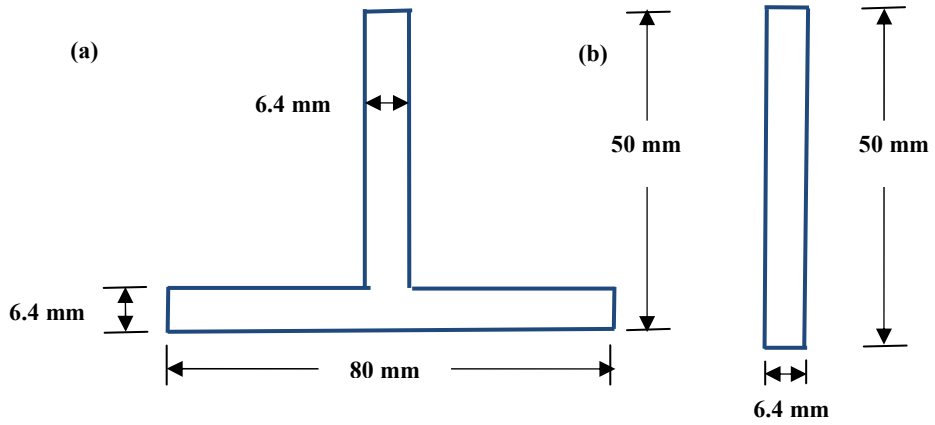

Figure 8.2 (a) Dimensions of (a) GFRP stiffeners and (b) webs of GFRP stiffeners of specimens B5 and B8

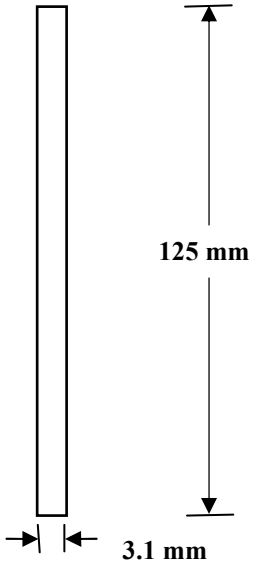

Figure 8.3 Dimensions of steel stiffeners of model of control specimen B9

Appendix B

B.1 Calculations for steel web panel

The ultimate load of the steel web panel with material nonlinearity only is given by Equation 8.1. The ultimate load of the web panel with the material and geometric nonlinearities is determined using Equation 8.2 to Equation 8.8.

Table 8.1 gives the calculations for the ultimate loads of the steel web panel.

$$V_p = \frac{\sigma_{yw} d_w t_w}{\sqrt{3}} + \frac{b_f t_f^2 \sigma_{yf}}{a} \quad \text{Equation 8.1}$$

$$V_{b,Rd} = V_{bw,Rd} + V_{bf,Rd} \leq \frac{\eta d_w t_w \sigma_{yw}}{\sqrt{3}\gamma_{M1}} \quad \text{Equation 8.2}$$

$$V_{bw,Rd} = \frac{\chi_w d_w t_w \sigma_{yw}}{\sqrt{3}\gamma_{M1}} \quad \text{Equation 8.3}$$

$$\lambda_w = 0.76 \sqrt{\frac{\sigma_{yw}}{\tau_{cr}}} \quad \text{Equation 8.4}$$

$$\varepsilon = \sqrt{\frac{235}{\sigma_{yw}}} \quad \text{Equation 8.5}$$

$$\chi_w = \frac{0.83}{\lambda_w} \text{ if } \lambda_w \geq 1.08 \text{ for non} - \text{rigid end post} \quad \text{Equation 8.6}$$

$$c = a\left[0.25 + \frac{1.6 b_f t_f^2 \sigma_{yf}}{d_w 2 t_w \sigma_{yw}}\right] \quad \text{Equation 8.7}$$

$$V_{bf,Rd} = \frac{b_f t_f^2 \sigma_{yf}}{c\gamma_{M0}}\left[1 - \left\{\frac{M_{Ed}}{M_{f,Rd}}\right\}^2\right] \quad \text{Equation 8.8}$$

Table 8.1 Calculations for ultimate loads of the steel web panel

Ultimate load (material nonlinearity only)							
Frame, $V_{psf} = b_f t_f^2 \sigma_{yf}/a$ (kN)	21.6	21.6	21.6	21.6	21.6	21.6	21.6
Web, $V_{psw} = A_s.\sigma_{ys}/\sqrt{3}$ (kN)	43.3	86.6	173.2	260	346	433	520
Ultimate load, $V_p = V_{psf} + V_{psw}$ (kN)	**65**	**108**	**195**	**281**	**368**	**455**	**541**
Ultimate load (material and geometric nonlinearities)							
<u>Contribution of web</u>							
Thickness of web, t_w (mm)	0.5	1.0	2.0	3.0	4.0	5.0	6.0
K (for simply supported square plate)	9.34	9.34	9.34	9.34	9.34	9.34	9.34
Shear buckling stress (GPa) $\tau_{cr} = \frac{\pi^2 KE}{12(1-\vartheta^2)}\frac{t_w^2}{d_w^2}$	.0017	.0069	0.028	0.062	0.111	0.173	0.249 $> \tau_{yw}$
$\lambda_w = 0.76\sqrt{\sigma_{yw}/\tau_{cr}}$	10.00	5.003	2.501	1.668	1.251	1.001	0.834
$\chi_w = 0.83/\lambda_w$ (for non-rigid end posts)	0.083	0.166	0.332	0.498	0.664	0.830	0.995
$V_{bw,Rd} = \frac{\chi_w d_w t_w \sigma_{yw}}{\sqrt{3}\gamma_{M1}}$ (kN)	3.59	14.37	57.47	129.3	229.9	359.2	517.3
<u>Contribution of flanges</u>							
$c = a[0.25 + 1.6 b_f t_f^2 \sigma_{yf}/d_w 2 t_w \sigma_{yw}]$ (mm)	355.4	240.2	182.6	163.4	153.8	148.0	144.2
Let applied load force on web panel (kN)	34	59	116	193	293	417	564
M_{Ed} = Load x a (kN-mm)	1700	29500	58000	96500	146500	208500	282000
$M_{f,Rd} = A_f.h_f.\sigma_{yf}$ (kN-mm)	406800	406800	406800	406800	406800	406800	406800
$V_{bf,Rd} = b_f t_f^2 \sigma_{yf}/c\gamma_{M0}[1 - \{M_{Ed}/M_{f,Rd}\}^2]$ (kN)	30.35	44.78	58.21	63.20	63.12	58.02	46.85
Ultimate load, $V_{b,Rd}$ of web panel = $V_{bw,Rd} + V_{bf,Rd}$ (kN)	33.9	59.1	115.7	192.5	293.0	417.2	563
Ultimate load, $V_{b,Rd}$ of web panel (kN)	**33.9**	**59.1**	**115.7**	**192.5**	**293.0**	**417.2**	***541**

* Ultimate plastic load of the web panel

B.2 Calculations for glass fabric-strengthened steel plate

Let in Figure 8.4(a) of the composite section,

t_s, t_f = thicknesses of steel and glass fabric sections (mm)

E_s = modulus of elasticity of steel = 205 GPa

E_f = modulus of elasticity of glass fabric = 13 GPa

t_n = distance of neutral axis of composite plate from the un-strengthened edge of the steel section

t_e = thickness of equivalent steel section based on flexural stiffness (mm)

V_p = ultimate plastic load of the composite section (kN)

V_{ps}, V_{pf}= ultimate plastic load of the of steel and glass fabric sections (kN)

σ_{ys}, σ_{yf} = tensile yield strength of the steel and glass fabric (GPa)

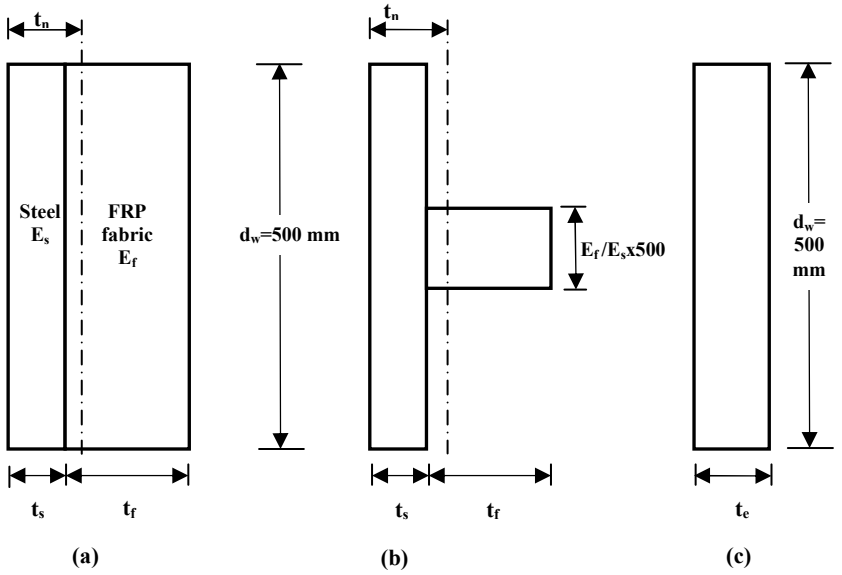

Figure 8.4 Conversion of glass fabric-strengthened plate to equivalent steel section

Location of neutral axis

Using Figure 8.4(b) the distance of the neutral axis, t_n, is given by Equation 8.9.

$$t_n = [\{(500 \times t_s)\ (t_s/2)\} + \{(500 \times E_f/E_s \times t_f)\ (t_s + t_f/2)\}] / [500 \times t_s + 500 \times E_f/E_s \times t_f]$$

Equation 8.9

Second moment of area of equivalent steel section

The second moment of area, I_{NA}, of the equivalent steel section, (b), is given by Equation 8.10.

$$I_{NA} = [500 \times t_s^3/12] + [(500 \times t_s)\ (t_s/2 - t_n)^2] + [E_f/E_s \times 500 \times t_f^3/12] + [(E_f/E_s \times 500 \times t_f)\ (t_s + t_f/2 - t_n)^2]$$

Equation 8.10

Equivalent steel section

Let 't_e' is thickness of equivalent steel section (mm) in Figure 8.4(c) and is given by Equation 8.11.

$$t_e = [(I_{NA} \times 12)/500]^{1/3} \qquad \text{Equation 8.11}$$

Table 8.2 gives the calculations for the elastic critical loads and the ultimate loads of the glass fabric-strengthened plate.

Table 8.2 Calculations for elastic critical and ultimate loads of the glass fabric-strengthened plate

Elastic critical load					
Thickness of steel, t_s (mm)	3.0	3.0	3.0	3.0	3.0
Thickness of fabric, t_f (mm)	3.0	6.0	9.0	12.0	15.0
Distance of n-axis, t_n (mm)	1.68	2.0	2.64	3.02	3.67
Second moment of area, I_{NA}, of the equivalent steel section (mm^4)	2001.2	5113.8	11679	22757	39282
Equivalent steel thickness based on flexural stiffness, t_e (mm)	3.63	4.961	6.532	8.157	9.873
Elastic critical load (kN) $V_{cr} = \frac{\pi^2 KE}{12(1-\upsilon^2)}\frac{t_e^3}{d_w}$	**165.6**	**422.7**	**964**	**1881**	**3238**
Ultimate load (material nonlinearity only)					
Steel, $V_{ps} = A_s.\sigma_{ys}/\sqrt{3}$ (kN)	259.7	259.7	259.7	259.7	259.7
Fabric, $V_{pf} + A_f.\sigma_{yf}/\sqrt{3}$ (kN)	90	180	270.0	360	450
Ultimate load, $V_p = V_{ps} + V_{pf}$ (kN)	**349.7** $> V_{cr}$	**439.7** $> V_{cr}$	**529.7** $< V_{cr}$	**619.7** $< V_{cr}$	**709.7** $< V_{cr}$
Ultimate load (material and geometric nonlinearities)					
Elastic critical load (kN)	165.6	422.7	964	1881	3238
K (for simply supported square plate)	9.34	9.34	9.34	9.34	9.34
Shaer buckling stress, $\tau_{cr} = V_{cr}/A$ (GPa)	0.0912	0.1703	0.2952	0.4610	0.6623
$\lambda_w = 0.76\sqrt{\sigma_{yw}/\tau_{cr}}$	1.378	1.009	0.766	0.613	0.512
$\chi_w = 0.83/\lambda_w$	0.602	0.823	1.083	1.354	1.621
$V_{bw,Rd} = \frac{\chi_w d_w t_w \sigma_{yw}}{\sqrt{3}\gamma_{M1}}$ (kN)	210.59	361.82	573.65	839.08	1150.4
Ultimate load, $V_{bw,Rd}$ (kN)	**210.59**	**361.82**	***529.7**	***619.7**	***709.7**

* Ultimate plastic load of the web panel

B.3 Calculations for glass fabric-strengthened steel web panel

Table 8.3 gives the calculations for the ultimate loads with (a) material nonlinearity and (b) material and geometric nonlinearities of the glass fabric-strengthened web panel.

Table 8.3 Calculations for ultimate loads of the glass fabric-strengthened web panel

Ultimate plastic load (material nonlinearity only)					
Steel frame, $V_{pfs} = b_f t_f^2 \sigma_{yfs}/a$	21.6	21.6	21.6	21.6	21.6
Steel web, $V_{pws} = A_s.\sigma_{yws}/\sqrt{3}$ (kN)	259.7	259.7	259.7	259.7	259.7
Fbric, $V_{pf} = A_f.\sigma_{yf}/\sqrt{3}$ (kN)	90	180	270.0	360	450
Ultimate load, $V_p = V_{psf} + V_{psw} + V_{pf}$ (kN)	**371.5**	**461.1**	**551.6**	**641.7**	**731.8**
Ultimate load (material and geometric nonlinearities)					
<u>Contribution of web</u>					
Thickness of steel, t_s (mm)	3.0	3.0	3.0	3.0	3.0
Thickness of fabric, t_f (mm)	3.0	6.0	9.0	12.0	15.0
Equivalent steel thickness, t_e (mm)	3.63	4.961	6.532	8.157	9.873
Elastic critical load (kN)	165.6	422.7	964	1881	3238
Shear buckling stress, $\tau_{cr} = V_{cr}/A$ (GPa)	0.0912	0.1703	0.2952	0.4610	0.6623
$\lambda_w = 0.76\sqrt{\sigma_{yw}/\tau_{cr}}$	1.378	1.009	0.766	0.613	0.512
$\chi_w = 0.83/\lambda_w$ (for non-rigid end posts)	0.602	0.823	1.083	1.354	1.621
$V_{bw,Rd} = \frac{\chi_w d_w t_w \sigma_{yw}}{\sqrt{3}\gamma_{M1}}$ (kN)	129.24	361.82	573.65	839.08	1150.4
<u>Contribution of flanges</u>					
$c = a[0.25 + 1.6 b_f t_f^2 \sigma_{yf}/d_w 2 t_w \sigma_{yw}]$ (mm)	163.4	156.7	148.2	142.6	139.1
Let applied load force on web panel (kN)	274	420	576	658	738
M_{Ed} = Load x a (kN-mm)	137000	210000	288000	329000	369000
$M_{f,Rd} = A_f.h_f.\sigma_{yf}$ (kN-mm)	68.91	72.86	75.71	77.63	78.96
$V_{bf,Rd} = b_f t_f^2 \sigma_{yf}/c\gamma_{M0}\left[1 - \{M_{Ed}/M_{f,Rd}\}^2\right]$ (kN)	62.82	57.73	46.14	38.06	28.33
Ultimate load, $V_{b,Rd}$ of web panel = $V_{bw,Rd} + V_{bf,Rd}$ (kN)	273.4	419.5	619.8	877.14	1178.7
Ultimate load of web panel	**273.4**	**419.5**	***551.6**	***641.7**	***731.8**

* Ultimate plastic load of the web panel

Appendix C Ultimate load calculations of steel plate-girder

C.1 Ultimate plastic load

The ultimate plastic load of the plate-girder is determined as under:

$$V_p \text{ of plate} - \text{girder} = \frac{4}{3} \text{x } [\frac{\sigma_{yw} d_w t_w}{\sqrt{3}} + \frac{b_f t_f^2 \sigma_{yf}}{a}] \text{ of test web panel}$$

$V_p = 4/3 \text{ x } [\{(0.3 \text{ x } 3 \text{ x } 500)/ 1.732\} + \{(300 \text{ x } 12^2 \text{ x } 0.3)/ 500\}]$

$V_p = 4/3 \text{ x } [259.8 + 25.92] = 380.865$

$V_p \approx 381$ kN

C.2 Ultimate loads

The ultimate load of the steel plate-girder is determined using the equations presented by (i) Basler (1961), (ii) Rockey et al (1978), (iii) Lee and Yoo (1999), (iv) British Standards 5950: Part1 (BS5950-I, 2000), and (v) Eurocode 3, EC3 (ENV3, 1997-1-5). Symbols and abbreviations are defined separately in the thesis.

Basler

Basler (1961) suggested Equation 8.12 for the ultimate load, V_{ult} of a shear panel.

$$V_{ult} = d_w t_w \left[\tau_{cr} + \frac{\sqrt{3}}{2} \frac{\tau_{yw}}{\sqrt{1+\alpha^2}} \left\{1 - \frac{\tau_{cr}}{\tau_{yw}}\right\}\right] \qquad \text{Equation 8.12}$$

V_{ult} of plate-girder = 4/3 of W_{ult} of test web panel

= 4/3 x (500x3) x [0.06231 + (√3x0.1732)/(2x √2){1-(0.06231/0.1732)}]

= **260 kN**

Rockey et al

Rockey et al (1978) suggested Equation 8.13 to determine the ultimate load, V_S, for the plate-girder predominantly loaded to shear.

$$V_s = V_{yw} \left[\frac{\tau_{cr}}{\tau_{yw}} + \sqrt{3} \text{Sin}^2\theta \left(\text{Cot}\theta - \frac{a}{d_w}\right) \frac{\sigma_t^y}{\sigma_{yw}} + 4\sqrt{3} \text{ Sin}\theta \left\{\sqrt{\frac{\sigma_t^y M_p^*}{\sigma_{yw}}}\right\}\right] \qquad \text{Equation 8.13}$$

Where,

$$\sigma_t^y = \sigma_{yw} \left[\frac{\sqrt{3}}{2} \frac{\tau_{cr}}{\tau_{yw}} \text{Sin}2\theta + \sqrt{1 + \left(\frac{\tau_{cr}}{\tau_{yw}}\right)^2 \left(\frac{3}{4} \text{Sin}^2\theta - 1\right)}\right] \qquad \text{Equation 8.14}$$

Where

Mp^* $= M_{pf}/ M_{pw} = 0.25\ b_f\ t_f^2\ \sigma_{yf} / t_w\ d_w^2\ \sigma_{yw}$

θ_d $= \tan^{-1}(a/d_w)$ [for square panels, $\theta_d = \tan^{-1}(a/d_w) = \tan^{-1}(500/500) = 45^0$]

θ $= 2\ \theta_d/3 = 30^0$

Table 8.4 gives the details of calculations of the ultimate load, V_s, of the steel plate-girder using the procedure given by Rockey et al (1978).

Table 8.4 Calculations for ultimate load of steel plate-girder (Rockey et al, 1978)

$M_{pf} = 0.25\ b_f\ t_f^2\ \sigma_{yf}$ (kN-mm)	3240
$M_{pw} = t_w\ d_w^2\ \sigma_{yw}$ (kN-mm)	22500
$Mp^* = M_{pf}/ M_{pw}$	0.0144
$\sigma_t^y = \sigma_{yw}\left[\frac{\sqrt{3}}{2}\frac{\tau_{cr}}{\tau_{yw}}\mathrm{Sin}2\theta + \sqrt{1+\left(\frac{\tau_{cr}}{\tau_{yw}}\right)^2\left(\frac{3}{4}\mathrm{Sin}^2\theta - 1\right)}\right]$	0.372 GPa
$V_s =$ $V_{yw}\left[\frac{\tau_{cr}}{\tau_{yw}} + \sqrt{3}\mathrm{Sin}^2\theta\left(\mathrm{Cot}\theta - \frac{a}{d_w}\right)\frac{\sigma_t^y}{\sigma_{yw}} + 4\sqrt{3}\,\mathrm{Sin}\theta\left\{\sqrt{\frac{\sigma_t^y\ M_p^*}{\sigma_{yw}}}\right\}\right]$ of test web panel	197.37 kN
V_s of plate-girder = 4/3 x V_s of test web panel	**263 kN**
$I_f/b^3t_w = [(300\text{x}\ 12^3)/12]/[500^3\text{x}3]$	115.2 x10^{-6}
$c = b[0.5(I_f/b^3t_w)/ (I_f/b^3t_w + 6.09)]$ (mm)	237.5

Lee and Yoo

Lee and Yoo (1999) proposed Equation 8.15 to determine the ultimate load, V_u, of the plate-girder.

$$V_u = R_d V_p (0.6C + 0.4) \qquad \text{Equation 8.15}$$

Where;

$$R_d = 0.8 + 0.2\left[\frac{\left\{\frac{d_w}{t_w}\frac{\sqrt{\sigma_{yw}}}{\sqrt{K}} - 6000\right\}}{6000}\right] \quad \text{for } \frac{6000\sqrt{K}}{\sqrt{\sigma_{yw}}} \le \frac{d_w}{t_w} \le \frac{12000\sqrt{K}}{\sqrt{\sigma_{yw}}}$$

$$C = 4.5\ \text{x}\ 10^7\ \frac{6000\ K/\sigma_{yw}}{\left(d_w/t_w\right)^2} \quad \text{for } \frac{d_w}{t_w} > 7500\sqrt{K/\sigma_{yw}}$$

V_p = ultimate plastic load (kN) = $A_w.\sigma_{yw}/\sqrt{3}$

R_d = strength reduction factor due to initial out-of-plane flatness D/120

σ_{yw} = yield strength of steel in web (psi)

K = Shear buckling constant proposed by Lee & Yoo = $K_{ss} + 0.8(K_{sf} - K_{ss})$

K_{ss} = K when all four edges of plates are simply supported

$K_{ss} = 5.34 + 4/ (a/d_w)^2$ for $a/d_w \geq 1.0$

K_{sf} = K when two opposite edges of plates are fixed and other two are simply supported

$K_{sf} = 8.98 + 5.6/(a/d_w)^2 - 1.99/(a/d_w)^2$ for $a/d_w \geq 1.0$

Table 8.5 gives the details of calculations of the ultimate load, V_s, of the steel plate-girder using the procedure given by Lee and Yoo (1999).

Table 8.5 Calculations for ultimate load of steel plate-girder (Lee & Yoo, 1999)

σ_{yw} = 0.3 GPa x 145000 (psi)	43500
$K_{ss} = 5.34 + 4/ (a/d_w)^2$	9.34
$K_{sf} = 8.98 + 5.6/(a/d_w)^2 - 1.99/(a/d_w)^2$	12.60
$K = K_{ss} + 0.8(K_{sf} - K_{ss})$	11.95
$d_w/t_w = 500/3 = 166.66$	167
$6000/ \sqrt{(K/\sigma_{yw})}$	99.4 > 167
$7500/ \sqrt{(K/\sigma_{yw})}$	124.3 < 167
$12000/ \sqrt{(K/\sigma_{yw})}$	199 > 167
$R_d = 0.8 + 0.2\left[\frac{\left\{\frac{d_w}{t_w}\frac{\sqrt{\sigma_{yw}}}{\sqrt{K}} - 6000\right\}}{6000}\right]$	0.936
$6000 \sqrt{(K/\sigma_{yw})}/ (d_w/t_w)$	0.597 < 167
$7500 \sqrt{(K/\sigma_{yw})}/ (d_w/t_w)$	0.745 < 167
$C = 4.5 \times 10^7 \frac{6000\, K/\sigma_{yw}}{\left(d_w/t_w\right)^2}$ for $\frac{d_w}{t_w} > 7500\sqrt{K/\sigma_{yw}}$	0.445
V_u of end web panel = $R_d V_p (0.6C + 0.4)$	162.2
V_u of plate-girder = 4/3 x V_u of end web panel	**216 kN**

British Standards

The British Standards 5950: Part 1 (BS5950-I, 2000) gives Equation 8.16 to Equation 8.18 for determining the ultimate load of plate-girders.

$$V_b = V_w + V_f \qquad \text{Equation 8.16}$$

$$V_w = q_w A_w \qquad \text{Equation 8.17}$$

$$V_f = \frac{P_v \frac{d_w}{a}\left[1-\left(f_f/\sigma_{yf}\right)^2\right]}{1+0.15\left[M_{pw}/M_{pf}\right]}$$

Equation 8.18

Table 8.6 gives the details of calculations of the ultimate load, V_b, of the steel plate-girder using the British Standards 5950: Part1 (BS5950-I, 2000).

Table 8.6 Calculations for ultimate load of steel plate-girder (BS5950-I, 2000)

Contribution of web	
q_w (From Table 21 of BS5950) GPa	0.093
V_w of test web panel= $q_w.A_w$ (kN)	139.5
Contribution of flanges	
$P_v = \sigma_{yw}A_w/\sqrt{3}$ (kN)	260
$M_{pw} = \sigma_{yw}.t_w\, d_w^2\, /4$ (kN-mm)	56,250
$M = P_v.\, a$ (kN-mm)	130000
$f_f = M/d_o A_f$ (GPa)	0.07053
$M_{pf} = \sigma_{yf}\, b_f\, t_f^2\, /4$ (kN-mm)	3,240
V_f of test panel (Equation 8.18) kN	68.15
V_b of plate-girder = 4/3 x [V_w + V_f] of test panel(kN)	**277 kN**

Eurocode 3

The procedure in Eurocode 3, EC3 (ENV1-5-1997) has been used to estimate the ultimate load of the steel plate-girder using Equation 8.2 to Equation 8.8.

Table 8.7 gives the details of calculations for determining the ultimate load, $V_{b,Rd}$, of the steel plate-girder using the procedure in EC3.

Table 8.7 Calculations for ultimate load of steel plate-girder (ENV 1-5-1993, 1997)

Contribution of web	
$V_{plastic} = \frac{\sigma_{yw} d_w t_w}{\sqrt{3}} + \frac{b_f t_f^2 \sigma_{yf}}{a}$ of test web panel (kN)	285.6
$V_{plastic}$ of plate-girder = 4/3 x $V_{plastic}$ of test panel (kN)	381
K (for simply supported square plate)	9.34
$\tau_{cr} = \frac{\pi^2 KE}{12(1-\vartheta^2)} \frac{t_w^2}{d_w^2}$	0.06231
$\lambda_w = 0.76\sqrt{\sigma_{yw}/\tau_{cr}}$	1.6676 > 1.08
$\chi_w = 0.83/\lambda_w$ (for non-rigid end posts)	0.4977
$V_{bw,Rd} = \frac{\chi_w d_w t_w \sigma_{yw}}{\sqrt{3}\gamma_{M1}}$ of test web panel (kN)	129.3
Contribution of flanges	
$c = a\left[0.25 + 1.6 b_f t_f^2 \sigma_{yf}/d_w 2 t_w \sigma_{yw}\right]$ (mm)	171.08
Let applied load on test web panel (kN)	203
M_{Ed} = Applied load x a (kN-mm)	103936
$M_{f,Rd} = A_f . h_f . \sigma_{yf}$ (kN-mm)	552960
$V_{bf,Rd} = b_f t_f^2 \sigma_{yf}/c\gamma_{M0}\left[1 - \{M_{Ed}/M_{f,Rd}\}^2\right]$ (kN)	73.08
$V_{b,Rd}$ of plate-girder = 4/3 x [$V_{bw,Rd}$ + $V_{bf,Rd}$] of test panel	**270 kN**

Appendix D Design ultimate loads of specimens B1 to B9 of author

D.1 Un-strengthened specimen B1 and FE model B9

Table 8.8 gives the calculations for the estimation of the ultimate loads, $V_{b,Rd}$, of the un-strengthened specimen B1 and FE model B9 using the procedure in EC3.

Table 8.8 Calculations for design ultimate loads of specimen B1 and FE model B9

Formula	Specimen B1	FE model B9
Contribution of web		
$V_{plastic} = \frac{\sigma_{yw} d_w t_w}{\sqrt{3}} + \frac{b_f t_f^2 \sigma_{yf}}{a}$ of test web panel (kN)	265.09	334.2
$V_{plastic}$ of specimen = 4/3 x $V_{plastic}$ of test panel (kN)	353	445
Aspect ratio of test web panel = a/d_w = 500/ 500	1.0	1.0
K (for square plate with simply supported boundary conditions)	9.34	9.34
$\tau_{cr} = \frac{\pi^2 KE}{12(1-\vartheta^2)} \frac{t_w^2}{d_w^2}$	0.06231	0.06231
$\lambda_w = 0.76 \sqrt{\sigma_{yw}/\tau_{cr}}$	1.594 > 1.08	1.809 > 1.08
$\chi_w = 0.83/\lambda_w$ (for non-rigid end posts)	0.521	0.459
$V_{bw,Rd} = \frac{\chi_w d_w t_w \sigma_{yw}}{\sqrt{3}\gamma_{M1}}$ of test web panel (kN)	123.58	140.3
Contribution of flanges		
$c = a[0.25 + 1.6 b_f t_f^2 \sigma_{yf}/d_w 2 t_w \sigma_{yw}]$ (mm)	179.15	168.08
Let applied load on test web panel (kN)	199	222
M_{Ed} = Applied load x a (kN-mm)	101888	113664
$M_{f,Rd} = A_f.h_f.\sigma_{yf}$ (kN-mm)	593510.4	608256.0
$V_{bf,Rd} = b_f t_f^2 \sigma_{yf}/c\gamma_{M0} [-\{M_{Ed}/M_{f,Rd}\}^2]$ (kN)	75.36	81.86
$V_{b,Rd}$ of plate-girder = 4/3 x [$V_{bw,Rd}$ + $V_{bf,Rd}$ (kN)] of test web panel	265	296
Design ultimate load	**265 kN**	**296 kN**

D.2 Specimens B2 and B5 with vertical GFRP stiffener(s)

Table 8.9 gives the calculations made for the ultimate loads, $V_{b,Rd}$, of the specimens B2 and B5 with vertical GFRP pultruded section stiffener(s) in the end web panel, test panel, using the design procedure.

Table 8.9 Calculations for design ultimate loads of specimens B2 and B5

Formula	Specimen B2		Specimen B5
	Approach 1	Approach 2	
Contribution of web			
Aspect ratio of test panel, a/d_w	0.5	---	0.5
Shear buckling co-efficient 'K' (for simple supported conditions) $= 5.34 + 4.0/(a/d_w)^2$	*25.36	**20.77	*25.36
$\tau_{cr} = \frac{\pi^2 KE}{12(1-\vartheta^2)}\frac{t_w^2}{d_w^2}$ (GPa)	0.169	0.1386	0.169
$\lambda_w = 0.76\sqrt{\sigma_{yw}/\tau_{cr}}$	0.9677 < 1.08	1.069 < 1.08	1.0978 > 1.08
$\chi_w = 0.83/\lambda_w$ (for non-rigid end posts)	0.857	0.777	0.756
$V_{bw,Rd} = \frac{\chi_w d_w t_w \sigma_{yw}}{\sqrt{3}\gamma_{M1}}$ of test panel (kN)	203.6	184.3	231.15
Contribution of flanges			
$c = \left[0.25 + 1.6 b_f t_f^2 \sigma_{yf}/d_w 2 t_w \sigma_{yw}\right]$ (mm)	179.15	179.15	168.08
Let applied load on test web panel (kN)	277	258	310
M_{Ed} = Applied load x a (kN-mm)	141824	132096	158720
$M_{f,Rd} = A_f.h_f.\sigma_{yf}$ (kN-mm)	593510.4	593510.4	608256
$V_{bf,Rd} = b_f t_f^2 \sigma_{yf}/c\gamma_{M0}\left[-\{M_{Ed}/M_{f,Rd}\}^2\right]$ (kN)	73.22	73.80	79.05
$V_{b,Rd}$ of plate-girder = 4/3 x $[V_{bw,Rd} + V_{bf,Rd}]$ of test panel	369	344	413
Design ultimate load	**369 kN**	**344 kN**	**413 kN**

* GFRP stiffeners assumed to satisfy the 'stiffness requirement' of design procedure

** First buckling mode from eigenvalue analysis used in design procedure

Determination of value of 'K' for specimen B2

In the second approach, the value of shear buckling co-efficient 'K' for the end web panel of specimen B2 with non-rigid (flexible) GFRP intermediate stiffeners was determined with the help of web buckling analysis as described in the design procedure, details as follows.

An FE model of the web plate in the end web panel with non-rigid (flexible) GFRP intermediate stiffeners was built using QSL8 element with an 8x8 mesh. The web plate was loaded in such a way that it was subjected to pure shear. Instead of the flanges and rigid transverse stiffeners, the web plate was subjected to simply supported boundary conditions in the same way for the steel plate described in Chapter 4. The eigenvalue analysis was carried out and the value of 'K' was obtained, Table 8.10.

Table 8.10 Calculations for value of 'K 'for GFRP-strengthened panel of specimens B2

Area of cross-section of web panel $A_w = t_w.d_w$ (mm^2)	1500
Applied shear load (kN)	80
Eigenvalue at first positive buckling mode	2.599
Elastic critical load, V_{cr} (kN) = Eigenvalue x applied shear	207.92
Critical shear stress, $\tau_{cr} = V_{cr}/ A_w$	0.1386
Shear buckling co-efficient, $K = 12(1-\upsilon^2) \tau_{cr} d_w^2/ t_w^2 \pi^2 E$	**20.77**

D.3 Specimen B8 with load-bearing GFRP stiffeners

The GFRP stiffeners used in test specimen B8 have been found to satisfy the 'strength and stiffness requirements' of the design procedure. Its design ultimate load has therefore been taken the same that, 296 kN, of FE model of the un-strengthened specimen B9.

D.4 Specimen B6 with a GFRP pultruded section stiffener

The diagonal GFRP stiffener used in specimen B6 is shown in Figure 8.5.

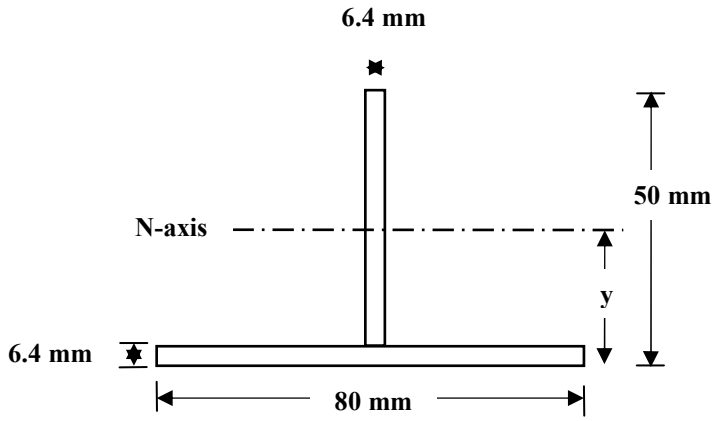

Figure 8.5 Cross-section of diagonal GFRP stiffener used in specimen B6

Table 8.11 shows the calculations for the estimation of the ultimate load of specimen B6 using design procedure.

Table 8.11 Calculations for design ultimate load of specimen of B6

Particulars	**Load (kN)**
Area of cross-section of GFRP stiffener, A_{GFRP} (mm^2) = (80 x 6.4) + (43.6 x 6.4)	791
Squash load of diagonal T-section GFRP pultruded section stiffener (at σ_y GFRP =250 MPa) = 791x0.25	197.75
Applied load required to squash diagonal GFRP stiffener =197.75/√2	139.8
Plastic ultimate load of end web panel of specimen B6 with diagonal stiffener (kN) = ([300 x 12^2 x 0.322]/500) + ([3 x 500 x 0.353]/1.732) + 139.8 = 27.8 + 305.7 + 139.8	473.3
EC3 ultimate load of un-strengthened end web panel of specimen B6= 0.75x296	222
Design ultimate load of strengthened web panel = 222+139.8 = 361.8 < 473.3 (OK)	361.8
Design ultimate load of specimen B6 = 4/3 x 361.8	**482 kN**

D.5 FRP fabric-strengthened specimens B3, B4 and B7

Table 8.12 gives the details of calculations made to estimate ultimate loads of specimens B3, B4 and B7 using the design procedure. Equivalent steel thicknesses of FRP fabric-strengthened webs of the specimens B3, B4 and B7 are determined using the 'flexural stiffness approach" and are given in Table 8.13.

Table 8.12 Calculations for design ultimate loads of specimens B3, B4 and B7

Formula	Specimen		
	B3	**B4**	**B7**
Contribution of web			
Thickness of steel, t_s (mm)	3.0	3.0	3.0
Thickness of fabric, t_f (mm)	6.2	10.5	4.0
Equivalent steel thickness based on flexural stiffness, t_e (mm) [see Table 8.13]	6.5	7.3	4.024
Shear buckling co-efficient, K	9.34	9.34	9.34
$\tau_{cr} = \frac{\pi^2 KE}{12(1-\vartheta^2)}\frac{t_w^2}{d_w^2}$	0.2925	0.373	0.112
$\tau_{yw} = \sigma_{yw}/\sqrt{3}$	0.158 $< \tau_{cr}$	0.158 $< \tau_{cr}$	0.204 $> \tau_{cr}$
$\lambda_w = 0.76\sqrt{\sigma_{yw}/\tau_{cr}}$	0.736 < 1.08	0.651 < 1.08	1.35 > 1.08
$\chi_w = 0.83/\lambda_w$	1.128	1.274	0.615
$V_{bw,Rd} = \frac{\chi_w d_w t_w \sigma_{yw}}{\sqrt{3}\gamma_{M1}}$ of FRP-str. panel (kN)	820.65	703.63	261.91
Contribution of flanges			
$c = a\left[0.25 + 1.6 b_f t_f^2 \sigma_{yf}/d_w 2 t_w \sigma_{yw}\right]$ (mm)	150.0	147.1	157.1
Let applied load on test panel (kN)	864	759	346
M_{Ed} = Applied load x a (kN-mm)	432000	379500	172875
$M_{f,Rd} = A_f.h_f.\sigma_{yf}$ (kN-mm)	593510	593510	608256
$V_{bf,Rd} = b_f t_f^2 \sigma_{yf}/c\gamma_{M0}\left[1-\{M_{Ed}/M_{f,Rd}\}^2\right]$ (kN)	43.61	55.89	83.41
$V_{b,Rd}$ of plate-girder = 4/3 $[V_{bw,Rd} + V_{bf,Rd}]$ of end web panel (kN)	1152	1012	461
$V_{plastic}$ of specimen = 4/3 x$[\frac{\sigma_{yw} d_w t_w}{\sqrt{3}} + \frac{b_f t_f^2 \sigma_{yf}}{a}$ of test panel] (kN)	1007	773	645
Design ultimate load	$\tau_{yw} < \tau_{cr}$ ***1007 kN**	$\tau_{yw} < \tau_{cr}$ ***773 kN**	$\tau_{yw} > \tau_{cr}$ **461 kN**

* Ultimate plastic load of specimen (plate-girder)

Equivalent steel thicknesses of fabric-strengthened webs in the test web panels of specimens B3, B4 and B7

Consider the composite section shown in Figure 8.4.

Location of neutral axis

Using Figure 8.4(b), the distance of the neutral axis, t_n, is given by Equation 8.9

Second moment of area of equivalent steel section

The second moment of area, I_{NA}, of the equivalent steel section, Figure 8.4(b), is given by Equation 8.10.

Equivalent rectangular steel section

Let 't_e' is thickness of equivalent rectangular steel section (mm) in Figure 8.4(c) and is given by Equation 8.11.

Table 8.13 gives the calculations for determination of equivalent steel thicknesses of FRP fabric-strengthened webs of the specimens B3, B4 and B7 using the 'flexural stiffness approach'.

Table 8.13 Calculations for equivalent steel thicknesses of fabric-strengthened webs in test web panels of B3, B4 and B7

Particulars	**Specimen No.**		
	B3	**B4**	**B7**
Thickness of steel web, d_1 (mm)	3.0	3.0	3.0
Thickness of FRP fabric layers, d_2 (mm)	6.2	10.5	4.0
Distance of neutral axis of composite section from un-strengthened edge of the steel web, t_n (mm)	2.725	2.272	1.773
Second moment of area, I_{NA}, of the equivalent steel section (mm^4)	11319	16597.4	2726.2
Equivalent steel thickness of FRP fabric-strengthened web, t_e (mm)	6.5	7.3	4.024

Appendix E Design of GFRP stiffeners used in specimens B2, B5, B6 and B8 of author

E.1 Vertical GFRP stiffeners of specimen B2

Required cross-section of steel stiffeners

Let thickness of intermediate steel stiffener, t_s = 4 mm (see Figure 8.6)

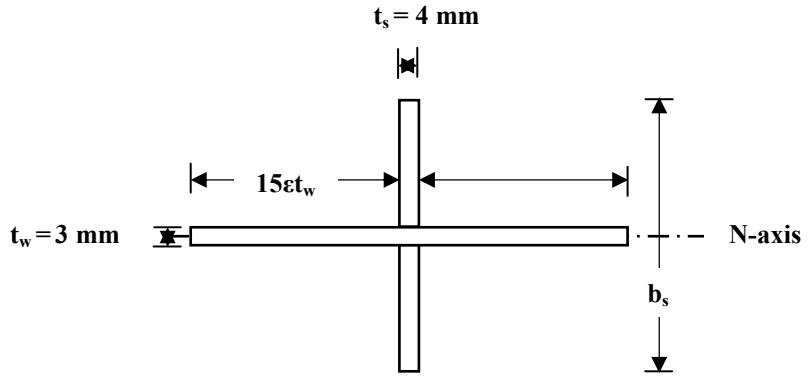

Figure 8.6 Required cross-section of intermediate steel stiffener for specimen B2

For $a/d_w = 1 < \sqrt{2} = 1.4142$, $I_{s\,min} \geq 1.5\, d_w^3\, t_w^3 / a^2$ $= 1.5 \times 500^3 \times 3^3 / 500^2$

$= 20{,}250$ mm^4

Similarly, $EI_{s\,min} = 20{,}250 \times 205$ $= 4.15 \times 10^6$ kN-mm^2

Length of web to be considered in determining $I_{s\,min}$ $= 2 \times 15\varepsilon t_w + t_s$

$= 2 \times 15 \times \sqrt{(235/274)} \times 3 + 4$ $= 87.4$ mm

For t_s = 4 mm, $I_s = 4 \times b_s^3/12 + 87.4 \times 3^3/12 \geq 20{,}250$ mm^4

$b_s \geq 39.039 \approx 40$ mm Two 20 x 4 mm steel stiffeners are required

EI of steel stiffeners only $= 205 \times 4 \times 40^3/12 = 4.37 \times 10^6$ kN-mm^2 $> 4.15 \times 10^6$ kN-mm^2 OK

Check for buckling of the stiffener

$b_s/t_s \leq 0.55\sqrt{(E/\sigma_y)}$

For E = 205 GPa and σ_y = 300 MPa, $0.55\sqrt{(E/\sigma_y)} = 0.55\sqrt{(205/0.3)} = 14.4$

$b_s/t_s = 20/4 = 5.0 < 14.4$ OK

Required cross-section of GFRP stiffeners

Let thickness of intermediate GFRP stiffener, t_s = 5 mm

EI of equivalent GFRP stiffener only $= 36 \times (5 \times b_s^3/12) = 4.37 \times 10^6$ kN-mm^2

$b_s = 66.03 \approx 66$ mm

Two 40 x 33 x 5 mm GFRP stiffeners are required

Check for buckling of the stiffener's web

$b_s/t_s \leq 0.55 \sqrt{(E/\sigma_y)}$

For E = 36 GPa and σ_y = 250 MPa, $0.55 \sqrt{(E/\sigma_y)} = 0.55 \sqrt{(36/0.25)} = 6.6$

$b_s/t_s = (33-5)/5 = 5.6 < 6.6$ OK

It shows that the cross-section, 40 x 25 x 5 mm, of each of the two GFRP stiffeners used in test specimen B2 is smaller than that required by the design procedure.

E.2 Vertical GFRP stiffener of specimen B5

Required cross-section of steel stiffener

Let thickness of intermediate steel stiffener, t_s = 4 mm (see Figure 8.7)

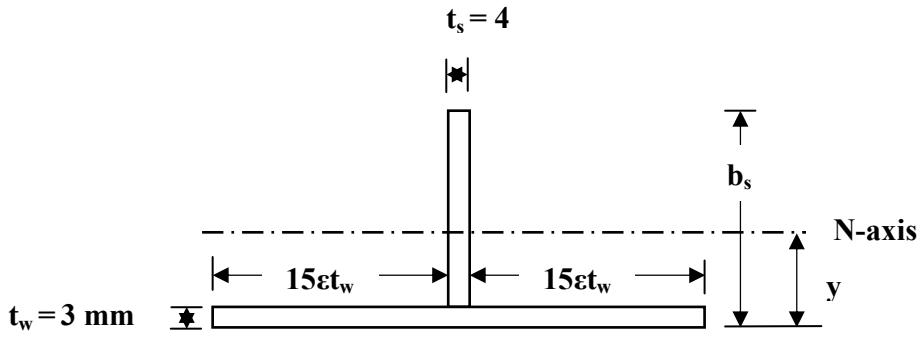

Figure 8.7 Required cross-section of intermediate steel stiffener for specimen B5

Length of web to be considered in determining $I_{s\,min}$ $= 2 \times 15\varepsilon t_w + t_s$

$= 2 \times 15 \times \sqrt{(235/353)} \times 3 + 4$ $= 77$ mm

For $a/d_w = 1 < \sqrt{2} = 1.4142$, $I_{s\,min} \geq 1.5\, d_w^3\, t_w^3 / a^2$ $= 1.5 \times 500^3 \times 3^3 / 500^2$

$= 20{,}250$ mm^4

Similarly, $EI_{s\,min} = 20{,}250 \times 205 = 4.15 \times 10^6$ kN-mm^2

For location of the neutral axis, take first moments of area

$y \times [(77 \times 3) + (4b_s)] = [(77 \times 3)(3/2) + (4b_s)(3 + bs/2]$

$y = [2b_s^2 + 12b_s + 346.5] / [4b_s + 231]$

For b_s = 30 mm, $y = 7.14$ mm, $I_s = 30{,}674$ mm^4 $> 20{,}250$ mm^4

One 30 x 4 mm steel stiffener is required

EI of the steel stiffener = $205 \times 30{,}674 = 6.3 \times 10^6$ kN-mm^2 $> 4.15 \times 10^6$ kN-mm^2 OK

Check for buckling of the stiffener

$b_s/t_s = 30/4 = 7.5 < 0.55 \sqrt{(E/\sigma_y)} = 14.40$ OK

Required cross-section of GFRP stiffener

Let thickness of intermediate GFRP stiffener, $t_s = 6.4$ mm (see Figure 8.8)

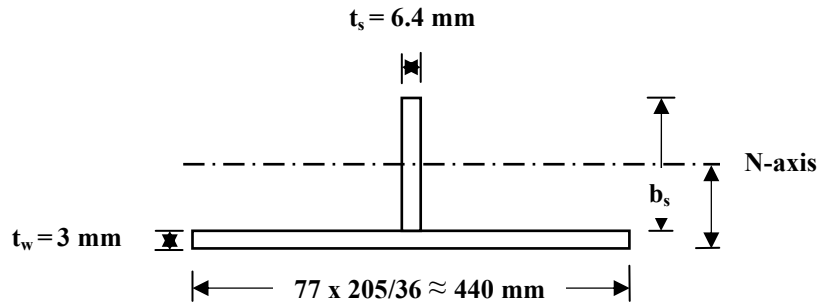

Figure 8.8 Required cross-section of intermediate GFRP stiffener for specimen B5

For location of neutral axis, take first moments of area (see Figure 8.8)

$$y \times [(440 \times 3) + (6.4b_s)] = [(440 \times 3)(3/2) + (6.4b_s)(3 + bs/2]$$

$$y = [3.2b_s^2 + 19.2b_s + 1980] / [6.4b_s + 1320]$$

For $b_s = 50$ mm, $y = 6.67$ mm, $I_s = 248{,}529$ mm^4

$EI = 36 \times 248{,}529 = 8.95 \times 10^6$ kN-mm^2 > > 4.15×10^6 kN-mm^2

For $b_s = 40$ mm, $y = 4.99$ mm, $I_s = 134{,}237$ mm^4

$EI = 36 \times 134{,}237 = 4.83 \times 10^6$ kN-mm^2 > 4.15x106 kN-mm^2 OK

One 80 x 40 x 6.4 mm GFRP stiffener is required

Check for buckling of the stiffener's web

$b_s/t_s = (40\text{-}6.4)/6.4 = 5.25 < 0.55 \sqrt{(E/\sigma_y)} = 6.6$ OK

It shows that the cross-section, 80 x 50 x 6.4 mm, of GFRP stiffener used in test specimen B5 is lager that that required by the design procedure.

E.3 Diagonal GFRP stiffener of specimen B6

EC3 ultimate load of un-strengthened test panel of specimen B6 = ¾ x 296= 221 kN

Test ultimate load of specimen B6 with diagonal GFRP stiffener = 437 kN

Test ultimate load of GFRP-strengthened panel of specimen B6 = ¾ x 437 = 328 kN

Additional load required due to diagonal GFRP stiffener = difference in ultimate loads of the un-strengthened and GFRP-strengthened web panels of B6 = 328-221 = 107 kN

In view of the above, the minimum of the Euler load and squash load of diagonal GFRP stiffener should be equal to or greater than 107 kN.

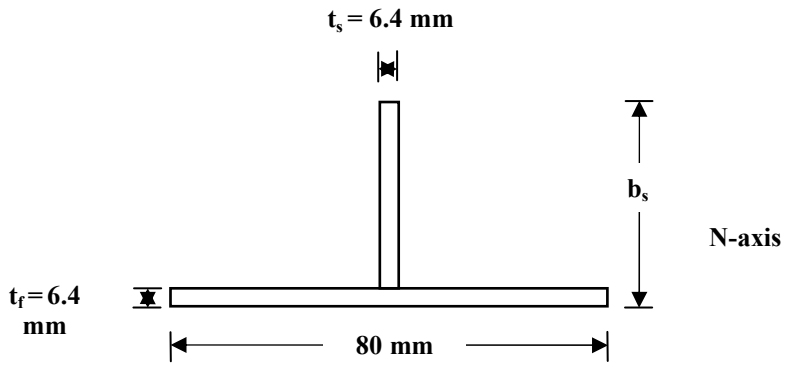

Figure 8.9 Required cross-section of diagonal stiffeners for specimen B6

Let 'b_s' is the overall depth of GFRP stiffener and other dimensions are as given in Figure 8.9.

Length of GFRP stiffener, L = diagonal of the web panel = 678 mm

For b_s = 45 mm, y = 10.53 mm, I_s = 116,781 mm^4

Euler Load, F_e, of GFRP stiffener = (π^2 x 36 x 116,781)/ 678^2

= 90 kN < 107 kN Not OK

Squash load, N_{pl}, of GFRP stiffener = [(80 x 6.4) + (38.6 x 6.4)] x 0.25

= 190 kN > 107 kN OK

For b_s = 48 mm, y = 11.41 mm, I_s = 141,118 mm^4

Euler Load, F_e, of GFRP stiffener = (π^2 x 36 x 141,118)/ 678^2

= 109 kN > 107 kN OK

Squash load, N_{pl}, of GFRP stiffener = [(80 x 6.4) + (41.6 x 6.4)] x 0.25

= 195 kN > 107 kN OK

One 80 x 48 x 6.4 mm GFRP stiffener is required

Check for buckling of the stiffener's web

$b_s/t_s = (48\text{-}6.4)/6.4 = 6.5 < 0.55\sqrt{(E/\sigma_y)} = 6.6$ OK

It shows that the cross-section, 80 x 50 x 6.4 mm, of GFRP stiffener used in test specimen B6 is larger than that required by the design procedure.

E.4 Load-bearing GFRP stiffeners of specimen B8

Required cross-section of steel stiffener

Stiffness requirement

Let thickness of intermediate steel stiffener, t_s = 5 mm (see Figure 8.10)

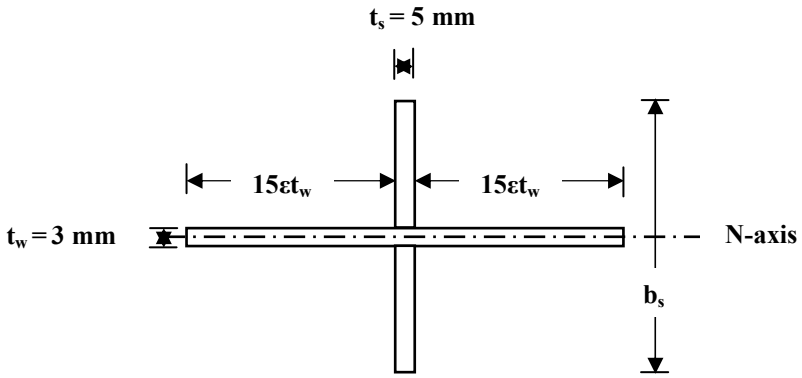

Figure 8.10 Required cross-section of load-bearing steel stiffeners for specimen B8

Length of web to be considered in determining $I_{s\,min}$ $= 2 \times 15\varepsilon t_w + t_s$

$= 2 \times 15 \times \sqrt{(235/353)} \times 3 + 5$ $= 78$ mm

For $a/d_w = 1 < \sqrt{2} = 1.4142$, $I_{s\,min} \geq 1.5\, d_w^3\, t_w^3 / a^2 = 1.5 \times 500^3 \times 3^3/500^2 = 20{,}250$ mm^4

Similarly, $EI_{s\,min} = 20{,}250 \times 205 = 4.15 \times 10^6$ kN-mm^2

For t_s = 5 mm, $I_s = 5 \times b_s^3/12 + 78 \times 3^3/12 \geq 20{,}250$ mm^4

$b_s \geq 36.25 \approx 40$ mm Two 20 x 4 mm steel stiffeners are required

EI of the steel stiffeners + web portion $= 205 \times [5 \times 40^3/12 + 78 \times 3^3/12]$

$= 5.5 \times 10^6$ kN-mm$^2 > 4.15 \times 10^6$ kN-mm^2 OK

Strength requirement

Length of steel stiffener, L = 500 mm

Maximum compressive strength on stiffener $\geq$ test load applied to the stiffener

$= 285$ kN

For b_s = 40 mm, I = 26841.1 mm^4

Euler load, F_e, of effective section of steel stiffener = (π^2 x 205 x 26841.1)/ 500^2

= 217.3 kN < 285 kN Not OK

Squash load, N_{pl}, of effective section of steel stiffener = [(78x3) + (40 x 5)] x 0.334

= 145kN < 285 kN Not OK

For b_s = 70 mm, I = 143086.4 mm^4

Euler load, F_e, of steel stiffener = (π^2 x 205 x 143086.4)/ 500^2

= 423 kN > 285 kN OK

Squash load, N_{pl}, of steel stiffener = [(78x3) + (70 x 5)] x 0.334

= 195 kN < 285 kN Not OK

For b_s = 100 mm,

Squash load, N_{pl}, of steel stiffener = [(78x3) + (100 x 5)] x 0.334

= 245 kN < 285 kN Not OK

For b_s = 120 mm,

Squash load, N_{pl}, of steel stiffener = [(78x3) + (120 x 5)] x 0.334

= 278 kN < 285 kN Not OK

For b_s = 130 mm,

Squash load, N_{pl}, of steel stiffener = [(78x3) + (130 x 5)] x 0.334

= 295 kN > 285 kN OK

Two 65 x 5 mm steel stiffeners are required

Check for buckling of the stiffener

b_s/t_s = 65/5 = 13.0 < 0.55 $\sqrt{(E/\sigma_y)}$ = 14.40 OK

Required cross-section of GFRP stiffener

Stiffness requirement

Let thickness of intermediate GFRP stiffener, t_s = 6.4 mm (see Figure 8.11)

Equivalent length of GFRP + web portion = 205/36 x 78 + 6.4 ≈ 450 mm

EI of equivalent GFRP stiffener + web portion

= 36 x [6.4x b_s^3/12 + 450 x 3^3/12] ≥ 4.41 x 10^6 kN-mm^2

b_s ≥ 60.82 ≈ 62 mm Two 31 x 6.4 mm GFRP stiffeners are required

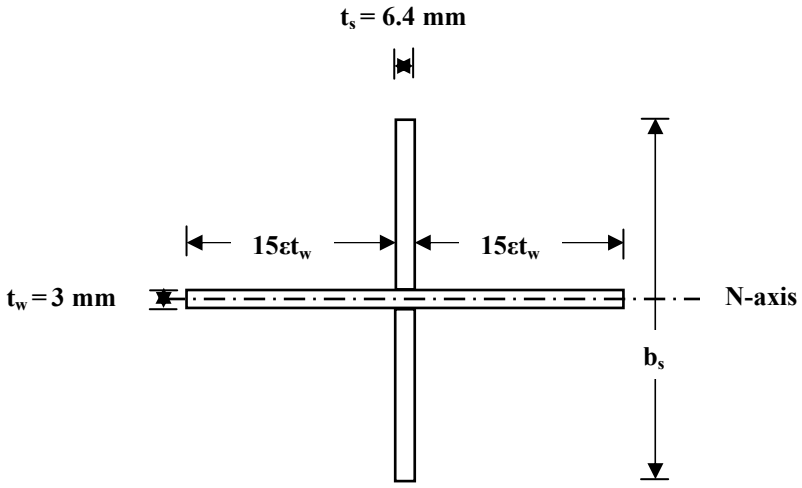

Figure 8.11 Required cross-section of load-bearing GFRP stiffeners for specimen B8

Strength requirement

Length of GFRP stiffener, L = 500 mm

Maximum compressive strength of stiffener ≥ test load applied to the stiffener

= 285 kN

For b_s = 62 mm, I = 128102.1 mm^4

Euler load, F_e, of effective section of GFRP stiffener = (π^2 x 36 x 128110)/ 500^2

F_e = 182 kN < 285 kN Not OK

Squash load, N_{pl}, of effective section of GFRP stiffener

N_{pl} = (78 x 3) x 0.353 + (135.6 x 6.4) x 0.25 = 299 kN > 285kN OK

For b_s = 70 mm, I = 183925.1 mm^4 F_e = 261 kN < 285 kN Not OK

For b_s = 80 mm, I = 274055 mm^4 F_e = 389 kN > 285 kN OK

Two 80 x 40 x 6.4 mm GFRP stiffeners are required

Check for buckling of the stiffener's web

b_s/t_s = (40-6.4)/6.4 = 5.25 < 0.55 $\sqrt{(E/\sigma_y)}$ = 6.6 OK

It shows that the cross-section, 80 x 50 x 6.4 mm, of each of the two GFRP stiffeners used in test specimen B8 is larger than that required by the design procedure.

Appendix F Design ultimate loads of specimens OB1 to OB3 of Okeil et al

F.1 Un-strengthened specimen OB1

Table 8.14 gives calculations for the estimation of the ultimate load of the un-strengthened specimen OB1 using the procedure in EC3.

Table 8.14 Calculations for design ultimate load of specimen OB1

Formula	Specimen OB1
Contribution of web	
$V_{plastic} = \frac{\sigma_{yw} d_w t_w}{\sqrt{3}} + \frac{b_f t_f^2 \sigma_{yf}}{a}$ of test web panel (kN)	318.6
$V_{plastic}$ of specimen = 4/3 x $V_{plastic}$ of test panel (kN)	425
K (for square plate with simply supported boundary conditions)	9.34
$\tau_{cr} = \frac{\pi^2 KE}{12(1-\vartheta^2)} \frac{t_w^2}{d_w^2}$	0.06868
$\lambda_w = 0.76 \sqrt{\sigma_{yw}/\tau_{cr}}$	1.61465 > 1.08
$\chi_w = 0.83/\lambda_w$ (for non-rigid end posts)	0.514
$V_{bw,Rd} = \frac{\chi_w d_w t_w \sigma_{yw}}{\sqrt{3}\gamma_{M1}}$ of test web panel (kN)	149.6
Contribution of flanges	
$c = a\left[0.25 + 1.6 b_f t_f^2 \sigma_{yf}/d_w 2 t_w \sigma_{yw}\right]$ (mm)	171.91
Let applied load on test web panel (kN)	228
M_{Ed} = Applied load x a (kN-mm)	118788
$M_{f,Rd} = A_f . h_f . \sigma_{yf}$ (kN-mm)	566900.1
$V_{bf,Rd} = b_f t_f^2 \sigma_{yf}/c\gamma_{M0}\left[1 - \{M_{Ed}/M_{f,Rd}\}^2\right]$ (kN)	78.66
$V_{b,Rd}$ of plate-girder = 4/3 x [$V_{bw,Rd}$ + $V_{bf,Rd}$] of test panel	304
Design ultimate load	**304 kN**

F.2 Specimen OB2 with two vertical GFRP stiffeners

Table 8.15 gives calculations for the estimation of the ultimate load of specimen OB2 with two vertical GFRP pultruded section stiffeners, one on each side of the test web panel.

Table 8.15 Calculations for design ultimate load of specimen OB2

Formula	Specimen OB2
Contribution of web	
Aspect ratio = a/d_w = 250/ 500	0.5
K (for simple supported conditions) = $5.34 + 4.0/(a/d_w)^2$	25.36
$\tau_{CR} = \frac{\pi^2 KE}{12(1-\vartheta^2)}\frac{t_w^2}{d_w^2}$	0.1865
$\lambda_w = 0.76\sqrt{\sigma_{yw}/\tau_{CR}}$	0.9798 < 1.08
$\chi_w = 0.83/\lambda_w$ (for non-rigid end posts)	0.847
$V_{bw,Rd} = \frac{\chi_w d_w t_w \sigma_{yw}}{\sqrt{3}\gamma_{M1}}$ of test web panel (kN)	246.46
Contribution of flanges	
$c = a\left[0.25 + 1.6 b_f t_f^2 \sigma_{yf}/d_w 2 t_w \sigma_{yw}\right]$ (mm)	172.0
Let applied load on test web panel (kN)	322
M_{Ed} = Applied load x a (kN-mm)	167762
$M_{f,Rd} = A_f.h_f.\sigma_{yf}$ (kN-mm)	566900.1
$V_{bf,Rd} = b_f t_f^2 \sigma_{yf}/c\gamma_{M0}\left[1-\{M_{Ed}/M_{f,Rd}\}^2\right]$ (kN)	75.09
$V_{b,Rd}$ of plate-girder = 4/3 x [$V_{bw,Rd}$ + $V_{bf,Rd}$] of test panel (kN)	429
Design ultimate load	**429 kN**

F.3 Specimen OB3 with a diagonal GFRP stiffener

Table 8.16 gives calculations for the estimation of the ultimate load of specimen OB3 using the design procedure.

Table 8.16 Calculations for design ultimate load of specimen of OB3

Particulars	**Load (kN)**
Area of cross-section of GFRP stiffener, A_{GFRP} by taking depth of stiffener equal to '0.55 $\sqrt{(E/\sigma_y)}$' and width of its flange equal to 125 mm = [125 x 9.5] + [0.5 5x $\sqrt{(17200/150)}$ x 9.5] (mm^2)	1719
Squash load of diagonal T-section GFRP pultruded section stiffener (at σ_y GFRP = 150 MPa) = 1719 x 0.15	257.85
Applied load required to squash diagonal GFRP stiffener = 257.85/$\sqrt{2}$	182.3
Plastic ultimate load of end web panel of specimen OB3 with diagonal stiffener (kN) = ([279 x 13^2 x 0.3]/508) + ([3.2 x 508x 0.31]/1.732) + 181.9 = 27.8 + 290.9 + 182.3	501.0
Test ultimate load of un-strengthened end web panel of specimen OB3 = 0.75x278	208.5
Design ultimate load of strengthened web panel = 208.5+182.3 = 390.8 < 501 (OK)	390.8
Design ultimate load of specimen OB3 = 4/3 x 390.8	**520 kN**

Appendix G Design of GFRP stiffeners of specimens OB2 and OB3 of Okeil et al

G.1 Vertical GFRP intermediate stiffeners of specimen OB2

Required cross-section of steel stiffener

Let thickness of intermediate steel stiffener, t_s = 5 mm (see Figure 8.12)

Length of web to be considered in determining $I_{s\,min}$ $= 2 \times 15\varepsilon t_w + t_s$

$= 2 \times 15 \times \sqrt{(235/310)} \times 3.2 + 4 = 88.6$ mm

For $a/d_w = 1 < \sqrt{2} = 1.4142$, $I_{s\,min} \geq 1.5\, d_w^3\, t_w^3 / a^2 = 1.5 \times 508^3 \times 3.2^3/508^2$

$= 24{,}696.2$ mm^4

Similarly, $EI_{s\,min} = 24{,}696.2 \times 205 = 5.12 \times 10^6$ kN-mm^2

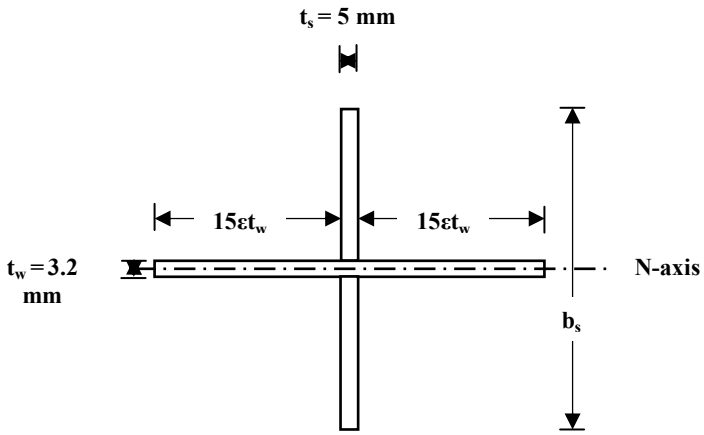

Figure 8.12 Required cross-section of intermediate steel stiffener for specimen OB2

For t_s = 5 mm, $I_s = 5 \times b_s^3/12 + 88.6 \times 3.2^3/12 \geq 24{,}696.2$ mm^4

$b_s = 38.86 \approx 40$ mm Two 20 x 5 mm steel stiffeners are required

EI of the steel stiffeners only $= 205 \times 5 \times 40^3/12 = 5.457 \times 10^6$ kN-mm^2

$> 5.12 \times 10^6$ kN-mm^2 OK

Check for buckling of the stiffener

$b_s/t_s \leq 0.55\sqrt{(E/\sigma_y)}$, For E = 205 GPa and σ_y = 300 MPa,

$0.55\sqrt{(E/\sigma_y)} = 0.55\sqrt{(205/0.3)} = 14.4$ $b_s/t_s = 20/5 = 4.0 < 14.4$ OK

Required cross-section of GFRP stiffener

Let thickness of intermediate GFRP stiffener, t_s = 8 mm

EI of equivalent GFRP stiffener only = $17.2 \times 8 \times b_s^3/12 = 5.467 \times 10^6$ kN-mm^2

$b_s = 77.78 \approx 80$ mm Two 60x40x8 mm GFRP stiffeners are required

Check for buckling of the stiffener's web

$b_s/t_s \leq 0.55\sqrt{(E/\sigma_y)}$ For E = 17.2 GPa and σ_y = 150 MPa, 0.55

$\sqrt{(E/\sigma_y)} = 0.55\sqrt{(17/0.15)} = 5.86$ $b_s/t_s = (40-8)/8 = 4.0 < 14.4$ OK

It shows that the cross-section, 140 x 128 x 9.5mm, of each of the two GFRP stiffeners used in test specimen OB2 is larger than that required by the design procedure.

G.2 Diagonal GFRP stiffener of specimen OB3

Test ultimate load of un-strengthened test panel of specimen OB3= ¾ x 278= 209 kN
Test ultimate load of specimen OB3 with diagonal GFRP stiffener = 435 kN
Test ultimate load of GFRP-strengthened panel of OB3 = ¾ x 435 = 327 kN
Additional load required due to diagonal GFRP stiffener = difference in ultimate loads of un-strengthened and GFRP-strengthened panels of OB3= 327-209 = 118 kN

In view of the above, the minimum of the Euler load and squash load of diagonal GFRP stiffener should be equal to or greater than 118 kN. Let 'b_s' is the overall depth of GFRP stiffener and other dimensions are as given in Figure 8.13. Length of the stiffener be taken as 700 mm as in the test specimen.

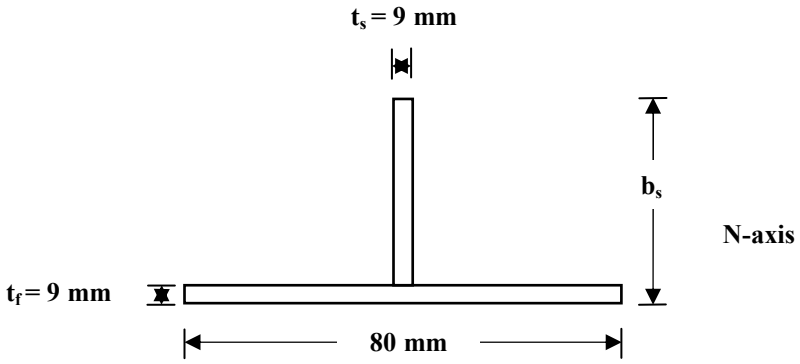

Figure 8.13 Required cross-section of diagonal stiffeners for specimen OB3

For b_s = 60 mm, y = 16.18 mm, I_s = 356,623 mm^4
Euler Load, F_e, of GFRP stiffener = (π^2 x 17.26 x 356,623)/ 700^2
= 124 kN > 118 kN OK
Squash load, N_{pl}, of GFRP stiffener = [(80 x 9) + (51 x 9)] x 0.15
= 177 kN > 118 kN OK
One 80 x 60 x 9 mm GFRP stiffener is required

Check for buckling of the stiffener's web

b_s/t_s = (60-9)/9 = 5.66 < 0.55 $\sqrt{(E/\sigma_y)}$ =5.86 OK

It shows that the cross-section, 140 x 128 x 9.5 mm, of diagonal GFRP stiffener used in test specimen OB3 is larger than that required by design procedure.

Appendix H Design ultimate loads of models of parametric studies

H.1 Design ultimate loads of models with diagonal stiffeners (First & second studies)

Table 8.17 and Table 8.18 give the calculations made for the estimation of the ultimate loads of models with diagonal stiffeners using the design procedure.

Table 8.17 Design ultimate loads of models with diagonal stiffeners (First study)

Thickness of web t_w (mm)	**(1) EC3 ultimate load of un-strengthened web panel (kN)**	**(2) * Squash load of diagonal steel & GFRP stiffeners = $A_s\sigma_{ys}/\sqrt{2}$ (kN)**	**Design ultimate load (kN) (1) + (2)**
0	21.6	---	22.1
0.5	34	31.8	65.8
1.0	59	31.8	90.8
2.0	116	31.8	148
3.0	193	31.8	225
4.0	293	31.8	325
5.0	417	31.8	449
6.0	541	31.8	573

*Squash load of steel and GFRP stiffeners is same because of the same areas of cross-section and yield strengths

Table 8.18 Design ultimate loads of models with diagonal stiffeners (Second study)

Diagonal steel stiffener		**Web thickness t_w (mm)**	**(1) EC3 Ultimate load of un-strengthened web panel (kN)**	**(2) Squash load of diagonal stiffeners = $A_s\sigma_{ys}/\sqrt{2}$ (kN)**	**Design ultimate load (kN) (1)+(2)**
d_s x t_s (mm)	**One or both sides**				
100 x 12	Both	0.5	34	509	543
100 x 12	Both	1.0	59	509	568
100 x 12	Both	2.0	116	509	625
100 x 12	Both	3.0	193	509	702
100 x 3	Both	3.0	193	127.3	320
25 x 12	Both	3.0	193	127.3	320
25 x 3	Both	3.0	193	32	225
100 x 12	One	3.0	193	255	448
100 x 3	One	3.0	193	64	257
25 x 12	One	3.0	193	64	257
25 x 3	One	3.0	193	16	209

H.2 Design ultimate loads of glass fabric-strengthened models

Table 8.19 gives the calculations made for the estimation of the ultimate loads of glass fabric-strengthened models using the design procedure.

Table 8.19 Calculations for design ultimate loads of glass fabric-strengthened models

Formula	Model				
	1	**2**	**3**	**4**	**5**
Contribution of web					
Thickness of steel, t_s (mm)	3.0	3.0	3.0	3.0	3.0
Thickness of fabric, t_f (mm)	3.0	6.0	9.0	12.0	15.0
Equivalent steel thickness based on flexural stiffness, t_e (mm)	3.6	4.96	6.53	8.16	9.78
Shear buckling co-efficient, K	9.34	9.34	9.34	9.34	9.34
$\tau_{cr} = \frac{\pi^2 KE}{12(1-\vartheta^2)}\frac{t_w^2}{d_w^2}$	0.0912	0.1704	0.295	0.461	0.662
$\tau_{yw} = \sigma_{yw}/\sqrt{3}$	0.1732 $> \tau_{cr}$	0.1732 $> \tau_{cr}$	0.1732 $< \tau_{cr}$	0.1732 $< \tau_{cr}$	0.1732 $< \tau_{cr}$
$\lambda_w = 0.76\sqrt{\sigma_{yw}/\tau_{cr}}$	1.378 > 1.08	1.009 < 1.08	0.766 < 1.08	0.613 < 1.08	0.512 < 1.08
$\chi_w = 0.83/\lambda_w$	0.602	0.823	1.083	1.354	1.623
$V_{bw,Rd} = \frac{\chi_w d_w t_w \sigma_{yw}}{\sqrt{3}\gamma_{M1}}$ of FRP-str. panel (kN)	210.6	361.8	573.86	839	1151.6
Contribution of flanges					
$c = a\left[0.25 + 1.6 b_f t_f^2 \sigma_{yf}/d_w 2 t_w \sigma_{yw}\right]$ (mm)	156.7	148.2	142.6	139.1	136.8
Let applied load on test panel (kN)	274	420	620	877	1152
M_{Ed} = Applied load x a (kN-mm)	137000	210000	310000	438500	576000
$M_{f,Rd} = A_f.h_f.\sigma_{yf}$ (kN-mm)	406800	406800	406800	406800	406800
$V_{bf,Rd} = b_f t_f^2 \sigma_{yf}/c\gamma_{M0}\left[1 - \{M_{Ed}/M_{f,Rd}\}^2\right]$ (kN)	62.8	57.7	41.5	7.3	0
$V_{b,Rd}$ of model = $[V_{bw,Rd} + V_{bf,Rd}]$ of fabric-strengthened web panel (kN)	274	419.5	620	877	1152
$V_{plastic}$ of model = $[\frac{\sigma_{yw} d_w t_w}{\sqrt{3}} + \frac{b_f t_f^2 \sigma_{yf}}{a}]$ of fabric-strengthened web panel] (kN)	371.5	461.5	551.6	641.7	731.7
Design ultimate load	$\tau_{yw} > \tau_{cr}$ **274 kN**	$\tau_{yw} > \tau_{cr}$ **419.5 kN**	$\tau_{yw} < \tau_{cr}$ ***551.6 kN**	$\tau_{yw} < \tau_{cr}$ ***641.7 kN**	$\tau_{yw} < \tau_{cr}$ ***731.7 kN**

* Ultimate plastic load of the fabric-strengthened web panel

H.3 Design ultimate loads of fabric-strengthened specimens B3, B4 and B7

Table 8.20 gives the details of calculations made to estimate ultimate loads of specimens B3, B4 and B7 with one layer of the carbon fabric and two layers each of the glass fabric, respectively, using the design procedure.

Table 8.20 Calculations for design ultimate loads of specimens B3, B4 and B7

Formula	Specimen		
	B3	**B4**	**B7**
Contribution of web			
Thickness of steel, t_s (mm)	3.0	3.0	3.0
Thickness of fabric, t_f (mm)	1.5	2.5	2.5
Equivalent steel thickness based on flexural stiffness, t_e (mm)	3.5	3.462	3.462
Shear buckling co-efficient, K	9.34	9.34	9.34
$\tau_{cr} = \frac{\pi^2 KE}{12(1-\vartheta^2)}\frac{t_w^2}{d_w^2}$	0.0845	0.08298	0.08298
$\tau_{yw} = \sigma_{yw}/\sqrt{3}$	$0.158 > \tau_{cr}$	$0.158 > \tau_{cr}$	$0.204 > \tau_{cr}$
$\lambda_w = 0.76\sqrt{\sigma_{yw}/\tau_{cr}}$	1.37 > 1.08	1.381 > 1.08	1.567 > 1.08
$\chi_w = 0.83/\lambda_w$	0.606	0.601	0.53
$V_{bw,Rd} = \frac{\chi_w d_w t_w \sigma_{yw}}{\sqrt{3}\gamma_{M1}}$ of FRP-str. panel (kN)	215.71	196.63	209.44
Contribution of flanges			
$c = a\left[0.25 + 1.6 b_f t_f^2 \sigma_{yf}/d_w 2 t_w \sigma_{yw}\right]$ (mm)	171.5	171.9	162.3
Let applied load on test panel (kN)	292	273	292
M_{Ed} = Applied load x a (kN-mm)	145875	136500	145875
$M_{f,Rd}$ = $A_f.h_f.\sigma_{yf}$ (kN-mm)	593510	593510	608256
$V_{bf,Rd} = b_f t_f^2 \sigma_{yf}/c\gamma_{M0}\left[1-\{M_{Ed}/M_{f,Rd}\}^2\right]$ (kN)	76.21	76.63	82.77
$V_{b,Rd}$ of plate-girder = 4/3 [$V_{bw,Rd}$ + $V_{bf,Rd}$] of end web panel (kN)	389	364	389
$V_{plastic}$ of specimen = 4/3 x[$\frac{\sigma_{yw} d_w t_w}{\sqrt{3}} + \frac{b_f t_f^2 \sigma_{yf}}{a}$ of test panel] (kN)	511	473	565
Design ultimate load	$\tau_{yw} > \tau_{cr}$ **389 kN**	$\tau_{yw} > \tau_{cr}$ **364 kN**	$\tau_{yw} > \tau_{cr}$ **389 kN**

* Ultimate plastic load of specimen (plate-girder)

References

Adams, R.D. (1990) *Fatigue strength tests and their limitations,* Adhesive and Sealant Engineering Materials Handbook, 3, Chapman and Hall publications.

Adams, R.D., Comyn, J. And Wake, W.C. (1997) *Structural adhesive joints in engineering,* Second edition, Springer publications.

AISC specifications (1961) *Design, fabrication and erection of structural steel for buildings*, November 30, 1961.

Alinia, M.M., and Dastfan, M. (2006) *Behaviour of thin steel plate shear walls regarding frame members,* Journal of Construction Steel Research, 62(7), 730-738.

Alinia, M.M., Gheitasi, A. and Shakiba, M. (2011) *Post-buckling and ultimate state of stresses of steel plate girders,* Thin-walled Structures, 49(4), 455-464.

Alinia, M.M., Shakiba, M. and Habashi, H.R. (2009) *Shear failure characteristics of steel plate girders,* Thin-walled Structures, 47(12), 1498-1506.

Al-Saidy, A.H., Klaiber, F.W. and Wipf, T.J. (2004) *Repair of steel composite beams with carbon-reinforced polymer plates*, Journal of Composite for Construction, 8(2), 163-172.

ANSI/AASHTO/AWS D1.5-96 (1996) Bridge Welding Code, American Association of State Highway and Transportation Officials (AASHTO) and American Welding Society (AWS), Washington DC, USA.

AS 4100 (1998) *Standards Australia*, Australian Standards for steel structures, Sydney, Australia.

Attari, N., Amziane, S. and Chemrouk, M. (2012) *Flexural strengthening of concrete beams using CFRP, GFRP and hybrid FRP sheets,* Construction and Building Materials, 37, 746-757.

Bakis, C.E., Bank, L.C., Brown V.L., Cosenza, E., Davalos, J.F., Lesko, J.J., Machida, A., Rizkalla, S.H. and Triantafillou, T.C. (2002) *Fibre-reinforced polymer composites for construction: State-of-art review*, Journal of Composites for Construction, 6(2), 73-87.

Basler, K., (1961) *Strength of plate-girders in shear*, Journal of Structural Design, Proceedings of the American Society Civil Engineers, ASCE Proc. No. 2967, 151-180.

BS 5950-1 (2000) *British standards for structural use of steelwork in building*, *Part 1: Code of practice for design – Rolled and welded sections*.

BS EN ISO 6892-1 (2009) *Metallic materials –Tensile testing- Part 1: Method of test at room temperature,* European Committee for Standardization, Brussels.

Cadei, J.M.C., Stratford, T.J.; Hollaway, L.C. and Duckett, W.G. (2004) *Strengthening metallic structures using externally bonded fibre-reinforced polymers*, Construction Industry Research and Information Association (CIRIA) Report No. C595, London UK.

Callister, W. D. (2000) *Materials Science and Engineering*, Fifth Edition, John Wiley and Sons, United States.

Case, J. and Chilver, A.H. (1971) *Strength of materials and structure*, Second Edition, Edward Arnold (publishers) Ltd, London, United Kingdom.

Chakrabarti, P.R., Millar, D. and Bandyopadhyay (2011) *Application of composites in Infrastructure Part-III, a brief report on research and development,* June 24, 2011, http://quakewrap.com/frp%20papers/Application-of-Composites-in-Infrastructure-Part-III-(a-brief-report-on-research-and-development).pdf (Accessed November 26, 2012).

Colombi, P. and Poggi, C. (2006) *An experimental and numerical study of elastic behaviour of steel beams reinforced by pultruded CFRP strips,* Composites Part B: Engineering, 37(1), 64-73.

Crocombe, A.D. and Adams, R.D. (1981) *Influence of spew fillet and other parameters on stress distribution in a single lap joints,* The Journal of Adhesion, 13(2), 141-155.

Czaderski, C. (2002) *Shear strengthening with pre-fabricated CFRP L-shaped plates: Test specimens S1 to S6,* EPMA Report No. 116/7, August 2002, Switzerland.

Czaderski, C. and Motavalli M. (2004) *Fatigue behaviour of CFRP L-shaped plates for shear strengthening of RC T-beams,* Composites Part B: Engineering, 35(4), 279-290.

D3039/D 3039M -08 (2008) *Standard method for tensile properties of polymer matrix composite materials,* American Society of Testing Materials (ASTM) Committee D30 on Composite Materials.

Da Silva, L., Cruz P.J. and Asio H.G. (1999) *A comparative assessment of the shear strength of slender steel beams,* Archives of Civil Engineering, 45(4), 587-613.

DURA RAL7001 (2012) *Pultruded GRP Profiles*, DURA Composites Limited, Essex, UK http://www.grpprofiles.com/dura_profile_standard_range.html (Accessed January 12, 2012).

DURAGRID T-3500 (2010) *Design Manual*, Strongwell Corporation, Bristol, Virginia USA, http://www.strongwell.com/PDFfiles/Pultruded%20Grating/DURADEK%20_and_%20DURAGRID%20Load%20Tables.pdf (Accessed August 03, 2010).

ENV 1993-1-1 (1993) *Eurocode 3: Design of steel structures, Part 1.1, General rules for buildings,* European Committee for Standardization, Brussels.

ENV 1993-1-4 (1996) *Eurocode 3: Design of steel structures, Part 1.4, General Rules - Supplementary rules for stainless steel,* European Committee for Standardization, Brussels.

ENV 1993-1-5 (2006) *Eurocode 3: Design of steel structures*, *Part 1.5, General rules and rules for buildings, Supplementary Rules for planar plated structures without transverse loading*, European Committee for Standardization, Brussels.

Fitch, D. (2007) *Design of steel plate and box girders*, http://www.sigi.ca/engineering/documents/plate_and_box_girder_design.pdf (Accessed September 10, 2012).

Harries, K.A., Peck, A.J. and Abraham, E.J. (2009) *Enhancing stability of structural steel sections using FRP*, Thin-Walled Structures, 47(10), 1092-1101.

Hendy, C.R., and Turco, E. (2008) N*umerical validation of simplified theories for design rules of transversely stiffened plate girders*, Structural Engineer, November 4, 2008.

Hoglund, T. (1997) *Shear buckling resistance of steel and aluminium plate girders,* Thin-Walled Structures, 29(1), 13-30.

Hoglund, T., (1973) *Design of thin plate I girders in shear and bending with special reference to web buckling*, Bulletin No. 94, Division of Building Statistics and Structural Engineering, Royal Institute of Technology, Stockholm, Sweden.

Hollaway, L. C. (2005) *Advances in adhesive joining of dissimilar materials with special reference to steels and FRP composites,* In Proceedings of the International Symposium on Bond Behaviour of FRP in Structures (BBFS), December 2005, 11-21.

Hollaway, L.C. (2010) *A review of present and future utilization of FRP composites in the civil infrastructure with reference to their important in-service properties*, Construction and Building Materials, 24(12), 2419-2445.

Hollaway, L.C. and Teng, J.G. (2008) *Strengthening and rehabilitation of civil infrastructures using fibre-reinforced polymers (FRP) composites*, The Institute of Materials, Minerals and Mining, Yoodhead Publishing Limited, Cambridge United Kingdom.

Imam, B. M. and Chryssanthopoulos, M. K. (2010) *A review of metallic bridge failure statistics,* In Bridge Maintenance, Safety and Management: Proceedings of the Fifth International IABMAS Conference, July 2010, 3275-3282.

Islam, S.M.Z. and Young, B. (2013) *Strengthening of ferritic stainless steel tubular structural members using FRP subjected to two-flange loading,* Thin-Walled Structures, 62, 179-190.

Johansson, B., Maquoi, R., Sedlacek, G., Müller, C., and Beg, D. (2007) *Commentary and worked examples to EN 1993-1-5, Plated Structural Elements*, Joint Report prepared under the JRC-ECCS cooperation agreement for the evolution of Eurocode 3 (programme of CEN / TC 250) , EUR 22898 EN-2007.

Lam, D., Cheong, T. and Chiew, S.P. (2004) *Structural steelwork -Design to limit state theory*, Third Edition, Oxford, United Kingdom.

Lang, C. (2008) *Composite patching of fatigue cracks in steel structures,* Ph.D. Thesis, School of Built Environment, Heriot-Watt University, Edinburgh, Scotland.

Lee, S.C. and Yoo, C.H. (1998) *Strength of plate girder web panels under pure shear,* Journal of Structural Engineering, 124(2), 184-194.

Lee, S.C. and Yoo, C.H. (1999) *Experimental study on ultimate shear strength of web panel,* Journal of Structural Engineering, 125(8), 838-846.

LUSAS, version 14.3 (2008) *Modeller reference manual,* Finite Element Analyses Limited, Surrey, United Kingdom.

Meier, U., Deuring, M., Meier, H. and Schwegler, G. (1992) *Strengthening of structures with CFRP laminates: Research and applications in Switzerland,* Advanced Composite Materials in Bridges and Structures, Canadian Society for Civil Engineering, Sherbrooke, Canada, 243-251.

Mostofinejad, D. and Kashani, A.T. (2013) *Experimental study on effect of EBR and EBROG methods of debonding of FRP sheets under shear strengthening of RC beams,* Composites Part B: Engineering, 45, 1704-1713.

Motavalli, M. and Czaderski, C. (2007) *FRP Composites for retrofitting of existing civil structures in Europe: State of art review,* International Conference on Composites and Polycon, American Composites Manufacturers Association, Tampa, Florida USA, October 17-19, 2007, 1-10.

NA to BS EN 1993-1-5:2006 (2008) *UK National Annex to Eurocode 3: Design of steel structures - Part 1-5: Plated structural elements*, European Committee for Standardization, Brussels.

Narmashiri, K., Jumaat, M.Z. and Sulon, N.H.R. (2010) *Shear strengthening of steel I-beams using CFRP strips*, Scientific Research & Essays, 5(16), 2155-2168.

Newman, G.M., Robinson, J.T. and Bailey, C. G. (2001) Fire safe design: A new approach to multi-storey steel-framed buildings. *SCI publication*, *288*(2).

Nilsen, C.L., Mydin, M.A.O. and Ramli, M. (2012) *Performance of lightweight thin-walled steel section: Theoretical and mathematical considerations*, Advances in Applied Science Research, 3(5), 2847-2859.

Okeil, A. M., Bingol, Y., and Chorkey, M. (2010) *Stiffening thin-walled structures using pultruded FRP sections*, *Highways for life and accelerated bridge construction,* FHWA Bridge Engineering Conference, Orlando, Florida, USA, April 8-9, 2010.

Okeil, A.M., Bingol, Y. and Ferdous, M.R. (2009a) *A novel technique for inhibiting buckling of thin-walled steel structures using pultruded glass FRP sections*, Journal of Composites for Construction, 13(6), 547-557.

Okeil, A.M. Bingol, Y. and Ferdous, M.R. (2009b) *Novel technique for stiffening steel structures*, Technical Report No. FHWA/LA.08/441, Federal Highway Administration, Department of Transportation, USA.

Okeil, A.M., Broussard, G. and Ferdous, M.R., (2011) *Strengthening-by-stiffening: Analysis Model Validation and Parametric Study*, First Middle East Conference on Smart Monitoring Assessment and Rehabilitation of Civil structures, Dubai, UAE, February 8-10, 2011, 1-9.

Photiou, N.K., Hollaway, L.C. and Chryssanthopoulos, M.K. (2006a) *Strengthening of an artificially degraded steel beam utilizing a carbon/glass composite system,* Construction and Building Materials, 20(1), 11-21.

Photiou, N. K., Hollaway, L. C. and Chryssanthopoulos, M. K. (2006b) *Selection of carbon-fibre-reinforced polymer systems for steelwork upgrading,* Journal of Materials in Civil Engineering, 18(5), 641-649.

PLIO-GRIP 7770/220 (2011) *PLIO-GRIP structural adhesives*, Ashland Performance Materials, Dublin, USA, http://www.ashland.com/products/pliogrip-structural-adhesives (Accessed August 03, 2010).

Presta, F., Hendy, C.R., and Turco, E. (2011) N*umerical validation of simplified theories for design rules of transversely stiffened plate girders*, Workshop on Eurocode 4-2, Composite Bridges, Stockholm, Sweden, March 17, 2011, 255-264.

Real, E., Mirambell, E. and Estrada, I. (2007) *Shear response of stainless steel plate girders,* Engineering Structures, 29(7), 1626-1640.

Rockey, K. C., Evans, H. R. and Porter, D. M. (1978) *A design method for predicting the collapse behaviour of plate girders*, Proceedings of Institution of Civil Engineers (ICE), 65(1), 85-112.

Rockey, K.C. and Skaloud, M. (1968) *Influence of flange stiffness upon the load carrying capacity of webs in shear*, 8th Congress of IABSE, Final Report, New York, USA.

Rockey, K.C. and Skaloud, M. (1972) *The ultimate load behaviour of plate-girders loaded in shear*, The Structural Engineer, 50(1), 29-47.

Rockey, K.C., Valtinat, G., and Tang, K.H., (1981) *The design of transverse stiffeners on webs loaded in shear –an ultimate load approach*, Proceedings of Institution of Civil Engineers (ICE), 71(4), 1069-1099.

Sparks, K. J. (Ed.). (2008) *Encyclopaedia Britannica 2008*, Encyclopaedia Britannica.

Sen, R., Liby, L. and Mullins, G. (2001) *Strengthening steel bridge sections using CFRP laminates,* Composites Part B: Engineering, 32(4), 309-322.

Sundarrraja, M.C. and Rajamohan, S. (2009) *Strengthening of RC beams in shear using GFRP inclined strips: An experimental study*, Construction and Building Materials, 23(2), 856-864.

Taljsten, B. (1997) *Strengthening of beams by plate bonding,* Journal of Materials in Civil Engineering, 9(4), 206-212.

Technowrap 2K™ (2011) Walker Technical Resources Limited, Aberdeen, UK, http://www.wtr.uk.com/index.asp?id=4&refID=30&contentID=30 (Accessed April 28, 2011).

Technowrap-2K structural adhesive (2011) Walker Technical Resources Limited, Aberdeen, UK, http://www.wtr.uk.com/index.asp?id=4&refID=41&contentID=41 (Accessed April 28, 2011).

Technowrap™ structural strengthening (2011) Walker Technical Resources Limited, Aberdeen, UK, http://www.wtr.uk.com/index.asp?id=4&refID=41&contentID=41 (Accessed April 28, 2011).

Timoshenko, S.P., and Krieger, S.W. (1959) *Theory of plates and shells,* Second Edition, MaGraw-Hill International Editions, Singapore.

Tomblin, J.S., Seneviratne, W., Escobar, Yoon, K.Y. and Harter, P. (2003) *Presentation on adhesive behaviour in aircraft applications, Key characteristics for advanced material control*, Federal Aviation Administration Workshop, September 16-18, 2003.

Tomblin, J.S., Yang, C. and Harter, P. (2001) *Investigation of thick bond line adhesive joints,* Report No. DOT/FAA/AR-01/33, Federal Administration Authority, Department of Transportation, USA.

Trahair, N.S., Bradford, M.A. and Nether cot, D.A. (2001) *The behaviour and design of steel structures to BS5950*, Third Edition-British, Taylor and Francis, London, United Kingdom.

Vallee, T. and Keller, T. (2006) *Adhesively bonded lap joints from pultruded GFRP profiles, Part-III: Effects of chamfers*, Composites Part B: Engineering, 37, p328-336.

Vatonec, M., Kelley, P.L., Brainerd, M.L. and Kivela, J.B. (2002) *Post strengthening of steel members with CFRP*, 47th International SAMPE Symposium and Exhibition 2002, Long Beach, CA, May 12-16, 2002, 941-954.

White, D.W. and Barker, M.G. (2008) *Shear resistance of transversely stiffened steel I-girders*, Journal of Structural Engineering, 134(9), 1425-1436.

Wonseok, C. and Sotelino, E.D. (2006) *Three-dimensional finite element modelling of composite girder bridges*, Engineering Structures, 28(1), 63-71.

Zhao, X.L. and Al-Mahaidi, R. (2009) *Web buckling of light steel beams strengthened with CFRP subjected to end-bearing forces*, Thin-Walled Structures, 47(10), 1029-1036.